



UNIVERSITY OF  
LIVERPOOL

# **Iridium-mediated C-H functionalisation under mild conditions**

Thesis submitted in accordance with the requirements of the University of Liverpool for the  
degree of Doctor in Philosophy by:

**Claudia GATTI**

January 2020



**PGR Policy on Plagiarism and Dishonest Use of Data**  
**PGR CoP Appendix 4 Annexe 1**

**PGR DECLARATION OF ACADEMIC HONESTY**

|                         |   |
|-------------------------|---|
| <b>NAME (Print)</b>     | Claudia Gatti   |
| <b>STUDENT NUMBER</b>   | 201145208   |
| <b>SCHOOL/INSTITUTE</b> | Physical Sciences - Stephenson Institute for Renewable Energy |
| <b>TITLE OF WORK</b>    | Iridium-mediated C-H functionalisation under mild conditions  |

*This form should be completed by the student and appended to any piece of work that is submitted for examination. Submission by the student of the form by electronic means constitutes their confirmation of the terms of the declaration.*

Students should familiarise themselves with Appendix 4 of the PGR Code of Practice: PGR Policy on Plagiarism and Dishonest Use of Data, which provides the definitions of academic malpractice and the policies and procedures that apply to the investigation of alleged incidents.

Students found to have committed academic malpractice will receive penalties in accordance with the Policy, which in the most severe cases might include termination of studies.

**STUDENT DECLARATION**

I confirm that:

- I have read and understood the University's PGR Policy on Plagiarism and Dishonest Use of Data.
- I have acted honestly, ethically and professionally in conduct leading to assessment for the programme of study.
- I have not copied material from another source nor committed plagiarism nor fabricated, falsified or embellished data when completing the attached material.
- I have not copied material from another source, nor colluded with any other student in the preparation and production of this material.
- If an allegation of suspected academic malpractice is made, I give permission to the University to use source-matching software to ensure that the submitted material is all my own work.

SIGNATURE.....

DATE.....

*Alla mia famiglia*

(To my family)

# Abstract

## Iridium-mediated C-H functionalisation under mild conditions

Claudia GATTI

This thesis discusses the design of new methods for C-H functionalisation mediated by iridium complexes. In this respect, two C-H functionalisations will be discussed: the iridium-mediated room-temperature sonochemical alkane dehydrogenation and the iridium-catalysed Michael-type hydroalkylation.

The first part is focused on the dehydrogenation of abundant and inexpensive alkanes to olefins, which can then be easily converted in a vast array of chemicals. However, alkane dehydrogenation is a highly challenging transformation and, both on industrial and laboratory-scale, the main problem is the high operating temperature (>150 °C). This issue was addressed exploiting the sonocatalytic approach, a combination of catalysis and sonochemistry. It was demonstrated that the soluble iridium complex  $\text{Ir}(\text{P}^i\text{Pr}_3)_2\text{H}_5$  can perform the dehydrogenation of a variety of alkanes under ultrasound irradiation at 25 °C, a significantly lower temperature than that reported for most known homogeneous systems. Although the complex only allows for a stoichiometric reaction, this is the first example of general one-step ultrasound driven dehydrogenation of alkanes at room temperature.

The second part focuses on hydroalkylation, an atom economical method for C-C bond formation starting from weakly C-H acidic nitriles as Michael-donors and cyclohexenone. This method provides a facile access to 3-substituted cyclohexanones containing a quaternary centre, important building blocks for the synthesis of pharmaceuticals and natural products. The methodology for the hydroalkylation has been previously optimised in the same group, together with an early scope of reagents. Following this, the focus was directed towards expanding the scope to pyridyl-substituted nitriles and conducting mechanistic studies. To get insights in the previously proposed catalytic cycle, it has been repeated stoichiometrically step by step. Several new intermediates have been identified and one of these was found to be an even more active catalyst than the starting iridium-pentahydride complex. These new results allowed to propose a revised catalytic cycle and the findings helped to improve the hydroalkylation method thanks to the use of an additive.

# Publications

**Room-temperature sonochemical alkane dehydrogenation**

Claudia Gatti, Alexey G. Sergeev, and Dmitry G. Shchukin

*Manuscript in preparation*

# Acknowledgements

This work has been a long journey and there are many people whom I would like to thank.

First of all, I would like to thank my supervisor, in particular Prof Dmitry Shchukin for the possibility of this adventure, the leadership and the support and Dr. Alexey Sergeev for the scientific guidance, patience and attention to details. You both helped me become a better and more confident scientist and person.

Second, I would like to thank Dr. Konstatin Luzyanin for the help with the project with uncountable hours spend together talking about and doing NMR. But mostly, thank you for the moral support during difficult moments and for always being available for a chat and a coffee. You helped me so much during the past four years and I learnt a lot from you.

I am grateful to my lab-mates. Marta, for her work on the hydroalkylation project and with Martin for having welcomed me in the lab, for the chemistry discussions, the music and the daily coffees. Robyn, for your smile, the chats and the mutual support, I wish you the best for your future. Mike, Xiaoliang, Paula and Marios, for all your help in the Stephenson lab and for always been available to help me carry the nitrogen.

I would like to thank the members of the Stephenson. Here I have found not only great colleagues, but also many friends. Gaia, thank you for all the guidance and wisdom and, together with Silvia and Stefano, thank you for always being there for me and back me up when I needed. Thank you to Charlotte and Verity for always being there for a laugh. Thank you to Andrea for the therapeutic complaining.

I gratefully acknowledge all the colleagues who I have had the pleasure to work with during these years, both from the Chemistry department and the Stephenson Institute for Renewable Energy. I would also like to thank Dr. Ben Mckeever-Abbas as well for allowing me to write the thesis after work in AstraZeneca.

Finally, my boyfriend Ale, where do I start? You helped me when I first arrived in Liverpool and you have not stopped ever since! Thank you for all the support during this journey, for always being there for me even in my bad moments, for encouraging me to push forward and not to give up. I could have not imagined this experience without you! *Grazie amore mio!*

*Infine, vorrei ringraziare tutta la mia famiglia. I miei genitori, Eliana ed Antonio, e mio fratello Marco per esserci sempre, nonostante la distanza. Grazie per aver accettato la mia decisione e per avermi aiutato lungo il cammino. Grazie per avermi fatto diventare la persona che sono! Vi voglio bene!*

# Abbreviations

List of abbreviated terms, in alphabetical order, used commonly throughout the thesis. Each term will be explained at their first use in the main text.

•)))))) - ultrasound irradiation

A - amplitude

AAD - alkane acceptorless dehydrogenation

acac - acetylacetonate

AD - alkane Dehydrogenation

Ad - adamantyl

aq - apparent quartet

ASAP - atmospheric solids analysis probe

at - apparent triplet

ATD - alkane transfer dehydrogenation

BDE - bond dissociation energy

bs - broad singlet

b.p. - boiling point

cat. - catalyst

C-C - carbon-carbon bond

C-H - carbon-hydrogen bond

COA - cyclooctane

COD - 1,5-cyclooctadiene

COE - cyclooctene

conc. - concentrated

Cp - cyclopentadienyl

Cp\* - pentamethylcyclopentadienyl

Cy - cyclohexyl

d - doublet

*d*-THF - deuterated THF

dct - dibenzo[*a,e*]cyclooctatetraene

dd - doublet of doublets

DFT - density functional theory

DSC - differential scanning calorimetry  
ee - enantiomeric excess  
eq. - equivalents  
EWG - electron withdrawing group  
GC - gas chromatography  
GC-FID - GC with flame ionisation detector  
HA - hydrogen acceptor  
HRMS - high resolution mass spectrometry  
Hz - hertz  
<sup>i</sup>Pr - *iso*-propyl  
ISTD - internal standard  
Isooctane - 2,2,4-trimethylpentane  
M - transition metal  
m – multiplet  
<sup>n</sup>Bu - *tert*-butyl  
NMR - nuclear magnetic resonance  
NOE - nuclear Overhauser effect  
q - quartet  
<sup>R</sup>PCP - 2,6-*bis*[di(R)phosphinomethyl]phenyl  
r.t. - room temperature  
T - temperature  
t - triplet  
TBA - 2,2-dimethylbutane, also neohexane  
TBAB - tetra-*n*-butylammonium bromide  
TBE - 3,3-dimethyl-1-butene, also *tert*-butylethylene  
<sup>t</sup>Bu - *tert*-butyl  
TEA - triethylamine  
*tert*-butylethylene - 3,3-Dimethyl-1-butene, also TBE  
TGA – thermogravimetric analysis  
THF - tetrahydrofuran  
TOF - turnover frequency  
TON - turnover number



# Table of contents

|   |     |
|---|-----|
| Abstract.....   | i   |
| Publications.....   | ii  |
| Acknowledgements .....  | iii |
| Abbreviations.....  | iv  |
| 1 Introduction .....  | 1   |
| 1.1 Introduction on C-H bond activation and functionalisation .....                       | 2   |
| 1.1.1 Background .....  | 2   |
| 1.1.2 History.....  | 3   |
| 1.1.3 Mechanism perspective.....  | 5   |
| 1.1.4 Conclusion.....   | 7   |
| 1.2 Alkane dehydrogenation.....   | 8   |
| 1.2.1 General introduction.....   | 8   |
| 1.2.2 Heterogeneous catalytic alkane dehydrogenation.....                                 | 9   |
| 1.2.3 Alternative synthetic strategies: homogeneous catalytic alkane dehydrogenation..... | 10  |
| 1.3 Transition-metal-mediated Michael additions .....                                     | 22  |
| 1.3.1 General introduction.....   | 22  |
| 1.3.2 Michael additions of activated C-H bonds.....                                       | 23  |
| 1.3.3 Hydroalkylation of weakly acidic C-H bonds.....                                     | 27  |
| 1.4 Sonochemistry .....   | 31  |
| 1.4.1 Introduction and fundamentals.....  | 31  |
| 1.4.2 Ultrasound and cavitation bubbles.....  | 32  |
| 1.4.3 Sonochemistry for organic reactions .....   | 33  |
| 1.5 Summary and objectives.....   | 38  |

|       |   |    |
|-------|---|----|
| 2     | Iridium-mediated room-temperature sonochemical alkane transfer dehydrogenation .....          | 39 |
| 2.1   | Introduction .....  | 40 |
| 2.1.1 | General introduction on alkane dehydrogenation .....  | 40 |
| 2.1.2 | Homogeneous catalytic alkane dehydrogenation .....  | 40 |
| 2.1.3 | Sonochemistry .....   | 43 |
| 2.1.4 | Summary and objectives.....   | 45 |
| 2.2   | Design of the apparatus.....  | 46 |
| 2.3   | Initial screening of complexes.....   | 49 |
| 2.3.1 | Synthesis of thermally and photochemically active catalysts.....                              | 49 |
| 2.3.2 | Screening of complexes .....  | 53 |
| 2.4   | Optimisation of the reaction conditions for the sonochemical experiments.....                 | 59 |
| 2.4.1 | Optimization of the concentration of the complex .....  | 59 |
| 2.4.2 | Influence of TBE concentration.....   | 60 |
| 2.4.3 | Amplitude optimization .....  | 62 |
| 2.4.4 | Time optimisation .....   | 62 |
| 2.4.5 | Control experiments .....   | 65 |
| 2.4.6 | Perfluoroalkane as cosolvent.....   | 66 |
| 2.5   | Distribution of alkenes.....  | 67 |
| 2.6   | Temporal control experiment.....  | 69 |
| 2.7   | Investigation of the deactivation of the complexes .....                                      | 71 |
| 2.7.1 | Possible deactivation pathways and their investigation.....                                   | 71 |
| 2.7.2 | TGA and DSC analyses of Ir(P <sup>i</sup> Pr <sub>3</sub> ) <sub>2</sub> H <sub>5</sub> ..... | 77 |
| 2.8   | Further screening of pentahydride complexes.....  | 80 |
| 2.8.1 | Synthesis of iridium-pentahydride analogues .....   | 80 |
| 2.8.2 | Screening of bisphosphine-iridium-pentahydride analogues.....                                 | 88 |
| 2.9   | Scope of alkanes .....  | 90 |

|         |  |     |
|---------|--|-----|
| 2.10    | Distinguishing between homogeneous and heterogeneous catalysis.....  | 93  |
| 2.11    | Conclusion.....  | 97  |
| 2.12    | Possible future plans.....   | 99  |
| 2.13    | Experimental section .....   | 101 |
| 2.13.1  | Materials and general procedures.....  | 101 |
| 2.13.2  | Equipment and methods.....   | 101 |
| 2.13.3  | Synthesis of the complexes.....  | 103 |
| 2.13.4  | Quantitative analysis method for sonochemical reactions .....  | 116 |
| 2.13.5  | Testing the stability of <i>n</i> -dodecane under ultrasound irradiation.....  | 118 |
| 2.13.6  | Screening of complexes .....   | 118 |
| 2.13.7  | Optimisation experiments for the sonochemical <i>n</i> -dodecane transfer dehydrogenation mediated by Ir(P <sup><i>i</i></sup> Pr <sub>3</sub> ) <sub>2</sub> H <sub>5</sub> ..... | 125 |
| 2.13.8  | Thermal <i>n</i> -dodecane transfer dehydrogenation mediated by ( <sup><i>Ad</i></sup> PCP)IrHCl with NaO <sup><i>t</i></sup> Bu .....   | 128 |
| 2.13.9  | Photochemical <i>n</i> -dodecane acceptorless dehydrogenation mediated by <i>trans</i> -Rh(PMe <sub>3</sub> ) <sub>2</sub> (CO)Cl.....   | 128 |
| 2.13.10 | Catalyst deactivation experiments .....  | 129 |
| 2.13.11 | Sonochemical transfer dehydrogenation of different alkanes mediated by Ir(P <sup><i>i</i></sup> Pr <sub>3</sub> ) <sub>2</sub> H <sub>5</sub> .....                                | 135 |
| 2.13.12 | Dct and Hg tests .....   | 136 |
| 3       | Iridium-catalysed Michael-type hydroalkylation of cyclohexenone with alkyl-aryl-nitriles .....   | 138 |
| 3.1     | Introduction .....   | 139 |
| 3.1.1   | Background on Michael additions .....  | 139 |
| 3.1.2   | Previous work carried out by the group on the Michael-type hydroalkylation reaction .....  | 140 |
| 3.1.3   | Summary and objectives.....  | 144 |
| 3.2     | Hydroalkylation of 2-cyclohexen-1-ones with di-substituted acetonitriles.....  | 145 |
| 3.2.1   | Catalyst screening for difficult substrates.....   | 145 |
| 3.2.2   | Scope of pyridyl-substituted acetonitriles .....   | 148 |
| 3.2.3   | Attempts for the ultrasound-promoted hydroalkylation .....   | 154 |

|   |     |
|---|-----|
| 3.3 Insights into the catalytic cycle of the iridium-catalysed Michael-type hydroalkylation of 2-cyclohexen-1-one with diphenylacetonitrile.....            | 157 |
| 3.3.1 Previously proposed catalytic cycle .....   | 157 |
| 3.3.2 Time monitoring experiments of the hydroalkylation reaction by GC ....  | 159 |
| 3.3.3 Time monitoring experiment of the hydroalkylation reaction by NMR spectroscopy .....  | 162 |
| 3.3.4 Investigation of C-H activation step: reactivity of the iridium-pentahydride catalyst with diphenylacetonitrile .....                                 | 165 |
| 3.3.5 Reactivity of iridium-pentahydride catalyst with cyclohexenone .....  | 169 |
| 3.3.6 Test of the isolated intermediates as catalysts.....  | 179 |
| 3.3.7 Investigation of C-C bond formation step: reactivity of the iridium-ylide-nitrile intermediate with cyclohexenone.....                                | 185 |
| 3.3.8 Revised catalytic cycle.....  | 188 |
| 3.3.9 Reactivity of iridium-phenoxide intermediate with diphenylacetonitrile  | 190 |
| 3.3.10 Reactivity of iridium-ylide-nitrile with phenol .....  | 196 |
| 3.3.11 Phenol as an additive to the Michael addition reaction.....  | 201 |
| <br>  |     |
| 3.4 Towards the dehydrogenation of 3-substituted cyclohexanones to <i>meta</i> -substituted phenols .....   | 211 |
| 3.4.1 Introduction and background .....   | 211 |
| 3.4.2 Attempts for the iridium-catalysed transfer dehydrogenation .....   | 212 |
| 3.4.3 Attempts for the ultrasound-promoted Stahl dehydrogenation.....   | 218 |
| <br>  |     |
| 3.5 Conclusions .....   | 221 |
| 3.6 Possible future plans.....  | 223 |
| 3.7 Experimental section .....  | 224 |
| 3.7.1 Materials and general procedures.....   | 224 |
| 3.7.2 Equipment and methods.....  | 224 |
| 3.7.3 Quantitative analysis methods for the catalytic experiments.....  | 225 |
| 3.7.4 Synthesis of the catalysts.....   | 228 |
| 3.7.5 Synthesis of the substrates .....   | 228 |
| 3.7.6 Catalyst screening for the iridium-catalysed hydroalkylation of 2-cyclohexen-1-one with <sup>i</sup> Pr- and Cy-substituted phenylacetonitriles ..... | 233 |

|        |   |     |
|--------|---|-----|
| 3.7.7  | Scope of the pyridyl-substituted acetonitrile substrates.....   | 235 |
| 3.7.8  | Attempted ultrasound-mediated Michael-type hydroalkylation of cyclohexenone with diphenylacetonitrile.....  | 238 |
| 3.7.9  | Independent synthesis and isolation of the intermediate complexes ....  | 239 |
| 3.7.10 | GC time monitoring experiments .....  | 244 |
| 3.7.11 | NMR time monitoring experiments .....   | 247 |
| 3.7.12 | Michael-type hydroalkylation catalysed by Ir(P <sup>i</sup> Pr <sub>3</sub> ) <sub>2</sub> H <sub>5</sub> with phenol as an additive (10 equivalents) .....   | 252 |
| 3.7.13 | Michael-type hydroalkylation catalysed by Ir(P <sup>i</sup> Pr <sub>3</sub> ) <sub>2</sub> H <sub>5</sub> with NaOPh as an additive .....   | 253 |
| 3.7.14 | Michael-type hydroalkylation of 2-cyclohexen-1-one with Cy-substituted phenylacetonitrile catalysed by Ir(P <sup>i</sup> Pr <sub>3</sub> ) <sub>2</sub> H <sub>5</sub> with phenol as an additive ..... | 254 |
| 3.7.15 | Dehydrogenation of 3-substituted cyclohexanones to <i>meta</i> -substituted phenols .....   | 255 |
| 4      | Conclusions .....   | 259 |
| 4.1    | Summary and conclusions .....   | 260 |
| 5      | References .....  | 263 |

1

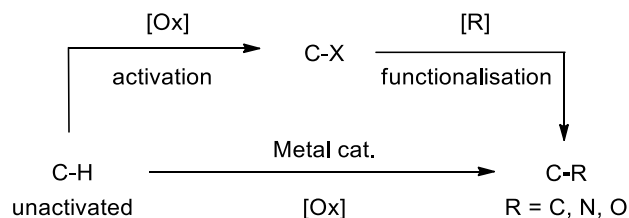
# Introduction

## 1.1 Introduction on C-H bond activation and functionalisation

### 1.1.1 Background

The direct functionalisation of C-H bonds represents an important class of transformations and a long-standing goal of chemists. Over the years these type of transformations have attracted a growing interest as they can lead the way to the atom-, step-economical and environmentally friendly synthesis of more complex organic compounds.<sup>1-2</sup>

C-C bond forming reactions constitute the backbone of organic synthesis.<sup>3</sup> Historically the functionalisation of a non-activated C-H bond included a pre-oxidation step to obtain the activated oxidised-substrate, which can be further reacted to achieve the desired functionalised product (Scheme 1.1).<sup>4-5</sup> The easiest way to reduce the number of steps in a synthesis is to decrease the number of functional groups manipulations. It can be achieved starting the construction of the C-C bond directly from the non-activated C-H bond precursor *via* a metal-catalysed C-H activation (Scheme 1.1). Therefore, C-H activation is conformed to the principle of step-economical and atom-economical synthesis due to the high utilisation of atoms.



Scheme 1.1 Metal-catalysed C-H activation strategy opposed to the classic synthetic approach.

The C-H transformation can generate new C-C, C-O and C-N bonds, directly accessing more complex molecules. Moreover, with this transformation also a new functionality can be introduced, providing further requirements for the synthesis of complicated structural frameworks. C-H activation is of interest not only to academia, but also many industrial processes involve the transformation of C-H groups, starting from simple molecules.<sup>6</sup>

The interest in C-H bond transformations relies also in the ubiquitous nature of C-H bonds in organic substances. The C-H bond is a general chemical unit present almost in all kinds of organic compounds, starting from simple alkanes and arenes, going to more complex organic molecules such as natural products and pharmaceuticals and ending with synthetic and biological polymers. Consequently, there is no surprise that the direct functionalisation of

this cheap and abundant feedstock represents an attractive strategy for the elaboration of more complex organic molecules, which has drawn a lot of attention in the past decades.

Even simple organic molecules, however, incorporate different types of unique C-H bonds, each one of them characterised by a specific acidity and, in general, low reactivity. Hence, to achieve a highly effective and selective C-H activation under mild reaction conditions is still a big challenge. An isolated C-H bond in a molecule has a low reactivity because of the high kinetic barriers associated with its cleavage. The C-H bond cleavage can be regarded as a homolytic cleavage or ionisation process and it is indeed related to the specific  $pK_a$  of that particular bond and hybridisation of the carbon atom. In Table 1.1 the bond dissociation energies for selected types of C-H bonds and their corresponding acidities and hybridisations are reported.<sup>2</sup> As it can be inferred from the table, in general, the metalation of  $C(sp^2)$ -H bonds is easier compared to  $C(sp^3)$ -H bonds, which require much higher reaction temperatures to achieve good catalytic activities.

Table 1.1 Bond dissociation energies (BDE) for selected C-H bonds and their relative carbon hybridisation and  $pK_a$  values.

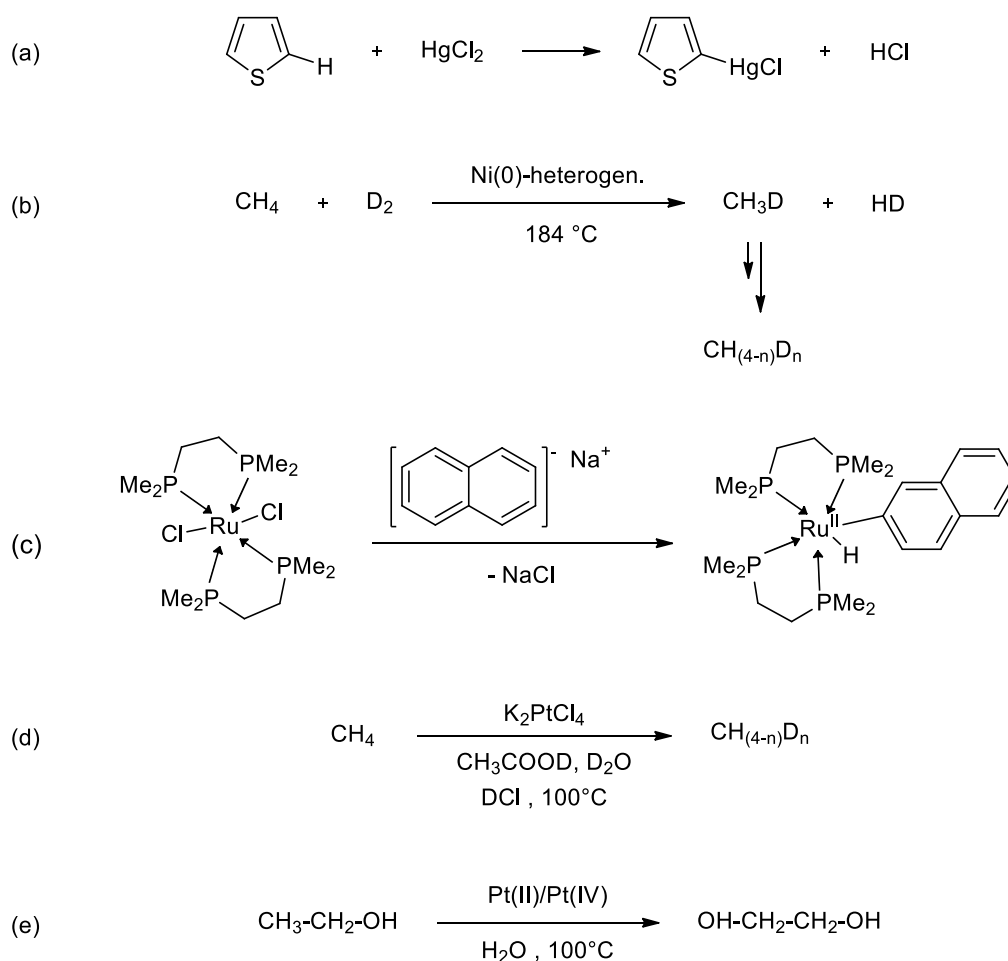
|               |                 |   |   |  |   |
|---------------|-----------------|---|---|--|---|
| BDE (kJ/mol)  | 522.2           | 460.2   | 410.8   | 397.9  | 389.9   |
|               | $H-C\equiv C-H$ | $\begin{array}{c} H_2C \\ \diagdown \\ C-H \\ \diagup \\ H \end{array}$ | $\begin{array}{c} H \\   \\ H_3C-C-H \\   \\ H \end{array}$ | $\begin{array}{c} CH_3 \\   \\ H_3C-C-H \\   \\ H \end{array}$ | $\begin{array}{c} CH_3 \\   \\ H_3C-C-H \\   \\ CH_3 \end{array}$ |
| $pK_a$        | ~25             | 44  | ~50   | ~50  | ~50   |
| hybridisation | $C(sp)$         | $C(sp^2)_{\text{vinyl}}$  | $C(sp^3)_1$   | $C(sp^3)_2$  | $C(sp^3)_3$   |

### 1.1.2 History

In 1883, the first example of an isolated alkyl C-H bond functionalisation has been reported by Hofmann. The C-H functionalisation was achieved under harsh acidic conditions employing oxygen- and nitrogen-radical species.<sup>7-8</sup> However, the earliest example of metal-promoted C-H activation was reported by Volhard only ten years later, involving the C-H activation of thiophene by mercury chloride (Scheme 1.2, eq. (a)).<sup>9</sup> However, it was only in 1936 that the term “C-H activation” appeared in the literature for the first time, describing a metal-catalysed process by Taylor.<sup>10</sup> The C-H bond of methane was cleaved on the surface of an heterogeneous nickel-catalyst to achieve various degrees of H-D exchange (Scheme 1.2,



eq. (b)). From that point forward a growing interest was granted on the C-H activation, as it started to be equated to the metal-mediated cleavage of carbon-hydrogen bonds in various compounds with a strong interest on the activation of saturated hydrocarbons. The first pioneers of this challenging field were Chatt, Garnett and Shilov in the late '60s. Chatt reported the 2 electrons reduction of ruthenium(II) to of ruthenium(0) followed by the oxidative addition of the C-H bond of neutral naphthalene (Scheme 1.2, eq. (c)).<sup>11</sup> Garnett described the alkanes and arenes deuteration by a palladium salt (Scheme 1.2eq. (d))<sup>12</sup> and Shilov, based on previous work, reported the chlorination and hydroxylation of alkanes by mixtures of platinum and palladium salts (Scheme 1.2, eq. (e)).<sup>13</sup> From these works the modern development of the C-H activation field started.

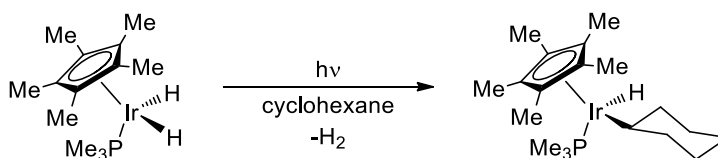


Scheme 1.2 First examples of C-H activations.

While at the beginning the term “C-H activation” was coined to describe a metal-mediated C-H cleaving process, with time it has become more and more popular. Nowadays, its use is so widespread across many different C-H functionalisation processes that drafting a consistent definition is difficult. However, it is worth clarifying few details. “Activation of a

bond”, in the context of a general chemical reaction, refers to any process where the reactivity of a specific bond is increased. It is indeed used by the chemical community to describe several different processes, such as activation of a bond by a substituent, or activation of a bond *via* formation of an intermediate between the substrate and another reagent. Because the term “C-H bond activation” is most frequently used in the organometallic area, in this context it refers to the formation of a complex, where the C-H bond interacts directly with the metal complex. Most of the time, this leads to the formation of an intermediate with a carbon-metal bond, however, “activation” of a bond does not necessarily mean “cleavage” of a bond.

In the modern days, C-H bond activation in the organometallic field is often equated with the concerted oxidative addition mechanism. The first example of C-H activation through oxidative addition has been reported in the ‘80s. Bergman, Graham and Jones described the addition of a C-H bond of an alkane to a low valent iridium complex with formation of an alkyl-hydride-iridium species under photochemical conditions (Scheme 1.3).<sup>14-16</sup> Mechanistic investigations showed that the oxidative addition takes place *via* a concerted mechanism, where the metal first activate the C-H bond with the formation of a dative bond and then the alkyl-hydride-metal species is formed. This work showed for the first time how metal species could activate, *via* a new process, a C-H bond characterised by very low reactivity like the one of alkanes, drawing a lot of attention and interest onto this new possibility.



Scheme 1.3 Oxidative addition of a non-activated alkane C-H bond to a Cp\*(PMe<sub>3</sub>)IrH<sub>2</sub> complex.

### 1.1.3 Mechanism perspective

In addition to the concerted oxidative addition pathway, many other C-H activation modes exists, depending mainly on the type of metal complex involved, i.e. identity and oxidation state, and the characteristics of the C-H bond to be activated, i.e. its acidity.<sup>17-18</sup> A plethora of C-H activation mechanisms exist, but they can be divided into two main classes. The first is the inner-sphere mechanism, which consists in the coordination of the C-H bond directly to the metal centre to form an organometallic species, which could undergo a cleavage event. The second class is the outer-sphere mechanism, where the C-H bonds undergoes insertion

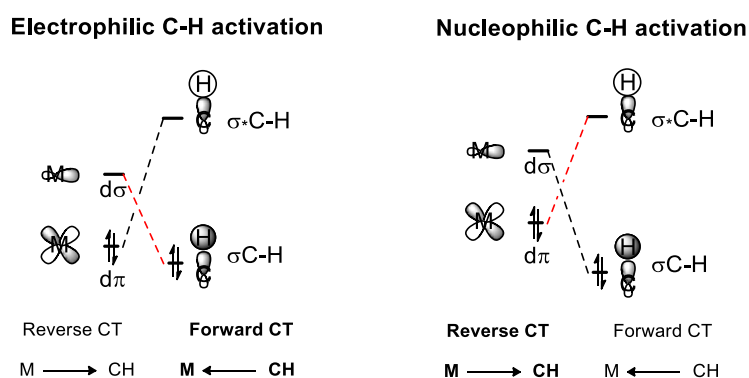
into a ligand of the metal complex.<sup>2</sup> The first type of mechanism is the most common one and it is the one which will be described more in detail.

Transition metals are particularly suited for the activation of C-H bond because the d orbitals of the metal present proper energies and symmetries that match the  $\sigma$ -bonding and  $\sigma^*$ -antibonding orbitals of the C-H bond.<sup>19</sup> With the coordination a two-path charge transfer (CT) takes place: the filled  $\sigma$  orbital of the C-H bond donates electron density to an empty d  $\sigma$  orbital of the metal (forward CT) and at the same time a filled metal d $\pi$  orbital donates electron density to the empty  $\sigma^*$  orbital of the coordinated C-H (back-bonding, reverse CT). This forward and backwards donation weakens the C-H bond (activation), eventually causing also the cleavage of the bond.

Many different types of inner-sphere mechanism exist, but they can be classified depending on the main direction of the charge transfer in the C-H activation step.<sup>2, 18, 20</sup>

High-valent electron-deficient (and cationic) late transition metals typically react *via* an electrophilic pathway (Scheme 1.4, left side). Those metals present low-energy d $\pi$  and d $\sigma$  orbitals, hence the coordination features a strong  $\sigma$ -donation over a weak  $\pi$ -back-donation, resulting in a predominant forward CT. Therefore, electron-poor catalysts in high oxidation state (Pd<sup>II</sup>, Pt<sup>II</sup>, Rh<sup>III</sup>, Ir<sup>III</sup>, Ru<sup>II</sup>) react *via* an electrophilic activation mechanism.

On the other hand, low-valent electron-rich metals usually react *via* a nucleophilic pathway (Scheme 1.4, right side). When this type of metals interacts with a C-H bond, the reverse CT dominates over the forward CT because of the higher energy d $\pi$  and d $\sigma$  orbitals. Hence, this type of process is most common for low oxidation state transition metals (Rh<sup>I</sup>, Ir<sup>I</sup>), which can highly benefit from the presence of strongly binding ligands, as  $\sigma$ -donating ligands such as phosphines, which can increase the electron-density on the metal centre.



Scheme 1.4 Orbital interactions for the electrophilic and nucleophilic C-H activation processes.

The electrophilic activation mechanism, typical for high-valent transition metals, normally takes place *via* a concerted metalation-deprotonation reaction. First the C-H bond

coordinates the metal centre and subsequently the activated bond is deprotonated by a ligand or by an external anion.<sup>2</sup> On the contrary, low-valent transition metals can react with a variety of mechanisms, from the classic oxidative-addition to  $\sigma$ -bond metathesis, passing through many different variants between these two main mechanisms.<sup>2</sup> Oxidative-addition is the most common mechanism for complexes made of electron-rich  $d^8$  late transition-metals which, with the C-H cleavage, give a species with  $d^6$  configuration in a transformation with low energetic cost. The desired functionalised product is then released *via* reductive-elimination for an overall transformation with no change in the oxidation state of the metal, as with the  $\sigma$ -bond metathesis.

To summarise, the nature and oxidation state of the metal centre defines the type of inner sphere mechanism that will take place, hence an electrophilic or nucleophilic C-H activation. Those two transformation types can undergo *via* a variety of different mechanisms, depending on both the metal and ligand characteristics.

#### 1.1.4 Conclusion

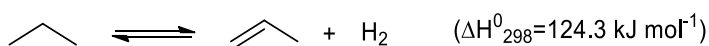
The field of activation and functionalisation of aliphatic C-H bonds is a fundamental challenge in organic chemistry, and it is clear from the previous examples that it covers a broad spectrum of different and challenging processes. While functionalisation of  $Csp^2$ -H bonds is common and well-studied, this work will focus on the more challenging functionalisation of  $Csp^3$ -H bonds. The aim is to present the contribution made to the ever-expanding field of transition-metal  $Csp^3$ -H functionalisation with two complementary approaches: dehydrogenation of alkanes and Michael-type hydroalkylation. In the following paragraphs the literature review on these selected types of C-H activation/functionalisation processes will be outlined. Then, a general background on sonochemistry will also be described to set the base on this unusual method for chemical activation.

## 1.2 Alkane dehydrogenation

### 1.2.1 General introduction

Alkanes are the most abundant and inexpensive hydrocarbons feedstocks available for the organic chemical industry. The majority of commercialised organic chemicals, such as acids, alcohols, ketones and aldehydes, derives from alkanes *via* one or more functionalisation steps.<sup>21</sup> Moreover, through their dehydrogenation to alkenes, which are much more reactive substrates, they can be converted into a large variety of compounds. In fact, alkenes are among the most versatile chemicals and perhaps the most important class of compounds in the chemical industry. Light olefins can be readily transformed into a vast array of value-added fine chemicals and pharmaceutical intermediates and represent also the building blocks for the production of a large number of polymers and oxygenates.<sup>22-24</sup>

Unfortunately, the catalytic functionalization of alkanes is one of the most challenging reactions in organic chemistry, as it requires the activation of strong carbon-hydrogen bonds. The chemical inertness of alkanes is reflected in one of their old names, “paraffins”, from the Latin *parum affinis*,<sup>13</sup> that means “lack of affinity with other materials”. From a chemical point of view, the dehydrogenation, is a one-step reaction that allows to convert paraffins into the corresponding olefin and molecular hydrogen (Scheme 1.5). However, the reaction is thermodynamically unfavoured because it is highly endothermic. Therefore, really high temperatures are needed (up to 900 °C). Also, the enthalpy required to dehydrogenate alkanes increases as the chain becomes shorter and a considerably larger amount of energy is indeed required to dehydrogenate light paraffins ( $\Delta H_{298}^0 = 117.6 \text{ kJ mol}^{-1}$  for isobutane,  $124.3 \text{ kJ mol}^{-1}$  for propane and  $137 \text{ kJ mol}^{-1}$  for ethane dehydrogenation).<sup>22</sup> The high dehydrogenation enthalpy has restricted the feasible applications of alkanes and most of the times high reaction temperatures are required.



Scheme 1.5 Propane Dehydrogenation.

Industrially, the inertness of this C-H bond has been overcome with the use of heterogeneous catalysts. Thus, alkane dehydrogenation has made it out to industrial applications, but these catalytic systems have some major drawbacks. First of all, they need very harsh reaction conditions and secondly they yield the product with low selectivity. To overcome this problem, scientists are developing alternative catalytic systems, based on homogenous catalysts. Up to date, however, despite the great advances, studies are still at a laboratory

exploration stage as the best systems still require relatively high temperatures. Therefore, the development of new efficient catalytic dehydrogenation systems is highly desirable.

## 1.2.2 Heterogeneous catalytic alkane dehydrogenation

C-H bonds represents the most ubiquitous chemical bond in nature and, as described earlier, at the same time they are one of the most difficult to cleave. The low reactivity of alkanes translates into severe reaction conditions, meaning as well that more than one possible product can often be formed, lowering selectivity. Thus, an additional problem to consider is the possible side reactions. Despite C-H bonds in paraffins are more reactive than C-C bonds, catalyst that favour the C-H over the C-C bond cleavage are required to avoid side reactions. Another complicating factor is that olefins are considerably more reactive than their corresponding alkanes, leading to further undesired side reactions. The side reactions that can occur are mainly of three types: hydrogenolysis, the hydrogen addition into a C-C bond leading to the formation of two smaller alkanes; cracking, the cleavage of a C-C bond to yield two smaller hydrocarbons; and isomerisation, the rearrangement of atoms within the molecule.<sup>22</sup> Thankfully, these side reactions are catalysed by specific catalytic sites, therefore they can be partially controlled through a careful catalyst design.

With an increasing demand for olefins, due to their wide range of applications, the technologies for alkane dehydrogenation have drawn a lot of attention. For the above mentioned reasons, several types of heterogeneous catalysts have been developed and found application in the petrochemical industry, where the heterogeneous catalytic alkane dehydrogenation is carried out on a large scale.<sup>25-27</sup> Up to date, several heterogeneous dehydrogenation processes have been commercialised. The major role in the dehydrogenation of light alkanes is played by two types of metal-supported catalysts: the chromium and platinum/tin-based catalysts. The chromium-based catalysts are typically composed of chromium oxides ( $\text{Cr}^{\text{III}}_2\text{O}_3$ ) dispersed on a porous alumina support, together with a doped alkaline metal.<sup>25</sup> The platinum-based catalysts are also supported on alumina as well, and they contain other inactive metals, preferably tin, to modify their catalytic properties.<sup>25</sup>

Heterogeneous dehydrogenation catalysts have been successfully used in industry as highly practical, but these catalysts show major drawbacks. They are based either on toxic chromium or precious platinum metals. The existing dehydrogenation methods are also limited to very simple molecules: styrene is produced from ethyl benzene and ethylene and propylene are obtained by catalytic steam cracking of low molecular alkanes.<sup>23</sup> These

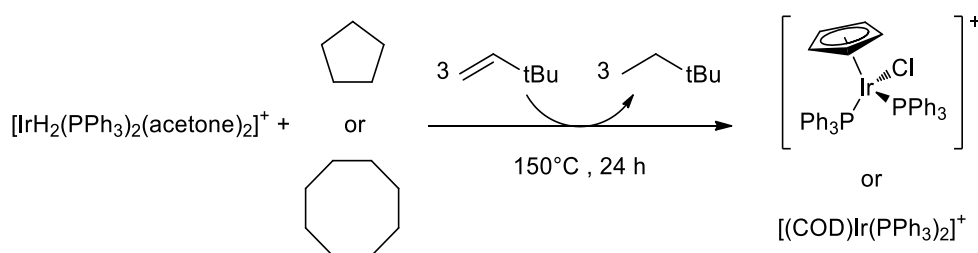
processes require very harsh reaction conditions (500-900 °C), in order for the favourable entropy for the loss of hydrogen to offset the unfavourable enthalpy of dehydrogenation, and also to overcome the relatively low activity of these catalysts. Moreover, the process requires even more energy because of the aforementioned side reactions (carbon-carbon bond cleavage and isomerisation). They lead to very poor product selectivities, which implies the need for separation steps.<sup>22</sup> Furthermore, the high energy demand results in the production of plentiful CO<sub>2</sub> emissions.

### 1.2.3 Alternative synthetic strategies: homogeneous catalytic alkane dehydrogenation

#### 1.2.3.1 Background

Because of the high temperature required for the heterogeneous alkane dehydrogenation, researchers have long been looking for a more sustainable and efficient approach to make olefins. The use of homogeneous transition metal catalysts is a cleaner and more promising route to olefins *via* dehydrogenation of alkanes. Over the past three decades, significant progress has been achieved in this field, with homogeneous catalysts that can operate at lower temperatures (<250 °C) and with better selectivities.<sup>28</sup> These results could be achieved thanks to some adjustments to drive the reaction towards the desired products, overcoming the endothermicity of the process.

While heterogeneous catalyst have been widely use for the dehydrogenation of light alkanes (ethane and less successfully propane and isobutane),<sup>29</sup> the first homogeneous system capable to dehydrogenate higher alkanes to the corresponding olefins with good chemoselectivities have been reported by Crabtree and co-workers in 1979.<sup>30</sup> The cationic Ir(III) complex  $[\text{IrH}_2(\text{PPh}_3)_2(\text{acetone})_2]^+[\text{BF}_4]^-$  was found to promote the first stoichiometric dehydrogenation of cyclopentane or cyclooctane (COA) in the presence of *tert*-butylethylene (TBE, 3,3-dimethyl-1-butene), to yield the corresponding cyclopentadienyl or 1,5-cyclooctadiene complexes in 30 to 70% yield (Scheme 1.6).



Scheme 1.6 Stoichiometric alkane transfer dehydrogenation with  $[\text{IrH}_2(\text{PPh}_3)_2(\text{acetone})_2]^+[\text{BF}_4]^-$ .

Further studies showed the addition of TBE to act as a “hydrogen acceptor”, thus driving the endothermic process of loss of H<sub>2</sub> and resulting in the catalytic generation of dehydrogenated products.<sup>31</sup> Among the common olefins, many factors make *tert*-butylethylene the most effective hydrogen acceptor. It hydrogenates rapidly, to produce *tert*-butylethane (TBA) and it is bulky enough to not strongly coordinate the metal centre. Also, it lacks an allylic C-H bonds, that could be cleaved by the metal leading to the formation of an allyl complex, strongly binding the metal centre, and therefore ending into catalyst deactivation.<sup>29</sup> When the dehydrogenation is carried out with the help of an hydrogen acceptor it is usually called “transfer dehydrogenation”.

Cyclooctane is usually chosen as the model substrate for this type of reaction. It is in fact one of the best substrates for dehydrogenation. In its tub conformation the transannular H...H repulsion destabilise the alkane with respect to the alkene, which does not have half of this interactions. This leads to a 5-7 kcal mol<sup>-1</sup> lower heat of dehydrogenation, compared to other alkanes.<sup>32</sup>

Similar stoichiometric cycloalkane dehydrogenations were reported by Felkin, using Re(PPh<sub>3</sub>)<sub>2</sub>H<sub>7</sub> as catalyst.<sup>33-35</sup> Soon thereafter, both Crabtree<sup>36-38</sup> and Felkin<sup>39-40</sup> independently reported the first catalytic homogeneous transfer dehydrogenations of alkanes. The best results have been obtained for the transfer dehydrogenation of cyclooctane with TBE at 150 °C, where the Ir(PPh<sub>3</sub>)<sub>2</sub>H<sub>5</sub> catalyst exhibited a TON of 70 over 5 days.<sup>39</sup> In 1990, Fujii and Saito<sup>41</sup> made the important observation that under reflux conditions, in the presence of Wilkinson-type complexes, the alkane is spontaneously converted into the corresponding olefin, reporting indeed the first example of acceptorless alkane dehydrogenation. In this study the hydrogen formed from the dehydrogenation is constantly removed by the reflux process, displacing the equilibrium towards the products, without the need for a hydrogen acceptor. The highest total TON of 13.4 was obtained with cyclooctane under thermal reaction conditions after 48 h, using Rh(P(*p*-tolyl)<sub>3</sub>)<sub>2</sub>Cl as catalyst. A similar approach was reported also by Crabtree,<sup>42</sup> with some improvements: the addition of a stream of argon to facilitate the removal of hydrogen and the use of perfluoroalkanes as solvent in order to reach higher temperatures.

A variety of similar homogenous systems have been developed, but the main issue of these systems was catalyst deactivation, mainly due to P-C bond cleavage of the phosphine ligand. To solve this problem, it was clear that a new class of catalysts, which had to be able to withstand the higher reaction temperatures required for an efficient alkane dehydrogenation, had to be developed.



### 1.2.3.2 Dehydrogenation of alkanes catalysed by iridium pincer complexes

In the search for an increased catalyst lifetime, the turning point was the development of pincer complexes.<sup>43-44</sup> The thermally very stable pincer phosphines gave catalysts characterised by very high stability and activity. This could be achieved because the degradation through P-C and C-H bond cleavage was difficult due to the constrained conformation of the ligand, which limits the access of the metal to these bonds.

These pincer complexes were firstly synthesised by Shaw,<sup>45</sup> who reported the preparation of bis(phosphine)based pincer Rh and Ir hydride chloride complexes (<sup>t</sup>BuPCP)MHCl (<sup>t</sup>BuPCP=2,6-bis[di(*tert*-butyl)phosphinomethyl]phenyl) (Figure 1.1). But only in 1996, this class of complexes has been investigated as hydrogen transfer catalysts by Jensen and Kaska,<sup>46</sup> who reported that iridium derivative (<sup>t</sup>BuPCP)IrH<sub>2</sub> was the best dehydrogenation catalyst, and not the rhodium counterpart. The pincer catalyst was tested for the transfer dehydrogenation of COA in the presence of the sacrificial hydrogen acceptor TBE; attaining TON of 82 at 150°C (Scheme 1.7). The complex displayed also excellent thermal stability at elevated temperatures (200 °C). Thanks to its exceptional stability, this iridium dihydride catalyst has been used over the years for the C-H activation of many different substrates (Scheme 1.8),<sup>29, 47-50</sup> in some cases to give aromatic products. In particular cyclohexane dehydrogenation to benzene could be achieved using excess acceptor olefin.<sup>48</sup>

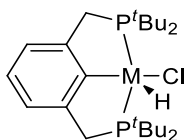
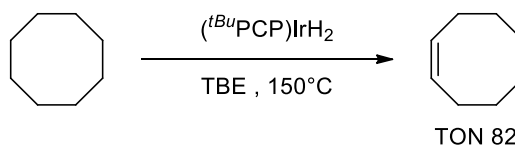


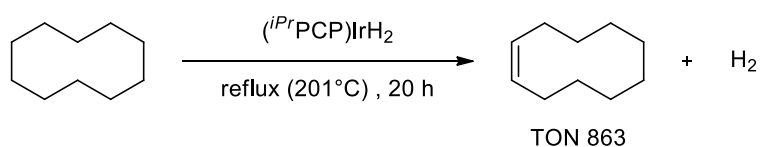
Figure 1.1 (<sup>t</sup>BuPCP)MHCl with M=Rh, Ir.



Scheme 1.7 Transfer dehydrogenation of COA in the presence of TBE with (<sup>t</sup>BuPCP)IrH<sub>2</sub> as the catalyst.

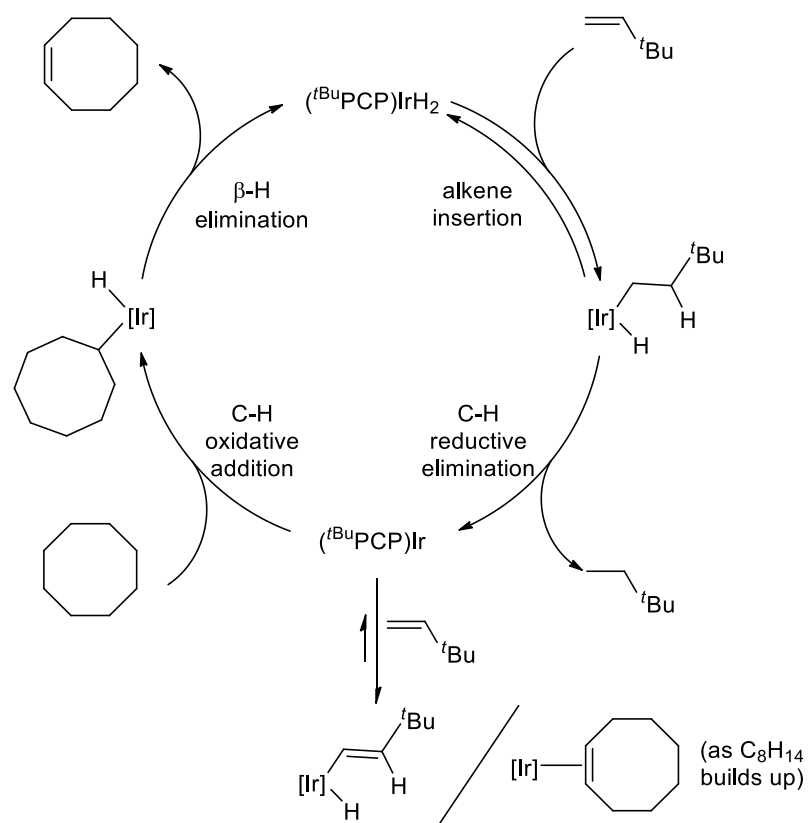


The high thermal stability of Ir pincer complexes enabled also to achieve the efficient acceptorless dehydrogenation under reflux condition.<sup>51</sup> At these high temperatures, the equilibrium was sufficiently shifted towards the dehydrogenated alkene, so that significant amounts of olefins were formed even without the use of a hydrogen acceptor. The sterically less-crowded (*i*PrPCP)IrH<sub>2</sub> catalyst afforded 863 TON in the dehydrogenation of cyclodecane to cyclodecene, obtained together with gaseous H<sub>2</sub>, which was removed from the system under stream of argon (Scheme 1.10). The same catalyst was used to perform the first acceptorless dehydrogenation of an acyclic alkane: *n*-undecane to undecene isomers.<sup>52</sup> This represents one of the most efficient catalytic systems for the acceptorless dehydrogenation under thermal conditions.



Scheme 1.10 Acceptorless dehydrogenation of cyclodecane with (*i*PrPCP)IrH<sub>2</sub> as the catalyst.

The reaction mechanism of transfer dehydrogenation of cyclooctane using TBE as hydrogen acceptor has been analysed in detail, both through kinetic studies<sup>53-54</sup> and theoretical calculations.<sup>55</sup> The proposed catalytic cycle, shown in Scheme 1.11, begins with the 16-electron iridium-dihydride species, which undergoes insertion of TBE in the Ir-H bond; subsequent reductive elimination of *tert*-butylethane (TBA) generates the reactive 14-electron iridium(I) complex. This species then undergoes oxidative addition of a C-H bond of the alkane substrate yielding the alkyl hydride, followed by  $\beta$ -hydride elimination to close the cycle, releasing the olefin and regenerating the iridium-dihydride species. However, the 14-electron species can also undergo an unproductive oxidative addition of TBE vinylic C-H bond to form a vinyl hydride; these two species are in rapid equilibrium. The catalyst resting state during the transfer dehydrogenation of *n*-alkanes is the (<sup>t</sup>BuPCP)Ir(1-alkene) complex, thus the obtained olefin inhibits catalytic reaction as it builds up, binding the (<sup>t</sup>BuPCP)Ir complex *via*  $\pi$ -coordination. Therefore, the easier dehydrogenation of cyclooctane with respect of *n*-alkanes is due to the weaker binding of COE to the Ir(I) centre than the 1-alkene.<sup>23</sup> In the case of acceptorless dehydrogenation the active complex (<sup>t</sup>BuPCP)Ir is generated *via* thermolytic loss of H<sub>2</sub> from (<sup>t</sup>BuPCP)IrH<sub>2</sub>, being the turnover-limiting step of the catalytic cycle.<sup>24</sup>



Scheme 1.11 Catalytic cycle for the cyclooctane transfer dehydrogenation with  $(t\text{BuPCP})\text{IrH}_2$  as catalyst.

To develop improved catalysts for alkane dehydrogenation, a large number of modifications on iridium PCP pincer complexes have been prepared, varying the electronic and steric properties. Some examples are reported in Figure 1.2. Mainly three strategies have been used for the modification of PCP ligands: 1) variations of the substituents either on the phosphorous atom or at the *para*-position of the aromatic backbone, 2) variation of the backbone itself and 3) variation of the linkers between the backbone and the phosphorus atom.

Although iridium pincer complexes have excellent thermal stability, they are still generally subjected to decomposition when heated above 200 °C for extended periods of time. Indeed, this decomposition is of particular concern with acceptorless dehydrogenations, which require higher temperatures and longer reaction times. In the effort to develop a more thermally stable complex, Goldman and co-workers<sup>56</sup> reported a highly stable adamantyl-substituted pincer iridium catalyst,  $(\text{Ad}^d\text{PCP})\text{IrH}_2$  (Figure 1.2, first complex on the second row). The adamantyl substituent was expected to be sterically and electronically similar to the *tert*-butyl group, but at the same time it was expected to be more resistant towards cyclometallation and P-C bond cleavage: the two most plausible pathways for catalyst decomposition. This adamantyl-substituted pincer iridium complex exhibited high thermal stability up to 250 °C, which allowed to achieve a higher catalytic activity for the acceptorless

dehydrogenation of cyclodecane and *n*-dodecane (Scheme 1.12). At the beginning the TOF were slightly lower than the ones obtained with the corresponding *iso*-propyl- and *tert*-butyl-substituted PCP-iridium complexes. However, over time the TON of (<sup>Ad</sup>PCP)IrH<sub>2</sub> exceeded the ones of the other two most active pincer catalysts.

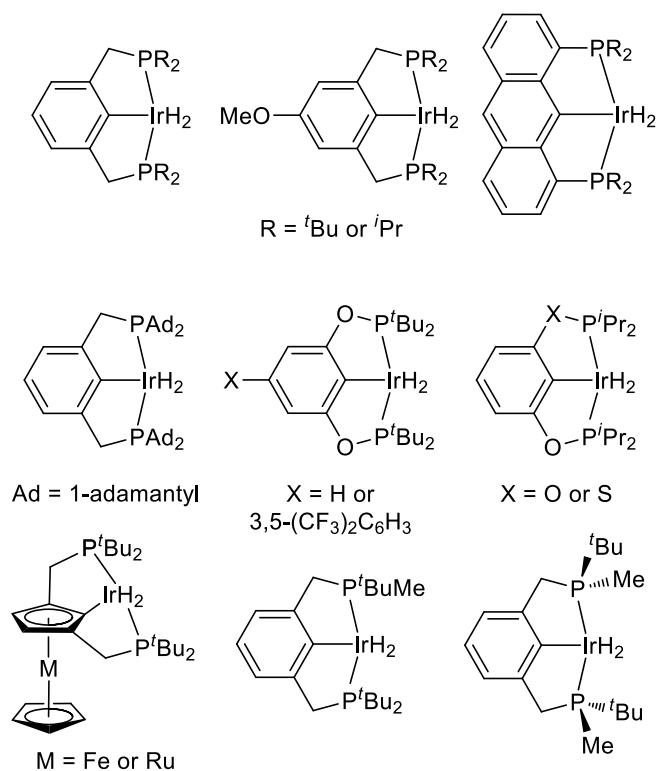
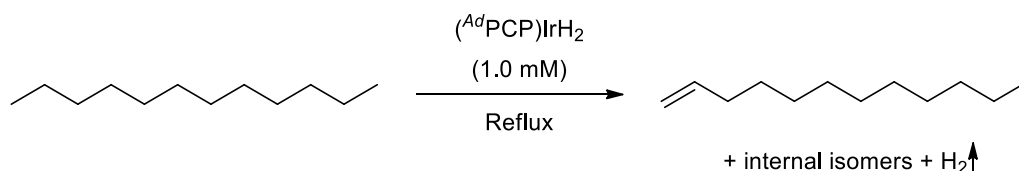


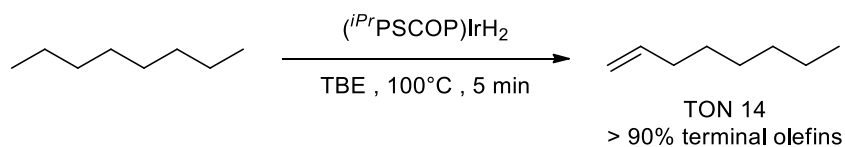
Figure 1.2 Different modification of PCP pincer complexes.<sup>23, 43</sup>



Scheme 1.12 Thermal acceptorless alkane dehydrogenation under reflux conditions with (<sup>Ad</sup>PCP)IrH<sub>2</sub> as catalyst.

Another notable modification of the classic PCP ligand was the substitution of the carbon of the methylen bridges between the phosphorous and the aromatic backbone for an heteroatom. Bisphosphinite iridium pincer complexes have been prepared independently by Brookhart<sup>57</sup> and Jensen,<sup>58</sup> (<sup>t</sup>BuPOCOP)IrH<sub>2</sub> and (<sup>i</sup>PrPOCOP)IrH<sub>2</sub> complexes respectively (Figure 1.2, second and third complex on the second row). These catalysts were proven to be more active by one order of magnitude than the classic (PCP)Ir systems for the transfer dehydrogenation of COA with TBE. However, they showed lower activity when linear alkanes were employed as substrates. Finally, Huang<sup>59</sup> reported a PSCOP-type pincer iridium complex, using sulphur and oxygen atoms as linkers that is highly active for transfer

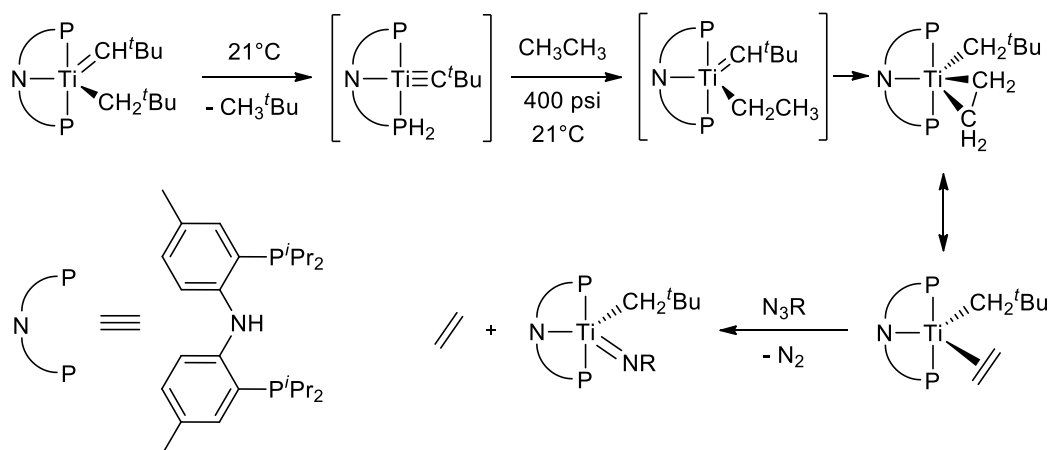
dehydrogenation of both linear and cyclic alkanes at 200 °C (Figure 1.2, third complex on the second row). This system represents one of the most active towards the homogeneous transfer dehydrogenation of COA with TBE and is also able to perform the transfer dehydrogenation of *n*-octane at 100 °C, affording the  $\alpha$ -olefin regioselectively (Scheme 1.13).



Scheme 1.13 Thermal transfer alkane dehydrogenation of *n*-octane at 100 °C with  $(iPrPSCOP)IrH_2$  as catalyst.

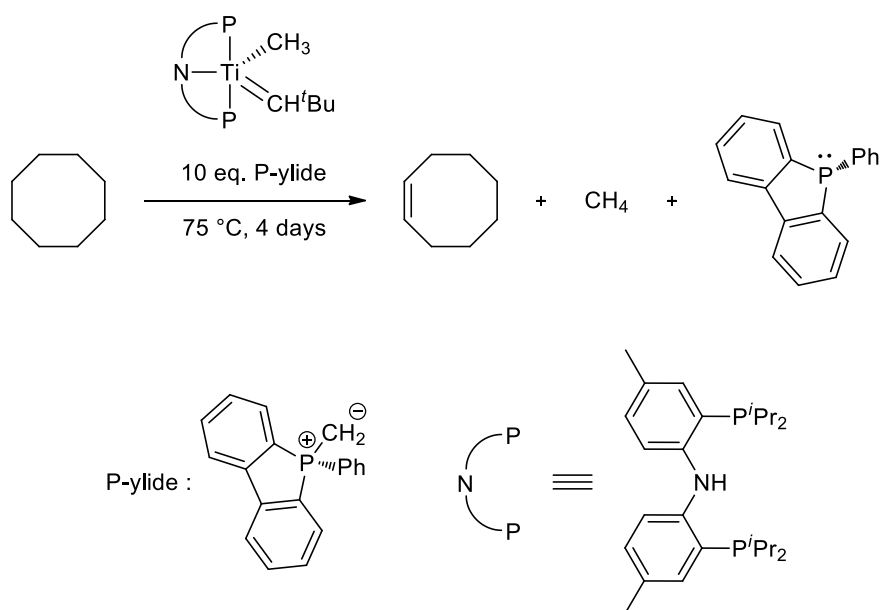
### 1.2.3.3 Towards milder approaches with titanium pincer complexes

In 2011 Mindiola and co-workers were able to achieve the dehydrogenation of alkanes under very mild conditions.<sup>60</sup> They reported that a titanium alkylidyne intermediate complex,  $(PNP)Ti\equiv C^tBu$  ( $PNP=N[2-P^iPr_2-4-methylphenyl]_2^-$ ), was able to activate the C-H bonds of ethane at 21 °C over 24 hours (Scheme 1.14). Starting from a titanium precursor, it first undergoes a  $\alpha$ -hydrogen abstraction with elimination of *tert*-butylethane to generate the titanium alkylidene intermediate. This complex activates ethane, subsequently the activated ethane ligand on the alkylidene intermediate undergoes  $\beta$ -hydrogen abstraction to the adjacent alkylidene ligand to yield a titanium ethylene adduct. Treatment of the reaction mixture with oxidants allows to release ethylene with formation of a titanium imido complex. Few years later the same group reported also the dehydrogenation of higher alkanes up to  $C_6$  by the same titanium complex with isolation of the relative  $\alpha$ -olefin complexes.<sup>61</sup> This is a remarkable transformation taking place at surprisingly low temperatures compared to previous thermal alkane dehydrogenation reaction. Unfortunately, it presents various drawbacks, i.e. it is still stoichiometric process which takes place under elevated alkane pressures and it can only be applied to short alkanes. Moreover, the release of the desired dehydrogenated product is only achieved in a two-step process thanks to the use of oxidants.



Scheme 1.14 Proposed mechanism for the stoichiometric dehydrogenation of ethane by a titanium-alkylidene intermediate complex.

Pursuing the studies on similar titanium alkylidene complexes, in 2017 Mindiola and his group showed how the addition of a specific phosphorus ylide as hydrogen acceptor could make the dehydrogenation reaction catalytic.<sup>62</sup> This system was able to perform the dehydrogenation of both linear ( $C_4$  to  $C_3$ ) and cyclic alkanes ( $C_6H_{12}$  and COA) to the corresponding olefins under only 75 °C, under milder conditions with TON between 0.2 and 3.2 (Scheme 1.15). Remarkable is the selectivity of the system: when linear alkanes were used as the substrate, they were converted into the corresponding terminal olefins. Unfortunately, the system required the use of 10 equivalent of a non-commercially available phosphorus-ylide.



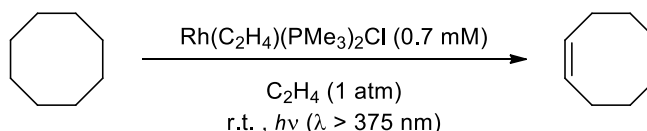
Scheme 1.15 Transfer alkane dehydrogenation under mild conditions catalysed by a titanium base-metal.

#### 1.2.3.4 Photocatalytic alkane dehydrogenation

Another way to achieve the alkane dehydrogenation is *via* a photochemical approach, although this area has been less investigated than the corresponding thermochemical approach. The photochemical activation can be considered as a greener approach towards alkane dehydrogenation, because the reaction can be performed at lower temperatures and often without the need of a hydrogen acceptor. The photochemical method aims to drive the endergonic process of alkane dehydrogenation with the use of light. However, the efficiency is not high because the photon energy greatly exceeds the reaction endothermicity and because any build-up of light-absorbing impurities can affect the photo-process.

The first example of photocatalytically active catalyst has been reported by Burk and Crabtree,<sup>37-38</sup> using the  $[\text{IrH}_2(\text{CF}_3\text{CO}_2)(\text{PCy}_3)_2]$  complex. This photochemical catalytic dehydrogenation was performed in the absence of TBE and no decomposition products were observed after 7 days of irradiation at 254 nm at room temperature (TON 7).

Tanaka and co-workers<sup>63-65</sup> developed a remarkable visible light-assisted transfer alkane dehydrogenation catalysed by the  $\text{Rh}(\text{C}_2\text{H}_4)(\text{PMe}_3)_2\text{Cl}$  species. The catalytically active species was generated *in situ* from the dimeric precursor  $[\text{Rh}(\text{PMe}_3)_2\text{Cl}]_2$  under ethylene atmosphere. Ethylene in this system was also needed as the hydrogen acceptor, required to push the reaction towards the desired dehydrogenated product. Interestingly, this system catalyses the dehydrogenation COA at room temperature, obtaining TOF of 77 (Scheme 1.16).



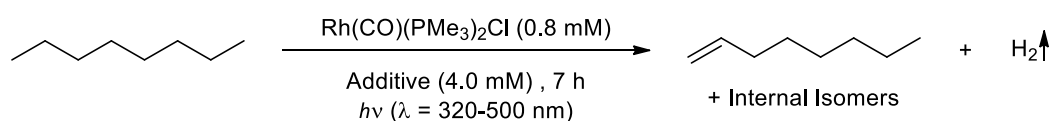
Scheme 1.16 Visible-light assisted transfer alkane dehydrogenation catalysed by  $\text{Rh}(\text{C}_2\text{H}_4)(\text{PMe}_3)_2\text{Cl}$

However, it was only with Tanaka<sup>66</sup> and Saito<sup>67</sup> that one of the most successful catalysts, the Vaska-type Rh complexes, started to be investigated for the photochemical dehydrogenation of alkanes. They both independently reported that the *trans*- $\text{RhCl}(\text{CO})(\text{PR}_3)_2$  ( $\text{R}=\text{Me}, \text{Et}, \text{Ph}$ ) was able to achieve the alkane dehydrogenation under mild conditions. Later Goldman and co-workers<sup>68-69</sup> extensively studied the mechanism of this transformation with the *trans*- $\text{RhCl}(\text{CO})(\text{PMe}_3)_2$  catalyst. With these studies they showed that the role of light was needed for the dissociation of CO from the complex, to yield a reactive rhodium complex that subsequently dehydrogenates the alkane to finally release the olefin. The catalytic species was regenerated by reaction with the previously liberated CO and release of molecular hydrogen to close the catalytic cycle. This process is considered to be the first example of a highly efficient photochemical alkane functionalisation *via* an



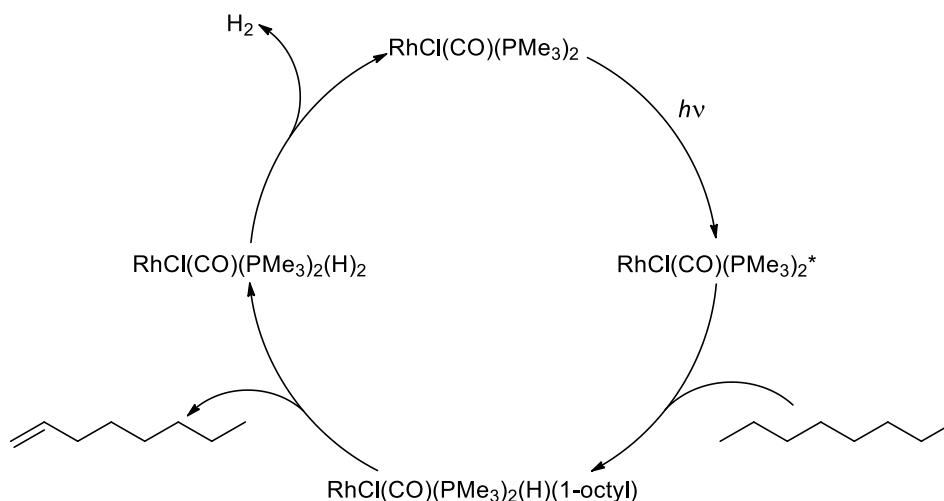
organometallic route. Although the promising results, the issue with the feasibility of photochemical processes on an industrial scale was the cause of the decreasing interest on this approach over the following years.

Very recently, Beller and co-workers,<sup>70</sup> reported a substantially improved system for the acceptorless alkane dehydrogenation with the same *trans*-RhCl(CO)(PMe<sub>3</sub>)<sub>2</sub> photocatalyst (Scheme 1.17). Thanks to 4,4'-bipyridine as an additive, the rhodium catalyst promoted the dehydrogenation of a large number of both cyclic and linear alkanes and also *N*-containing heterocycles (liquid organic hydrogen carriers). With this improved system and a careful reactor design, excellent TONs up to almost 3000 are obtained over 7 hours.



Scheme 1.17 UV-light driven acceptorless alkane dehydrogenation catalysed by *trans*-RhCl(CO)(PMe<sub>3</sub>)<sub>2</sub>.

The same group, trying to tackle the catalyst deactivation issues, carried out a thorough mechanistic investigation, supported by both spectroscopic and theoretical methods. They corrected the previously proposed mechanism for CO release not happening and they proposed a mechanistic model without CO dissociation (Scheme 1.18). They also reported that, using ethyl formate or CO<sub>2</sub> as a CO-releasing stabilizer, higher efficiency can be achieved.<sup>71</sup> The catalyst decomposition was caused by the natural loss of CO from the complex with subsequent formation of inactive rhodium nanoparticles. They hypothesise that the addition of formate or CO<sub>2</sub> stabilised the catalyst, possibly favouring the formation of dimeric species, therefore decreasing the complex decomposition impeding the loss of CO. Under these newly optimised conditions the *trans*-RhCl(CO)(PMe<sub>3</sub>)<sub>2</sub> catalyst promoted the photochemical acceptorless alkane dehydrogenation with TON over 5000. Moreover, this transformation was achieved with temperatures below 90 °C, appreciatively mild for this type of transformations.



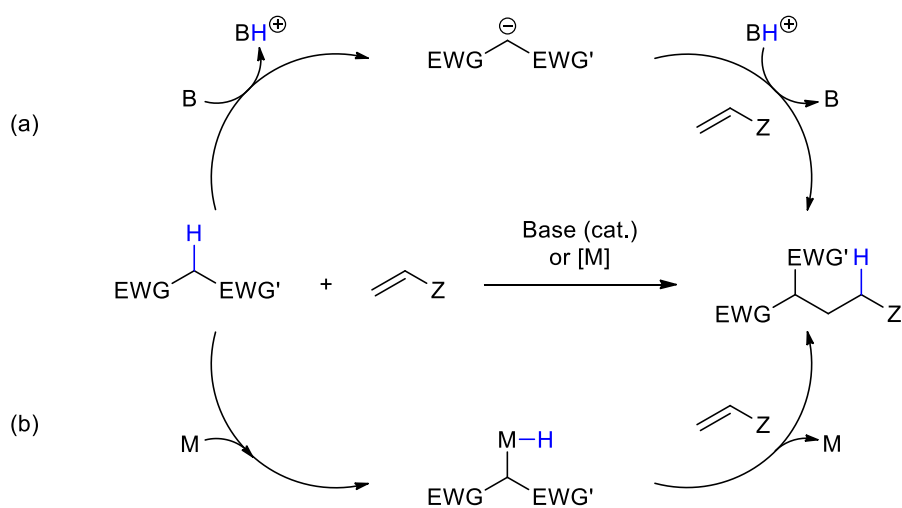
Scheme 1.18 Proposed mechanistic pathway<sup>71</sup> for the UV-light driven acceptorless alkane dehydrogenation catalysed by *trans*-RhCl(CO)(PMe<sub>3</sub>)<sub>2</sub>.

To summarise, transition-metal-mediated alkane dehydrogenation has been widely investigated in the literature, both with thermal and photochemical approaches. However, there are only few systems that operate under milder conditions and all of them present few issues: from multi step processes, to the use of expensive stoichiometric reagents, to difficulties for large scale development. Therefore, there is still much room for improvement towards an efficient room-temperature alkane dehydrogenation.

## 1.3 Transition-metal-mediated Michael additions

### 1.3.1 General introduction

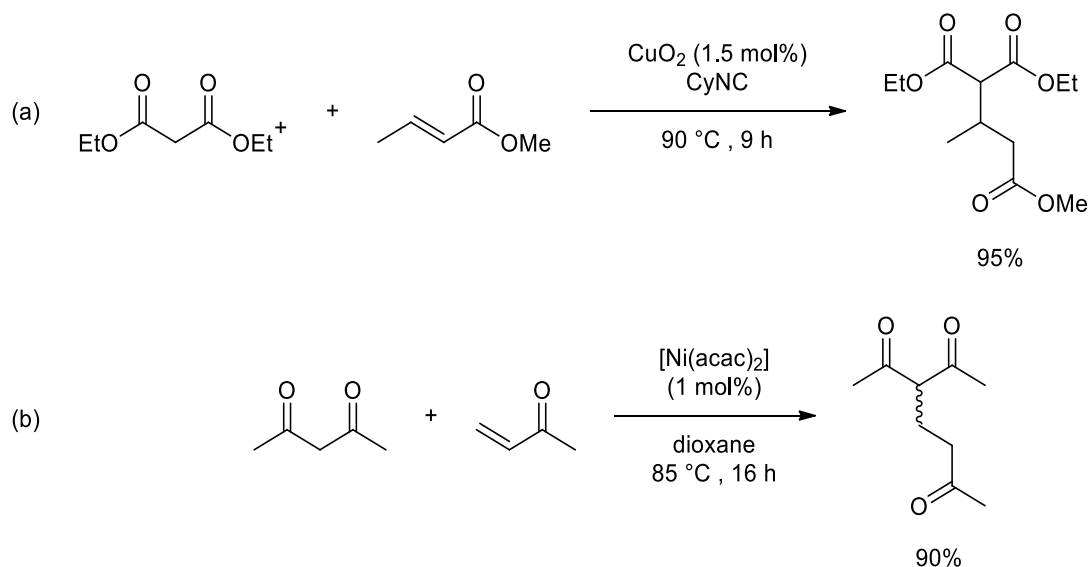
Michael addition reactions are one of the most powerful C-C bonds forming reactions as they can be applied for the synthesis of various compounds bearing a wide range of functional groups. The Michael addition is a conjugate 1,4-addition of a resonance stabilized carbanion, the Michael-donor, to an activated  $\alpha,\beta$ -unsaturated species, the Michael-acceptor. For classic Michael addition reactions, the Michael-donor is a nucleophile bearing two electron-withdrawing groups (EWG) to enhance the acidic nature of the  $-\text{CH}_2$  group. On the other hand, Michael-acceptors are  $\alpha,\beta$ -unsaturated compounds with activated double bonds. A strong base, usually an alkali hydroxides or alkoxides, is needed to deprotonate the Michael-donor (Scheme 1.19, path a).<sup>3</sup> However, the harsh conditions provided by the base can also trigger competing side-reactions and favour the formation of undesired side-products. To solve this issue, many transition-metal catalysts have been developed which are able to perform this addition under neutral conditions *via* C-H activation and are now commonly used (Scheme 1.19, path b).<sup>72</sup> The catalytic C-H activation allows the direct addition of Michael-donor, without the need of stoichiometric pre-activation of the nucleophile, making this process more atom-economical. The alternative mechanism, through which the catalyst operates, allowed the nucleophile scope to be expanded to less acidic substrates. Many examples are reported in the literature of activated C-H bonds bearing two electron-withdrawing groups, which highly increase the acidity and therefore the reactivity of the C-H bond at the  $\alpha$ -carbon atom.<sup>1</sup> These substrates include active methylene compounds such as malonates,  $\beta$ -ketoesters,  $\beta$ -diketones, malonates, carboxylic acid derivatives, etc. On the other hand, the scope of non-activated C-H substrates is quite narrow.



Scheme 1.19 Possible mechanism for the Michael addition reaction: pathway (a) shows a base promoted reaction, pathway (b) shows the mechanism for a transition metal-catalysed Michael addition.

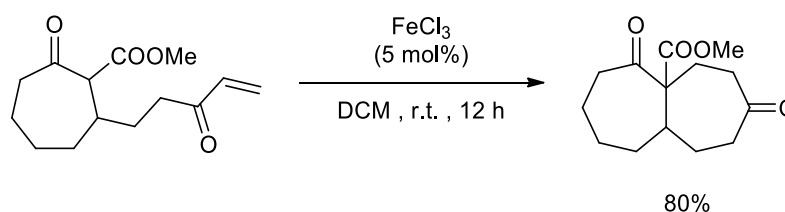
### 1.3.2 Michael additions of activated C-H bonds

The first Michael addition catalysed by a transition metal has been described in 1972 by Kinoshita and co-workers.<sup>73</sup> They reported that a binary system composed of copper oxide and cyclohexyl-isocyanide was able to catalyse the Michael addition of various  $\beta$ -diketones and  $\beta$ -diketoesters to activated olefins, such as diethyl malonate acceptor in high yields (Scheme 1.20, a). Another early work, in 1980, on this new type of Michael addition reactions reported the addition of  $\beta$ -dicarbonyls to a variety of activated alkenes catalysed by nickel acetylacetonate (Scheme 1.20, b).<sup>74</sup>



Scheme 1.20 Early works of the Michael addition catalysed by transition metal complexes.

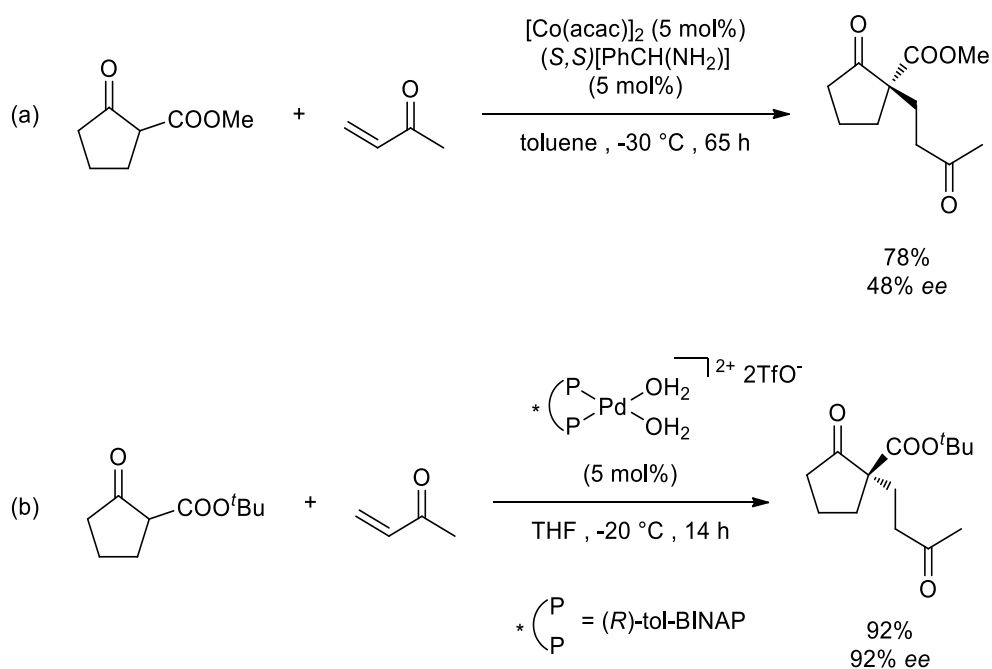
Over the years many different metal species have been investigated as catalyst for the Michael addition. Christoffers<sup>75</sup> carried out an extensive work focusing in particular on iron species. A focus in the group was the use of a cheap catalyst such as hydrated iron(III) chloride to catalyse the Michael addition of various nucleophiles, such as ketoesters and diketones, to vinyl ketones, including quinones. In particular, they reported in 1998 an example of intramolecular Michael addition of a ketoester to a vinyl ketone shown in Scheme 1.21.<sup>76</sup>



Scheme 1.21 Iron-catalysed Michael addition of substrates with activated C-H bonds bearing two electron-withdrawing groups. Intramolecular alkylation of a vinyl ketone with a  $\beta$ -ketoester.

These Michael addition reactions and many others have proven to be highly efficient and, therefore, their enantioselective version has also been widely investigated over the years.<sup>72</sup> Asymmetric 1,4-addition reactions allow the construction of stereocentres in a single step and, therefore, they are of high synthetic interest. Depending on the type of reaction, the stereocentre can be generated either on the Michael-donor or Michael-acceptor side.<sup>1</sup> The first example of enantioselective Michael addition has been reported by the Hammer's group in 1984.<sup>77</sup> They described the addition of  $\beta$ -ketoesters to a vinyl ketone catalysed by cobalt acetylacetonate, although with modest enantiomeric excess (Scheme 1.22, a). Platinum- and palladium-based systems for the Michael addition appeared much later near the years

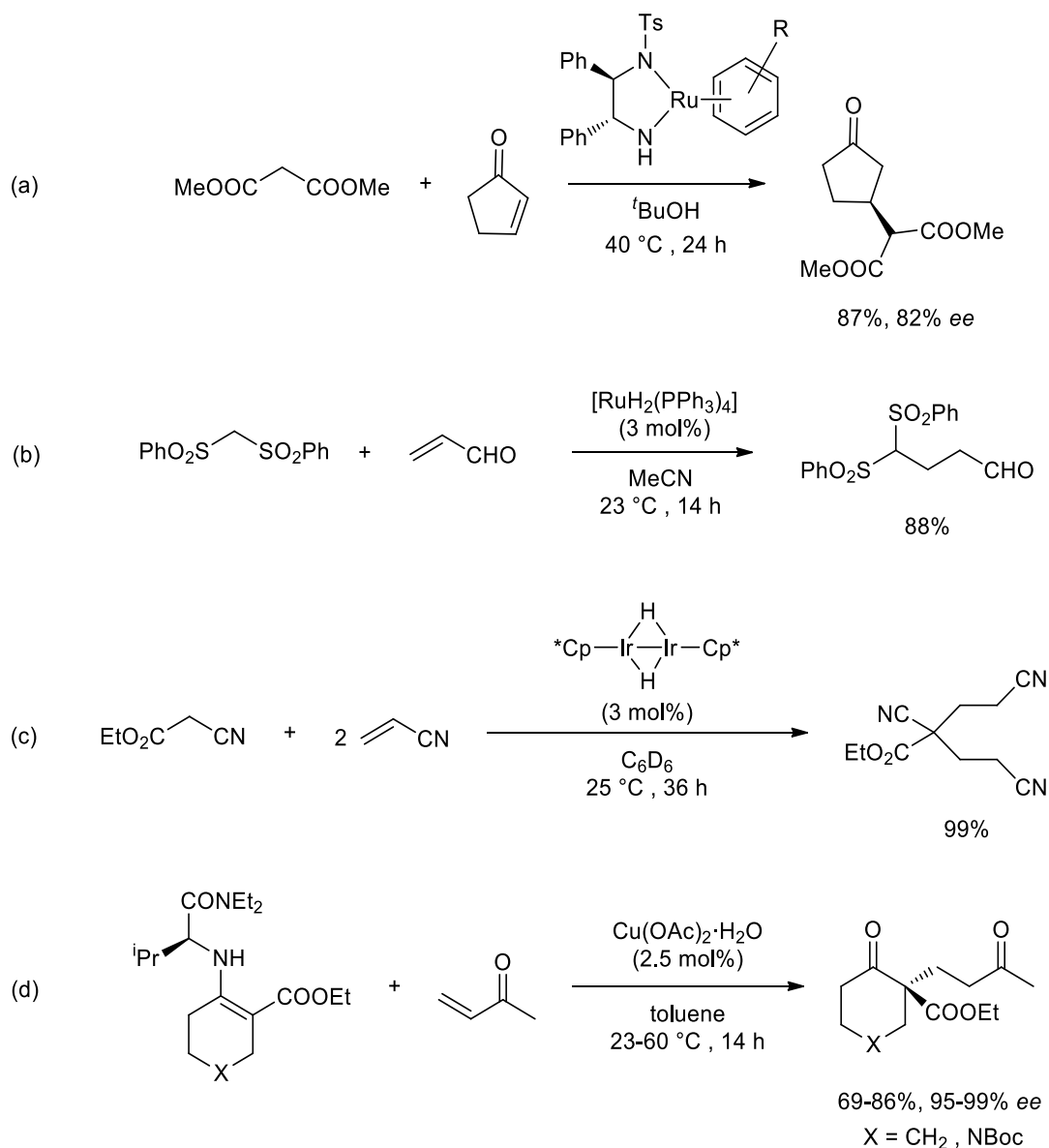
2000.<sup>78</sup> However, with their development and introducing the use of a chiral ligand, much better results could be achieved. Sodeoka reported the use of a chiral palladium complex able to catalyse the Michael addition of both open and cyclic  $\beta$ -ketoesters and  $\beta$ -diketones to vinyl ketones, in high yields and excellent enantioselectivities up to a remarkable 99% enantiomeric excess.<sup>79</sup> An example is reported in Scheme 1.22, b.



Scheme 1.22 Enantioselective Michael addition reaction of substrates with activated C-H bonds bearing two electron-withdrawing groups. (a) Cobalt-catalysed and (b) Pd-catalysed asymmetric addition of a cyclic  $\beta$ -ketoester to a vinyl ketone.

Various transition metal catalysts have been developed able to catalyse many variants of Michael addition, broadening the scope of both Michael-donors and acceptors, also in an asymmetric fashion. Examples are the use of a chiral ruthenium amino complex reported by Ikariya<sup>80</sup> and the Michael addition of disulfone-methylene compounds to activated olefins by Mateo, also with a ruthenium catalyst (Scheme 1.23, a and b respectively).<sup>81</sup> Regarding group 9 transition-metals, Wakatsuki reported a binuclear iridium hydride complex able to catalyse a double Michael addition of ethyl-cyanoacetate to 2 equivalents of acrylonitrile in excellent yields (Scheme 1.23, c).<sup>82</sup> The use of cobalt and rhodium catalysts has also been explored.<sup>72, 77, 83</sup> As previously described, group 10 metal complexes such as of platinum and palladium have been investigated, together with nickel.<sup>74, 78-79</sup> The use of cheaper metals as copper or silver have also been reported.<sup>72, 84</sup> Copper catalysts have drawn a lot of attention in the field of Michael additions. Christoffers and Mann, after an extensive screening of copper complexes, concluded that copper acetate was the best one able to mediate the Michael

addition of chiral enamines of ketoesters to vinyl ketones, with the construction of quaternary stereocentres thanks to chiral amine auxiliaries (Scheme 1.23, d).<sup>85</sup> Lanthanide complexes have also been studied and examples of Michael additions mediated by complexes of lanthanum, europium and ytterbium have been reported.<sup>86-88</sup>



Scheme 1.23 Examples for the Michael addition of various C-H activated substrates catalysed by different transition metal catalysts. (a) Ruthenium-catalysed enantioselective alkylation of  $\alpha,\beta$ -unsaturated ketones with  $\beta$ -diesters. (b) Ruthenium-catalysed Michael addition of disulfones to an activated olefin. (c) Iridium-catalysed Michael addition of cyanoesters to acrylonitrile. (d) Copper-catalysed Michael addition of enamine to vinyl ketone.

Although the literature described many transition-metal and lanthanide complexes able to efficiently mediate Michael addition reaction, they all require the use of activated C-H substrates as nucleophiles, which means that the Michael-donors bear two electron-

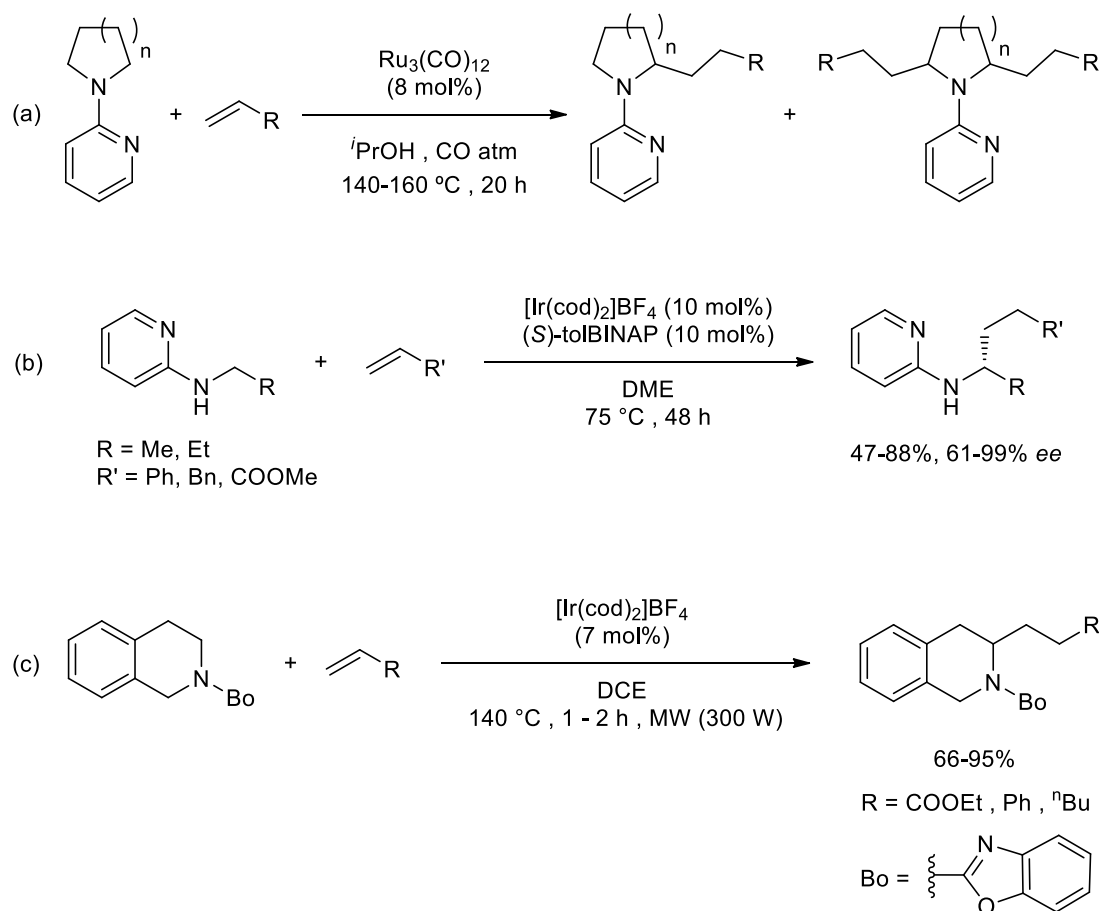
withdrawing groups. This requirement places some strict limits on the scope of possible nucleophiles.

### 1.3.3 Hydroalkylation of weakly acidic C-H bonds

Although there is a wide literature for the Michael addition of activated C-H nucleophiles containing two electron-withdrawing groups, Michael-donors containing less acidic C-H bonds have proven to be more challenging substrates. Therefore, much fewer examples have been reported in the literature for the Michael addition of non-activated nucleophiles.

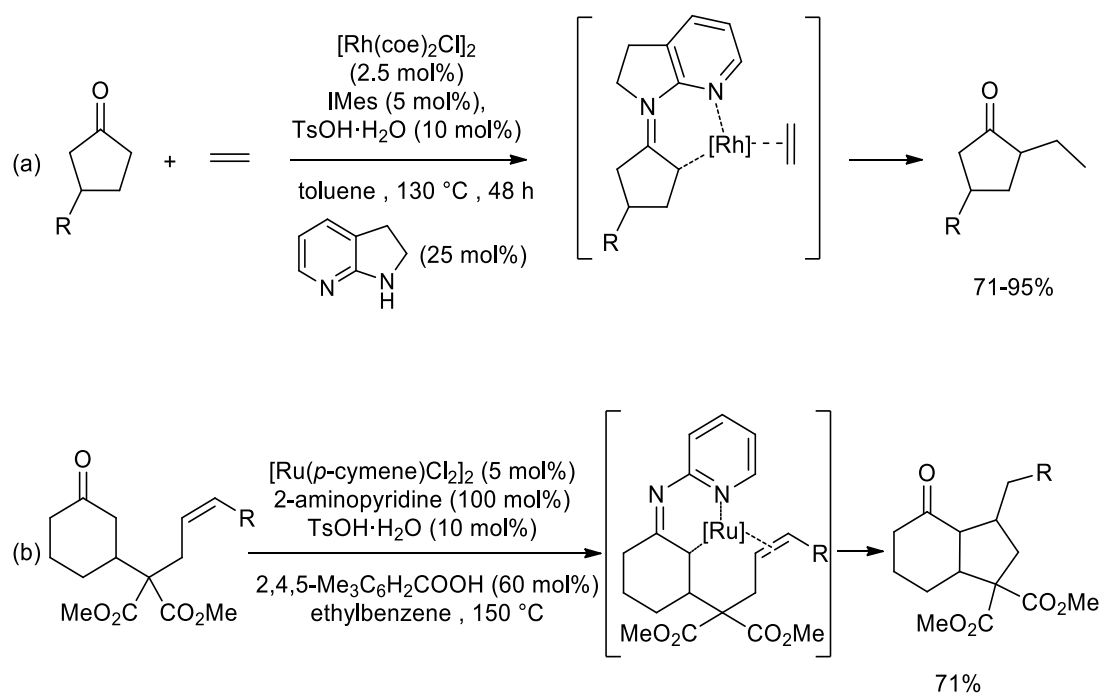
The Michael-type hydroalkylation of weakly acidic C-H bonds has been performed *via* direct C-H activation, often facilitated by the presence of directing groups such as carbonyls and N-heterocycles. Murai and co-workers in 2001 were the first to report a direct alkylation of an amine  $\alpha$ -C-H bond to various substituted olefins catalysed by tri-ruthenium dodecacarbonyl (Scheme 1.24, a).<sup>89</sup> Their approach was successful, thanks to the presence of a pyridine substituent on the nitrogen acting as a directing group. However, the system yields a mixture of mono- and di-alkylated products. Another example of the use of pyridines as directing groups has been reported in 2012 by Shibata.<sup>90</sup> By using a chiral cationic iridium catalyst, they were able to develop an enantioselective method for the alkylation of substituted olefins with alkyl-amino-pyridines with good yields and enantiomeric excess (Scheme 1.24, b). Only two years later, Opatz and Laham used the same iridium complex to activate the C-H bond in  $\alpha$ -position to a secondary amine.<sup>91</sup> They used a benzoxazole moiety as chelating group, which can be easily introduced on the substrate and be removed after the alkylation. Excellent yields were obtained with also good selectivities for the monoalkylated product (Scheme 1.24, c).





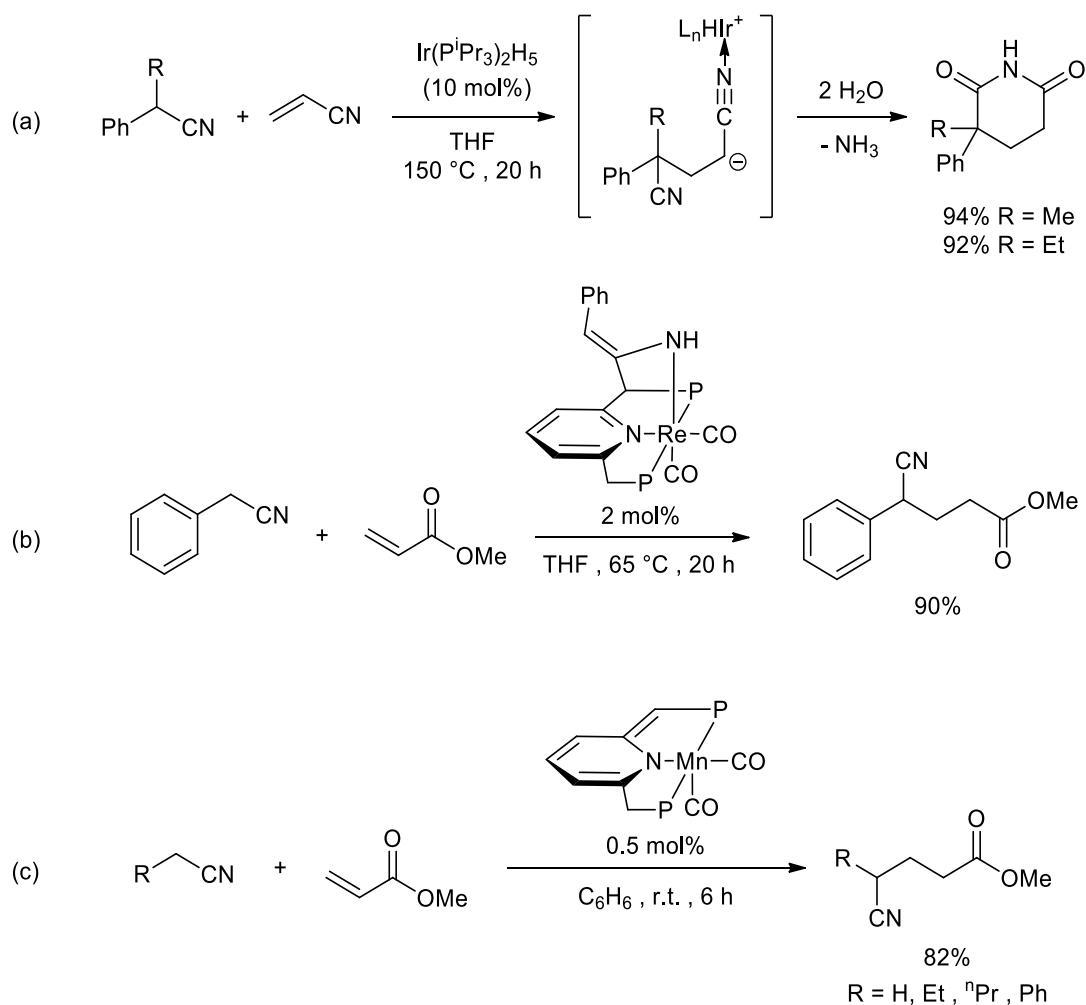
Scheme 1.24 Transition-metal catalysed hydroalkylation reactions of non-activated nucleophiles to substituted olefins mediated by N-containing directing groups. (a) Ruthenium-catalysed alkylation of C-H bonds adjacent to nitrogen atoms. (b) Iridium-catalysed enantioselective C-H alkylation of alkyl-amino-pyridines to substituted olefins. (c) Iridium-catalysed C-H alkylation of C-H bonds adjacent to nitrogen atom bearing a removable directing group.

Another example of the use of non-activated substrates is found in the  $\alpha$ -alkylation of aliphatic ketones. Dong and co-workers reported an example of cooperative-catalysis between a rhodium and an enamine ligand to achieve the insertion of simple olefins into the  $\alpha$ -C-H bond of ketones.<sup>92</sup> The role of the 1,2-dihydro-7-azaindole ligand is to simultaneously activate the ketone, with the formation of an enamine, and to direct the rhodium-mediated alkylation into the right  $\alpha$ -position.<sup>93</sup> The mono-alkylation is achieved selectively at the less hindered  $\alpha$ -carbon with olefins ranging from ethylene to 1-hexene and styrene. A large number of functional groups are also tolerated as substituents on the ketone, i.e. hydroxyls, esters, substituted phenyls and amines. The following year the same group adopted a similar strategy for the intramolecular alkylation of alkyl- and aryl-olefins using a ruthenium-catalyst and 2-aminopyridine as bifunctional ligand.<sup>94</sup> Again, a range of functional groups were tolerated.



Scheme 1.25 Metal-enamine cooperative catalysis for the  $\alpha$ -alkylation of cyclic ketones. (a) Rhodium-catalysed alkylation of substituted cyclopentanones with ethylene. (b) Ruthenium-catalysed intramolecular alkylation of cyclohexanones with olefins.

Very few examples are reported in the literature about the use of non-activated acetonitriles. Their use as nucleophiles in metal-catalysed alkylations is, in fact, complicated because of the low C-H acidity.<sup>95</sup> In 2003, Murahashi and co-workers reported the first breakthrough in the field with the alkylation of olefins with di-substituted acetonitriles to synthesise glutarimides.<sup>96</sup> They reported the addition of benzyl nitriles to acrylonitrile mediated by a pentahydride-iridium catalyst. The obtained alkylated product that subsequently undergoes hydrolysis to yield the desired glutarimides in high yields (Scheme 1.26, a). The nitrile scope reported by Murahashi described the use of various C-H acidic nitriles, however, it included also two non-activated nucleophiles with a weakly acidic tertiary C-H bond. More recently two examples have been reported, by Milstein and co-workers, for the alkylation of methyl acrylate with non-activated nitriles mediated by pincer-type metal catalysts. In 2013 they reported the Michael addition of benzyl cyanide to various  $\alpha,\beta$ -unsaturated ketones and esters with moderate to good yields (Scheme 1.26, b).<sup>97</sup> Again, the alkylation was enabled *via* metal-ligand cooperation between the rhenium metal centre and an unusual PNP-chelating ligand. Later, in 2016, they expanded the scope of Michael-donors to aliphatic-nitriles for the first time.<sup>98</sup> This time a PNP-manganese catalyst was promoting the addition of those nitriles to  $\alpha,\beta$ -unsaturated ketones and esters with various degrees of success (Scheme 1.26, c).



Scheme 1.26 Michael addition of non-activated acetonitriles to olefins mediated by various transition-metal catalysts. (a) Iridium-catalysed synthesis of glutarimides *via* Michael addition of phenylacetone nitriles to acrylonitrile. (b) Rhenium-catalysed Michael addition of benzyl-cyanide to methyl acrylate. (c) Manganese-catalysed Michael addition of aliphatic nitriles to methyl acrylate.

To summarise, there are many examples reported in the literature for the hydroalkylation, including Michael addition, of nucleophiles with activated C-H bonds mediated by various transition-metal catalysts. Instead, the literature for Michael-donors with non-activated C-H bonds is scarce. In particular, most of C-H nucleophiles have primary or secondary  $\alpha$ -C-H bonds. Michael additions with weakly acidic tertiary C-H bonds have yet to be investigated and the development of these reactions would allow not only to expand the scope of Michael-donors, but also a simple access to products with quaternary centres of high synthetic interest.

## 1.4 Sonochemistry

### 1.4.1 Introduction and fundamentals

In the recent years, due to the increased environmental consciousness both in the research and industrial environment, scientists have been working to answer the need for greener synthetic approaches. This resulted in an increased interest in employing more environmentally friendly methodologies in order to minimise the chemical wastes, improve the atom economy and reduce energy consumption. In this regard, ultrasound-assisted organic synthesis appeared as a greener approach able to answer this challenge. The features that makes the ultrasound approach so desirable are increased reactivity and reaction rates, higher selectivity with formation of cleaner products in higher yields and lower energy demand for a reaction.<sup>99</sup>

Sound is the propagation of pressure waves through a physical elastic medium, i.e. air or liquid. Human hearing is between 16 Hz and about 18 kHz. Beyond the upper limit sound is inaudible and it is therefore defined as ultrasound.<sup>99</sup> The frequencies used in sonochemistry are generally between 20 kHz and 2 MHz.<sup>99-100</sup> The European Society of Sonochemistry defines sonochemistry as “the application of ultrasound to chemical reactions and processes”. This is possible because the sound above 20 kHz and up to 2 MHz can generate a great amount of acoustic energy and hence affect the chemical reactivity.<sup>101</sup> In Figure 1.3 the various frequency ranges of sound and the frequencies applied in the field of sonochemistry are reported. The conventional power ultrasound, between 20 and 40 kHz, is the one used in common laboratory equipment, such as the ultrasonic cleaning baths that can be found in any chemistry laboratory. However, ultrasound can reach much higher frequencies and the use of sonochemistry is being extended to a much broader range, up to 2 MHz. This high energy ultrasound can be used in organic reactions since it provides specific activations, but the chemical consequences of high-intensity ultrasounds do not arise from an interaction between acoustic waves and matter at a molecular or atomic level. In fact, first the wavelength of ultrasound is much larger than the molecular dimensions, and secondly the average energy is not even enough to modified the ro-vibrational levels.<sup>99</sup> Instead, the driving force in sonochemistry is cavitation. High frequency ultrasound above 5 MHz does not produce any cavitation and this range is indeed used for medical applications, i.e. imaging.

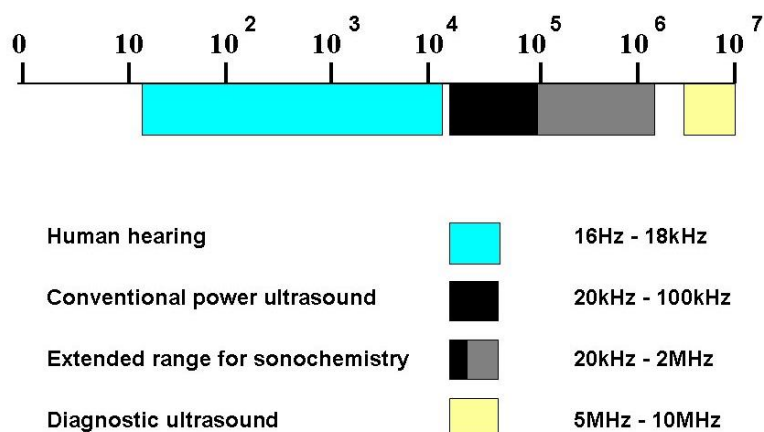


Figure 1.3<sup>100</sup> Sound frequency ranges

## 1.4.2 Ultrasound and cavitation bubbles

Ultrasound is propagated through the liquid *via* a series of compression and rarefaction waves induced in the molecules of the liquid medium (Figure 1.4). In the case of a sufficiently high power, when the negative pressure of the rarefaction cycle exceeds the attractive forces between the molecules of the liquid, a cavitation bubble is created. This bubble increases in size over a few cycles, however, the acoustic field experienced by the bubble is not stable due to the interference caused by other bubbles forming and resonating around it. As a result, some bubbles will grow till reaching an unstable size, causing a violent collapse.

The implosion of these cavities establishes the environment enabling the chemical reaction to occur. Each cavitation bubble acts as a localised micro-reactor. With the implosion, the vapours inside the cavity are compressed, generating intense heat that raises the temperature of the liquid immediately surrounding the cavity, creating a local *hot spot*. The temperature of this region is extremely high (5000 °C), but the region itself is so small that the heat dissipates immediately. In fact, this event occurs with a lifetime of about  $10^{-7}$  s and cooling rates above  $1000 \text{ K s}^{-1}$ .<sup>99</sup> At any given time, indeed, the bulk solution remains at room temperature.<sup>99-100, 102</sup> Therefore, the substrate undergoes a sort of thermal activation, with the difference that this highly energetic state, deriving from the collapsing bubble, can be better controlled by carefully varying the frequency and intensity of ultrasounds. The vapour pressure of the solvent also plays a role in determining the energy released with this phenomenon.

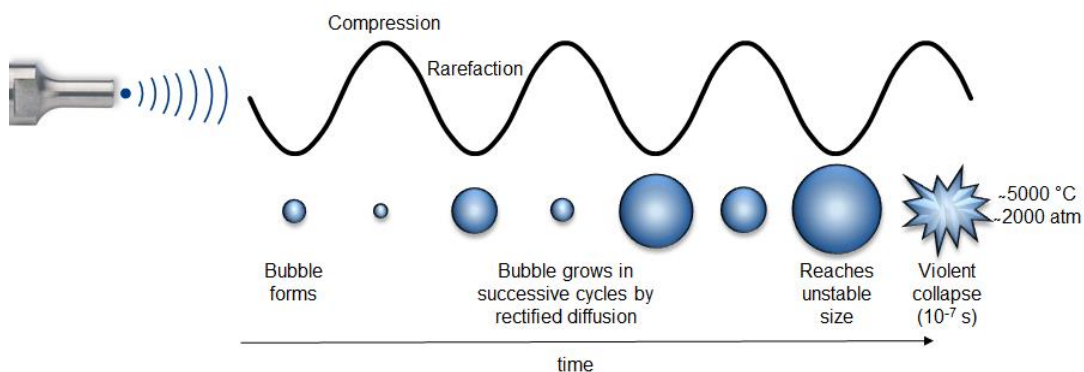


Figure 1.4 Sound propagation in a liquid showing cavitation bubble formation and collapse.

Studies have provided evidence of three regions of sonochemical activity in a sonicated system<sup>103</sup> (Figure 1.5). The first zone is the gaseous region of the cavitation bubble, here extreme conditions are produced. In order for a chemical to experience these extreme conditions during the collapse of the cavitation bubble, it must enter the bubble and so it should be volatile. The second zone is the gas-liquid transition region, characterised by intermediate temperatures and pressures and containing the less volatile components of the reaction mixture. Finally, the third zone consists of the bulk liquid phase subjected to intense shear forces.

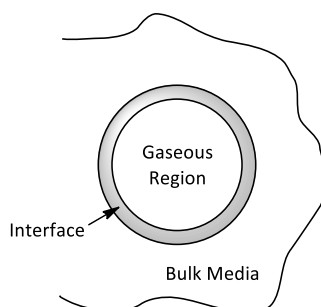


Figure 1.5 Cavitation in a homogeneous liquid: three reaction zones of sonochemical reactions (Shell model)

### 1.4.3 Sonochemistry for organic reactions

Sonochemical energy differs from other traditional energy sources in duration, pressure and energy per molecule. This correlation is visually explained in Figure 1.6,<sup>102</sup> where the sonochemical energy can be compared to other forms of energy such as thermo- or photochemical. As it can be observed, ultrasound is an efficient method for delivering high amounts of energy, in the form of high temperatures and pressures in an extremely short period of time. The short timescale of the sonochemical events makes this chemical activation method

similar to photochemical activation. However, in the case of sonochemistry the activation is thermal, rather than electronic, indeed showing similarities with classic thermal activations.

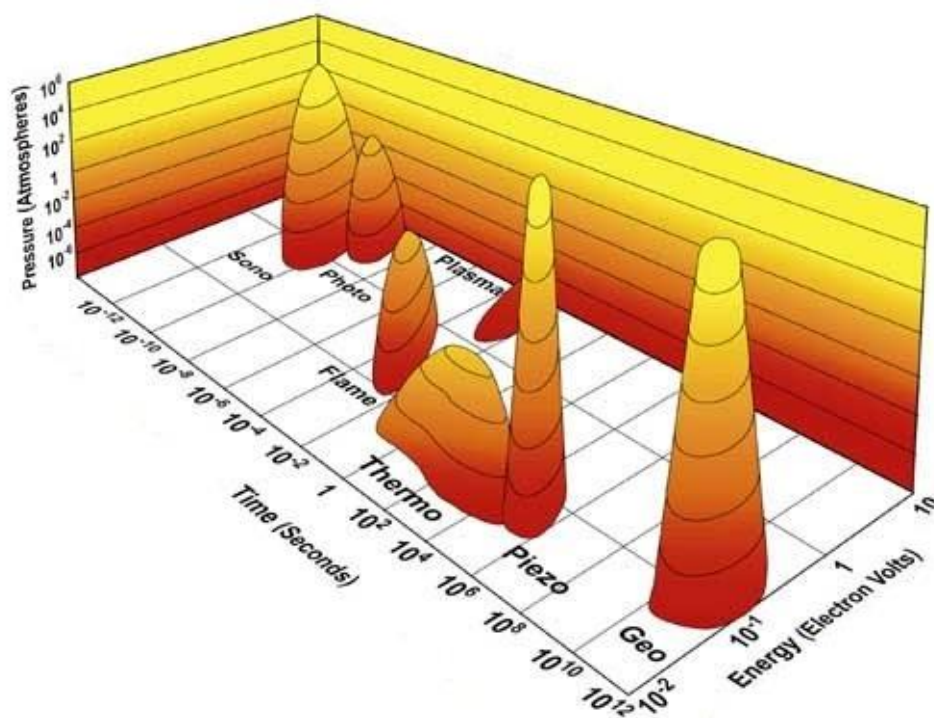
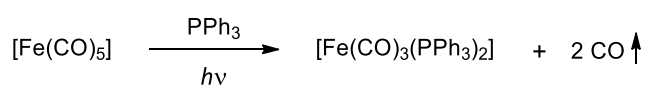


Figure 1.6<sup>102</sup> Ultrasound in relation to other forms of energy. The three axes represent the timescale of the interaction between the energy and matter, the pressure produced and the energy per molecule released.

Sonochemistry also shows some features typical of photochemical reactivity. In particular, the effect of high-intensity ultrasound on a variety of metal carbonyls is the general phenomenon of sonochemical ligand dissociation.<sup>104</sup> For example, thermolysis of  $[\text{Fe}(\text{CO})_5]$  gives highly divided iron powder. This type of multiple ligand dissociation is not available from ordinary thermal processes, because under thermal conditions it is really hard to control.<sup>104-105</sup>  $[\text{Fe}(\text{CO})_5]$  is photosensitive with respect to substitution of CO. In the presence of  $\text{PPh}_3$ ,  $[\text{Fe}(\text{CO})_3(\text{PPh}_3)_2]$  is formed from  $[\text{Fe}(\text{CO})_5]$  (Scheme 1.27).<sup>106</sup> Similar substitution pattern is observed when  $[\text{Fe}(\text{CO})_5]$  is treated with ultrasound in the presence of triphenylphosphine (Scheme 1.28).<sup>104</sup>

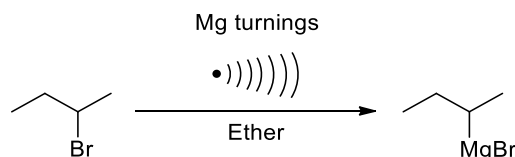
Thus, sonochemistry resembles thermal activation for some aspects, but it has some similarities with photochemical activation as well.



Scheme 1.27 Photochemical ligand exchange of  $\text{Fe}(\text{CO})_5$  with triphenylphosphine.

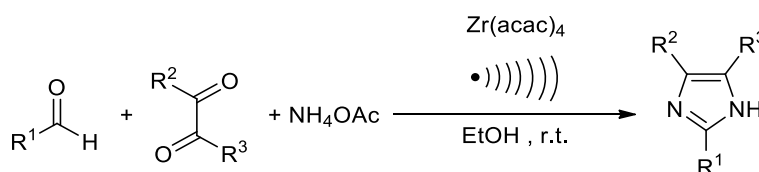






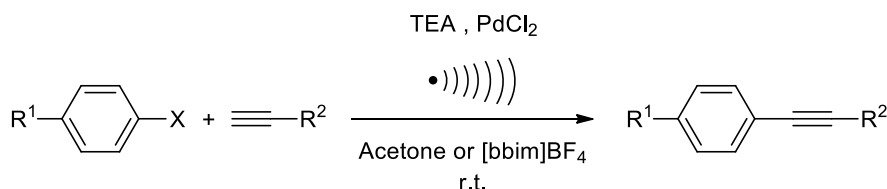
Scheme 1.30 Grignard reagent synthesis under ultrasound irradiation.

In the field of catalysis, a novel, simple, efficient and green methodology has been reported by Khosropour<sup>107</sup> for the synthesis of 2,4,5-tri-substituted imidazoles under ultrasound irradiation from condensation reaction of aldehydes, benzyls and ammonium acetate through a zirconium(IV) acetylacetonate catalyst (Scheme 1.31). The procedure offers excellent yields, shorter reaction times and milder conditions.



Scheme 1.31 Ultrasound-promoted synthesis of 2,4,5-tri-substituted imidazoles catalysed by  $Zr(acac)_4$ .

The Sonogashira reaction, Pd-catalysed coupling of aryl halides and terminal acetylenes, is usually conducted in the presence of a Cu-cocatalyst, amine and phosphine ligand. The application of ultrasound has been very useful to soften the conditions, so that the reaction can occur at room temperature (Scheme 1.32). Srinivasan<sup>108</sup> reported the Sonogashira reaction to proceed at 30 °C in acetone or ionic liquid as solvent under ultrasound irradiation to give enhanced reaction rates, excellent chemo-selectivity and high yields in the absence of copper cocatalyst and phosphine ligand. Analysis showed that Pd(0) nanoparticles are formed under ultrasound irradiation and they act as catalyst for the reaction. Examples are reported in the literature also for the ultrasound promoted Heck,<sup>109</sup> Henry<sup>110</sup> and Suzuki type reactions.



Scheme 1.32 Sonogashira reaction under ultrasound irradiation catalysed by Pd(0) nanoparticles

These are only a few examples, but they can give an idea of the broad range of applications and achievements that ultrasound irradiation can reach among chemical reactions. In conclusion, chemists have exploited the use of ultrasounds to overcome in many

cases the synthetic limitations, improving reactivity and selectivity. Sonochemistry is an expanding field, whose applications can be found for a wide range of chemical systems. Although it has more than eight decades of history, there is still large room for improvement regarding the use of ultrasounds in chemical systems, particularly in the field of homogeneous catalysis.

## 1.5 Summary and objectives

As evident from the many examples discussed in the previous sections, the research on C-H functionalisation made a considerable progress over the past few decades. Activation of aliphatic C-H bonds by transition-metal complexes has become a fast-developing field, especially in the past 20 years. Once, harsh reaction conditions were considered obligatory to achieve satisfactory yields and selectivities. Catalyst design has been crucial to improve those processes, together with the use of activated substrates and directing groups. However, still the temperatures required for the C-H activation were not always mild. The aim of this work is to describe the contribution to the ever-developing field of C-H activation under mild conditions, by focusing on two different transformations.

The second chapter will focus on the alkane dehydrogenation under mild conditions, providing a more energy and cost-effective route to the corresponding olefins. The aim is to achieve the alkane C-H activation at room-temperature by combining the use of a transition-metal catalyst with the ultrasonic treatment of the solution. The steps for the development and improvement of this system will be described.

In the third chapter the development of a mild Michael addition reaction will be examined. Further studies will be carried out to improve a previously developed system for the Michael-type activation of weakly C-H acidic nitriles to cyclohexenones under mild conditions. In particular, the reaction mechanism will be investigated and a catalytic cycle for this hydroalkylation reaction will be proposed. The use of ultrasound will be also applied to this system to try to perform this transformation at room temperature.

2

Iridium-mediated room-  
temperature sonochemical alkane  
transfer dehydrogenation

## 2.1 Introduction

### 2.1.1 General introduction on alkane dehydrogenation

Dehydrogenation of abundant and inexpensive saturated hydrocarbons is the most economical route for the production of olefins, which can be easily further converted in a vast array of organic chemicals. For this reason, the C-H activation of alkanes is one of the most investigated reactions in organic synthesis for its great potential value in applications. Alkane dehydrogenation is a highly challenging process and on an industrial scale is achieved with heterogeneous catalysis under very harsh conditions, with reaction temperatures even above 900 °C. Therefore, in the recent years, many homogeneous catalysts able to perform this reaction have been developed, but they still mainly require relatively high temperatures, with most efficient systems working above 150 °C. Although several homogeneous systems able to perform the catalytic alkane dehydrogenation have been discovered, only few of them are able to operate under relatively mild conditions. In this work this issue is addressed using a new method, combination of catalysis and sonochemistry.

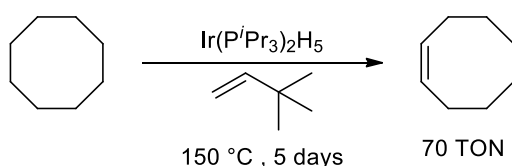
### 2.1.2 Homogeneous catalytic alkane dehydrogenation

The promoting effects of catalysis on organic transformations are well known. Due to the disadvantages of the heterogeneous alkane dehydrogenation, researchers have been looking for a more efficient way to obtain olefins. A cleaner and more promising route to their production involves the dehydrogenation of alkanes over homogeneous transition metal catalysts and, in the past three decades, significant advantages have been made on these studies. In fact, the corresponding homogeneous catalysts can operate at lower temperatures (<250 °C) with better selectivities. However, as already mentioned, dehydrogenation is an endothermic process and so it needs to be driven in some way. Several methods have been employed, from the use of a sacrificial hydrogen acceptor in the transfer alkane dehydrogenation, to the removal of the formed molecular hydrogen upon acceptorless thermal or photochemical activation; all of them mediated by metal derivatives.

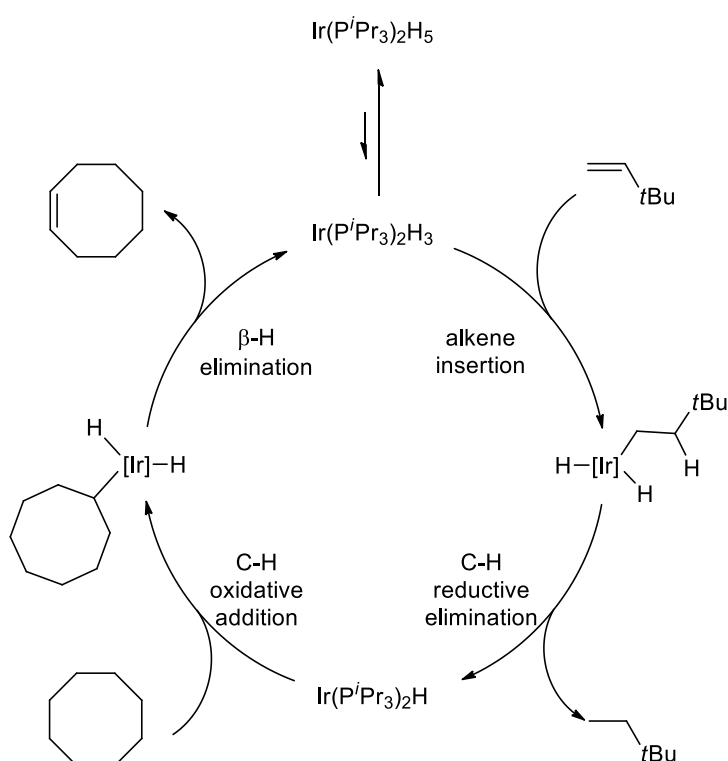
#### 2.1.2.1 Thermochemical alkane dehydrogenation

Crabtree<sup>36-38</sup> and Felkin<sup>39-40</sup> independently reported the first catalytic homogeneous transfer dehydrogenations of alkanes mediated by iridium bis(trialkylphosphine) complexes. The Ir(*i*-Pr<sub>3</sub>)<sub>2</sub>H<sub>5</sub> catalyst afforded 70 TON over 5 days for the transfer dehydrogenation of cyclooctane with *tert*-butylethylene at 150 °C (Scheme 2.1).<sup>39</sup> The catalytic cycle for this

remarkable transformation is reported in Scheme 2.2. The cycle starts with the iridium pentahydride which is activated by loss of a hydrogen molecule. The complex then undergoes insertion of TBE in the Ir-H bond; subsequent reductive elimination of *tert*-butylethane (TBA) generates the reactive 14-electrons Ir(I) complex. This species undergoes oxidative addition of a C-H bond of the alkane substrate yielding the iridium alkyl hydride; subsequent  $\beta$ -hydride elimination closes the cycle producing the olefin and regenerating the iridium trihydride. TBE acts as a “hydrogen acceptor”, its addition drives the endothermic process of loss of H<sub>2</sub>, resulting in the catalytic generation of dehydrogenated products.<sup>31</sup> Cyclooctane is usually chosen as the model substrate for this type of reaction; it is in fact one of the best substrates for dehydrogenation. The easier dehydrogenation of cyclooctane with respect of *n*-alkanes is due to the weaker binding of COE to the Ir(I) centre than the 1-alkene.<sup>31</sup>



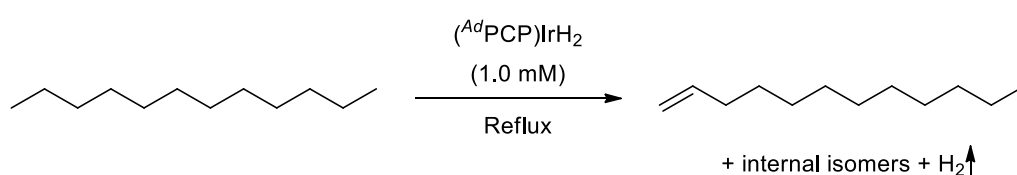
Scheme 2.1 Transfer dehydrogenation of cyclooctane with *tert*-butylethylene catalysed by Ir(<sup>i</sup>Pr<sub>3</sub>)<sub>2</sub>H<sub>5</sub>.



Scheme 2.2 Catalytic cycle for the transfer dehydrogenation of cyclooctane catalysed by Ir(<sup>i</sup>Pr<sub>3</sub>)<sub>2</sub>H<sub>5</sub>.

Many other homogeneous systems have been developed, but the main problem remained the catalyst deactivation. To overcome this issue, systems based on pincer

complexes began to flourish. This new class of catalyst was able to withstand the higher reaction temperatures at which the alkane dehydrogenation seemed to occur more efficiently, resulting in higher activity. Various pincer complexes have been developed able to catalyze both the transfer and acceptorless dehydrogenation of both linear and cyclic alkanes. In 2010, Goldman and co-workers<sup>56</sup> designed an adamantyl-substituted pincer iridium catalyst, (<sup>Ad</sup>PCP)IrH<sub>2</sub>, able to withstand decomposition at 250 °C over long periods of time, showing higher activity towards alkane dehydrogenation. This new system has been tested for the acceptorless dehydrogenation of cyclodecane and *n*-dodecane with excellent results (Scheme 2.3).



Scheme 2.3 Thermal acceptorless alkane dehydrogenation under reflux conditions with (<sup>Ad</sup>PCP)IrH<sub>2</sub> as catalyst.

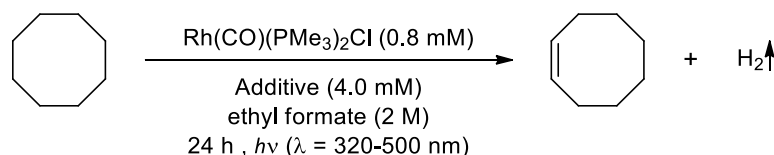
Worth to mention are some attempts to achieve the alkane dehydrogenation under milder conditions using a base-metal by Mendiola and co-workers. In 2011 they reported that the titanium alkylidyne complex (PNP)Ti≡C<sup>t</sup>Bu (PNP=N[2-P<sup>i</sup>Pr<sub>2</sub>-4-methylphenyl]<sub>2</sub>), can activate the C-H bond of ethane at room temperature, ethylene can then be released in a subsequent step *via* oxidation by azides (see Scheme 1.14, Chapter 1).<sup>60</sup> Later on in 2017, the same group showed that the alkylidene complex (PNP)Ti=CH<sup>t</sup>Bu(CH<sub>3</sub>) is able to catalyze the transfer dehydrogenation of various alkanes under relatively mild conditions (75 °C) (see Scheme 1.15, Chapter 1). However this process could only achieve TON between 0.2 and 3.2 over 4 days of reaction and required the use of a rather expensive phosphine ylide as the sacrificial hydrogen acceptor.<sup>62</sup>

### 2.1.2.2 Photochemical alkane dehydrogenation

While the thermocatalytic dehydrogenation of alkanes have been well explored, the light-driven alkane dehydrogenation is much less investigated. To avoid the use of sacrificial acceptor and to allow the reaction to be performed at lower temperatures, photocatalytic processes have been considered as a greener option for alkane dehydrogenation, where the light drives the endergonic process of alkane dehydrogenation.

Recently, Beller and co-workers,<sup>70</sup> reported an improved acceptorless catalytic system with the *trans*-RhCl(CO)(PMe<sub>3</sub>)<sub>2</sub> photocatalyst in the presence of 4,4'-bipyridine as an additive. This system could reach TONs of almost 3000 for the cyclooctane dehydrogenation,

with a recorded reaction temperature within the region of 85-88 °C. After a careful mechanistic investigation, they were able to further improve the system by using ethyl formate or CO<sub>2</sub> as CO-releasing stabilisers, obtaining catalyst TON up to 5350 for cyclooctane dehydrogenation (Scheme 2.4).<sup>71</sup>



Scheme 2.4 UV-light driven acceptorless alkane dehydrogenation catalysed by trans-RhCl(CO)(PMe<sub>3</sub>)<sub>2</sub>.

Worth to mention is also the system developed by Tanaka,<sup>63-65</sup> able to perform the visible light-assisted transfer alkane dehydrogenation mediated by Rh(C<sub>2</sub>H<sub>4</sub>)(PMe<sub>3</sub>)<sub>2</sub>Cl in the presence of ethylene as the hydrogen acceptor and catalyst activator. At room temperature, TOF of 77 were obtained for the dehydrogenation of COA (Scheme 1.16, Chapter 1).

To summarise, many examples have been reported in the literature for both thermal and photochemical transition-metal-mediated alkane dehydrogenation. However, only few systems are able to operate under mild conditions and still suffer from problems such as multi step processes, the need for expensive stoichiometric reagents or difficulties towards a large-scale development. Therefore, it is still a long way to reach an efficient room-temperature alkane dehydrogenation.

### 2.1.3 Sonochemistry

A growing interest in employing more environmentally friendly methodologies has arisen in recent years in order to minimize the quantities of chemical disposals and energy consumptions. In this regard, ultrasonic irradiation has emerged as a mean to achieve the so called “green” chemistry by enhancing the reactivity, increasing the selectivity and lowering the energy demand of a reaction.<sup>99</sup>

High-intensity ultrasound can be used as a method for chemical activation and the driving force for the reaction is the cavitation phenomenon (Figure 2.1). Successive compression and rarefaction cycles of the ultrasound wave cause the formation, growth and subsequent violent collapse of cavitation bubbles in the solvent medium. With the implosion, a *hot spot* is formed, characterised by extremely high temperatures and pressures. This event has a lifetime of about 10<sup>-7</sup> s, cooling rates above 1000 K s<sup>-1</sup> and the area is so limited that at any time during the process the bulk of the liquid remains at room temperature.<sup>99-100, 102</sup> The hot spots give rise to different reaction zones: an internal gaseous region of the cavitation



bubble, characterised by the most extreme conditions; this is surrounded by the interface zone, the gas-liquid transition region. All these hot spots are then surrounded by the bulk of the liquid phase under room temperature. Indeed, extreme conditions are created on a microscale and the substrate in this region can be considered to undergo a sort of thermal activation.

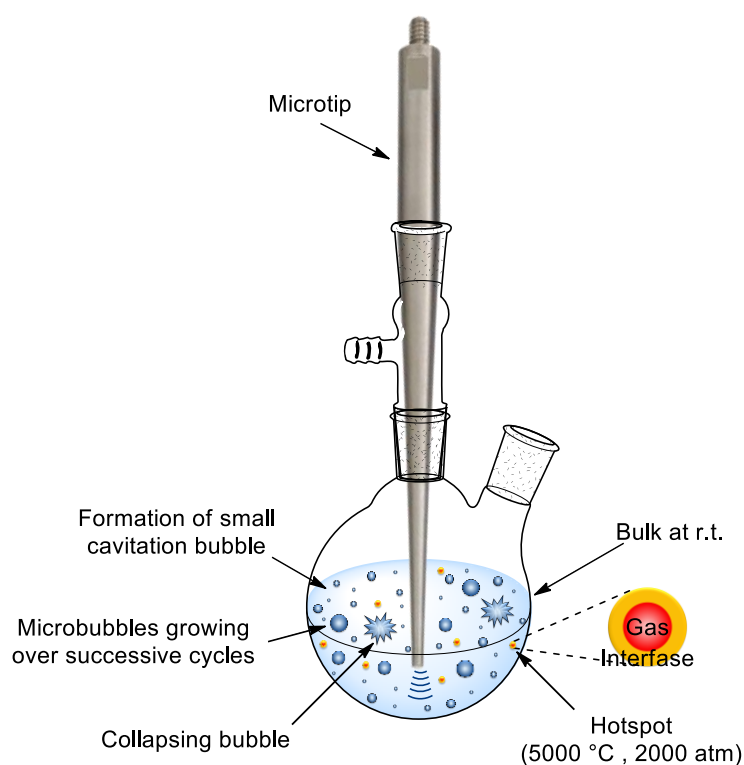


Figure 2.1 Scheme of the experimental set-up with cartoon of the cavitation process.

Sonochemistry has also some similarities with photochemical reactivity. In fact as described in the previous chapter, metal complexes subjected to high-intensity ultrasound can undergo a sonochemical dissociation of the ligands,<sup>104</sup> or they can form new reactive intermediates or species that are not usually observed in regular reactions. Moreover, organometallic reactions irradiated with ultrasound can easily show an acceleration of the reaction or a different product distribution or selectivity. For all those reasons, the use of a metal complex in the ultrasound-mediated organic synthesis can present some advantages such as improved yields, simpler procedure, shorter reaction times and milder conditions (low temperature); resulting overall in a simple, efficient and green procedure.<sup>99</sup>

Thus, sonochemistry for some aspects resembles thermal activation and on the other hand it has some similarities with photochemical activation. Chemists have exploited the use of ultrasounds for different applications and for a wide range of chemical systems, however

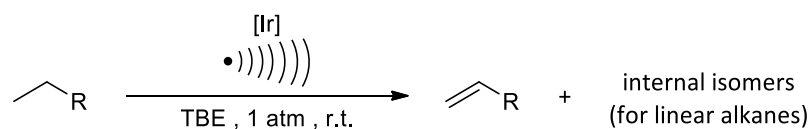
there is still large room for improvement regarding the use of sonochemistry to improve chemical systems, in particular in the field of homogeneous catalysis.

#### 2.1.4 Summary and objectives

The diminishing levels of the world's oil reserves is cause of concern for future energy sources, indeed an efficient use of the current and not yet developed resources has become crucial. In this area the use of a catalyst in a transformation becomes a way to achieve an environmentally friendly and atom economical process. Through catalytic alkane dehydrogenation, abundant and inexpensive hydrocarbons can be converted into the corresponding olefins, value-added chemical as starting material for many chemical transformations of industrial interest. Heterogeneous dehydrogenation catalysts have already been successfully applied in industry; however, they are effective only for short alkanes (C<sub>2</sub>-C<sub>4</sub>), they proceed under extremely high temperatures (500-900 °C) and with very low product selectivity. On the other hand, tremendous progress has been made in the field of homogeneous catalysts in the past 35 years. Nowadays the most successful systems are the class of the thermally stable pincer-type Ir complexes. Despite its wider substrate scope and moderate product selectivity, the homogeneous alkane dehydrogenation reaction still suffers from relatively harsh reaction conditions due to the elevated operating temperatures required for the thermal approaches (usually >150 °C); on the other hand, photochemical approaches have the problem of a difficult application on a large-scale. Alternative thermal approaches using titanium base-metal have been developed, but they are either multi-step stoichiometric transformations or require the use of expensive hydrogen acceptor to drive the reaction. Indeed, the development of a milder methodology is desirable.

The aim of the project was to develop a mild sonochemical alkane dehydrogenation process, providing a more energy and cost-effective route to the corresponding olefins. The innovation with respect to the state of art will consist in the activation of the substrate through the ultrasonic treatment of the reaction solution at room temperature. This process takes place in the presence of a homogeneous complex operating at the cavitation interface to mediate the transformation of the alkane into the corresponding alkene.

Thus, this chapter is aimed to develop and improve the following sonochemical system:



Scheme 2.5 General scheme for the sonochemical alkane transfer dehydrogenation.

## 2.2 Design of the apparatus

The instrument used to generate the ultrasound is a sonic dismembrator (Fisher Scientific™ Model 705). It is composed of a generator, a converter and the horn/probe with the replaceable tip (Figure 2.2). For reactions that can be performed under air, the probe is directly inserted into the reaction vessel as depicted in Figure 2.2 and immersed into the solution for few millimetres according to the probe size. To perform a reaction under air, the only requirement for the reaction vessel is to have high walls to contain the solution once it is agitated by the ultrasound. However, the catalytic alkane dehydrogenation reactions need to be performed under inert atmosphere to avoid catalyst decomposition, indeed in this case the reaction vessel had to be connected to the horn, sealing any possible opening. Hence, a suitable reactor had to be developed in order to be able to perform the reactions under inert atmosphere. The development of this reactor has been based on custom-built sonochemical reactors which have been reported in the literature.<sup>102</sup> A 25 mL round-bottom flask was used for the sonochemical experiments. The vessel had a side-arm with a Teflon-ring lined glass stopper or a silicon rubber septum for sample addition and extraction without exposing the reaction mixture to air. The instrument generates an electrical signal which is converted by the transducer to a mechanical vibration, this vibration is transmitted down the length of the horn where the tip longitudinally expands and contracts. Because of this movement the glass flask could not be directly connected to the horn. At first, a rubber septum was used to connect the flask to the horn. Different septum materials were also tested, but all of them were burnt after few seconds because of the high frictional heat produced by the intense vibration of the horn. The best approach was found by employing a rigid PTFE sleeve to connect the neck of a flask adapter to the tip. Moreover, the flask adapter was equipped with a PTFE screw-thread connector, allowing to connect the entire system to the Schlenk line through a rubber hose (Figure 2.3). Flask adapters with different lengths have been tested to find the optimal one, able to guarantee that the horn was immersed into the solution by one and a half length its tip diameter, the optimal depth as per specification of the instrument to guarantee efficient power delivery. Throughout the time of sonication, the microtip was cooled by a continuous stream of compressed air at its conjunction with the reactor.

The reactor developed had some limitations as it was not completely air tight. Although there was a PTFE sleeve between the glassware part and the microtip and the glassware connections were equipped with 2 PTFE rings, over time the up and down movement of the microtip caused small leaks of air into the system which could not be controlled and led to the decomposition of the complex (Section 2.7.1.2). To solve this problem a new custom-

made reactor was developed in collaboration with QSONICA (Figure 2.4). However, its realisation would have been too expensive and for that reason this solution has been abandoned.



Figure 2.2 Fisher Scientific™ FB-705 Sonic dismembrator components description

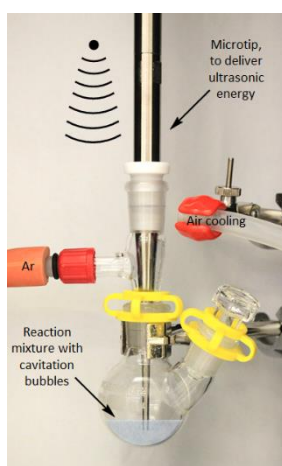


Figure 2.3 Sonochemical reactor used.

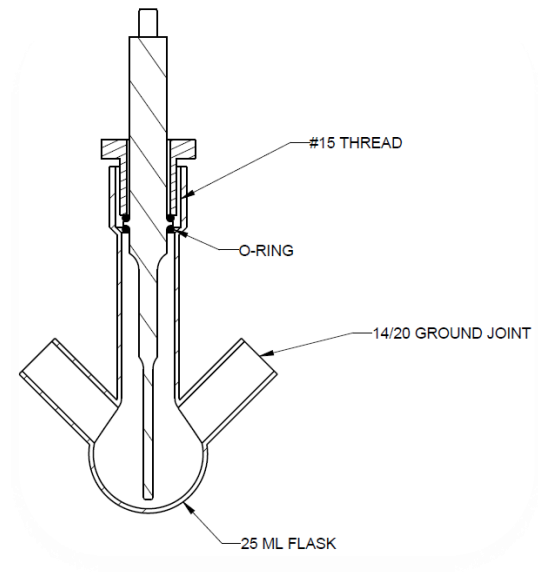


Figure 2.4 Drawing of the new custom reactor developed in collaboration with QSONICA.

## 2.3 Initial screening of complexes

In order to develop a system for the sonochemical alkane dehydrogenation, as a starting point, the complexes to be tested as catalysts had to be chosen and synthesised. Due to the similarities between thermal, photochemical and sonochemical activation, the catalysts reported in the literature to be the best ones for the thermal and photochemical alkane dehydrogenation were chosen. Then these complexes were tested for the sonochemical alkane dehydrogenation using the proper sonochemical reactor previously developed. Along with these reactions, an analytical method for the quantitative analysis of those was also optimised.

### 2.3.1 Synthesis of thermally and photochemically active catalysts

The first step was to choose the model highly active homogeneous alkane dehydrogenation catalysts for the envisioned sonochemical dehydrogenation. On one hand, ultrasonic irradiation of liquids produces acoustic cavitation: the rapid formation, growth and implosive collapse of vapour filled microbubbles. This generates short-lived *hot spots* with peak temperatures of up to 5000 °C and nanosecond lifetimes. These extraordinary high temperatures created during the microbubble implosion, give rise to a similarity between sonochemistry and thermal activation. On the other hand, as previously described, the effect of ultrasound on some complexes causes the general phenomenon of ligand dissociation, as happens in many photochemical reactions. Due to the similarities between thermal, photochemical and sonochemical activation, the complexes that were tested in the first place are those highly active in the corresponding thermal or photochemical reactions and they are reported in Figure 2.5.

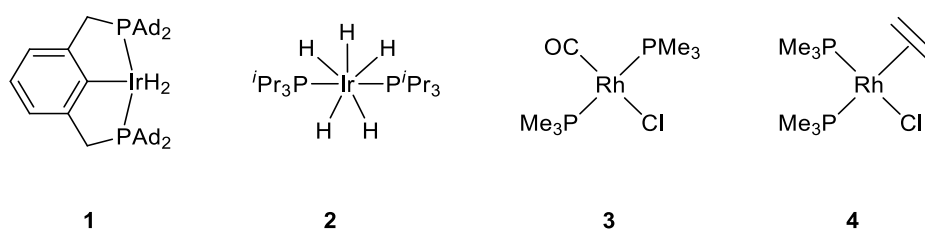
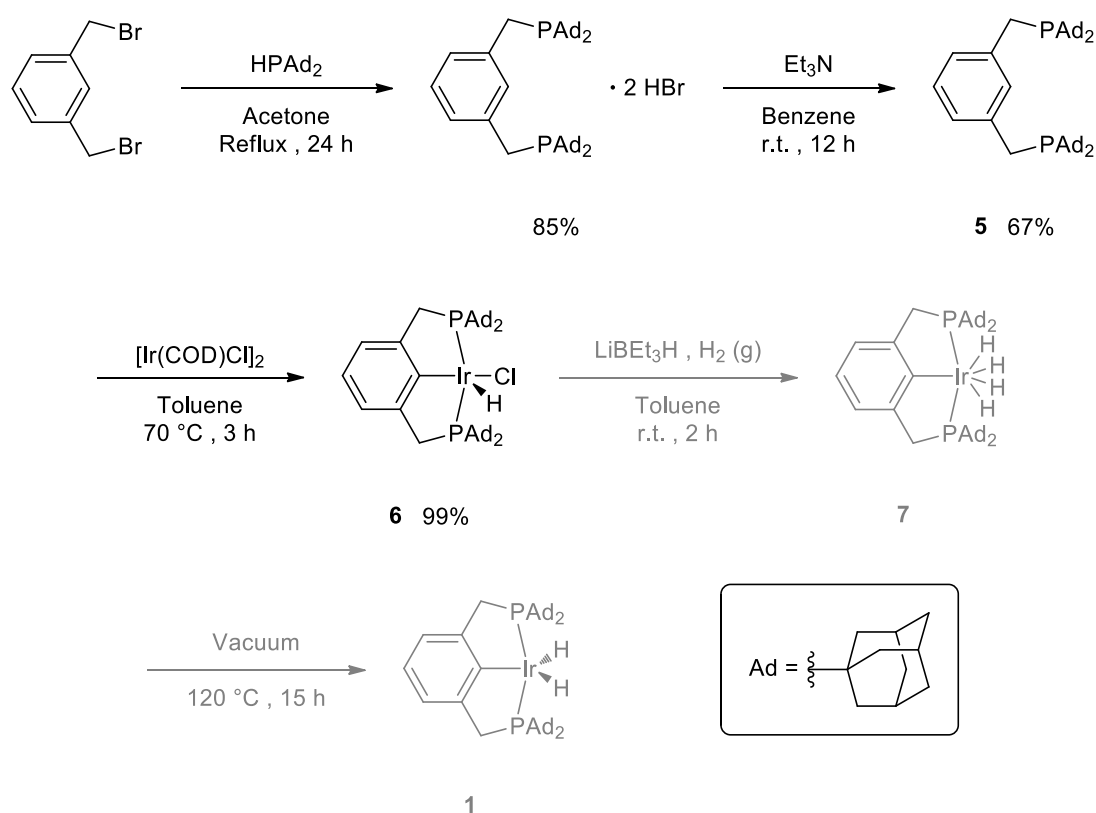


Figure 2.5 Thermally or photochemically active catalyst to be tested for the sonochemical alkane dehydrogenation.

The complex (<sup>Ad</sup>PCP)IrH<sub>2</sub> (**1**) has catalytic activity comparable with other PCP-Ir catalysts, but it was chosen because of its much higher thermal stability, thanks to the adamantyl groups that prevent catalyst deactivation. Its synthesis was described by Goldman,<sup>56</sup> who also

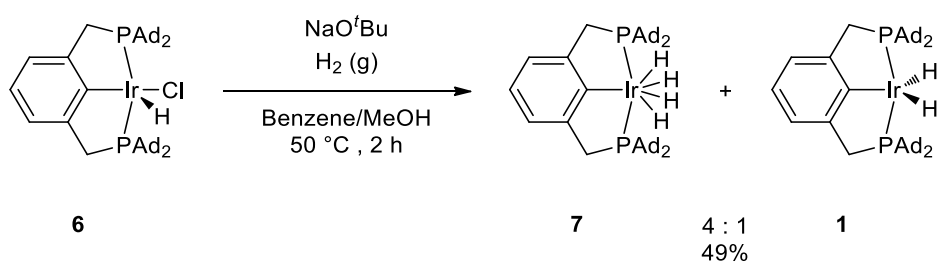
tested it for the acceptorless dehydrogenation of cyclodecane and *n*-dodecane. To synthesise the complex, the same synthetic approach (Scheme 2.6) has been applied. The ligand **5** was synthesised by reaction of 1,3-dibromoxylene with di-1-adamantylphosphine, the obtained product was purified in the presence of triethylamine. Complexation of the ligand to yield the pincer-iridium complex **6** was achieved using  $[\text{Ir}(\text{COD})\text{Cl}]_2$  dimer as the iridium source. The pincer-iridium complex **6** could then be converted into the desired hydrides **7** and **1** by treatment with the superhydride  $\text{LiBEt}_3\text{H}$  under hydrogen atmosphere at room temperature. The first three steps proceeded smoothly, but unfortunately, the last steps in order to cleanly obtain the desired dihydride complex **1** were not successfully performed.



Scheme 2.6 Synthesis of  $(\text{AdPCP})\text{IrHCl}$  (**6**) and attempts for the synthesis of  $(\text{AdPCP})\text{IrH}_2$  (**1**).

In order to successfully perform the last hydrogenation step, many synthetic pathways were investigated, varying the reagents and reaction conditions (ratios, temperature and pressure), but in every attempt a mixture of complexes **6**, **7** and **1** was obtained. A brand new superhydride has been purchased from another supplier, to be sure that the problem was not decomposed  $\text{LiBEt}_3\text{H}$ . A different approach has been tested, by using  $\text{NaO}^t\text{Bu}$  or  $\text{KO}^t\text{Bu}$  in benzene under  $\text{H}_2$  atmosphere at room temperature. The two bases were used separately both in slight and large excess. The synthesis was performed at higher temperature, or performed in a sealed Schlenk bomb, but in every case a mixture of products and unreacted

reagent was obtained. The reaction progress was also monitored by NMR under the different conditions in order to find the best way to shift the equilibrium; but in all the experiments, after some time the displacement of the chloride stopped to proceed and even after 2 days a considerable amount of the complex **6** was still present. Moreover, to make sure this incomplete conversion was not due to the solvents not being dry enough, a Karl-Fisher Titration was performed on both dry toluene and benzene, but in both cases the amount of water detected was below 10 ppm. Addition of trace amounts of water was also tested. In fact, for the synthesis reported in the literature the authors could have used a “wet” solvent and the trace amount of water could have facilitated the chloride abstraction *via* hydrogen bonding. Based on this same idea, addition of methanol from trace amounts to excess was also tested. This hypothesis appeared to be correct and after optimisation of the reaction conditions, full conversion of complex **6** was obtained with a benzene/MeOH ratio of 2:1 at 50 °C for 3 hours (Scheme 2.7) in the presence of NaO<sup>t</sup>Bu and H<sub>2</sub>. The product was obtained as a mixture of the tetra-hydride **7** and dihydride species **1** in 49% yield with a 4:1 ratio. Attempts in the conversion of **7** into **1** was performed by heating the mixture at 120 °C under vacuum as described in the literature.<sup>56</sup> Unfortunately, all lead to product decomposition even at lower temperature. Therefore, the complex was used in the sonochemical experiments as a mixture of the two hydride species **7** and **1**. Using the dihydride/tetrahydride mixture for the catalysis experiments has already been reported in the literature to give satisfactory results.<sup>111</sup>



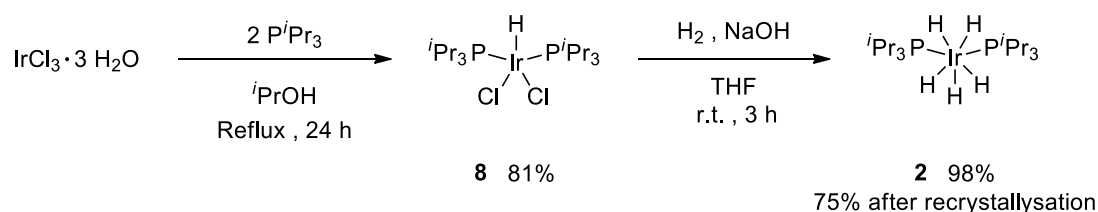
Scheme 2.7 Synthesis of Ir(<sup>Ad</sup>PCP)H<sub>4</sub> / Ir(<sup>Ad</sup>PCP)H<sub>2</sub> (7/1).

Complex **6** was also used in the sonochemical tests, together with NaO<sup>t</sup>Bu, in order to generate *in situ* the catalytically active 14 electron species [Ir(<sup>Ad</sup>PCP)]. This approach was already applied to many other (PCP)IrHCl complexes.<sup>25</sup> In the paper Goldman and co-workers also reported that the Ir(<sup>Ad</sup>PCP)HCl complex was obtained in a 70:30 ratio with its analogue Ir(<sup>Ad</sup>PCP)HBr,<sup>56</sup> with the bromide impurity coming most probably from the ligand synthesis (bromide ions from the HBr impurity, not fully eliminated by the purification with triethylamine). To use complex **6** in the sonochemical reaction, this should have been clean



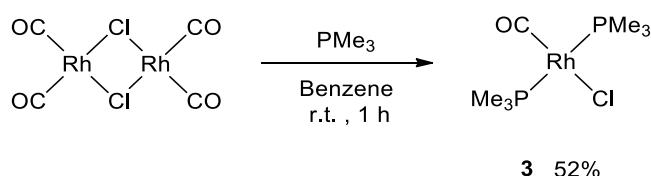
and 100% pure. Therefore, ligand **5** had to be purified before using it in the complexation step. After different attempts, a recrystallization procedure from chloroform and methanol was optimised and the ligand **5** was obtained in 67% yield. The purified phosphine **5** was then employed in the synthesis of **6**, the Ir(<sup>Ad</sup>PCP)HCl species was obtained with no other impurities.

The Ir(P<sup>*i*</sup>Pr<sub>3</sub>)<sub>2</sub>H<sub>5</sub> complex (**2**) was also synthesised according to the literature procedure.<sup>112</sup> This has been reported to be one of the first complexes found to be active for the catalytic homogeneous transfer dehydrogenation.<sup>39</sup> The literature method for its synthesis was improved slightly by adding a recrystallization step of the final isolated complex in order to decrease the variation between different batches. In fact, it was observed that the colour of different batches can vary from off-white to light-brown due to very small amount of impurities, not detectable by NMR spectroscopy. However, after the recrystallisation step, the final complex **2** was isolated as clear colourless crystals from all batches. The recrystallisation was performed from hexane layered with methanol in 1:3 ratio with an overall yield of 75% (Scheme 2.8).



Scheme 2.8 Synthesis of Ir(P(*i*Pr<sub>3</sub>)<sub>2</sub>H<sub>5</sub>) (**2**).

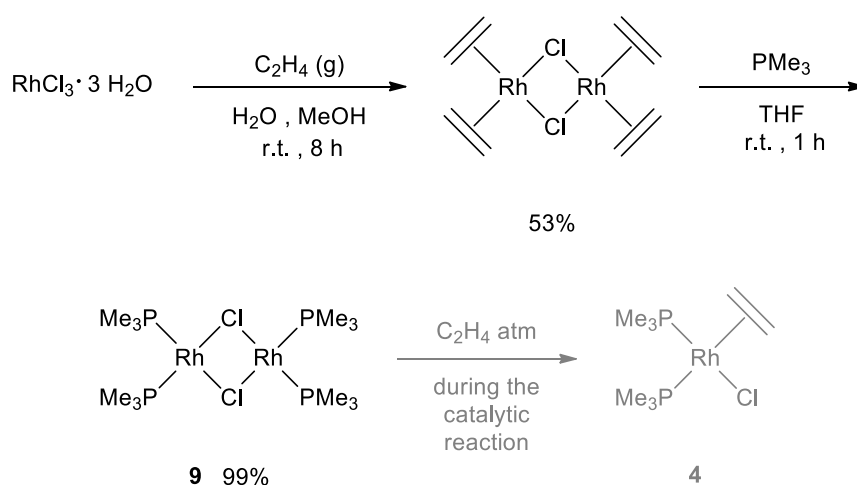
Then, some catalysts active in the photochemical alkane dehydrogenation were chosen: complex Rh(CO)(PMe<sub>3</sub>)<sub>2</sub>Cl (**3**) active under UV light<sup>66, 70</sup> and complex Rh(C<sub>2</sub>H<sub>4</sub>)(PMe<sub>3</sub>)<sub>2</sub>Cl (**4**) active under visible light irradiation.<sup>63-65</sup> The first one was synthesised from [Rh(CO)<sub>2</sub>Cl]<sub>2</sub> dimer according to synthetic procedures reported in the literature<sup>113-114</sup> (Scheme 2.9).



Scheme 2.9 Synthesis of complex Rh(CO)(PMe<sub>3</sub>)<sub>2</sub>Cl (**3**).

The second photocatalyst **4**, that is the catalytically active species, cannot be isolated because it rapidly decomposes when brought to dryness. Therefore, for the sonochemical reactions, complex **4** was prepared *in situ* from [Rh(PMe<sub>3</sub>)<sub>2</sub>Cl]<sub>2</sub> (**9**) under ethylene atmosphere,<sup>64</sup> whose function was both to activate the catalyst and to act as the hydrogen

acceptor. The dimeric precursor **9** was obtained as described in the literature (Scheme 2.10).<sup>115-118</sup> Some difficulties were encountered during the synthesis and characterisation of dimer **9** as not well described in the literature. The NMR spectra first recorded in  $d^8$ -toluene or  $d^1$ -chloroform showed a decomposed compound, most probably due to the complex undergoing oxidative addition with the solvent. When  $d^6$ -benzene was used, as reported in the literature,<sup>117</sup> clean spectra were obtained, but the  $^{31}\text{P}$ -NMR spectrum showed unusual chemical shifts and a very broad peak. This was probably due to the coalescence between the signals of the free and the complexed triphenylphosphine. However, mass spectrometry confirmed the desired complex was obtained.



Scheme 2.10 Synthesis of  $[\text{Rh}(\text{PMe}_3)_2\text{Cl}]_2$  (**9**).

### 2.3.2 Screening of complexes

Once a reliable reactor was developed and the catalysts to be tested were synthesised, the sonochemical alkane dehydrogenation was addressed. To the best of our knowledge, this type of alkane dehydrogenation has never been attempted before, since no examples are reported in the literature, *n*-dodecane dehydrogenation was chosen as model reaction to test the complexes. Before beginning to test the complexes, the stability of *n*-dodecane under ultrasound treatment had to be evaluated. It has been previously reported in the literature that alkanes, when subjected to ultrasound irradiation, undergo a series of C-C bond cleavage and radical rearrangements, releasing as the main products hydrogen, methane, ethylene and acetylene.<sup>119-120</sup> However some considerations need to be made on those results. In fact, formation of those species is in the order of micromolar concentrations in neat alkane and their formation was observed after prolonged sonication of over 50 hours.

When *n*-dodecane was subjected to sonication with the ultrasonic processor developed in this project, it did not appear to undergo any detectable degradation, therefore it was chosen as the model alkane substrate. The previously synthesised catalysts were assessed for the sonochemical dehydrogenation of *n*-dodecane (Figure 2.6). Together with the synthesised complexes, the activity of other commercially available complexes was investigated, such as Vaska complex (**11**) and Wilkinson catalyst (**12**) as those are structurally similar to the other chosen complexes. Moreover, complex **2** was examined alone and also in conjunction with the free <sup>*i*</sup>PrPCP phosphine, in order to generate *in situ* the corresponding Ir(<sup>*i*</sup>PrPCP)<sub>2</sub> complex (**10**). Complex **10** was in fact reported to be one of the most active catalysts for the thermal alkane dehydrogenation, even if not one of the most thermally stable.<sup>24</sup>

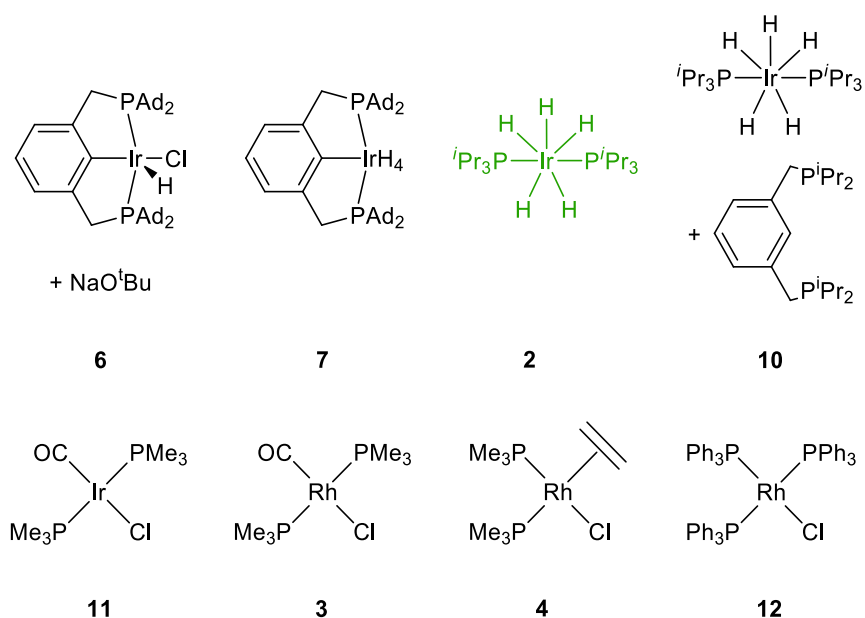


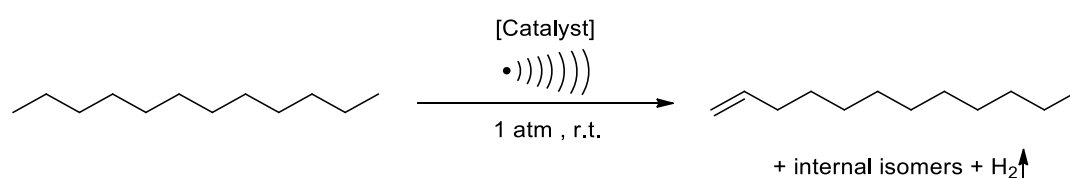
Figure 2.6 Complexes tested as catalysts for the alkane dehydrogenation.

For the sonochemical tests, a water bath was employed to cool down the reaction mixture, in order to maintain the solution at room temperature as high temperatures reduce the cavitation. In fact, the sonic dismembrator used for the experiments is a powerful equipment releasing a high amount of energy *via* ultrasound irradiation. Part of this energy is released in the form of heat, which causes the temperature of the solution to increase substantially if it is not allowed to properly dissipate. Thus, the need for a water bath to keep the reaction temperature under control. The water bath used is not temperature controlled, therefore room temperature means 25 ± 3 °C.

All the results for the sonochemical tests are reported in Table 2.1 and Table 2.2. To begin with, an amplitude of 50% was chosen; amplitude is a measurement of the excursion of the tip of the probe and it is directly proportional to the intensity of ultrasound. Because the

amount of energy delivered with ultrasound per unit of time is extremely high, the reactions were initially analysed after 10 minutes of sonication. Longer sonication times were also tested. The time reported in Table 2.1 and Table 2.2 is active sonication time, while the overall time of the reaction is higher (total reaction time = active sonication time x 2 - 10 mins). This is because, as already mentioned, delivering a high amount of energy causes the system to overheat. For this reason, the sonication was turned on and off every other 10 minutes. The catalyst concentration chosen was 1 mM, taking again as reference the paper by Goldman.<sup>56</sup> Before subjecting the reaction mixture to ultrasound irradiation, it was sonicated in a classic ultrasound bath for few seconds until all the complex was solubilised. All complexes tested were fully soluble in *n*-dodecane unless noted otherwise.

Table 2.1 Sonochemical *n*-dodecane acceptorless dehydrogenation by different complexes.



| Entry | t (min) | Catalyst   | TON <sup>a</sup> |
|-------|---------|--|------------------|
| 1     | 10      | Rh(PMe <sub>3</sub> ) <sub>2</sub> (CO)Cl ( <b>3</b> ) | < 0.1            |
| 2     | 10      | Ir( <sup>Ad</sup> PCP)HCl ( <b>6</b> ) <sup>b</sup>    | < 0.1            |
| 3     | 20      | Ir( <sup>Ad</sup> PCP)HCl ( <b>6</b> ) <sup>b</sup>    | < 0.1            |

Experimental conditions: reactions are carried out in neat *n*-dodecane (5 mL) at room temperature (25 ± 3 °C), under argon atmosphere, with a water cooling bath and with the microtip being cooled by a continuous stream of compressed air. The system is equipped with an outlet needle on the side neck of the flask in order to allow to perform the reaction under a stream of argon. Complex concentration is 1 mM. Amplitude is 50%. (a) TONs and are based on quantitative GC analysis using isooctane as the internal standard. (b) NaO<sup>t</sup>Bu (1.2 eq. with respect to the complex) is added to the reaction mixture in order to activate complex **6**.

The photocatalyst **3** and the thermally active catalyst **6**, together with NaO<sup>t</sup>Bu as the base for activation, were tested for both the acceptorless and the transfer *n*-dodecane dehydrogenation. First the acceptorless dehydrogenation was investigated as more desirable. For this type of dehydrogenation, the system was also equipped with an outlet needle on the side neck of the flask in order to allow the reaction to be performed under a flow of argon. This was required to expel the hydrogen produced during the acceptorless dehydrogenation and push the equilibrium of the reaction towards the products. To start with, complexes **3** and **6** were tested with 50% amplitude and for 10 minutes of sonication

(Table 2.1, entries 1 and 2). When using either of the complexes, no formation of dodecenes was observed. Doubling the reaction time to 20 minutes of active continuous sonication for the acceptorless *n*-dodecane dehydrogenation with **6** and base also did not lead to any product formation (Entry 3).

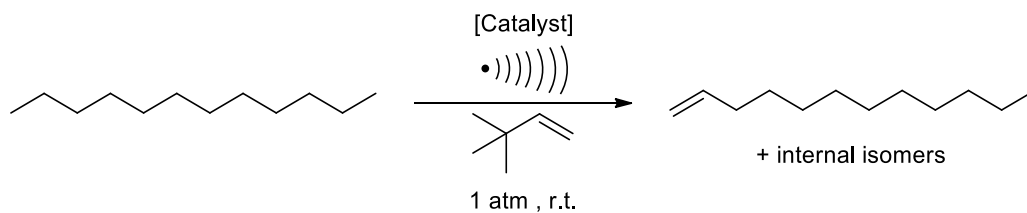
Due to no positive results, the same complexes were tested for the sonochemical transfer dehydrogenation, again with 50% amplitude and 10 minutes of sonication (Table 2.2, entries 1 and 2). Formation of the desired product was not observed; indeed, the focus was directed on the investigation of complex **6**: the amplitude was increased first to 80% and then to 100% (Entries 3 and 4), but once again no positive results were obtained. The catalyst loading was then increased from 1 to 5 mM (Entry 5) maintaining the amplitude at 50%, but still no product was observed. Therefore, the amplitude was increased to 100%, and the reaction time extended up to 1 hour of active sonication time (Entries 6-8), but the result did not change. Recovering the complex **6** after the sonochemical reaction showed that it did not undergo any activation under sonochemical conditions, despite the addition of NaO<sup>t</sup>Bu, meaning that it was not converted to the corresponding hydride catalyst **7** or **1**. During the thermocatalytic reactions instead, by the mean of NaO<sup>t</sup>Bu, the catalyst was converted to the corresponding dihydride species, the catalytically active complex. Under sonochemical conditions instead, it seemed that the NaO<sup>t</sup>Bu was not able to activate the complex. This could be due to the poor solubility of NaO<sup>t</sup>Bu in *n*-dodecane at room temperature, preventing the reaction with the complex, and indeed the activation. If complex **6** was not converted into the active species **1**, this could be the reason why this specific PCP-type catalyst was not active under ultrasound. Therefore, using directly the dihydride species in the sonochemical reaction could be the solution. Other catalysts planned to be investigated (**9**, **11**, **2** and **10**) are then tested with 50% amplitude for 10 minutes (Entries 9-12) none of them showing activity under these conditions. The same complexes, together with **3** and **7**, are evaluated increasing the amplitude setting to 100% and the time to 1 hour of sonication (Entries 13-18). Results are all negative except for the iridium pentahydride catalyst **2** with a turnover number of 0.93 (Entry 16). Together with those complexes, also **7** is assessed under the same conditions, but unfortunately it was not soluble in *n*-dodecane even after sonication in the sonicating bath, routinely performed before each reaction to fully solubilise the complex obtaining a homogeneous solution. Nevertheless, the reaction mixture appeared as a heterogenous solution, complex **7** is tested anyway showing no ability to dehydrogenate the dodecane (Entry 18). The Ir(<sup>i</sup>PrPCP)H<sub>2</sub> (**10**) complex is proposed to be generated directly *in situ*, through a ligand exchange between the phosphines of complex **2** and <sup>i</sup>PrPCP-H, reaction

that is entropically favoured (Entries 12 and 17). It has been decided to attempt to generate complex **10** upon mixing **2** and the pincer ligand due to previous difficulties in the synthesis and isolation of pincer-iridium-hydride complexes. For both tests performed in entries 12 and 17, no dodecenes formation is observed. As the pentahydride complex **2** itself is active under the conditions employed in entry 16 and no product is observed with the addition of the free PCP-phosphine (Entry 17), can be concluded that complex **2** is most probably reacting with the free pincer-phosphine to form the desired complex **10**, however it is not active for this kind of transformation under ultrasound.

To summarise, from the catalyst screening can be concluded that for the sonochemical *n*-dodecane transfer dehydrogenation, the photocatalytically active catalysts **3** and **4** seem to be inactive towards alkane dehydrogenation under sonochemical conditions. The same can be said for the pincer-type iridium complexes **6**, **7** and **10**; however up to date this class of complexes is the one reported to be best one for alkane dehydrogenation under thermocatalytic conditions. Instead the iridium penta-hydride complex **2** is the only one showing activity for the alkane dehydrogenation under sonochemical conditions, nevertheless its poor thermal activity compared to pincer-iridium complexes.

Worth to mention is that this complex does not form any dehydrogenation product at lower amplitude for 10 minutes of sonication (Entry 11), but when the intensity is increased to 100% amplitude and the reaction mixture treated with ultrasound for 1 hour, dodecenes are detected and a TON of 0.9 is obtained (Entry 16). Therefore, the unique activity of this iridium-pentahydride complex is further investigated with the optimisation of the reaction conditions.

Table 2.2 Screening of complexes for the sonochemical *n*-dodecane transfer dehydrogenation.



| Entry | A (%) | t (min) | Catalyst  | C <sub>cat</sub> (mM) | TON <sup>a</sup> |
|-------|-------|---------|---|-----------------------|------------------|
| 1     | 50    | 10      | Rh(PMe <sub>3</sub> ) <sub>2</sub> (CO)Cl ( <b>3</b> )  | 1                     | < 0.1            |
| 2     | 50    | 10      | Ir( <sup>Ad</sup> PCP)HCl ( <b>6</b> ) <sup>b</sup>   | 1                     | < 0.1            |
| 3     | 80    | 10      | Ir( <sup>Ad</sup> PCP)HCl ( <b>6</b> ) <sup>b</sup>   | 1                     | < 0.1            |
| 4     | 100   | 10      | Ir( <sup>Ad</sup> PCP)HCl ( <b>6</b> ) <sup>b</sup>   | 1                     | < 0.1            |
| 5     | 50    | 10      | Ir( <sup>Ad</sup> PCP)HCl ( <b>6</b> ) <sup>b</sup>   | 5                     | < 0.1            |
| 6     | 100   | 10      | Ir( <sup>Ad</sup> PCP)HCl ( <b>6</b> ) <sup>b</sup>   | 5                     | < 0.1            |
| 7     | 100   | 20      | Ir( <sup>Ad</sup> PCP)HCl ( <b>6</b> ) <sup>b</sup>   | 5                     | < 0.1            |
| 8     | 100   | 60      | Ir( <sup>Ad</sup> PCP)HCl ( <b>6</b> ) <sup>b</sup>   | 5                     | < 0.1            |
| 9     | 50    | 10      | [Rh(PMe <sub>3</sub> ) <sub>2</sub> Cl] <sub>2</sub> ( <b>9</b> ) <sup>c</sup>                                  | 1                     | < 0.1            |
| 10    | 50    | 10      | Ir(PMe <sub>3</sub> ) <sub>2</sub> (CO)Cl ( <b>11</b> )   | 1                     | < 0.1            |
| 11    | 50    | 10      | Ir(P <sup>i</sup> Pr <sub>3</sub> ) <sub>2</sub> H <sub>5</sub> ( <b>2</b> )                                    | 1                     | < 0.1            |
| 12    | 50    | 10      | Ir(P <sup>i</sup> Pr <sub>3</sub> ) <sub>2</sub> H <sub>5</sub> + <sup>i</sup> PrPCP ( <b>10</b> ) <sup>d</sup> | 1                     | < 0.1            |
| 13    | 100   | 60      | Rh(PMe <sub>3</sub> ) <sub>2</sub> (CO)Cl ( <b>3</b> )  | 1                     | < 0.1            |
| 14    | 100   | 60      | [Rh(PMe <sub>3</sub> ) <sub>2</sub> Cl] <sub>2</sub> ( <b>9</b> ) <sup>c</sup>                                  | 1                     | < 0.1            |
| 15    | 100   | 60      | Ir(PMe <sub>3</sub> ) <sub>2</sub> (CO)Cl ( <b>11</b> )   | 1                     | < 0.1            |
| 16    | 100   | 60      | Ir(P <sup>i</sup> Pr <sub>3</sub> ) <sub>2</sub> H <sub>5</sub> ( <b>2</b> )                                    | 1                     | 0.9              |
| 17    | 100   | 60      | Ir(P <sup>i</sup> Pr <sub>3</sub> ) <sub>2</sub> H <sub>5</sub> + <sup>i</sup> PrPCP ( <b>10</b> ) <sup>d</sup> | 1                     | < 0.1            |
| 18    | 100   | 60      | Ir( <sup>Ad</sup> PCP)H <sub>4</sub> ( <b>7</b> )   | 1                     | < 0.1            |
| 19    | 100   | 60      | Rh(PPh <sub>3</sub> ) <sub>3</sub> Cl ( <b>12</b> )   | 1                     | < 0.1            |

Experimental conditions: reactions are carried out in neat *n*-Dodecane (5 mL) at room temperature (25 ± 3 °C), under argon atmosphere, with a water cooling bath and with the microtip being cooled by a continuous stream of compressed air. TBE concentration is 0.1 M. (a) TONs and are based on quantitative GC analysis using isoctane as the internal standard. (b) NaO<sup>t</sup>Bu (1.2 eq. with respect to the complex) is added to the reaction mixture in order to activate complex **6**. (c) Providing the system with an inlet and outlet needle, ethylene (1 atm) is bubbled through the solution during the reaction to generate the catalytically active complex **4**, fulfilling also the role of hydrogen acceptor instead of TBE. (d) Attempt in the generation of Ir(<sup>i</sup>PrPCP)H<sub>2</sub> in situ from Ir(P<sup>i</sup>Pr<sub>3</sub>)<sub>2</sub>H<sub>5</sub> and the free phosphine <sup>i</sup>PrPCP-H (1.5 eq. with respect to the complex).

## 2.4 Optimisation of the reaction conditions for the sonochemical experiments

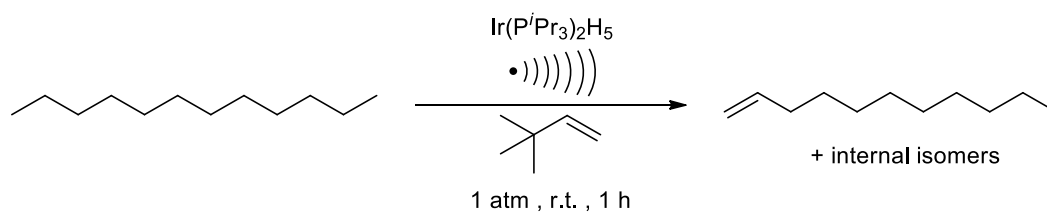
Once an active complex for the sonochemical alkane dehydrogenation has been identified, efforts have been focused on improving the yields of the system. The transfer dehydrogenation of *n*-dodecane is chosen again as model reaction to be optimised by systematically varying the different parameters of the system. The model reaction has been tested at different catalyst and TBE concentrations, amplitude settings and reaction times. Below are the details for the different optimisation processes. In the end a catalyst concentration of 5 mM and a reaction time of 1 hour have been chosen as benchmark conditions with an optimal TBE/catalyst ratio of 20 under 100% amplitude.

### 2.4.1 Optimization of the concentration of the complex

At first, the effect of the concentration of the complex on the sonochemical transfer *n*-dodecane dehydrogenation was investigated. Results are reported in Table 2.3. The catalyst loading was increased from 1 mM to 5 mM, with a rise of the activity of the system from 0.93 to 1.20 TON (Entries 1 and 2). Further increments in the concentration of the pentahydride complex to 50 mM seem to have a detrimental effect (Entry 3). It is worth to note that when the concentration of the iridium complex is increased, therefore the TBE/Ir ratio decreases and indeed, for the experiment reported in entry 3, only 2 equivalents of hydrogen acceptor (TBE) are available per molecule of iridium complex. Indeed, to ensure that the detrimental effect is not due to the low amount of hydrogen acceptor available per equivalent of iridium, the concentration of TBE was also increased to 1 M to compensate the increment in the amount of iridium complex (Entry 4) (the importance of the amount of TBE will be further explained in the following Section 2.4.2). The TON for the test with increased TBE/Ir ratio improved slightly, however with a value of 0.41 (Entry 4), it is still much smaller than the result with lower catalyst loadings (Entry 2).



Table 2.3 Optimisation of complex concentration for the sonochemical *n*-dodecane transfer dehydrogenation promoted by Ir(P<sup>*i*</sup>Pr<sub>3</sub>)<sub>2</sub>H<sub>5</sub> (**2**).



| Entry | TBE/Ir | C <sub>Ir</sub> (mM) | TON <sup>a</sup> |
|-------|--------|----------------------|------------------|
| 1     | 100    | 1                    | 0.93             |
| 2     | 20     | 5                    | 1.20             |
| 3     | 2      | 50                   | 0.20             |
| 4     | 20     | 50                   | 0.41             |

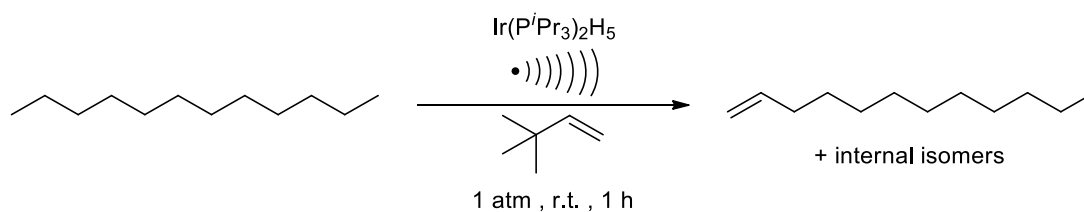
Experimental conditions: reactions are carried out in neat *n*-dodecane (5 mL) at room temperature (25 ± 3 °C) for 1 h, under argon atmosphere, with a water cooling bath and with the microtip being cooled by a continuous stream of compressed air. Amplitude is 100%. TBE concentration is 0.1 M except for entry 4 where is 1 M. (a) TONs are based on quantitative GC analysis using isooctane as the internal standard.

## 2.4.2 Influence of TBE concentration

The influence of the *tert*-butylethylene concentration on the system activity was evaluated and results are reported in Table 2.4. From the results reported in the table, the activity of the system shows a clear trend with an initial increase in activity with the increase of the TBE concentration from 0 to 0.10 M (Entries 1 and 2). However, a further increase in the TBE concentration causes a drop in the system activity (Entries 3 and 4). This is consistent with literature data, which have already shown the importance of a fine tune of the amount of TBE used, in fact it was found that the transfer dehydrogenation can be inhibited by excess TBE.<sup>23, 46, 48</sup> Optimisation of the concentration of the hydrogen acceptor showed without any doubt that for the sonochemical system investigated the optimal TBE/iridium ratio is 20:1 (Entry 2). Indeed, under sonochemical conditions, a lower concentration of TBE seems to be optimal as opposed to similar reactions under thermal conditions. In fact, in the latter, the best TBE/iridium ratio is reported to be 100:1 when iridium pincer-complexes are used as catalysts.<sup>24</sup> An explanation for that can be that under sonochemical conditions the reaction takes place in the hotspot, arising from the implosion of a cavitation bubble. The cavitation bubble is formed predominantly by TBE as it is the compound with lower boiling point of the system investigated. From this, it can be inferred that the hotspot has a higher local TBE

concentration with respect to the bulk of the solution and consequently a presumably higher local TBE/Ir ratio. This can justify why the sonochemical system is active at an apparent lower TBE/Ir ration, compared to the literature example under thermal conditions.

Table 2.4 Optimisation of TBE concentration for the sonochemical *n*-dodecane transfer dehydrogenation promoted by Ir(P<sup>*i*</sup>Pr<sub>3</sub>)<sub>2</sub>H<sub>5</sub> (**2**).



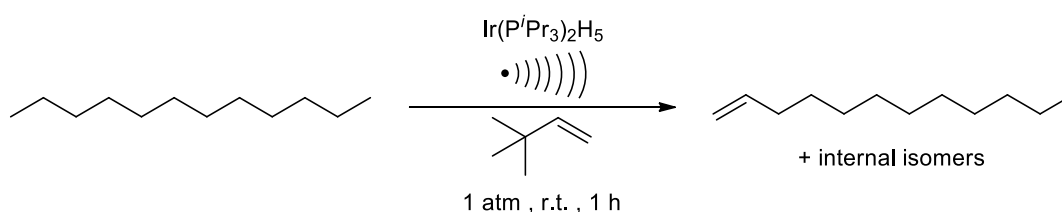
| Entry | TBE/Ir | C <sub>TBE</sub> (M) | TON <sup>a</sup> |
|-------|--------|----------------------|------------------|
| 1     | 10     | 0.05                 | 0.50             |
| 2     | 20     | 0.10                 | 1.20             |
| 3     | 100    | 0.50                 | 0.29             |
| 4     | 200    | 1.00                 | 0.15             |

Experimental conditions: reactions are carried out in neat *n*-dodecane (5 mL) at room temperature (25 ± 3 °C) for 1 h, under argon atmosphere, with a water cooling bath and with the microtip being cooled by a continuous stream of compressed air. Amplitude is 100%. Ir(P<sup>*i*</sup>Pr<sub>3</sub>)<sub>2</sub>H<sub>5</sub> concentration is 5 mM. (a) TONs are based on quantitative GC analysis using isooctane as the internal standard.

### 2.4.3 Amplitude optimization

The effect of the applied power, as ultrasound amplitude, was investigated. An increase of the amplitude showed highly significant positive effects on the TON of the reaction investigated and the results are reported in Table 2.5. Doubling the amplitude percentage from 50 to 100% resulted in almost a double TON for the dodecane dehydrogenation (Entries 2 and 3). To verify that the dehydrogenation was actually promoted by the ultrasounds, a test reaction has been stirred for the same amount of time without any ultrasonic treatment. Analysis of the sample showed that no significant amount of alkene products could be detected, confirming that the dehydrogenation was facilitated by the ultrasound irradiation.

Table 2.5 Optimisation of amplitude value for the sonochemical *n*-dodecane transfer dehydrogenation promoted by Ir(P<sup>i</sup>Pr<sub>3</sub>)<sub>2</sub>H<sub>5</sub> (**2**).



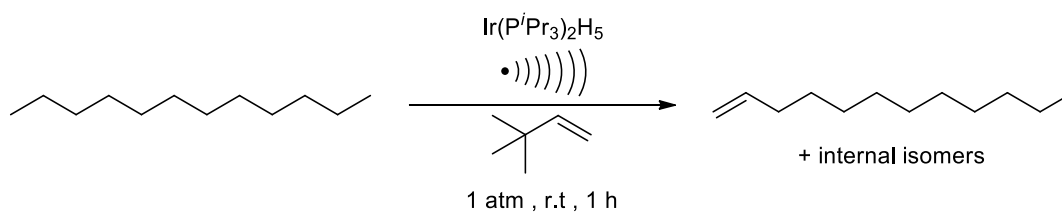
| Entry | A (%) | TON <sup>a</sup> |
|-------|-------|------------------|
| 1     | 0     | < 0.1            |
| 2     | 50    | 0.70             |
| 3     | 100   | 1.20             |

Experimental conditions: reactions are carried out in neat *n*-dodecane (5 mL) at room temperature (25 ± 3 °C) for 1 h of active sonication, under argon atmosphere, with a water cooling bath and with the microtip being cooled by a continuous stream of compressed air. Ir(P<sup>i</sup>Pr<sub>3</sub>)<sub>2</sub>H<sub>5</sub> concentration is 5 mM. TBE concentration is 0.1 M. (a) TONs are based on quantitative GC analysis using isooctane as the internal standard.

### 2.4.4 Time optimisation

Next, the reaction time was optimised. The results for such optimisation are reported in Table 2.6. As it can be observed from the data, the turnovers increased up to 1.2 TON for 1 hour of active sonication (Entry 5), after which time the reaction drastically slowed down, as it seemed to have reached a steady level (Entries 6-8). Indeed, even longer reaction times seemed not to be able to boost the dehydrogenation making the reaction catalytic.

Table 2.6 Optimisation of processing time for the sonochemical *n*-dodecane transfer dehydrogenation promoted by Ir(P<sup>i</sup>Pr<sub>3</sub>)<sub>2</sub>H<sub>5</sub> (**2**).



| Entry | t (h) | TON <sup>a</sup> |
|-------|-------|------------------|
| 1     | 0     | 0.00             |
| 2     | 0.2   | 0.38             |
| 3     | 0.3   | 0.65             |
| 4     | 0.7   | 0.94             |
| 5     | 1     | 1.20             |
| 6     | 2     | 1.22             |
| 7     | 3     | 1.27             |
| 8     | 4     | 1.28             |

Experimental conditions: reactions are carried out in neat *n*-dodecane (8 mL) at room temperature ( $25 \pm 3$  °C), under argon atmosphere, with a water cooling bath and with the microtip being cooled by a continuous stream of compressed air. The time reported in the table refers to the time of active sonication. Amplitude is 100%. Ir(P<sup>i</sup>Pr<sub>3</sub>)<sub>2</sub>H<sub>5</sub> concentration is 5 mM. TBE concentration is 0.1 M. At the required time, an aliquot of 0.5 mL of the reaction is taken and properly processed for analysis. (a) TONs are based on quantitative GC analysis using isooctane as the internal standard.

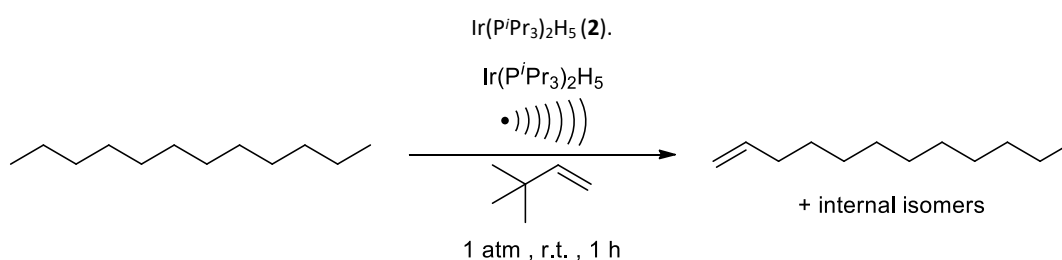
To investigate the reason for the modest TONs, the yield of alkene vs. reaction time was studied for different alkanes. In fact, the performance of the catalyst can be substrate specific and the concentration/time profiles for different alkanes were evaluated. A shorter alkane (*n*-hexane) and a cyclic one (cyclooctane, COA) have been chosen. From the graph in Figure 2.7 it can be observed that all three alkanes tested seemed to behave in a similar way, formation of the dehydrogenation product proceeded relatively fast for the first few minutes of the reaction up to 1 hour, after which the reaction seemed to stop. Comparing the trends for the first hour of reaction, *n*-hexane seemed to react faster compared to *n*-dodecane. On the other hand, cyclooctane appeared to be less active towards the dehydrogenation compared to the linear alkane. Initially, the reason for difficult improvement of the system was thought to be the reaction being only stoichiometric and not catalytic. However, an exactly similar deactivation trend over time for the cyclooctane, showing a much lower yield,



## 2.4.5 Control experiments

Control experiments were performed to confirm the need for all the parameters (Table 2.7). As already shown, ultrasound irradiation was essential to provide the energy necessary for the dehydrogenation to take place (Entry 2). Moreover, the control experiments indicate also that both the iridium complex and the hydrogen acceptor were essential for this transformation (Entries 3 and 4 respectively). An additional experiment was run using  $\text{IrCl}_3 \cdot 3\text{H}_2\text{O}$  as the iridium source (Entry 5). Iridium chloride was the precursor used for the synthesis of the active iridium pentahydride complex and can form easily iridium (0) metal. This experiment was run to check if the activity observed was caused by the iridium metal formed during the reaction and indeed if a simpler iridium complex could facilitate the transformation. The outcome of this experiment shows that iridium chloride is not able to promote the reaction.

Table 2.7 Control experiments for the sonochemical *n*-dodecane transfer dehydrogenation promoted by

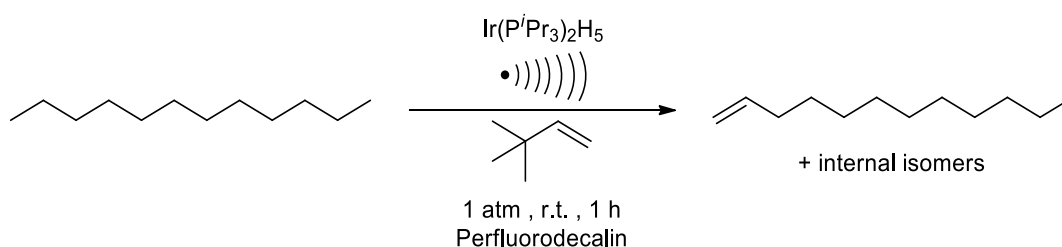


| Entry | A (%) | $C_{\text{IrH}_5}$ (mM) | $C_{\text{TBE}}$ (M) | $C_{\text{IrCl}_3 \cdot 3\text{H}_2\text{O}}$ (mM) | TON <sup>a</sup> |
|-------|-------|-------------------------|----------------------|--|------------------|
| 1     | 100   | 5                       | 0.1                  | -  | 1.18             |
| 2     | -     | 5                       | 0.1                  | -  | < 0.1            |
| 3     | 100   | -                       | 0.1                  | -  | < 0.1            |
| 4     | 100   | 5                       | -                    | -  | < 0.1            |
| 5     | 100   | -                       | 0.1                  | 5  | < 0.1            |

Experimental conditions: reactions are carried out in neat *n*-dodecane (5 mL) at room temperature ( $25 \pm 3$  °C) for 1 h of active sonication, under argon atmosphere, with a water cooling bath and with the microtip being cooled by a continuous stream of compressed air. (a) TONs are based on quantitative GC analysis using isoctane as the internal standard.

## 2.4.6 Perfluoroalkane as cosolvent

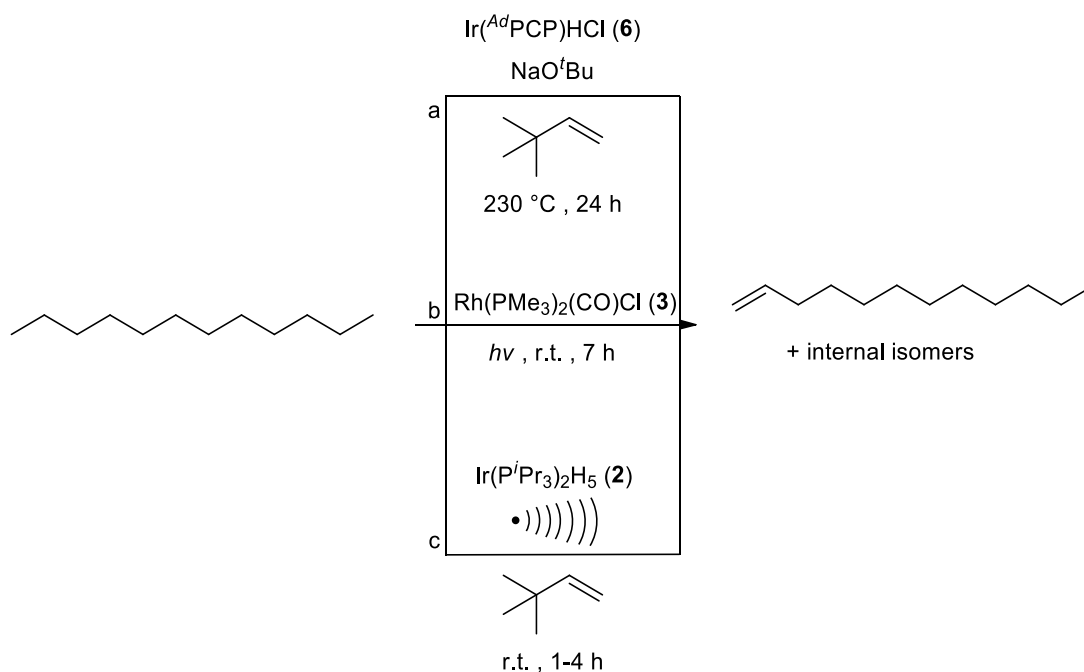
Together with the deactivation of the complex, another reason for the low activity could be attributed to the use of the alkane as solvent (neat reaction), due to a poor cavitation, i.e. abundant formation of cavitation bubbles and subsequent implosion. This problem could be overcome by running the reaction in a more appropriate solvent, such as perfluoroalkanes, which have been reported to be better solvents for sonochemical reactions.<sup>99</sup> It is known that the type of solvent has a profound effect on the sonochemical reactions.<sup>121</sup> Decreasing the solvent volatility increases the intensity of the cavitation collapse, i.e. the maximum temperature reached during the bubble collapse, which consequently relates to the rates of the sonochemical reaction. Moreover, perfluoroalkanes have already been used as cosolvents for the alkane dehydrogenation as reported by Crabtree and co-workers.<sup>42</sup> Aiming to improve the acceptorless dehydrogenation the authors discovered that using the alkane substrate as the reaction medium can sometimes be limiting in terms of the temperature at which the reaction can be conveniently run. Indeed, they solved the problem by using perfluoroalkanes as cosolvents in order to reach higher temperatures. The sonochemical tests were run using perfluorodecalin as solvent with *n*-dodecane concentration of 0.5 M (Scheme 2.11). The alkane was not soluble in perfluorodecalin, indeed 2 phases formed. But under ultrasound irradiation, they were effectively mixed together forming an emulsion, that dissipated once the ultrasound was turned off. For the quantitative analysis the *n*-dodecane phase was separated and analysed by GC as usual. A TON of 0.64 was recorded. However, this result cannot be considered a quantitative representation of the alkene generated, because in the perfluorodecalin phase there was still some trace amount of alkane and alkene (as observed by <sup>1</sup>H-NMR). Unfortunately, a quantitative evaluation of the dissolved amount of alkene and alkane from the NMR spectrum could not be achieved, due to the complexity of the system resulting in not well resolved signals.



Scheme 2.11 Sonochemical *n*-dodecane transfer dehydrogenation in perfluorodecalin as solvent medium.

## 2.5 Distribution of alkenes

The quantitative analyses of the sonochemical reactions were performed by gas-chromatography. When using *n*-dodecane as the substrate, a mixture of different dodecene isomers was obtained. Therefore, when observing the GC chromatogram, after the broad *n*-dodecane peak' many different small peaks were observed. It is interesting to note that the ratio between those peaks was different, depending on the type of energy used to conduct the reaction. Various *n*-dodecane dehydrogenation reactions, using different energy sources were examined (Scheme 2.12). A thermochemical reaction was run using the same conditions reported in the literature<sup>56</sup> and complex **6** together with NaO<sup>t</sup>Bu as catalyst, yielding a TON of 56.6. The same alkane dehydrogenation was tested under photochemical activation using complex **3** and the conditions from the literature,<sup>70</sup> obtaining a TON of 68.7. Finally, the developed sonochemical reaction was evaluated using the optimised conditions. Results are reported for both 1 hour and 4 hours of active sonication, with a TON of 1.03 and 1.11 respectively.



Scheme 2.12 (a) Thermochemical *n*-dodecane dehydrogenation. (b) Photochemical *n*-dodecane dehydrogenation. (c) Sonochemical *n*-dodecane dehydrogenation.

The mixtures of dodecene isomers from the three tests were then analysed by GC to calculate the relative ratios (Table 2.8). Five main isomer peaks could be identified and, as expected, the terminal isomer (1-alkene at 6.36 min identified using the corresponding standard) was not the major product in neither of the cases. It is interesting to note that for



the thermo- and photo-promoted experiments the ratio between the various isomers was almost identical, while for the sonochemical experiments it was definitively different, both after 1 or 4 hours of reaction. Moreover, for the ultrasound-driven experiments the isomerisation of the different isomers seemed to converge over time towards the formation of the isomer species corresponding to the fourth peak of the chromatogram with retention time of 6.56 minutes belonging to one of the internal dodecene isomers.

Table 2.8 Comparison between the ratios of the various dodecene isomers formed in *n*-dodecane dehydrogenation reactions promoted by different energy sources (see Scheme 2.12 for details on conditions).

| Retention Time<br>(min)  | Ratio of different isomers for different reactions |               |              |   |
|--------------------------|--|---------------|--------------|---|
|                          | Thermochemical                                     | Photochemical | Sonochemical |   |
| 6.27                     | 10   | 10            | 2            | 1 |
| 6.36 <sup>a</sup>        | 4  | 4             | 1            | 1 |
| 6.41                     | 1  | 1             | 2            | 2 |
| 6.56                     | 3  | 4             | 4            | 8 |
| 6.7                      | 1  | 1             | 1            | 2 |
| <b>Reaction Time (h)</b> | 24   | 7             | 1            | 4 |

<sup>a</sup> Terminal isomer

## 2.6 Temporal control experiment

Having established the optimal reaction conditions for the sonochemical alkane dehydrogenation, the reaction was investigated in more detail. A temporal control experiment over the activation of the dehydrogenation was performed (Figure 2.8). The purpose of the experiment was to distinguish between two possible scenarios: the role of the ultrasound irradiation is to activate the catalyst which then mediate the dehydrogenation at room temperature without the need of ultrasound or the ultrasound is needed to perform also the dehydrogenation step. In the first case the reaction will keep running after stopping the ultrasound irradiation, in the second case instead the reaction will stop as the ultrasound irradiation is turned off. Indeed, this experiment assessed the activation of the reaction over time while the ultrasound irradiation was intermittently turned on and off at given time intervals. Aliquots of the reaction mixture were taken periodically for the quantitative analyses.

As it can be observed from Figure 2.8, alkane dehydrogenation stopped completely in the absence of ultrasound, and it restarted efficiently after re-exposure to ultrasound. The rapid response time observed, with a fast switching between activation and deactivation period, could be explained with the rapid timescale of sonochemical events (hotspot lifetime  $10^{-7}$  s).<sup>122</sup> Quantitative GC analyses of the samples clearly showed no product yield increase when the ultrasound was turned off, suggesting that ultrasound irradiation promoted the dehydrogenation. From the point of view of what happens to the complex, there are two possible explanations. First, ultrasound irradiation allows the formation of an activated metal species which has a short lifetime and it is thought to exist only under ultrasound irradiation. Second, ultrasound stimulus creates the unusual conditions at which the complex can operate by providing the required energy. However, with the data available it was not possible to distinguish between the two hypotheses. Nevertheless, it could be confirmed that the ultrasound irradiation is required to perform the dehydrogenation step.

These experiments with on/off ultrasound cycles demonstrated that the dehydrogenation could be stopped and restarted by controlling the ultrasound stimulus. Indeed, ultrasound can temporally control the dehydrogenation rate. This is important because, ideally in the future, it could be used as a physical modality for temporal control of the reaction.

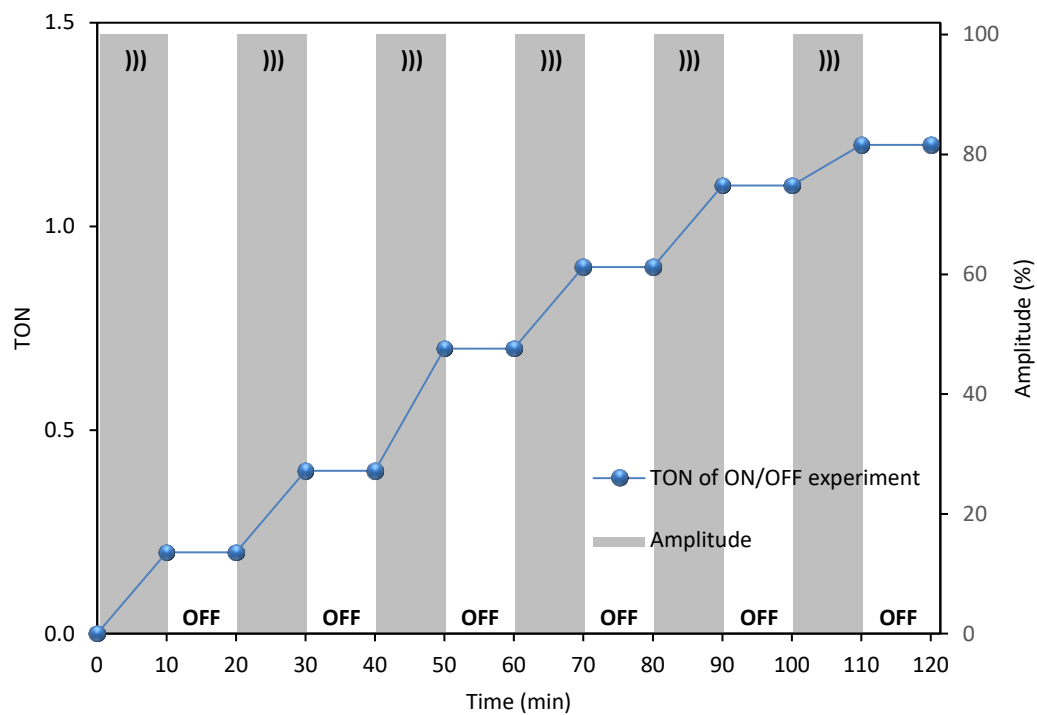


Figure 2.8 Temporal control experiment for the sonochemical *n*-dodecane transfer dehydrogenation through intermittent switching on/off the ultrasound probe. In each cycle the US is turned on for 10 min at 100% amplitude and then turned off for another 10 min.

## 2.7 Investigation of the deactivation of the complexes

### 2.7.1 Possible deactivation pathways and their investigation

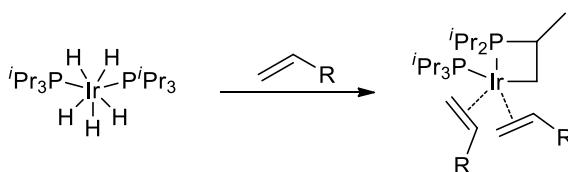
The loss of activity with the increasing reaction time could be owed to the deactivation of the system. Identifying the deactivation pathway could be useful to develop some strategies to suppress the deactivation and, therefore, increase the turnover numbers for this process. Deactivation of the system in analysis could occur *via* many forms: degradation of the ligand, leak of the apparatus leading to admission of air, inhibition by product-poisoning or general metal complex decomposition *via* other specific pathways.

Usually, any catalyst that is active enough to break a C-H bond in an alkane, is sufficiently reactive to attack its own ligands, leading indeed to catalyst deactivation. This is a common issue for homogeneous alkane dehydrogenation in general.

#### 2.7.1.1 Degradation of the ligand by cyclometalation or P-C bond cleavage

Two are the main degradation pathways for P-donor ligands such as the triisopropylphosphines of complex **2**: cyclometalation and P-C bond cleavage.

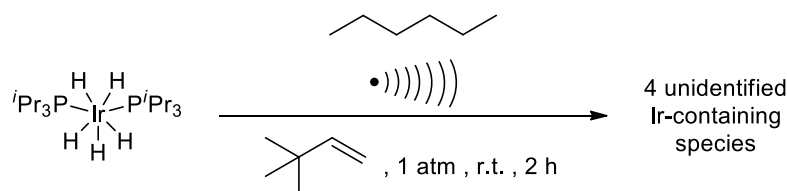
A metal centre can react with a C-H bond in the phosphine ligand to form a M-C bond, in a process called cyclometalation. The triisopropylphosphine ligand investigated can cyclometalate *via* activation of the C-H bond in  $\beta$ -position, resulting in an internal oxidative addition of the phosphine ligand (Scheme 2.13). Examples have been reported in the literature for the synthesis of similar cyclometalated Ir phosphine complexes bearing shorter alkanes (R=H, Me).<sup>123</sup>



Scheme 2.13 System deactivation by ligand degradation *via* cyclometalation.

To probe whether the cyclometalated complex was really formed during the reaction, the isolation of the deactivated complex from the reaction mixture was attempted (Scheme 2.14). *n*-Hexane was used as the alkane substrate as it is more volatile than *n*-dodecane in order to simplify the isolation of the iridium complexes by removal of the solvent by reduced pressure together with the hydrogen acceptor. Indeed, a mixture of the iridium species was obtained, which should be ideally predominantly constituted by the decomposed iridium complex. The mixture isolated from the sonochemical reaction was then analysed by NMR

spectroscopy (Section 2.13.10.1). The  $^1\text{H}$ -NMR spectrum showed a series of multiplets in the aliphatic region and no hydride peak was observed. The  $^{31}\text{P}$ -NMR showed also the presence of 4 major phosphine species and, most importantly, no peak was identified as a doublet, as it would be for the cyclometalated product (Figure 2.9). However, a double-cyclometalated complex, although extremely unlikely due to its high steric hindrance, could still be an option in agreement with the results.



Scheme 2.14 Sonochemical test for the isolation of the decomposed metallic species.

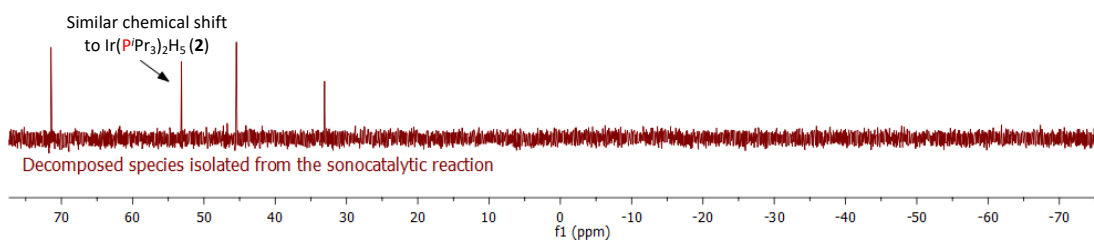
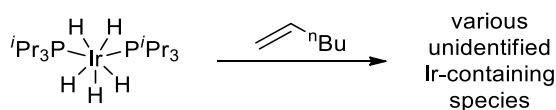


Figure 2.9  $^{31}\text{P}\{^1\text{H}\}$ -NMR spectrum (298 K,  $\text{d}^4$ -THF, 202 MHz) of the isolated decomposed iridium species.

As the decomposed complex from the sonochemical test was obtained as a mixture of different species, some experiments were performed to try to shed light on the complex deactivation. To do so, alternative synthetic approaches were applied aiming to isolate and identify the decomposed metallic species from  $\text{Ir}(\text{P}^i\text{Pr}_3)_2\text{H}_3$  and 1-hexene, adapting procedures reported in the literature for the synthesis of analogue cyclometalated complexes.<sup>123</sup> Unfortunately, despite the significant effort to do so, all those attempts to synthesise the decomposed catalyst were unsuccessful. Instead, they afford a complex mixture of free phosphine and various different phosphine iridium complexes not precisely identified (Scheme 2.15, more details and spectra in Section 2.13.10.2 of the experimental part).



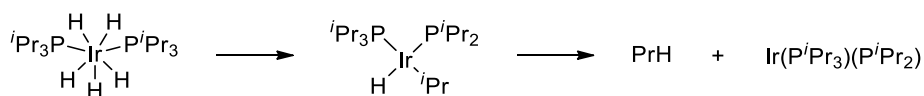
Scheme 2.15 General scheme for the attempts in the synthesis of the deactivated metal complex.

However, some considerations could be made from those results. As explained above, the cyclometalated complex was not formed, because in the  $^{31}\text{P}$ -NMR spectrum 2 doublets should be observed, while only singlets were present. Moreover, it appears clear that in the presence of the alkene the complex was not thermally stable. However, by comparing the  $^{31}\text{P}$ -NMR spectra of the different experiments reported in the experimental section, it seems that the same four species formed under ultrasound irradiation cannot be seen in any of the thermal experiments (for spectra see experimental part, Section 2.13.10.2). This result suggests that the complex decomposition might be related with its behaviour under sonochemical conditions (Section 2.7.1.4).

Although no cyclometalated products was isolated, the presence of this cyclometalation reaction was supported by the fact that a solution of complex **2** in a deuterated solvent, such as  $\text{C}_6\text{D}_6$ , showed an extensive incorporation of deuterium into the methyl groups of the phosphine ligands over time. This is likely to occur *via* a reversible C-H cyclometalation of the ligand, C-D oxidative addition/C-H reductive elimination of the deuterated solvent to the metal atom and, lastly, reductive elimination with disruption of the metallacycle, resulting in the formation of the C-D bond in the phosphine ligand.<sup>124-125</sup> Probably, such cyclometalation reaction was indeed still present, but it was not permanently deactivating the catalyst, because it is reversible.

Cyclometalation, because it is often reversible, is indeed much less problematic than P-C bond cleavage, which is most of the times irreversible.<sup>125-126</sup> Metal complexes bearing tertiary phosphines are liable to undergo P-C bond scission and a well-known problem for alkane dehydrogenation catalysts is thermal decomposition.<sup>24-25</sup> P-C bond cleavage has been reported in the literature for the alkane dehydrogenation catalysed by  $\text{IrH}_2(\eta^2\text{-O}_2\text{CCF}_3)(\text{P}\{p\text{-FC}_6\text{H}_4\}_3)_2$ .<sup>38</sup> or  $\text{IrH}_2(\text{CF}_3\text{COO})(\text{P}\{\text{C}_6\text{H}_{11}\}_3)_2$ <sup>42</sup> developed by Crabtree and co-workers. With the system under analysis, the decomposition of complex **2** could arise from the cleavage of the phosphine ligands with release of propane. This reaction might be an important deactivation pathway for the complex, but it is often missed because of the small amount of propane formed, which detection is hard and, moreover, it can easily escape the reaction mixture. In fact, with the methods of analyses at hand, this deactivation pathway could not be proved, but similar breakage of the phosphine ligand of the iridium-pentahydride complex **2** have been previously reported.<sup>39, 126-127</sup> The decomposition probably occurred *via* oxidative migration of the alkyl group to the metal centre, followed by reductive elimination of the obtained alkyl-iridium species with a hydride (Scheme 2.16).<sup>38, 128</sup> It appeared indeed

plausible that P-C cleavage of the phosphine ligand might be a possible reason for the system deactivation.



Scheme 2.16 System deactivation by ligand degradation *via* P-C cleavage.

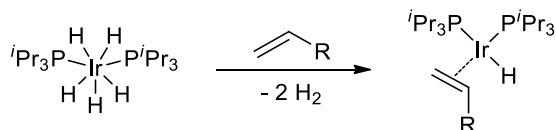
### 2.7.1.2 Leak in the apparatus leading to admission of air

Another common deactivation pathway for phosphine ligands was their oxidation to phosphine oxides. A leak in the system, inducing the build-up of molecular oxygen, could be the suspected cause of the ligand oxidation and result in the system deactivation. The starting solutions were colourless to light yellow at the start of the reactions. The colour subsequently darkened to a deep yellow while the reaction was carried out, to finally afford at the end a dark-green/olive solution. Most probably, the decomposition of complex **2** by molecular oxygen to standard phosphine oxides could be excluded, as in this case the colour of the solution would be blue. Moreover, from the NMR spectra of the isolated decomposed catalyst no phosphine oxide was observed. However, it cannot be excluded that the iridium centre itself might react with molecular oxygen to give inactive species.

Another observation could be made. At the start of the sonochemical tests the reaction mixture appears clear and perfectly homogeneous, while at the end a fine particulate was formed (probably deactivated iridium metal particles). As mentioned as well in Section 2.10, the presence of mercury does not significantly affect the yield of the dehydrogenated product, indicating that these metal particles were not involved in the reaction. Indeed, they might be the result of complex decomposition and system deactivation. Although those particles appeared to be insoluble in *n*-hexane, when isolated and dissolved in *d*<sup>8</sup>-THF for the analyses, they formed a homogeneous solution (*discussed in* Section 2.7.1.1). The formation of this particulate could be caused by both reaction with molecular oxygen and/or by the behaviour of the complex under ultrasound irradiation (*discussed in* Section 2.7.1.4). The building-up of molecular oxygen from a leak in the system could cause the complex decomposition *via* pathways other than formation of phosphine oxides. The problem of a leak was also the cause of the low reproducibility of the results.

### 2.7.1.3 Inhibition by product poisoning

Another possible deactivation pathway was the catalyst being poisoned by the product. The alkene product produced during the reaction could competitively bind to the metal leading to deactivation (Scheme 2.17).



Scheme 2.17 System deactivation by inhibition from product poisoning.

To probe the possibility of product inhibition, other experiments were performed. The standard sonochemical test was carried out, but after one hour of reaction a second aliquot of catalyst was added. The graph below (Figure 2.10) shows that the activity of the second batch of complex was not decreased, showing the usual activity pattern. This result supports the fact that the presence of the product is not the cause of the system deactivation. Moreover, it could be observed that the hydrogen acceptor was not completely consumed, but its concentration was still high enough to allow the reaction to take place.

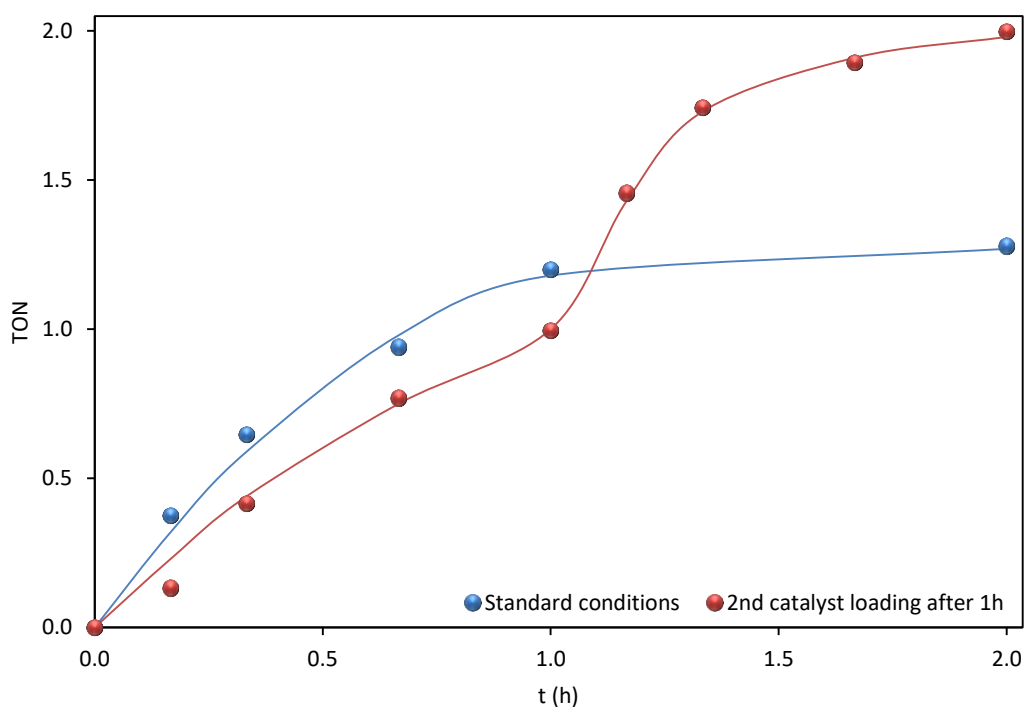


Figure 2.10 Time monitoring of the complex deactivation over time for the alkane transfer dehydrogenation under standard conditions and when a second aliquot of catalyst is added halfway through the reaction. Test to check the complex inhibition by the product.



To further support that the deactivation is not due to product inhibition, another experiment was run where 1 equivalent of alkene, with respect to the iridium complex, was added to the reaction mixture directly at the beginning of the reaction. The reaction was then time-monitored up to 1 hour to observe the alkene formation and compare it with the standard reaction. As can be deduced from the graph below (Figure 2.11), the reaction showed no product inhibition. The activity of the complex was comparable for both experiments carried out in the absence and in the presence of the alkene product; the small differences in the TON can be taken upon the difficulties in the reproducibility of the reaction.

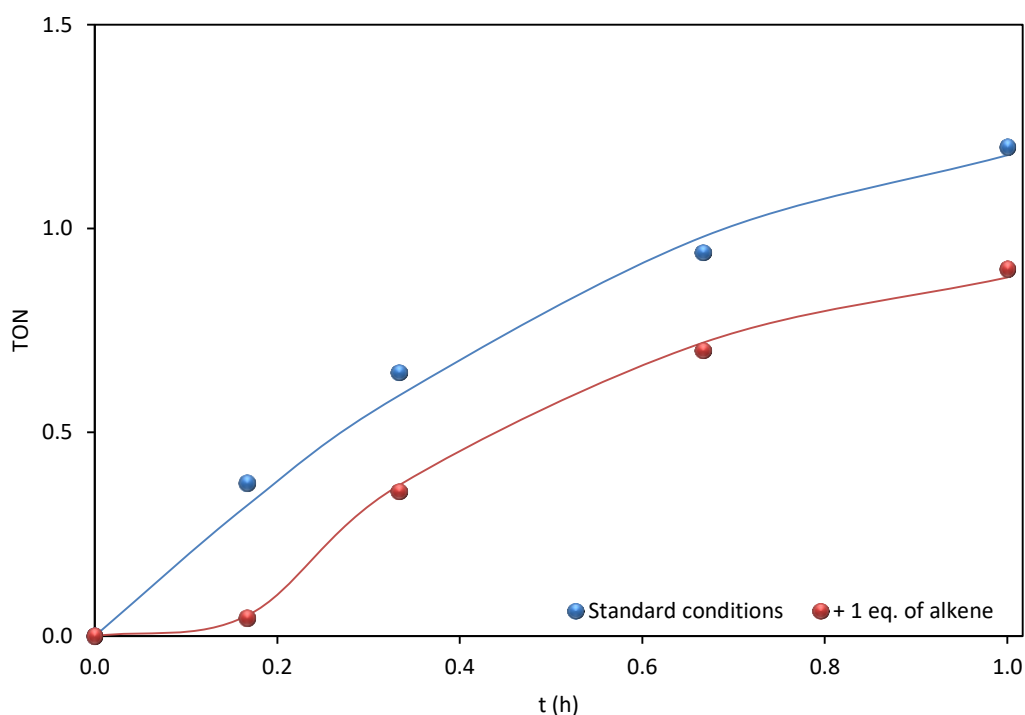


Figure 2.11 Time monitoring of the complex deactivation over time for the alkane transfer dehydrogenation under standard conditions (blue line) and when an equivalent of *n*-dodecene is added at the beginning of the reaction (red line). Test performed to check the complex inhibition by the product.

#### 2.7.1.4 Possible metal complex decomposition by ultrasound

To summarise, the deactivation by cyclometalation and product inhibition could be excluded, while P-C cleavage and decomposition due to an air leak cannot yet be ruled out. Besides, as inferred before, by comparison of the different  $^{31}\text{P}$ -NMR spectra the deactivated species formed under sonochemical conditions cannot be obtained *via* a thermal approach. Indeed, it seems plausible that the deactivation might be related to the complex stability under ultrasound irradiation.

Moreover, from the pattern of the time optimisation experiments from Figure 2.7, it can be hypothesised that the initial decomposed complex catalysed the subsequent further decomposition of more complex. This is suggested by the sudden decrease of the reaction rate after one hour of reaction, regardless of the type of substrate used.

To conclude, it seems that the maximum number of TON which can be achieved is limited by the competition between the dehydrogenation process and the various deactivation pathways, as the activity dropped significantly after one hour. It is difficult to identify those pathways due to the complexity of the reaction mixture and no conclusive considerations could be made regarding the deactivation mode of the complex. However, decomposition products from the sonochemical experiments differed from the species obtained from the other experiments carried out under thermal conditions. Decomposition of the complex is indeed most probably connected to its stability under ultrasound.

### 2.7.2 TGA and DSC analyses of $\text{Ir}(\text{P}^i\text{Pr}_3)_2\text{H}_5$

To obtain more insights into the stability and decomposition products of complex **2**, TGA and DSC analyses were carried out. As the complex was air sensitive, to avoid decomposition, the TGA was performed under nitrogen atmosphere. From the TGA curve in the graph (Figure 2.12, red curve), a 2% mass increase could be observed at the beginning, possibly due to small oxidation of the complex. The five hydrides were probably the first ones to be lost, but as they only account for the 1% of the total mass loss, their loss cannot be unequivocally identified. The complex looked to be mostly stable up to 133 °C. The highest mass loss, to the 68% of the total mass balance, accounts for the loss of one of the two phosphine ligands (plus hydrides). The derivative of the TGA curve confirmed that the loss of the phosphine started after 133 °C with the highest decomposition rate and it was quantitative after 290 °C. It is interesting to note that, even though the temperature was increased up to 700 °C, the final point of complete decomposition was not reached.

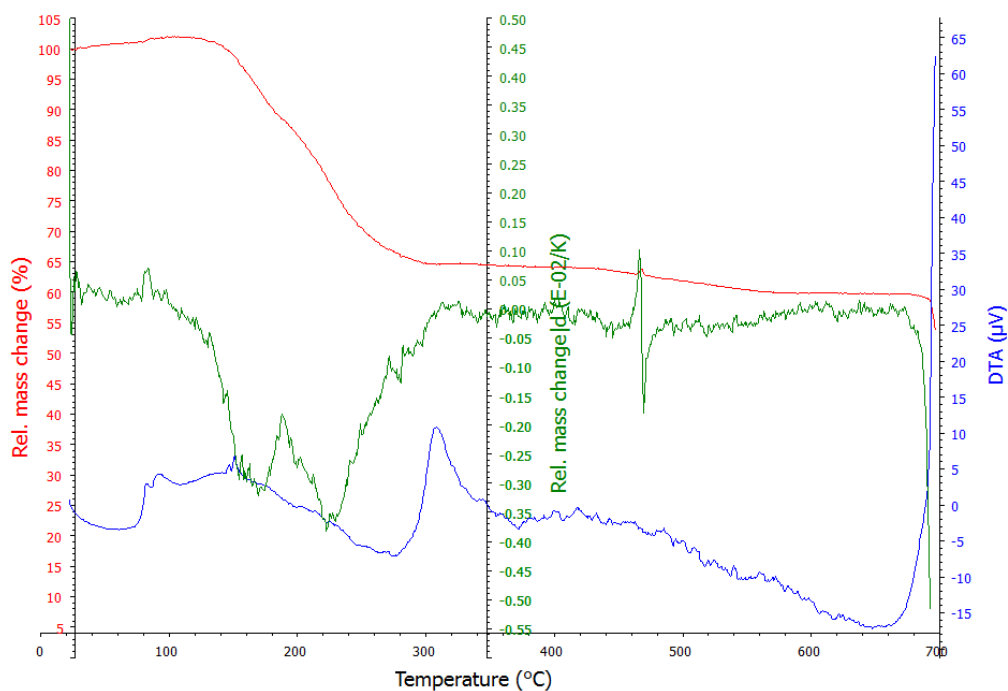


Figure 2.12 TGA analysis for  $\text{Ir}(\text{P}^i\text{Pr}_3)_2\text{H}_5$  (**2**) from room temperature to 700 °C at 5 °C/min. The red trace shows the relative mass change as the temperature is increased, decomposition starts at 133 °C. The green trace is the derivative of the relative mass change with the increasing of the temperature. The blue trace represents the differential thermal analysis as a function of the temperature.

As for the TGA, also the DSC analysis was carried out under nitrogen stream, to avoid decomposition of the complex by oxidation. The DSC was performed up to 120 °C when the complex started to decompose, as observed from the TGA. The compound was subjected to successive heating and cooling cycles, when it melted and solidified, respectively. As it can be observed from the graph (Figure 2.13), melting of the complex occurred consistently at 91-92 °C with an endothermic process of around 66 J/g. The complex solidified at a lower temperature, 67 °C, with an exothermic process liberating again around 66 J/g. The consistence between the energy of solidification and melting, even over successive cycles, suggests that the complex does not decompose during this phase transitions.

Table 2.9 Details of DSC analysis of Ir(P<sup>i</sup>Pr<sub>3</sub>)<sub>2</sub>H<sub>5</sub> (**2**).

| Rate<br>(°C/min) | T<br>(°C) | Rate<br>(°C/min) | Curve  | Area<br>(J/g) | T <sub>Peak</sub><br>(°C) |
|------------------|-----------|------------------|--------|---------------|---------------------------|
| 5                | 0         | 2                | -      | -             | -                         |
| 5                | 120       | 2                | Blue   | -65.36        | 91.7                      |
| 5                | 0         | 2                | Purple | 65.74         | 67.1                      |
| 5                | 120       | 2                | Red    | -66.26        | 91.2                      |

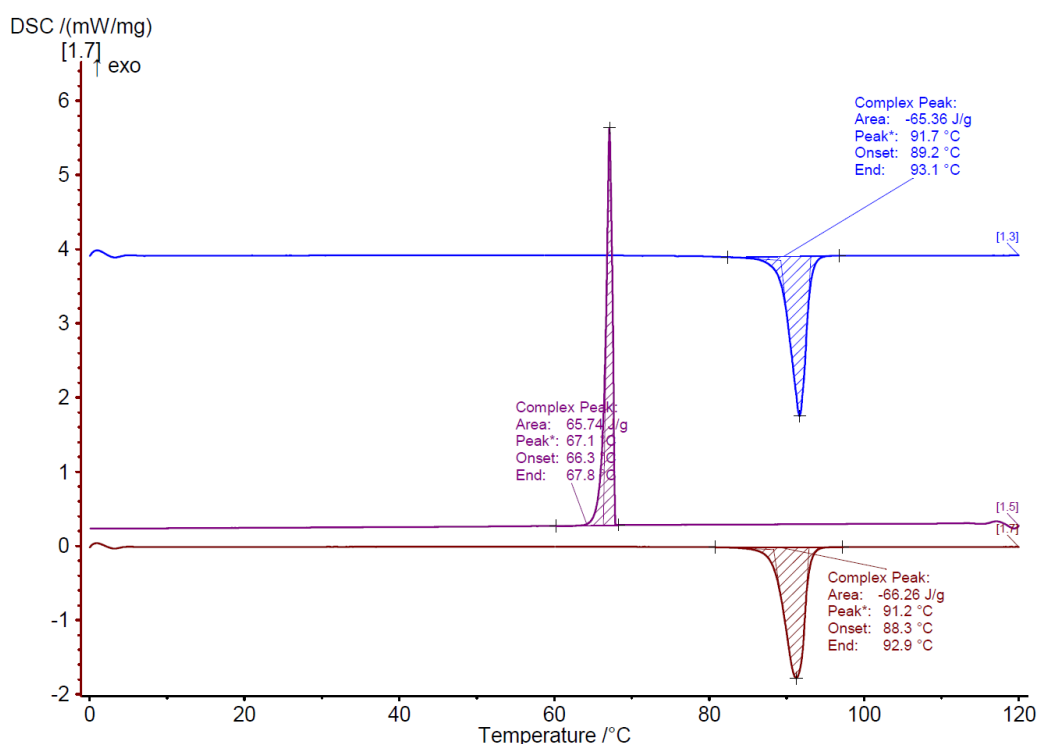


Figure 2.13 DSC analysis of Ir(P<sup>i</sup>Pr<sub>3</sub>)<sub>2</sub>H<sub>5</sub> (**2**). The red and blue traces represent the heating cycles, while the purple trace represents the cooling cycle.

Unfortunately, sometimes, as in this case, is particularly hard to identify the product of the decomposition of complex **2**. Therefore, to make a better use of the time, the attention was directed from the study of the deactivation of this complex to the investigation of the activity of some of its analogues with the hope to decrease the decomposition and therefore increase the activity.

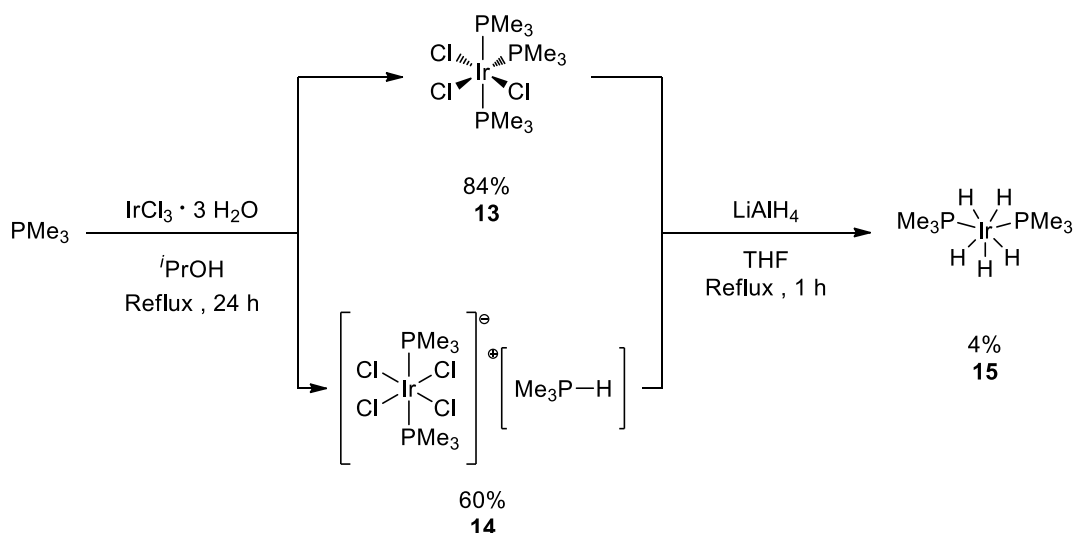
## 2.8 Further screening of pentahydride complexes

The issue of catalyst deactivation led to explore the possibility of avoiding this problem by replacing the *iso*-propyl groups on the phosphines with various substituents. With those modification, the hope was to alter the phosphine ability to influence the activity and stability of the system by varying the electronic and steric properties, possibly making the complex more stable towards deactivation.<sup>129</sup> Hopefully, other bisphosphine iridium-pentahydride systems, which should be capable to promote the alkane dehydrogenation, would also deactivate less readily, thus leading to a greater number of catalytic turnovers. The performance of a catalyst is greatly dependent on the balance between the rate of the product formation and the rate of the system deactivation. Lowering the complex decomposition rate would result in the increase of the yield of the reaction and indeed improvement of the turnover number of the process. Different analogue complexes were indeed synthesised and examined for the *n*-dodecane transfer dehydrogenation.

### 2.8.1 Synthesis of iridium-pentahydride analogues

It is known in the literature that by changing one or more of the three organic substituents in tri-substituted phosphine ligands, their steric and electronic properties can be manipulated.<sup>129</sup> These properties are also manifested in the catalytic properties of the metal centre.<sup>129</sup> With this in mind, various iridium-pentahydrides bearing different trialkyl-phosphines were synthesised and tested for the alkane dehydrogenation.

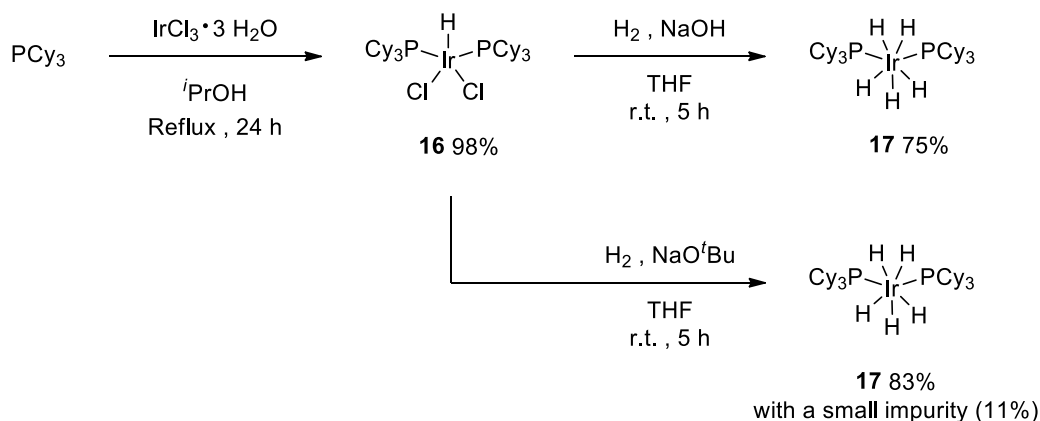
First, the isopropyl substituent was substituted with a methyl group. The resulting Ir(PMe<sub>3</sub>)<sub>2</sub>H<sub>5</sub> complex **15** did not have any carbon in β-position, making the deactivation by cyclometalation, or P-C bond cleavage, not viable according to the classic mechanism. Moreover, its very low steric hindrance may favour the alkane activation. Complex **15** was synthesised following the literature procedure, with some modifications (Scheme 2.18).<sup>130</sup>



Scheme 2.18 Synthesis of Ir(PMe<sub>3</sub>)<sub>2</sub>H<sub>5</sub> (**15**).

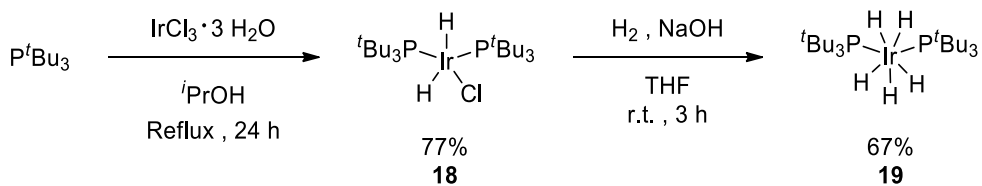
For the synthesis of the chloride-phosphine-iridium complex **13** or **14**, the same reaction conditions used for **8** were chosen (see Section 2.3.1), drastically improving the literature yields.<sup>130</sup> The formation of one or the other possible species (either **13** or **14**) was dictated by the temperature: a vigorous reflux led preferably to the formation of complex **13**, as the *mer*-isomer.<sup>130</sup> For the following step, the reduction, the conditions used for the synthesis of Ir(P<sup>*i*</sup>Pr<sub>3</sub>)<sub>2</sub>H<sub>5</sub> **2** were tested (see Section 2.3.1), but no product was observed, even when at higher temperature. Therefore, the use of a reducing agent, LiAlH<sub>4</sub> as reported in the literature,<sup>130</sup> was investigated. The reaction worked as expected and the crude product was then purified *via* sublimation.

Next, various complexes bearing bulkier ligands were synthesised. The increased steric bulk of the ligand should stabilise the metal towards oxidation by air and for the same reason, ideally, also increase the stability under ultrasound irradiation. Ir(PCy<sub>3</sub>)<sub>2</sub>H<sub>5</sub> complex **17** has cyclohexyl-substituted phosphines and its synthesis was performed adapting the procedure used for **2** (Scheme 2.19). Interesting to note, when using NaO<sup>*t*</sup>Bu as reported in the literature,<sup>131</sup> the product was obtained in 83% yield with an impurity that accounted for 11% of the total crude mass (by <sup>31</sup>P-NMR). The material was then discarded.



Scheme 2.19 Synthesis of Ir(PCy<sub>3</sub>)<sub>2</sub>H<sub>5</sub> (**17**).

Another complex with bulky ligands synthesised is Ir(P<sup>*t*</sup>Bu<sub>3</sub>)<sub>2</sub>H<sub>5</sub> (**19**), again with the hope that the bulkier ligands would stabilise the metal centre towards air oxidation and ultrasound treatment. Complex **19** was synthesised following the reported literature procedure (Scheme 2.20).<sup>132</sup>

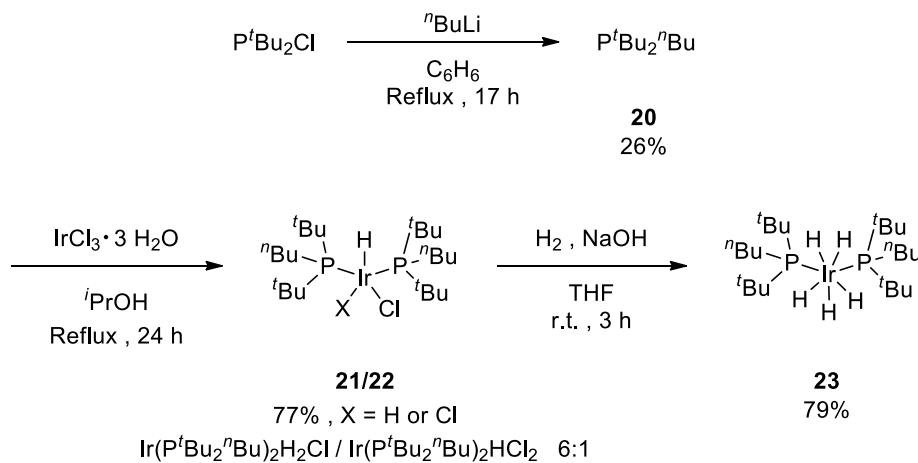


Scheme 2.20 Synthesis of Ir(P<sup>*t*</sup>Bu<sub>3</sub>)<sub>2</sub>H<sub>5</sub> (**19**).

For the first step the literature yields were improved diluting the reaction mixture, in order to fully solubilise the phosphine.<sup>132</sup> It is interesting to note that the dihydride-monochlorinated complex **18** was formed, not the monohydride-dichloride complex **8**. This was most probably because the iridium cannot accommodate anymore two big chlorine atoms due to the bulkier tritertbutylphosphine ligands.

The next step was to synthesise analogue complexes bearing a phosphine with different electronic properties. The novel iridium pentahydride complexes Ir(P<sup>*t*</sup>Bu<sub>2</sub><sup>*n*</sup>Bu)<sub>2</sub>H<sub>5</sub> (**23**) was synthesised by substituting a *tert*-butyl group with a *n*-butyl one. Moreover, another complex bearing unsymmetrical phosphines was also synthesised, by substituting the two *tert*-butyl groups with the even bulkier adamantyl ones to obtain Ir(PAd<sub>2</sub><sup>*n*</sup>Bu)<sub>2</sub>H<sub>5</sub> (**24**). In both cases, one of the three alkyl groups on the phosphine was substituted with a *n*-butyl group. This resulted in a slightly lower steric hindrance together with an increased acidity of the iridium complex (according to the trends reported in the literature for similar complexes),<sup>133</sup> making the cyclometalation less favoured. Similar unsymmetrical phosphine complexes have been

reported in the literature,<sup>134-135</sup> but those are the first iridium complexes bearing di-*tert*-butyl(butyl)phosphine and di-adamantyl(butyl)phosphine as ligands.



Scheme 2.21 Synthesis of Ir(P<sup>t</sup>Bu<sub>2</sub><sup>n</sup>Bu)<sub>2</sub>H<sub>5</sub> (**23**).

For the synthesis of complex **23**, first the unsymmetrical di-*tert*-butyl(butyl)phosphane (**20**) was synthesised according to the literature procedure (Scheme 2.21).<sup>136</sup> The phosphine was isolated as a mixture with benzene in a 1:1 ratio, in a 26% yield calculated by NMR. The low yield was probably caused by a significant amount of phosphine being removed together with the benzene. Therefore, the crude material was used directly in the following step without further manipulation. For future trials, the phosphine synthesis could be improved by using a low boiling ether instead of benzene as the solvent, allowing an easier isolation. The Ir(P<sup>t</sup>Bu<sub>2</sub><sup>n</sup>Bu)<sub>2</sub>HCl<sub>2</sub> complex (**22**) was synthesised adapting the procedure used for the isopropyl analogue **8**. In the optimised synthesis, the desired complex was isolated by simply concentrating the reaction mixture under reduced pressure. From the NMR spectra the isolated product appeared to be a mixture of 2 different compound: Ir(P<sup>t</sup>Bu<sub>2</sub><sup>n</sup>Bu)<sub>2</sub>H<sub>2</sub>Cl (**21**) and Ir(P<sup>t</sup>Bu<sub>2</sub><sup>n</sup>Bu)<sub>2</sub>HCl<sub>2</sub> (**22**) in a 6:1 ratio. By substituting a *tert*-butyl group with a *n*-butyl one, the steric bulk of the ligand decreased, making more room for a possible second chloride ligand. This was an intermediate situation between the bulkiness of complex **18**, Ir(P<sup>t</sup>Bu<sub>3</sub>)<sub>2</sub>HCl<sub>2</sub>, and the lower hindrance of complex **8**, Ir(P<sup>i</sup>Pr<sub>3</sub>)<sub>2</sub>H<sub>2</sub>Cl, where the coordination space on the iridium atom led to the formation of a mixture of two different species. This result was supported by considering the cone angle of the phosphine ligands (Table 2.10). As it can be seen from the table, the P<sup>t</sup>Bu<sub>3</sub> ligand is the one with the highest cone angle value and it was the only one forming an iridium complex which was not able to accommodate two chloride ligands, forming Ir(P<sup>t</sup>Bu<sub>3</sub>)<sub>2</sub>H<sub>2</sub>Cl (**18**).



Table 2.10 Values of the Tolman cone angles  $\theta$  for different phosphines.

| Entry | Ligand                            | $\theta$ (deg) <sup>a</sup> |
|-------|-----------------------------------|-----------------------------|
| 1     | PMe <sub>3</sub>                  | 118                         |
| 2     | P <sup>n</sup> Bu <sub>3</sub>    | 132                         |
| 3     | P <sup>i</sup> Pr <sub>3</sub>    | 160                         |
| 4     | P <sup>t</sup> Bu <sub>2</sub> Me | 161                         |
| 5     | P <sup>t</sup> Bu <sub>2</sub> Et | 165                         |
| 6     | PCy <sub>3</sub>                  | 170                         |
| 7     | P <sup>t</sup> Bu <sub>3</sub>    | 182                         |

(a) Values as reported in the literature.<sup>137-138</sup>

Exact value of the cone angle for the P<sup>t</sup>Bu<sub>2</sub><sup>n</sup>Bu ligand could not be found in the literature, but according to the trends obtained by substituting one of the *tert*-butyl ligands with either a methyl or an ethyl group (Entries 4 and 5), it can be assumed that the cone angle for P<sup>t</sup>Bu<sub>2</sub><sup>n</sup>Bu ligand would be around 165-170 degrees. Moreover, the theoretical value can be calculated as reported in Equation 1: for an unsymmetrical ligand the effective angle can be defined by a model that minimise the sum of the half angles.<sup>137</sup> Therefore, according to the values of  $\theta$  for P<sup>n</sup>Bu<sub>3</sub> and P<sup>t</sup>Bu<sub>3</sub> reported in the table (Entries 2 and 7), the theoretical cone angle for P<sup>t</sup>Bu<sub>2</sub><sup>n</sup>Bu is 165.3 deg. The predicted value of the cone angle can explain why this time a mixture of the mono- and di-hydride iridium complex was formed (**21** and **22**).

$$\theta = \frac{2}{3} \sum_{i=1}^3 \frac{\theta_i}{2} \quad \text{Equation 1}$$

According to the results from the NMR spectra, the geometries for the two complexes were the ones reported in Figure 2.14. Complex **21** has the chloride in apical position of a square base pyramidal geometry, while **22** has the hydride atom in the same apical position. This is the same geometry adopted by the isopropyl analogue according to the literature.<sup>124</sup> The mixture of the two species does not need to be separated as it can be directly used in the synthesis of the pentahydride derivative, obtaining in the end just one species. The Ir(P<sup>t</sup>Bu<sub>2</sub><sup>n</sup>Bu)<sub>2</sub>H<sub>5</sub>, complex **23**, was obtained again with the general pentahydride procedure. It is important for this last step to perform the reaction at a temperature no lower than 25 °C, as otherwise the reaction does not go to completion even with longer reaction times. The final complex **23** was isolated in 67% yield. The exact assignment of the different CH<sub>2</sub> atoms to the peaks of the NMR spectra was possible thanks to COSY and HSQC experiments.

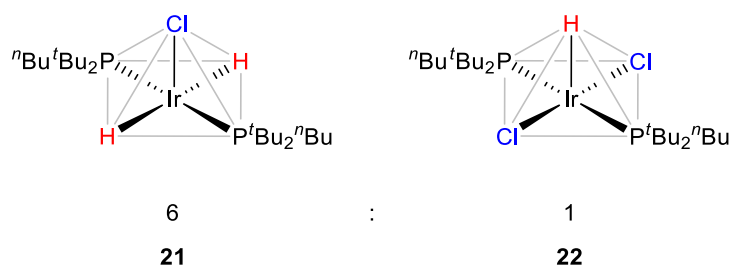
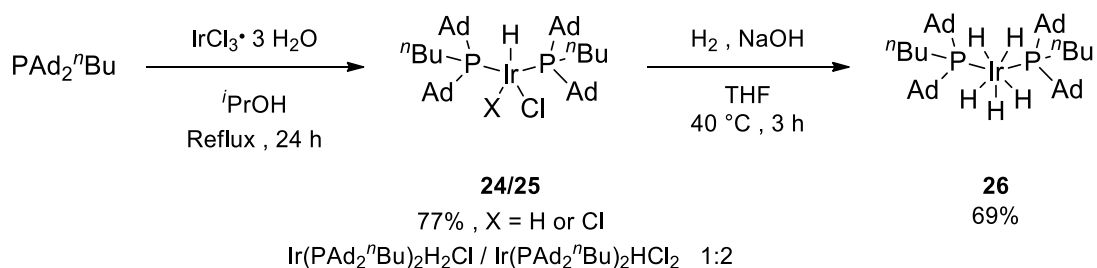


Figure 2.14 Expected geometries for  $\text{Ir}(\text{P}^t\text{Bu}_2^n\text{Bu})_2\text{H}_2\text{Cl}$  and  $\text{Ir}(\text{P}^t\text{Bu}_2^n\text{Bu})_2\text{HCl}_2$  with relative ratio.

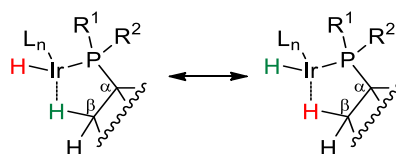
Next, a similar complex  $\text{Ir}(\text{PAd}_2^n\text{Bu})_2\text{H}_5$  (**26**) was synthesised, with the phosphine bearing two adamantyl groups and one *n*-butyl group (Scheme 2.22). After the first step, a mixture of the mono- and di-hydride iridium species was obtained,  $\text{Ir}(\text{PAd}_2^n\text{Bu})_2\text{H}_2\text{Cl}$  (**24**) and  $\text{Ir}(\text{PAd}_2^n\text{Bu})_2\text{HCl}_2$  (**25**), this time in a 1:2 ratio.



Scheme 2.22 Synthesis of  $\text{Ir}(\text{PAd}_2^n\text{Bu})_2\text{H}_5$  (**26**).

Moreover, according to the NMR spectra, it seemed that complex **25**, the monohydride, was present as 2 different rotamers in a 1:1 ratio. Unfortunately, full characterisation of this complex was difficult due to its low solubility. This was the reason why a  $^{13}\text{C}$ -NMR spectrum could not be recorded. The mass spectrum confirmed only the skeleton of the complex  $[\text{Ir}(\text{PAd}_2^n\text{Bu})_2]^+$ . As before, the mixture was used directly in the synthesis of the corresponding pentahydride complex **26**. The usual procedure was followed, but the temperature was increased to 40 °C in order to reach full conversion. Higher temperatures led to the formation of various by-products. Once again, solubility problems did not allow the  $^{13}\text{C}$ -NMR spectrum to be recorded. According to the proton and phosphorus spectra the product appeared to be the desired one, result supported also from the mass spectra. However, a question remains on the number of hydrides bonded to the iridium centre, which is assumed to be five from analogies with the other similar complexes. However, from the mass spectrum, only the “naked” diphosphine-iridium complex was observed  $[\text{Ir}(\text{PAd}_2^n\text{Bu})_2]^+$ . Moreover, from the  $^1\text{H}$ -NMR spectrum, the integral value of the hydride signal was lower than five, even when longer delay times (up to 30 s) were used to acquire the spectrum. The low integral value could be explained indeed with a hydrogen exchange between the hydride and the hydrogen atoms

of the ligand (Scheme 2.23), with the rate of this exchange being much faster than the NMR timescale. This process takes place *via* formation of an agnostic bond between the iridium and the hydrogen in  $\beta$ -position of the phosphine ligand, process particularly favoured with bulky ligands, such as  $\text{PAd}_2^n\text{Bu}$ , which form also a stable 5-membered ring. Therefore, this exchange process for this type of ligand was really fast, even at room temperature. However, the same process was also present for the hydride-chloride analogue and all the others pentahydride analogues, but it was much slower and consequently negligible.



Scheme 2.23 Hydrogen exchange in  $\text{Ir}(\text{PAd}_2^n\text{Bu})_2\text{H}_5$  (**26**).

It is quite common for polyhydride complexes to have structures that cannot be unequivocally demonstrated by NMR.<sup>139</sup> Their fluxional behaviour often precludes an unambiguous structural assignment based exclusively on NMR, requiring necessarily the use of other methods such as x-ray crystallography. Unfortunately, despite the efforts, suitable crystals for x-ray could not be obtained for this complex. However, the complex was tested for the sonochemical alkane dehydrogenation.

In conclusion, five different diphosphine-iridium pentahydride complexes have been synthesised (Figure 2.15), two of which have never been previously reported (complexes **23** and **26**). Their activity towards the alkane dehydrogenation was then tested under ultrasound irradiation.

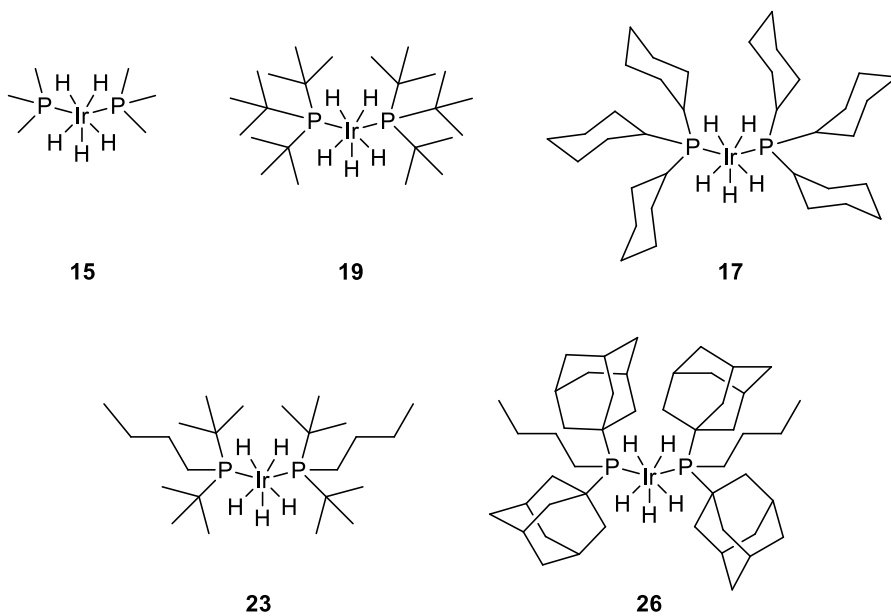
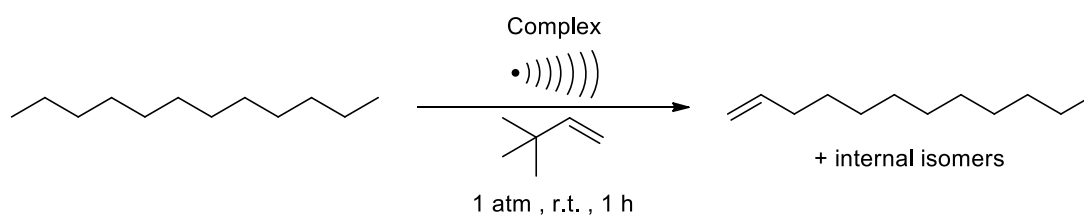


Figure 2.15 Iridium-pentahydride complexes synthesised to be tested for the sonochemical alkane dehydrogenation.

## 2.8.2 Screening of bisphosphine-iridium-pentahydride analogues

The synthesised complexes (Figure 2.15) were tested for the transfer alkane dehydrogenation under sonochemical conditions using *n*-dodecane as the benchmark substrate. Deoxygenated solution of the pentahydride analogues and TBE in *n*-dodecane were subjected to 1 hour of active sonication under the optimised conditions. Results are reported in Table 2.11. All analogues of the Ir(P<sup>*i*</sup>Pr<sub>3</sub>)<sub>2</sub>H<sub>5</sub> complex were inactive in the model dehydrogenation reaction.

Table 2.11 Screening of pentahydride complexes for the sonochemical *n*-dodecane transfer dehydrogenation.



| Entry | Catalyst   | Time (h) | TON <sup>a</sup> |
|-------|--|----------|------------------|
| 1     | Ir(P <sup><i>i</i></sup> Pr <sub>3</sub> ) <sub>2</sub> H <sub>5</sub> ( <b>2</b> )                        | 1        | 1.18             |
| 2     | Ir(PMe <sub>3</sub> ) <sub>2</sub> H <sub>5</sub> ( <b>15</b> )  | 1        | < 0.1            |
| 3     | Ir(P <sup><i>t</i></sup> Bu <sub>3</sub> ) <sub>2</sub> H <sub>5</sub> ( <b>19</b> )                       | 1        | < 0.1            |
| 4     | Ir(PCy <sub>3</sub> ) <sub>2</sub> H <sub>5</sub> ( <b>17</b> )  | 1        | < 0.1            |
| 5     | Ir(PCy <sub>3</sub> ) <sub>2</sub> H <sub>5</sub> ( <b>17</b> )  | 2        | < 0.1            |
| 6     | Ir(P <sup><i>i</i></sup> Bu <sub>2</sub> <sup><i>n</i></sup> Bu) <sub>2</sub> H <sub>5</sub> ( <b>23</b> ) | 1        | < 0.1            |
| 7     | Ir(P <sup><i>i</i></sup> Bu <sub>2</sub> <sup><i>n</i></sup> Bu) <sub>2</sub> H <sub>5</sub> ( <b>23</b> ) | 2        | < 0.1            |
| 8     | Ir(PAd <sub>2</sub> <sup><i>n</i></sup> Bu) <sub>2</sub> H <sub>5</sub> ( <b>26</b> )                      | 1        | < 0.1            |

Experimental conditions: reactions are carried out in neat *n*-dodecane (5 mL) at room temperature (25 ± 3 °C) for the time reported in the table, under argon atmosphere, with a water cooling bath and with the microtip being cooled by a continuous stream of compressed air. Amplitude is 100%. The complex concentration is 5 mM. TBE concentration is 0.1 M. (a) TONs are based on quantitative GC analysis using isooctane as the internal standard.

When the complex with the small trimethylphosphine ligand, **15**, was tested in the sonochemical reaction (Entry 2), the colour of the reaction mixture remained yellow until the end of the reaction. Therefore, as hypothesised, the less hindered complex seems to be more stable towards decomposition, which was presumably *via* P-C cleavage of the phosphine ligand. Unfortunately, the variation in the steric and electronic properties of the complex makes it also inactive under our operating conditions. Changing the phosphine to a bulkier P<sup>*t*</sup>Bu<sub>3</sub>, complex **19** (Entry 3), even if probably making the complex more stable towards air

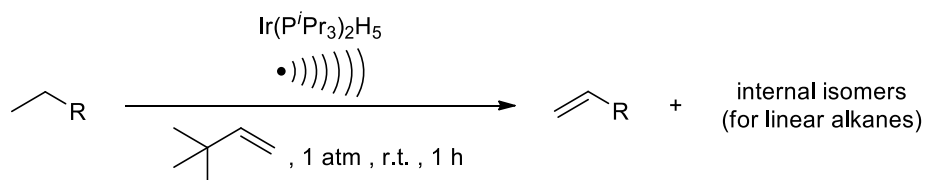
oxidation, seemed to increase the rate of the P-C cleavage and consequently decrease catalyst lifetime. This could be the explanation for the extremely low activity of the complex. A faster decomposition was also supported by the observation that the colour of the reaction mixture darkened from yellow to deep green after just few minutes of sonication, much faster than what happens when  $\text{Ir}(\text{P}^i\text{Pr}_3)_2\text{H}_5$ , complex **2**, was employed. Then, a slightly less hindered complex was tested, **17**. In this way, the steric bulk of the ligand was increased compared to complex **2**, hoping to further stabilise the metal centre, but not as much as with complex **19**, promoting the deactivation pathways. Unfortunately, again the sonochemical tests of this complex had shown that it was inactive towards alkane dehydrogenation under ultrasound irradiation (entry 4). Moreover, the tricyclohexylphosphine ligand made the complex not fully soluble in dodecane, forming a white suspension, even after sonication. The complexes bearing unsymmetrical phosphine ligands were also tested.  $\text{Ir}(\text{P}^t\text{Bu}_2{}^n\text{Bu})_2\text{H}_5$ , complex **23**, has a phosphine with a cone angle very similar to that of  $\text{Ir}(\text{P}^i\text{Pr}_3)_2\text{H}_5$ .<sup>137-138</sup> Although its similarity with the active pentahydride, even this complex had not shown any catalytic activity (entry 6). However, it is worth to note that the complex seemed to be more stable according to the changes in colour of the reaction mixture. The last new pentahydride complex **26** was then tested (Entry 8). Again, the changes in steric and electronic properties resulted in a complete deactivation of the system. Complexes **17** and **23** were also tested for longer reaction times, up to 2 hours of active sonication (Entries 5 and 7), but unfortunately only formation of traces of alkenes was observed.

Complex **2**, bearing the triisopropylphosphine, still appeared to be the most active compared with all the other complexes tested, being completely inactive or affording the desired dehydrogenated products only in trace amounts. The synthesis and subsequent sonochemical tests of other analogous complexes have been abandoned because even a small variation in the nature of the ligands leads to unpredictable results of drastically decreasing the activity of the system.

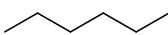
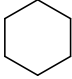
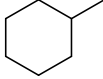
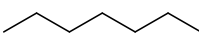
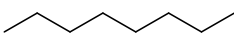
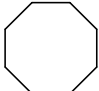
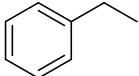

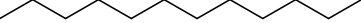
## 2.9 Scope of alkanes

As explained before, complex **2** was the most active for the sonochemical alkane dehydrogenation. To investigate the alkane scope of this reaction, complex **2** and 20 equivalents of TBE were screened in various solutions of different alkanes. Results are reported in Table 2.12.

Table 2.12 Scope of alkanes for the sonochemical transfer dehydrogenation.



### Alkane Scope (TON<sup>a</sup>)

|   |   |   |   |   |
|---|---|---|---|---|
|    |    |    |     |  |
| 1.2 <sup>b</sup><br>(0.2)   | 0.81<br>(0.03)  | 0.15<br>(0.04)  | 1.1 <sup>b</sup><br>(0.6)   | 0.8<br>(0.2)  |
|  |  |  |  |   |
| 0.7<br>(0.2)  | 0.58<br>(0.05)  | 1.2<br>(0.4)  | 1.19<br>(0.03)  |   |

Experimental conditions: reactions are carried out in neat alkane (5 mL) at room temperature ( $25 \pm 3$  °C) for 1 hour, under argon atmosphere, with a water cooling bath and with the microtip being cooled by a continuous stream of compressed air. Amplitude is 100%.  $\text{Ir}(\text{P}'\text{Pr}_3)_2\text{H}_5$  concentration is 5 mM. TBE concentration is 0.1 M. (a) TONs are based on quantitative GC analysis using isooctane as the internal standard and are reported as an average of two concordant runs. The number in parenthesis is the margin of error calculated with the z-score consistent for 99% confidence interval. (b) *n*-Dodecane is used as ISTD for the GC analysis.

To minimise the contribution from the reproducibility issues previously described (Section 2.2), each experiment was performed at least twice to ensure consistency. TONs were then reported as an average together with the margin of error as previously done in the literature.<sup>62</sup> The margin of error was calculated with the z-score consistent for the 99% confidence interval as in Equation 2.

$$\begin{aligned} \text{Margin of error} &= z \times \frac{\sigma}{\sqrt{n}} && \text{Equation 2} \\ z &= z\text{-score } (z_{99\%} = 2.58) \\ \sigma &= \text{relative standard deviation} \\ n &= \text{number of tests} \end{aligned}$$

As it can be seen, the conversion was limited by catalyst deactivation, with *n*-hexane showing a similar TON value to *n*-octane, *n*-decane and *n*-dodecane, 1.2, 1.2 and 1.19 respectively. Therefore, it can be assumed that all the linear alkanes have a similar activity towards the dehydrogenation, regardless of the chain length. This means that the small differences in the results between the dehydrogenation of *n*-heptane and *n*-octane, 1.1 and 0.8 TONs, compared to *n*-hexane and *n*-dodecane, can be owned to the issues of the apparatus.

The product alkene was always obtained as a mixture of linear and internal isomers, except for cyclic alkanes when only one isomer was formed. Surprisingly, the TONs for the formation of cyclohexene and cyclooctene, 0.81 and 0.7 TON respectively, were lower than the corresponding linear counterparts. This is an unusual result because, in general, cyclic alkanes are much more suitable for the dehydrogenation with respect to the linear ones. This is because of the higher C-H bond enthalpy of linear alkanes, which makes their back-hydrogenation more exothermic, and also because they are more prone to product inhibition, due to the stronger binding of linear olefins to the catalyst.<sup>32</sup> The fact that the rate of the dehydrogenation usually correlates with the stability of the alkene product, suggests that the rate determining step is the  $\beta$ -H-elimination from the alkyl-hydride intermediate.<sup>23</sup> Instead in the system analysed, based on the results, the rate determining step might be the C-H activation, which is known to be slower for cyclooctane compared to its linear analogue.<sup>140</sup> In fact, because the dehydrogenation usually proceeds *via* an oxidative addition, the process results very sensitive to the steric effects. Under sonochemical conditions those effects could be predominant, favouring the dehydrogenation of linear alkanes over the cyclic counterparts.

This is further supported by the case of methylcyclohexane dehydrogenation. Methylene cyclohexane is the preferred kinetic product, as reported in the literature.<sup>40</sup> This



is because the C-H activation occurs preferentially on the terminal position with the attack on the primary carbon, favouring the oxidative addition process. Subsequent isomerisation of the alkene product yields 1-methylcyclohexene as the major product from cyclohexane as reported in the literature.<sup>38</sup> In the sonochemical experiment after 1 hour of sonication, 0.15 TON was obtained as a mixture of approximately 1:1 of methylenecyclohexane/methylcyclohexene isomers.

This result, where the linear alkane appeared to undergo dehydrogenation in higher yields than the cyclic homologue, is also supported by the measurements of the relative kinetic reactivities of various types C-H bonds of alkanes. The same complex **2** was used as the dehydrogenation catalyst, but under thermal conditions. Those reactivities were experimentally found to be approximately: *sec*-alkyl-H (CH<sub>2</sub> in cyclohexane) 1; *iso*-alkyl-H (CH<sub>3</sub> in methylcyclohexane) 8; and *n*-alkyl-H (CH<sub>3</sub> in *n*-hexane) >60.<sup>40</sup>

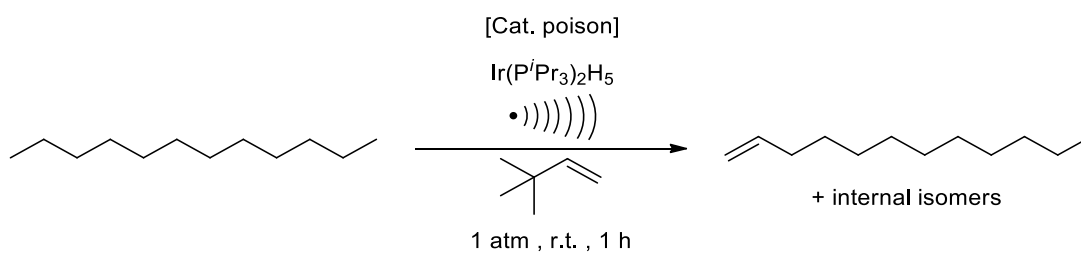
The effect of the complex decomposition was also influencing the result. The system deactivation was becoming more severe because less reactive substrates were tested, such as going from *n*-hexane, to cyclohexane, to methylcyclohexane. This might be because the deactivation rate remains constant, but the rate of product formation decreases drastically when moving to a less reactive substrate. This affected the rate ratio, and the system deactivation appeared to be faster as less alkenes were formed.

The last alkane tested was ethylbenzene. It was investigated due to its dehydrogenation product was styrene, which is one of the largest produced olefin on industrial scale, with 20 million tonnes per year.<sup>141</sup> Under sonochemical conditions it was obtained with 0.58 TON after 1 hour of active sonication.

Different alkanes, from C<sub>6</sub> to C<sub>12</sub>, were tested as substrates for the sonochemical alkane dehydrogenation promoted by an iridium pentahydride complex. Although TONs were low and the reaction cannot be considered catalytic yet, the results are extremely important as they show feasibility for the sonochemical approach. Different types of alkanes have been tested with the linear ones, which appear to be easier dehydrogenated compared to their cyclic counterparts. Although the reaction is only slightly more than stoichiometric, it is a proof of concept and the results could be further improved in the future by solving the problem of system deactivation.

## 2.10 Distinguishing between homogeneous and heterogeneous catalysis

From the literature it is well known that the starting Ir-pentahydride complex is a homogeneous catalyst,<sup>39</sup> but there is no mention about its behaviour under ultrasound irradiation. The aim was to determine whether the active iridium species is heterogeneous or homogeneous. Even if complex **2** is known to be a soluble metal complex, under ultrasonic irradiation it may decompose to give a heterogeneous species in the form of metal powder, film or colloidal form, not necessarily as visible precipitate. Moreover, under the reaction conditions investigated, ultrasound provides an unusual reaction environment and iridium nanoparticles could be generated thanks to the ultrasonic treatment, making the reaction heterogeneous.<sup>142</sup> As mentioned in Section 2.7.1.4, it is important to consider that in the reaction mixture over time the formation of some solid particles can be observed. A question also remains whether the activity observed was due to the homogeneous or heterogeneous component of the system, the above-mentioned solid particles. Therefore, experiments were run to understand if the sonochemical reaction was a homogeneous or heterogeneous system. The most typical test to check whether the solid particles formed are the actual catalyst would be to isolate those particles and then test them as catalyst in the system. Unfortunately, due to the high air sensitivity of the components this could not be done, therefore different methods have been investigated. Addition of selective poisons is often used in the attempt to distinguish between authentic homogeneous catalysts and heterogeneous analogues.<sup>143</sup> Suitable ones have been chosen and applied to our system (Scheme 2.24).



[Cat. poison] = Dibenzo[*a,e*]cyclooctatetraene (dct),  $\text{Hg}^0$



Scheme 2.24 Iridium poisoning experiments with dct.

First, a test to prove the homogeneity of the metal complex was carried out. This consisted in the addition of dibenzo[*a,e*]cyclooctatetraene (dct) to the reaction mixture. This compound is an excellent ligand and has been previously reported in the literature to be used as efficient selective poison for homogeneous iridium complexes.<sup>144</sup> The dct strongly binds to the metal centre killing the activity and acting as a “suicide inhibitor”. It strongly binds to the complex as an olefin does and cannot dissociate from the iridium centre anymore. Therefore, the iridium complex cannot form anymore the coordinatively unsaturated species required for the catalysis, but it forms a catalytically inert complex with the dct ligand. On the other hand, its rigidity also prevents it from binding the surface of heterogeneous catalysts, therefore it will not impede their catalytic activity.

Concerning the system under analysis, the dct could not be added from the beginning of the reaction, otherwise it would immediately bind to the homogeneous iridium-pentahydride complex and kill the activity of the complex.<sup>144</sup> An experimental protocol had to be developed. First the reaction was run for 10 minutes, aiming to produce the catalytically active complex and only then the dct was added to the reaction mixture. The response of the system to the dct poisoning was then detected by comparison between the TON obtained after 10 minutes and the TON obtained after 1 hour of ultrasound irradiation under the same conditions.

As it can be observed from the graph (Figure 2.16), at first a reaction was run using 1 equivalent of dct compared to the metal, but the reactivity pattern observed was just slightly affected compared to the standard reaction carried out in the absence of poison. The ratio of dct was then increased to 10 equivalents compared to the iridium complex and this time

the reaction was inhibited confirming the homogeneity of the active complex. As it can be seen from the graph, the TON obtained after 10 minutes remained constant and no further alkene formation could be observed even after 1 hour. This experiment was also run a second time to confirm that the inactivity was really due to the effect of the dct and not to a leak in the system.

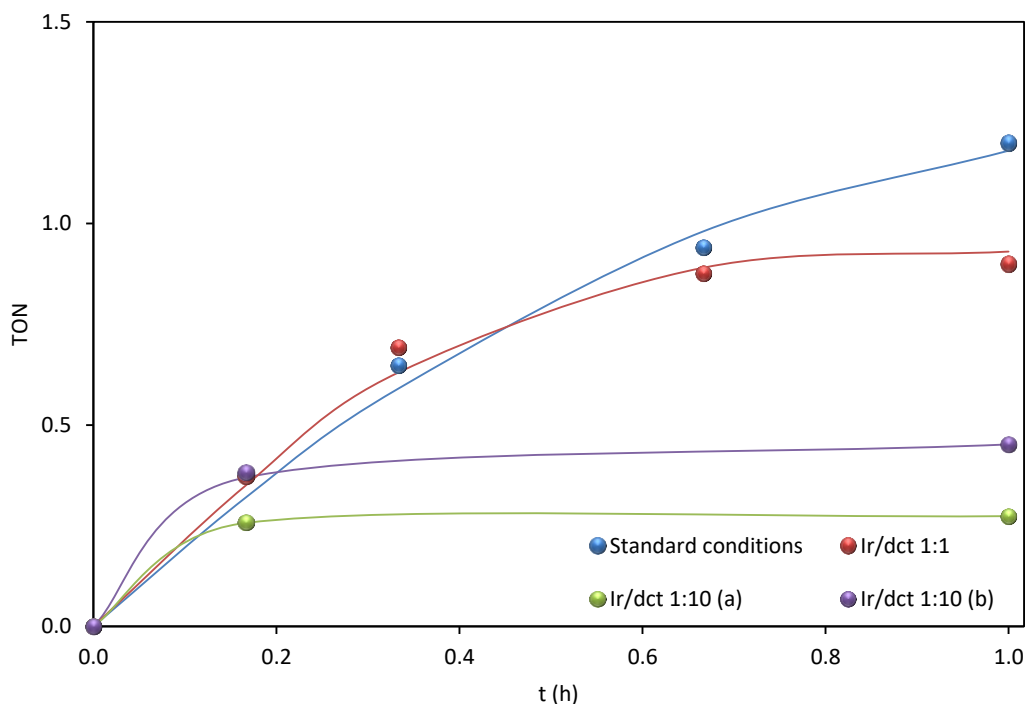


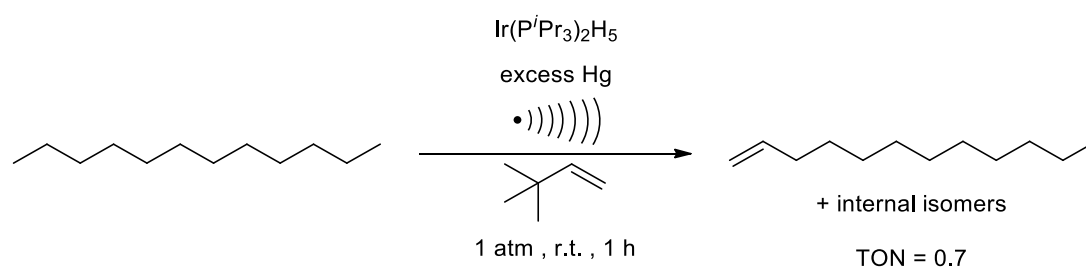
Figure 2.16 Effects of the addition of dct to the sonochemical *n*-dodecane dehydrogenation.

A second test was also carried out to further support the homogeneity of the active complex. Liquid mercury is used as a complementary test because it is reported to be a popular poisoning test for heterogeneous metal complexes.<sup>142-143</sup> Mercury reacts with the surface of the metal particles, deactivating the complex.<sup>145</sup> If a metal-catalysed process stops in the presence of mercury, then it must be a heterogeneous catalyst. Although this last assumption has been recently disproven with the example of false-positive results with palladium complexes,<sup>146</sup> this type of poisoning test was used on the sonochemical process, assuming to be reliable as long as consistent results with the dct test were obtained.

As mentioned before, a homogeneous transition metal complex can form heterogeneous soluble metal particles, which can be easily missed because not observable by the naked eye as for some colloidal solutions. Moreover, forcing reaction conditions, as the ultrasound, facilitates the formation of heterogeneous complexes, hypothesis which is supported by the formation of dark reaction solutions or precipitates.<sup>142</sup> Often, the transition metal complex

added to the reaction mixture is not the true catalyst, but a precursor which is then converted *in situ* into the catalytically active species that might be heterogeneous.

To avoid misleading conclusions, it was important that the mercury was in contact with the entire reactor: this could be guaranteed by using the Hg(0) in excess and a proper mixing of the solution, granted by the ultrasound induced stirring. An excess amount of mercury compared to the iridium complex was added to the reaction mixture at the beginning of the reaction (500 equivalents) (Scheme 2.25). The addition of mercury had little to no effect on the rate of the reaction, further supporting the hypothesis of the homogeneous reaction (TON=0.7). Indeed, the system passed the mercury poison test ruling out the possibility of deposited metal or nanoparticles contributing to the alkane dehydrogenation.



Scheme 2.25 Mercury poisoning test for the iridium-mediated sonochemical alkane dehydrogenation.

To summarise, the reaction was investigated and reliable conclusions could be drawn based on the outcome of these experiments. The dct poisoning experiment previously described was complementary to the mercury poisoning one. The reaction was completely inhibited with 10 equivalents of dct, and the mercury drop test had a little effect on the reaction rate. Those two combined results are strong evidence for an authentically homogeneous reaction. The dct and mercury tests complement each other, and they are both consistent with the fact that the sonochemical alkane dehydrogenation reaction is promoted by a homogeneous iridium species.

## 2.11 Conclusion

In this chapter the first example of ultrasound driven dehydrogenation of alkanes at room temperature has been reported. Although the iridium pentahydride complex presented showed only a small turnover, the concept of using ultrasound as the energy source, in combination with a hydrogen acceptor, provides an unprecedented route towards transfer dehydrogenation of alkanes, transforming this inexpensive hydrocarbon feedstocks into value-added commodity chemicals. This new approach also offers a key advantage compared to other processes: mild reaction conditions, with the reaction temperature of 25 °C being significantly lower than that reported for known homogeneous systems.<sup>24-25, 28, 39, 43, 61-62, 70, 147</sup>

A sonochemical reactor able to conduct catalytic reactions under inert atmosphere has been assembled.

Different homogeneous catalysts reported in the literature to be active for the alkane dehydrogenation have been synthesised and tested for the sonochemical transfer alkane dehydrogenation, but the iridium complex **2** was the only one found to be effective under our operating conditions.

This preliminary screening of complexes for the model sonochemical dehydrogenation of alkanes identified  $\text{Ir}(\text{P}^i\text{Pr}_3)_2\text{H}_5$  **2** as the catalyst able to perform this transformation by the means of acoustic cavitation. A system optimisation allowed to slightly increase the TON and the highest yield obtained of desired alkene product was 1.2 TON. According to the optimisation performed, the use of the iridium complex had to be combined with a hydrogen acceptor under ultrasound irradiation to drive the reaction.

Temporal control experiment showed that the dehydrogenation takes place only under ultrasound irradiation, indeed, in the future ultrasound could be used as a physical mode to control the proceeding of the reaction.

A major challenge with this approach was the complex decomposition and it was probably the main cause of the low turnover efficiency under the reported conditions. To further study the developed system, preliminary tests on the catalyst deactivation processes were conducted. These studies indicated that some decomposition pathways could be excluded, such as cyclometalation and product inhibition. The most probable cause for complex decomposition appeared to be related to its stability under ultrasound irradiation. However, no conclusive information could be obtained on the deactivated system.

A series of literature reported bisphosphine-iridium-pentahydride complexes bearing different trialkyl-phosphine ligands with smaller and larger steric bulk were also synthesised and tested, together with two novel bisphosphine-iridium-pentahydride complexes bearing

unsymmetrical trialkyl-phosphine ligands. Unfortunately, when tested for the sonochemical alkane transfer dehydrogenation, all of them were either inactive or afforded alkenes in traces. Surprisingly, even small variations in the alkyl groups on the phosphine ligands seemed to extremely affect the activity of the system.

This sonochemical process represented a new route for the transfer dehydrogenation of alkanes C<sub>6</sub>-C<sub>12</sub> to a mixture of terminal and internal olefins as well as of cyclic alkanes C<sub>6</sub> and C<sub>8</sub> and ethylbenzene. While examining the scope of this reaction, a counter-intuitive reactivity of the alkenes was observed, where linear alkanes were more easily dehydrogenated compared to the cyclic counterparts. Additionally, more complex substrates such as ethylbenzene were also dehydrogenated with more difficulty.

To investigate the homogeneity or heterogeneity of the reaction, dct and mercury tests have been carried out. Those two tests complemented each other and both highlighted that the sonochemical alkane dehydrogenation reaction was promoted by a homogeneous iridium species.

In conclusion, in contrast to classical alkane dehydrogenation, the method developed allowed the use of ultrasound as the alternative energy source. The system is still in its early stages of development, with some issues that need to be addressed. It was demonstrated that the iridium pentahydride complex could activate a C-H bond of various alkanes under ultrasound irradiation and *tert*-butylethylene as the hydrogen acceptor, providing a mild route to their dehydrogenation, with the reaction temperature of 25 °C being significantly lower than the ones reported for most known homogeneous systems. The feasibility of the sonochemical dehydrogenation for different alkanes have also been shown.

Promising preliminary results for the sonocatalytic transfer alkane dehydrogenation have been obtained, supporting the original idea behind the project. This is an unprecedented encouraging result, which also represents the first example of a conceptually new alkane dehydrogenation promoted by ultrasound. This is a good starting point on the way to develop a cleaner and more sustainable synthetic route to obtain olefins under mild conditions, exploiting the use of ultrasound irradiation in the presence of a homogeneous catalyst, with the potential for the development of a new catalytic version.

## 2.12 Possible future plans

The development of this general method for the mild alkane dehydrogenation needs to be further investigated. Up to date, the system does not show high activity. The optimised conditions only allow for a turnover of 1.2, but it is a good starting point to work further on the system optimisation and in principle achieving a catalytic reaction.

An extensive catalyst screening for the dehydrogenation of alkanes should be conducted. For this purpose, as even small variations in the phosphine alkyl groups seemed to drastically affect the activity of the system, an extensive screening is necessary, including also complexes that does not have any resemblance to the active one. Moreover, other iridium complexes could be considered as alternative catalysts. Many ones have been described as effective catalysts for the alkane dehydrogenation, especially pincer iridium complexes which are amongst the most active.<sup>43</sup> Another possibility is a class of rhenium polyhydride complexes, for example the  $\text{Re}(\text{PPh}_3)_2\text{H}_7$  developed by Felkin.<sup>33</sup>

As discussed, during the studies of this approach for the alkane dehydrogenation, decomposition of the iridium species has been observed. Unfortunately, the decomposed species could not be identified as well as for the exact deactivation process. The investigation has been abandoned due to time constraints, but further studies of the system might be helpful to shed some light on the complex decomposition. For example, as described in this work, the reaction mixture changed colour over time, therefore an *in situ* UV-vis analysis of the solution might give some more information on the metal species.

Additionally, as described previously, the reactor developed had some limitations because it was not completely airtight. During the reaction, the up and down movement of the microtip caused small leaks which cannot be controlled and contributed to the decomposition of the complex. To improve this problem, it might be worth to invest in the developed of custom-made reactor from QSONICA, which will guarantee strictly air free conditions.

An extended catalyst screening and/or a more in-depth analyses in the attempt to minimise the catalyst deactivation could, hopefully, lead to an improvement of the system making the sonochemical alkane dehydrogenation a catalytic process.

Moreover, the developed process in this project could be applied to the dehydrogenation of shorter alkanes such as propane and butane, which are gases and would require a specific set-up and analysis procedure. This possibly could be done *via* a similar set up to the one used by Beller and co-workers for the alkane dehydrogenation under UV-irradiation.<sup>70</sup> For example, in the case of butane the alkane must be gently bubbled in the reaction mixture



during the total time of the reaction. The reaction vessel must be equipped with a gas cooling trap to collect the butane/butenes mixture which would escape from the reaction vessel. The system has been designed and planned to show the applicability of the developed method to shorter alkanes but remains a near future work due to the limited time available.

## 2.13 Experimental section

### 2.13.1 Materials and general procedures

All reactions and manipulations were performed under argon atmosphere either in a glovebox or using standard Schlenk techniques and apparatus. All glassware and magnetic stirring bars were kept in an oven at 120 °C for at least two hours and let to cool down under vacuum before use.

The alkanes for the catalytic reactions were dried over 4 Å molecular sieves, degassed by several freeze-pump-thaw cycles and stored in an Argon-atmosphere glovebox or Sure/Stor™ flasks under argon.

Solvents used in the syntheses were dried and distilled under argon by standard procedures<sup>148</sup> and stored under an Argon atmosphere. THF, Et<sub>2</sub>O, toluene, hexane, and chloroform were dried by distillation over Na-benzophenone ketyl. MeOH was distilled over CaH<sub>2</sub>. Anhydrous benzene was purchased from Alfa Aesar and stored under argon in the glovebox. All distilled solvents were stored either in Sure/Stor™ flasks under argon or in the glovebox. Acetone and <sup>1</sup>PrOH were degassed by several freeze-pump-thaw cycles, stored in Sure/Stor™ flasks under argon and used fresh.

Deuterated solvents were purchased from Cambridge Isotopes; they were degassed by several freeze-pump-thaw cycles and stored over 4 Å molecular sieves under an argon atmosphere in Sure/Stor™ flasks.

All other reagents were used as received without any further purification. All chemicals were purchased from commercial suppliers (Merck Sigma-Aldrich, Alfa Aesar, Strem Chemicals, Pressure Chemicals, Cambridge Isotopes, TCI, VWR or Fisher chemical companies).

### 2.13.2 Equipment and methods

For catalytic reactions, quantitative analyses were performed by gas chromatography on an Agilent 7890A GC system equipped with a DB-WAXETR column (Fused Silica Capillary Column 60 m x 0.25 mm x 0.25 μm film thickness) or on an Agilent 6890N network GC system equipped with a ZB-WAX column (Fused Silica Capillary Column 30 m x 0.25 mm x 0.25 μm film thickness). Both GC were equipped with an FID detector. For details on instruments parameters see Section 2.13.4.

Nuclear Magnetic Resonance (NMR) spectra were acquired on a Bruker Avance III 500 MHz, Bruker 400 MHz and Bruker DPX 400 MHz spectrometers. Chemical shifts for <sup>1</sup>H-NMR

and  $^{13}\text{C}$ -NMR are reported in ppm relative to a peak of residual solvent with ppm as reported in the literature,<sup>149</sup> for  $^{31}\text{P}$ -NMR relative to  $\text{H}_3\text{PO}_4$ . The data are reported as follows: chemical shift in ppm ( $\delta$ ); multiplicity; coupling constants in Hz (J); integration, assignment. The splitting patterns are designated as follows: s (singlet), d (doublet), t (triplet), q (quartet), m (multiplet), dd (doublet of doublets), dt (doublet of triplets), br (broad).

Mass spectrometry analyses were conducted by the EPSRC UK National Mass Spectrometry Facility at Swansea University. Samples of compounds were sent to Swansea University in sealed ampullas under argon. Spectra were acquired under argon on an Agilent QTOF 6540 using EI and ASAP ionisation methods.

The TGA were performed on a Linseis STA PT-1000 (TG-DSC/DTA) Thermogravimetric Analyser. The DSC were performed on a Netzsch DSC 214 Polyma.

The glovebox used was argon filled Innovative Technologies PureLab HE cp-1.

Sonochemical experiments were performed using a Sonic Dismembrator Ultrasonic Processor (Fisher Scientific™, Model 705, 50/60 Hz, 700 W): equipped with a 1/8" Microtip (Fisher Scientific™, Catalog n. F6318); inside a Sound Enclosure (Fisher Scientific™, Catalog n. F622B).

The light source for the photocatalytic experiment was a Xe DC ARC LAMP, Newport, Model 66902, lamp power 50-500 W (set at 300 W), equipped with a water-cooling system. The UV-filter, supposed to cut the UV-contamination, was removed.

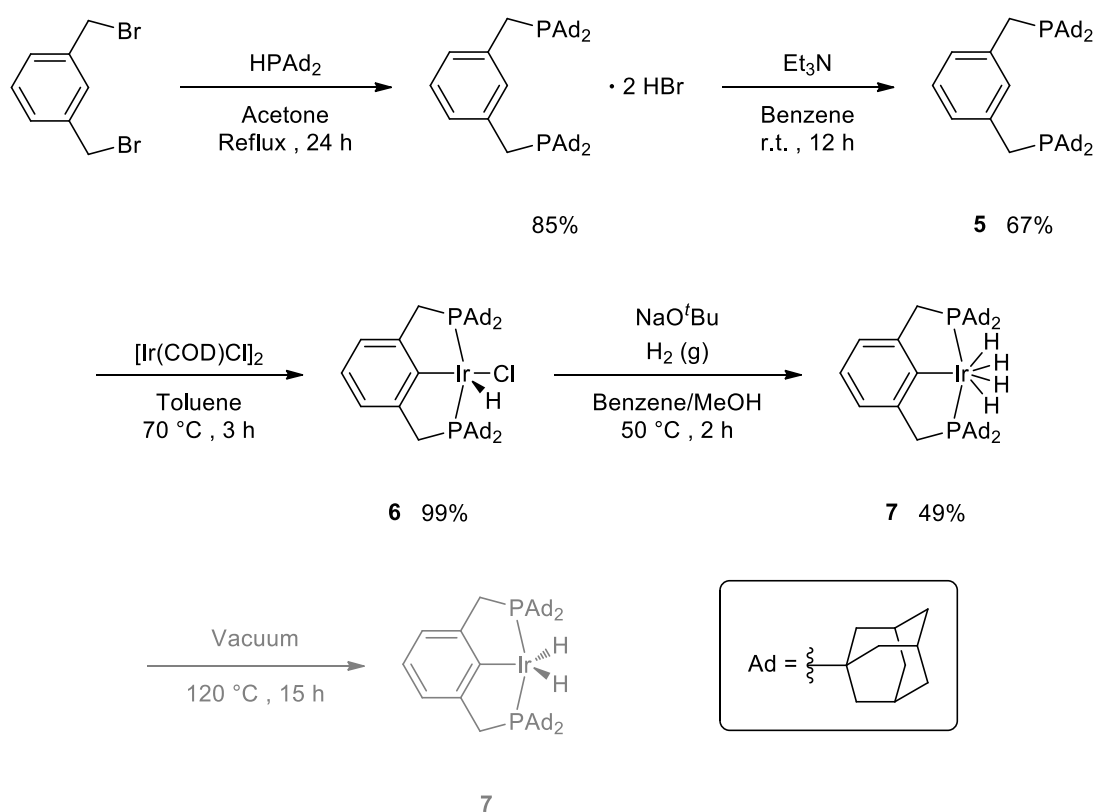
## 2.13.3 Synthesis of the complexes

### 2.13.3.1 Catalysts from the literature

#### 2.13.3.1.1 Synthesis of Ir(<sup>Ad</sup>PCP)H<sub>4</sub> and attempts for the synthesis of Ir(<sup>Ad</sup>PCP)H<sub>2</sub>

The literature procedure<sup>56</sup> has been followed with some modifications as described.

Synthetic route:

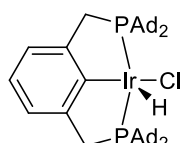


**Synthesis of <sup>Ad</sup>PCP-H (5).**<sup>56</sup> A mixture of di-1-adamantylphosphine (1.5 g, 5.02 mmol) and 1,3-dibromobenzene (0.65 g, 2.48 mmol) in degassed acetone (60 mL) was heated to reflux for 24 h. Once cooled to room temperature, the solvent was cannulated out and the white precipitate was dried under vacuum. The salt was transferred into the glovebox, benzene (60 mL) and TEA (0.54 g, 5.37 mmol) were added and the mixture was stirred overnight. The next morning the yellowish solution was separated *via* cannula filtration to remove the Et<sub>3</sub>N·HBr salt. The mother liquor was then concentrated to dryness to obtain a light yellow solid. Crude yield 1.48 g, 85%.

**Recrystallization to eliminate the ammonium salt impurity.** The yellowish phosphine (770 mg) was dissolved in chloroform (15 mL), then methanol (40 mL) was added and the solution was cooled in an ice-bath in order for the phosphine to precipitate. The solution was

then cannulated out and the remaining solid was washed with methanol. A white crystalline solid was obtained. Yield 521 mg, 67%.

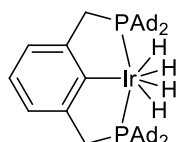
$^1\text{H}$  NMR (500 MHz, d-Toluene):  $\delta$  7.74 (s, 1H, *ipso*Ar-H), 7.34 (d,  $^3J_{\text{H-H}}=7.6$  Hz, 2H, Ar-H), 7.22 (t,  $^3J_{\text{H-H}}=7.5$  Hz, 1H, Ar-H), 2.85 (d,  $^2J_{\text{P-H}}=2.4$  Hz, 4H, bridging-CH<sub>2</sub>), 1.95 (s, 24H, 12Ad-CH<sub>2</sub>( $\alpha$ )), 1.88 (s, 12H, 12Ad-CH( $\beta$ )), 1.69 (s, 24H, 12Ad-CH<sub>2</sub>( $\gamma$ )).  $^{31}\text{P}\{^1\text{H}\}$  NMR (202 MHz, d-Toluene):  $\delta$  28.5 (s). NMR data are in accordance with the literature.<sup>56</sup>



**Synthesis of ( $^{\text{Ad}}\text{PCP}$ )IrHCl (6).**<sup>56</sup> A mixture of  $^{\text{Ad}}\text{PCP-H}$  (209 mg, 0.30 mmol) and  $[\text{Ir}(\text{COD})\text{Cl}]_2$  (99 mg, 0.15 mmol) in toluene (8.5 mL) was heated at 70 °C for 3 h under H<sub>2</sub> atmosphere. Once the solution cooled to room temperature, the solvent was removed under reduced pressure to yield a dark brown-red solid. Yield 280 mg, 99%.

$^1\text{H}$  NMR (500 MHz, C<sub>6</sub>D<sub>6</sub>):  $\delta$  7.01-7.01 (m, 3H, Ar-H), 3.29 (d,  $^2J_{\text{H-H}}=17.5$  Hz, 2H, CH<sub>2</sub>(H<sub>a</sub>)), 3.12 (d,  $^2J_{\text{H-H}}=17.4$  Hz, 2H, CH<sub>2</sub>(H<sub>b</sub>)), 2.16-2.57 (m, 24H, Ad-CH<sub>2</sub>), 1.81-1.87 (m, 12H, Ad-CH), 1.51-1.69 (m, 24H, Ad-CH<sub>2</sub>), -43.15 (t,  $^2J_{\text{P-H}}=11.95$  Hz, 1H, Ir-H).  $^{31}\text{P}\{^1\text{H}\}$  NMR (202 MHz, C<sub>6</sub>D<sub>6</sub>):  $\delta$  57.4 (d,  $^2J_{\text{P-H}}=25.3$  Hz). NMR data are in accordance with the literature.<sup>56</sup>

Used in the sonochemical experiments as Ir( $^{\text{Ad}}\text{PCP}$ )HCl and activated *in situ* with NaO<sup>t</sup>Bu (1.2 eq.).



**Synthesis of ( $^{\text{Ad}}\text{PCP}$ )IrH<sub>4</sub> (7).** A mixture of Ir( $^{\text{Ad}}\text{PCP}$ )HCl (251.1 mg, 0.27 mmol) and NaO<sup>t</sup>Bu (33.8 mg, 0.35 mmol) in benzene (25 mL) was prepared in a Schlenk flask. Methanol (12.5 mL) was added to the mixture and hydrogen was bubbled through the reaction mixture until the dark red solution turned yellow. The reaction was heated at 50 °C for 3 h under hydrogen atmosphere. Once the reaction mixture was cooled down, methanol (10 mL) was added to precipitate the product which was collected *via* cannulation and washed with cold methanol (3 x 10 mL). The solid was dried under vacuum for 30 min to obtain a light-yellow powder. Total yield 118 mg, approximately 49%.

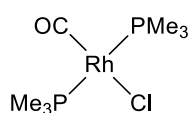
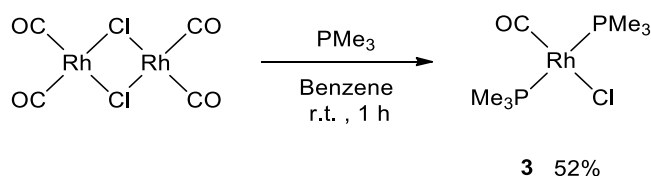
Product distribution calculated from NMR data: 70% Ir( $^{\text{Ad}}\text{PCP}$ )H<sub>4</sub>, 18% Ir( $^{\text{Ad}}\text{PCP}$ )H<sub>2</sub>, 12% unknown phosphine hydride species. All attempts to separate or interconvert the products into one single species failed. Used in the sonochemical experiments as a mixture of the two hydride species.  $^1\text{H}$  NMR (500 MHz, C<sub>6</sub>D<sub>6</sub>):  $\delta$  7.22-7.55 (m, 3H, Ar-H), 3.48-3.66 (m, 4H, 2CH<sub>2</sub>), 1.21-2.64 (m, 60H, 4Ad), -9.20 (t,  $^2J_{\text{P-H}}=10.75$  Hz, 4H, Ir-H<sub>4</sub>), -12.02 (m, Ir-H<sub>x</sub>), -19.28 (m, 2H, Ir-H<sub>2</sub>).  $^{31}\text{P}\{^1\text{H}\}$  NMR (202 MHz, C<sub>6</sub>D<sub>6</sub>):  $\delta$  73.35 (s, PIr-H<sub>4</sub>), 76.64 (s, PIr-H<sub>x</sub>), 80.79 (s, PIr-H<sub>2</sub>).

Attempts for the hydrogenation step to **synthesise (<sup>Ad</sup>PCP)IrH<sub>2</sub> (1)**:

- Reducing agent and bases tested: LiEt<sub>3</sub>H (fresh bottle) in toluene, KO<sup>t</sup>Bu or NaO<sup>t</sup>Bu in Benzene;
- Base used in different amounts: from 1.2 eq. to large excess;
- Reaction performed at different temperatures: r.t., 50 °C, 80°C (in a Schlenk bomb);
- Reaction progress monitored by NMR: complete conversion was never achieved;
- Titration of H<sub>2</sub>O content in Toluene and Benzene: low ppm amounts;
- Addition of trace amounts of H<sub>2</sub>O (in the paper they could have used a “wet” solvent and the traces amounts of water could have facilitated the chloride abstraction);
- Addition of MeOH from trace amounts to excess (same idea as for H<sub>2</sub>O: due to its high polarity it could facilitate the chloride abstraction).

#### 2.13.3.1.2 Synthesis of trans-Rh(CO)(PMe<sub>3</sub>)<sub>2</sub>Cl

The literature procedure<sup>113-114</sup> has been followed. Synthetic route:



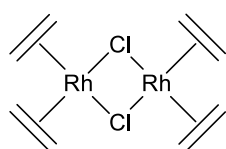
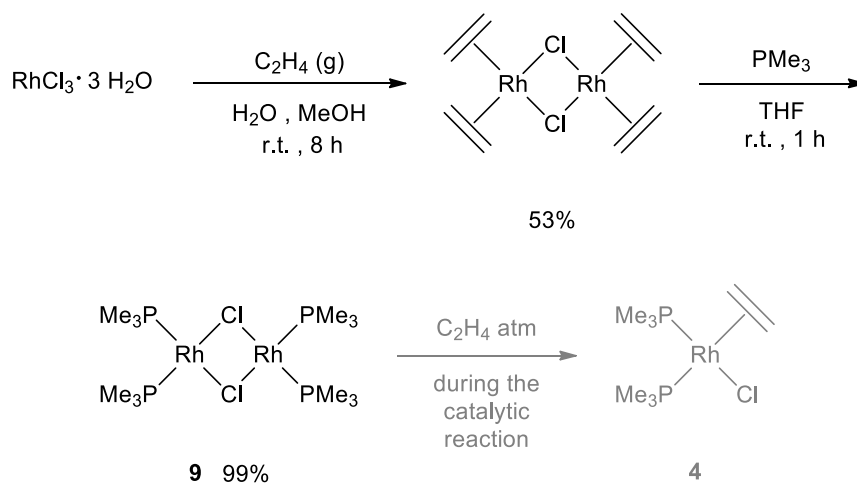
**Synthesis of trans-Rh(CO)(PMe<sub>3</sub>)<sub>2</sub>Cl (3).** Trimethylphosphine (73.8 mg, 0.97 mmol) was added dropwise to a solution of [Rh(CO)<sub>2</sub>Cl]<sub>2</sub> (85 mg, 0.22 mmol) in benzene (1 mL) at room temperature under vigorous stirring.

After the CO evolution ceased (the solution stopped fizzing), the mixture was stirred for 1 hour. Formation of a yellow precipitate was observed. The solution was concentrated under reduced pressure, the solid was dissolved in hot methanol, cooled very slowly to 0 °C and placed in the freezer overnight. At -77 °C, the solution was cannulated out and the yellow prisms washed with cold MeOH and then cold hexane. The yellow crystalline solid was dried under vacuum. Yield 73 mg, 52%.

<sup>1</sup>H NMR (500 MHz, d-Toluene): δ 1.16 (s, 18H, CH<sub>3</sub>). <sup>31</sup>P{<sup>1</sup>H} NMR (202 MHz, d-Toluene): δ -10.46 (s). NMR data are in accordance with the literature.<sup>113-114</sup> MS (EI+): m/z 318.0-319.9 (mol. peak) [Rh(CO)(PMe<sub>3</sub>)<sub>2</sub>Cl]<sup>+</sup>, 289.9-292.0 [Rh(PMe<sub>3</sub>)<sub>2</sub>Cl]<sup>+</sup>, 254.0 [Rh(PMe<sub>3</sub>)<sub>2</sub>]<sup>+</sup>, 177.9 [RhPMe<sub>3</sub>]<sup>+</sup>.

### 2.13.3.1.3 Synthesis of $[\text{Rh}(\text{PMe}_3)_2\text{Cl}]_2$

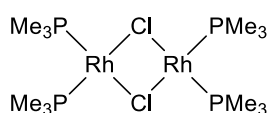
Synthesised according to literature procedure.<sup>115-118</sup> Synthetic route:



#### Synthesis of $[\text{Rh}(\text{C}_2\text{H}_4)_2\text{Cl}]_2$ .<sup>115-116</sup> $\text{RhCl}_3 \cdot 3\text{H}_2\text{O}$ (135.2 mg, 0.51 mmol)

was solubilised in distilled, degassed water (0.3 mL), then MeOH (3.4 mL) was added and ethylene purged through the reaction mixture and left bubbling for 8 hours. The solution was cannulated out, the orange solid was washed with MeOH and  $\text{Et}_2\text{O}$  and dried under vacuum. Yield 52.5 mg, 53%.

$^1\text{H}$  NMR (500 MHz,  $\text{CDCl}_3$ ):  $\delta$  3.12 (bs, 16H,  $8\text{CH}_2$ ).  $^{13}\text{C}\{^1\text{H}\}$  NMR (101 MHz,  $\text{CDCl}_3$ ):  $\delta$  61.51 (d,  $^1J_{\text{C-Rh}}=65.9$  Hz, 8C,  $8\text{CH}_2$ ). NMR data are in accordance with the literature.<sup>115-116</sup>

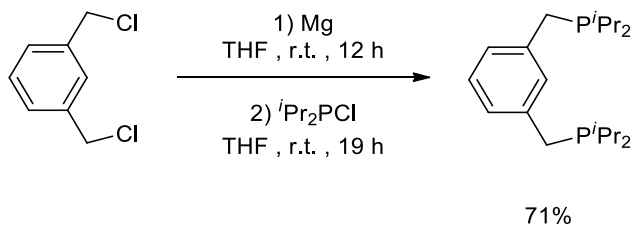


#### Synthesis of $[\text{Rh}(\text{PMe}_3)_2\text{Cl}]_2$ (9).<sup>117-118</sup> Trimethylphosphine (73.8

mg, 0.97 mmol) was added dropwise to a solution of  $[\text{Rh}(\text{C}_2\text{H}_4)_2\text{Cl}]_2$  (89.5 mg, 0.23 mmol) in THF (2.5 mL) upon vigorous stirring. After ethylene evolution ceased, the mixture was stirred for additional 20 minutes. The solvent was removed under reduced pressure and the product was obtained as a light brown-orange solid. Yield 134 mg, 99%.  $^1\text{H}$  NMR (500 MHz,  $\text{C}_6\text{D}_6$ ):  $\delta$  1.11 (d,  $^2J_{\text{H-P}}=4.6$  Hz, 36H,  $12\text{CH}_3$ ).  $^{31}\text{P}\{^1\text{H}\}$  NMR (202 MHz,  $\text{C}_6\text{D}_6$ ):  $\delta$  -21.24 (bs). NMR data are in accordance with the literature.<sup>117-118</sup> HRMS (ASAP)  $m/z$ : found 580.9341 for  $[\text{RhH}(\text{PMe}_3)_2\text{Cl}]^+$ , calculated for  $[\text{M}+\text{H}]^+ = [\text{C}_{12}\text{H}_{37}\text{Cl}_2\text{P}_4\text{Rh}_2]^+ = 580.9333$ .

#### 2.13.3.1.4 Synthesis of <sup>i</sup>PrPCPH

Synthesised by Marta Fernandez-Gimenez according to literature procedure.<sup>150</sup> Synthetic route:

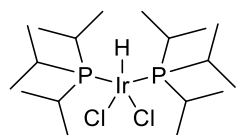
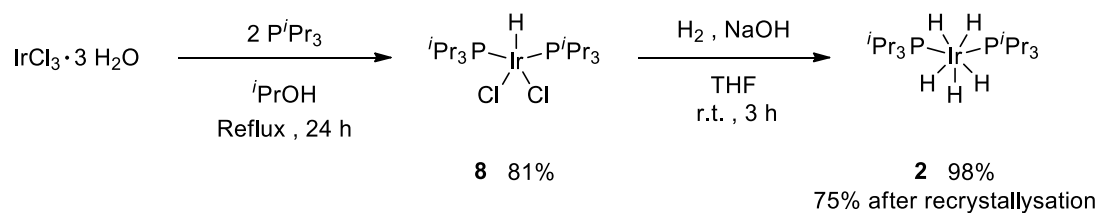


A 500 ml three-neck round bottom flask equipped with magnetic stirring, an addition funnel and a condenser was charged with Mg turnings (1.49 g, 60.8 mmol) and THF (21 ml). To this mixture 1,2-dibromoethane (0.2 ml, 2.32 mmol) was added at room temperature. The mixture was gently heated until ethylene evolution was observed. Then, *m*-dichloro-xylene in THF (190 ml) was added dropwise followed by THF (16.5 ml). The reaction mixture was stirred for 12 hours at room temperature. Filtration to remove excess Mg followed by titration of this solution with *n*-butanol and menthol using 1,10-phenanthroline as an indicator, revealed formation of the desired 1,3-bis[(chloromagnesium)methyl]benzene product in 92% yield. The resulting Grignard reagent (4.5 g, 14.4 mmol) was added at 0 °C to a solution of <sup>i</sup>Pr<sub>2</sub>PCl (4.50 g, 28.8 mmol) in THF (91.5 ml). At the end of the addition, the mixture was allowed to warm up to room temperature and stirred for additional 19 hours. The solvent was removed under reduced pressure and the crude product was extracted with dry ether (3 x 100 ml). The solution was filtered through Celite<sup>®</sup> to remove solid MgCl<sub>2</sub>. The crude product was purified by vacuum distillation, bp: 105 °C (2·10<sup>-3</sup> mm Hg). The desired product was obtained as an orange oil. Yield 3.44 g, 71%. <sup>1</sup>H NMR (250 MHz, CDCl<sub>3</sub>) δ 7.23-6.93 (m, 4H, Aromatic-H), 1.77-1.53 (m, 4H, CH), 1.08-0.88 (m, 24H, CH<sub>3</sub>). <sup>31</sup>P{<sup>1</sup>H} NMR (101 MHz, CDCl<sub>3</sub>) δ 11.1 (s, P<sup>i</sup>Pr<sub>2</sub>). NMR data are in accordance with the literature.<sup>150</sup>



### 2.13.3.1.5 Synthesis of Ir(P<sup>*i*</sup>Pr<sub>3</sub>)<sub>2</sub>H<sub>5</sub>

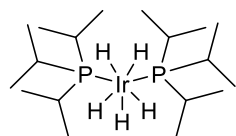
The literature procedure<sup>112</sup> has been slightly improved. Synthetic route:



**Synthesis of Ir(P<sup>*i*</sup>Pr<sub>3</sub>)<sub>2</sub>HCl<sub>2</sub> (**8**).** A solution of IrCl<sub>3</sub>·H<sub>2</sub>O (964.9 mg, 2.7 mmol) and triisopropylphosphine (1.36 g, 8.5 mmol) in degassed <sup>*i*</sup>PrOH (14.2 mL) was heated to reflux for 24 hours. Over time the colour of the solution changed from yellow to brown/red. Once cooled down, the solution was cannulated out and the remaining solid was washed with degassed <sup>*i*</sup>PrOH and then dried under vacuum overnight to yield a purple powder. Yield 1.292 g, 81%.

Once cooled down, the solution was cannulated out and the remaining solid was washed with degassed <sup>*i*</sup>PrOH and then dried under vacuum overnight to yield a purple powder. Yield 1.292 g, 81%.

<sup>1</sup>H NMR (500 MHz, CDCl<sub>3</sub>) δ 2.86-3.33 (m, 6H, 6CH), 1.35 (dd, <sup>3</sup>J<sub>H-P</sub> = 13.9, <sup>2</sup>J<sub>H-H</sub> = 7.1 Hz, 36H, 12CH<sub>3</sub>), -49.13 (t, <sup>2</sup>J<sub>H-P</sub> = 11.4 Hz, 1H, IrH). <sup>31</sup>P{<sup>1</sup>H} NMR (202 MHz, CDCl<sub>3</sub>) δ 31.98 (s). NMR data are in accordance with the literature.<sup>112</sup>



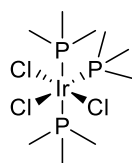
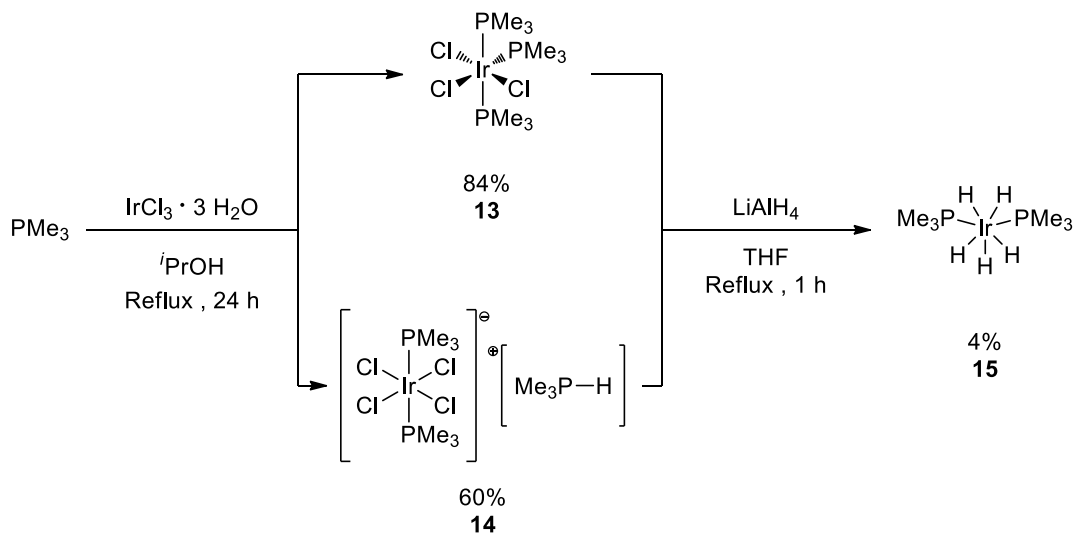
**Synthesis of Ir(P<sup>*i*</sup>Pr<sub>3</sub>)<sub>2</sub>H<sub>5</sub> (**2**).** Complex **8** (1.277 g, 2.2 mmol) and crushed NaOH (8.78 g, 219.5 mmol) were dissolved in THF (73 mL). The reaction mixture was stirred under H<sub>2</sub> atmosphere for 3 h, during which the colour changes from purple to pale yellow. The solvent was removed under reduced pressure and the solid was washed many times with distilled degassed water. The yellowish solid was dried under vacuum overnight. Crude yield 1.104 mg, 98%. The complex was recrystallized from hexane layered with MeOH (1:3 ratio), left for 3 days in the freezer to obtain large transparent colourless crystals. The solvent was then cannulated out, the crystals were rinsed with cold MeOH and then dried under vacuum. Yield 853.1 mg, 75%.

The solvent was removed under reduced pressure and the solid was washed many times with distilled degassed water. The yellowish solid was dried under vacuum overnight. Crude yield 1.104 mg, 98%. The complex was recrystallized from hexane layered with MeOH (1:3 ratio), left for 3 days in the freezer to obtain large transparent colourless crystals. The solvent was then cannulated out, the crystals were rinsed with cold MeOH and then dried under vacuum. Yield 853.1 mg, 75%.

<sup>1</sup>H NMR (500 MHz, d-Toluene) δ 1.83 - 1.52 (m, m, 6H, 6CH), 1.14 (dd, <sup>3</sup>J<sub>H-P</sub> = 13.6, <sup>2</sup>J<sub>H-H</sub> = 7.0 Hz, 36H, 12CH<sub>3</sub>), -10.93 (t, <sup>2</sup>J<sub>H-P</sub> = 12.2 Hz, 5H, IrH<sub>5</sub>). <sup>31</sup>P{<sup>1</sup>H} NMR (202 MHz, d-Toluene) δ 45.64 (s). NMR data are in accordance with the literature.<sup>112</sup>

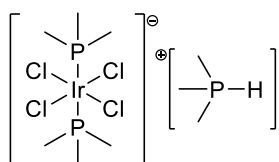
### 2.13.3.1.6 Synthesis of Ir(PMe<sub>3</sub>)<sub>2</sub>H<sub>5</sub>

The synthetic procedure has been adapted from the literature<sup>130</sup> and from the synthesis of **2**. Synthetic route:



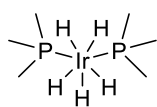
**Synthesis of *mer*-Ir(PMe<sub>3</sub>)<sub>2</sub>Cl<sub>3</sub> (**13**).** A solution of IrCl<sub>3</sub>·H<sub>2</sub>O (1.5 g, 4.3 mmol) and trimethylphosphine (1.686 g, 22.2 mmol) in degassed *i*PrOH (23 mL) was heated to reflux for 24 hours. Over time the colour of the solution changed from green to light brown and then yellow. Once cooled down, the solution was cannulated out and the remaining solid was washed with cold degassed *i*PrOH and then dried under vacuum overnight to yield a yellow crystalline solid. Yield 1.88 g, 84%.

<sup>1</sup>H NMR (500 MHz, C<sub>6</sub>D<sub>6</sub>) δ 1.38 (t, <sup>2</sup>J<sub>H-P</sub> = 3.9 Hz, 18H, 2*trans*-P(CH<sub>3</sub>)<sub>3</sub>), 1.13 (d, <sup>2</sup>J<sub>H-P</sub> = 10.5 Hz, 9H, P(CH<sub>3</sub>)<sub>3</sub>). <sup>31</sup>P{<sup>1</sup>H} NMR (202 MHz, C<sub>6</sub>D<sub>6</sub>) δ -42.34 (d, <sup>2</sup>J<sub>P-P</sub> = 19.3 Hz, 2P, 2*trans*-P(CH<sub>3</sub>)<sub>3</sub>), -47.66 (t, <sup>2</sup>J<sub>P-P</sub> = 19.3 Hz, 1P, P(CH<sub>3</sub>)<sub>3</sub>). NMR data are in accordance with the literature.<sup>130</sup>



**Synthesis of [Ir(PMe<sub>3</sub>)<sub>2</sub>Cl<sub>4</sub>]<sup>-</sup> [HPMe<sub>3</sub>]<sup>+</sup> (**14**).** A solution of IrCl<sub>3</sub>·H<sub>2</sub>O (545.2 mg, 1.5 mmol) and trimethylphosphine (404.2 mg, 5.0 mmol) in degassed *i*PrOH (8.0 mL) was heated to reflux for 24 hours. Over time the colour of the solution changed from green to light brown. Once cooled down, the solution was cannulated out and the remaining solid was washed with degassed *i*PrOH and then dried under vacuum overnight to yield a pinkish powder. Yield 507 mg, 60%.

<sup>1</sup>H NMR (500 MHz, d-DMSO) δ 1.66 (s, 18H, 2*trans*-P(CH<sub>3</sub>)<sub>3</sub>), 1.41 (t, <sup>2</sup>J = 3.9 Hz, 9H, P(CH<sub>3</sub>)<sub>3</sub>). <sup>31</sup>P{<sup>1</sup>H} NMR (202 MHz, d-DMSO) δ -42.31 (s, 1P, HP(CH<sub>3</sub>)<sub>3</sub>), -45.79 (s, 2P, 2*trans*-P(CH<sub>3</sub>)<sub>3</sub>). NMR data are in accordance with the literature.<sup>130</sup>

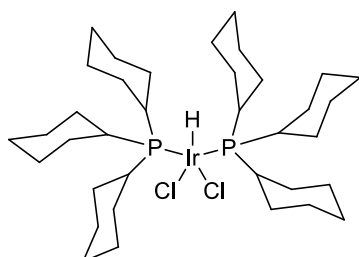
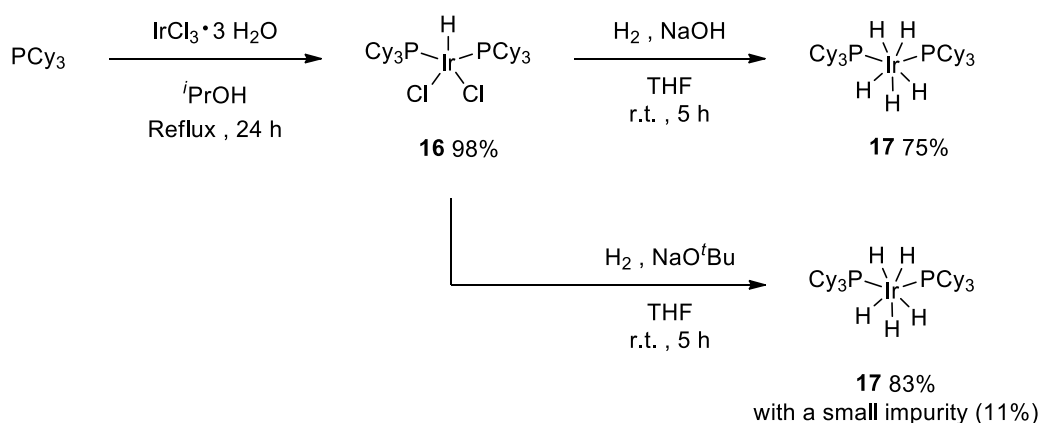


**Synthesis of Ir(PMe<sub>3</sub>)<sub>2</sub>H<sub>5</sub> (15).** Complex **13** (1.09 mg, 2.1 mmol) was dissolved in dry THF (19 mL) and LiAlH<sub>4</sub> (573.8 mg, 15.12 mmol) was slowly added portion-wise over 5 minutes at room temperature under vigorous stirring. The mixture was heated to reflux for 1 hour. Over time the colour of the solution changed from light pink to yellowish. Once cooled down, the solution was cannulated out to remove most of the unreacted LiAlH<sub>4</sub> and the solids were washed with dry THF (5 ml). The cannulated solution was slowly quenched according to Fieser work-up: water (0.5 mL) followed by an aqueous solution of 15% w/w NaOH (0.5 mL) and again water (1.5 mL). A second cannulation was carried out washing the remaining solids again with dry THF (3 ml) and collecting the liquid. The solvent was removed under reduced pressure to obtain a white/yellow solid. Crude yield 526.7 mg 73%. Sublimation of the solid was carried out at room temperature under vacuum using a cold finger, leaving the system under vacuum overnight to yield white solids. Yield 28.6 mg, 4%.

<sup>1</sup>H NMR (500 MHz, d-Tol) δ 1.39 (t, <sup>2</sup>J = 3.1 Hz, 18H, 2P(CH<sub>3</sub>)<sub>3</sub>), -9.76 (t, <sup>2</sup>J<sub>H-P</sub> = 13.9 Hz, 5H, IrH<sub>5</sub>). <sup>31</sup>P{<sup>1</sup>H} NMR (202 MHz, d-Tol) δ -56.87 (s). NMR data are in accordance with the literature.<sup>130</sup>

### 2.13.3.1.7 Synthesis of Ir(PCy<sub>3</sub>)<sub>2</sub>H<sub>5</sub>

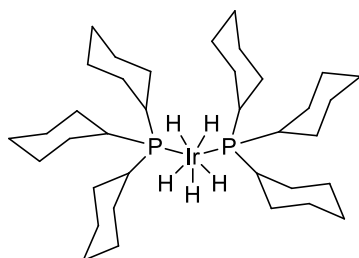
The synthetic procedure has been adapted from the synthesis of **2**. Synthetic route:



**Synthesis of Ir(PCy<sub>3</sub>)<sub>2</sub>HCl<sub>2</sub> (16).** A solution of IrCl<sub>3</sub>·H<sub>2</sub>O (203.3 mg, 0.6 mmol) and tricyclohexylphosphine (478.9 mg, 1.7 mmol) in degassed *i*PrOH (3 mL) was heated to reflux for 24 hours. The colour of the solution changed from green to brownish after few minutes, to become

purple/brown the next day. Once cooled down, the solution was cannulated out and the solid was washed with degassed *i*PrOH and then dried under vacuum overnight to yield a pink powder. Yield 459.0 mg, 98%.

$^1\text{H}$  NMR (500 MHz,  $\text{C}_6\text{D}_6$ )  $\delta$  3.10 - 1.17 (m, 66H, 6Cy), -47.75 (t,  $^2J_{\text{H-P}} = 10.8$  Hz, 1H, IrH).  $^{31}\text{P}\{^1\text{H}\}$  NMR (202 MHz,  $\text{C}_6\text{D}_6$ )  $\delta$  21.99 (d,  $^2J_{\text{H-P}} = 10.8$  Hz). NMR data are in accordance with the literature.<sup>131</sup>



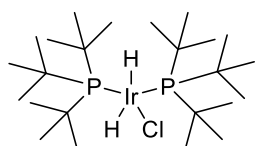
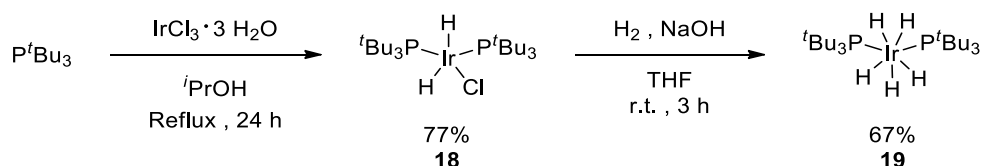
**Synthesis of  $\text{Ir}(\text{PCy}_3)_2\text{H}_5$  (17).** Complex **16** (99.8 mg, 0.12 mmol) and crushed NaOH (480.5 mg, 12.0 mmol) were dissolved in dry THF (4.5 mL). The reaction mixture was stirred under  $\text{H}_2$  atmosphere for 3 h, during which the colour changed from brown to pale yellow. The solvent was removed under reduced pressure and the solid was washed many times with distilled degassed water. The solid was dried under vacuum overnight to yield a white powder. Yield 68.5 mg, 75%.

$^1\text{H}$  NMR (500 MHz,  $\text{C}_6\text{D}_6$ )  $\delta$  2.20 - 1.15 (m, 66H, 6Cy), -10.55 (t,  $^2J_{\text{H-P}} = 12.1$  Hz, 5H, IrH<sub>5</sub>).  $^{31}\text{P}\{^1\text{H}\}$  NMR (202 MHz,  $\text{C}_6\text{D}_6$ )  $\delta$  32.10 (s). NMR data are in accordance with the literature.<sup>131</sup>

$^1\text{H}$  NMR (500 MHz,  $\text{C}_6\text{D}_6$ )  $\delta$  2.20 - 1.15 (m, 66H, 6Cy), -10.55 (t,  $^2J_{\text{H-P}} = 12.1$  Hz, 5H, IrH<sub>5</sub>).  $^{31}\text{P}\{^1\text{H}\}$  NMR (202 MHz,  $\text{C}_6\text{D}_6$ )  $\delta$  32.10 (s). NMR data are in accordance with the literature.<sup>131</sup>

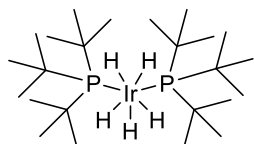
### 2.13.3.1.8 Synthesis of $\text{Ir}(\text{P}^t\text{Bu}_3)_2\text{H}_5$

The synthetic procedure has been adapted from the synthesis of **2**. Synthetic route:



**Synthesis of  $\text{Ir}(\text{P}^t\text{Bu}_3)_2\text{HCl}_2$  (18).** A solution of  $\text{IrCl}_3 \cdot \text{H}_2\text{O}$  (100.7 mg, 0.3 mmol) and tritertbutylphosphine (170.0 mg, 0.9 mmol) in degassed *i*PrOH (1.5 mL) was heated to reflux for 24 hours. Over time the colour of the solution changed from green to dark brown. Once cooled down, the solution was cannulated out and the remaining solid was washed with degassed *i*PrOH and then dried under vacuum overnight to yield an orange-brown powder. Yield 137.5 mg, 77%.

$^1\text{H}$  NMR (500 MHz,  $\text{C}_6\text{D}_6$ )  $\delta$  1.52 (t,  $^3J_{\text{H-P}} = 13.9$  Hz, 54H), -34.68 (t,  $^2J_{\text{H-P}} = 13.9$  Hz, 1H).  $^{31}\text{P}\{^1\text{H}\}$  NMR (202 MHz,  $\text{C}_6\text{D}_6$ )  $\delta$  75.38 (s). NMR data are in accordance with the literature.<sup>132</sup>



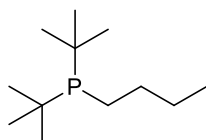
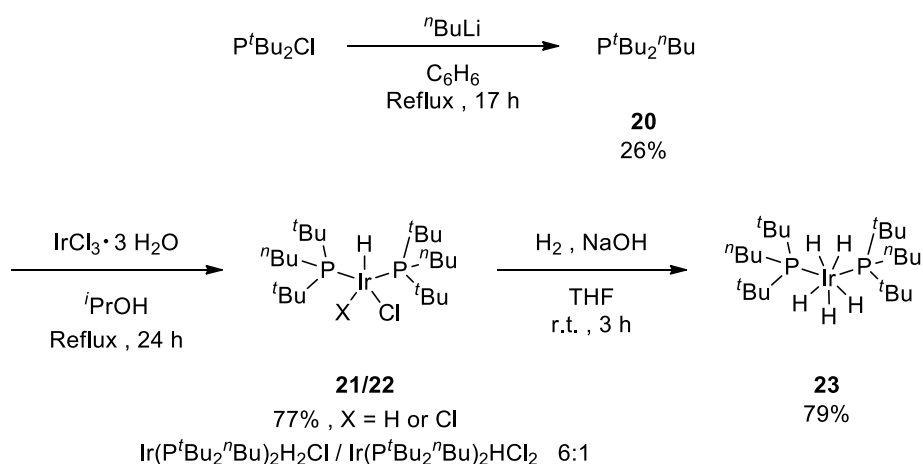
**Synthesis of Ir(P<sup>t</sup>Bu<sub>3</sub>)<sub>2</sub>H<sub>5</sub> (19).** Complex **18** (95.2 mg, 0.15 mmol) and crushed NaOH (605.3 mg, 15.0 mmol) were dissolved in dry THF (5.4 mL). The reaction mixture was stirred under H<sub>2</sub> atmosphere for 3 h, during which the colour changed from brown to light grey. The solvent was removed under reduced pressure and the solid was washed many times with distilled degassed water. The solid was dried under vacuum overnight to yield a light brown powder. Yield 60.6 mg, 67%.

<sup>1</sup>H NMR (500 MHz, C<sub>6</sub>D<sub>6</sub>) δ 1.49 (t, <sup>3</sup>J<sub>H-P</sub> = 5.8 Hz, 11H), -10.39 (t, <sup>2</sup>J<sub>H-P</sub> = 11.8 Hz, 1H). <sup>31</sup>P{<sup>1</sup>H} NMR (202 MHz, C<sub>6</sub>D<sub>6</sub>) δ 82.91 (s). NMR data are in accordance with the literature.<sup>132</sup>

### 2.13.3.2 New complexes

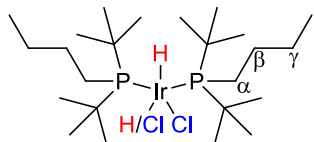
#### 2.13.3.2.1 Synthesis of Ir(P<sup>t</sup>Bu<sub>2</sub><sup>n</sup>Bu)<sub>2</sub>H<sub>5</sub>

The synthesis of the phosphine has been adapted from the literature<sup>136</sup> and the complexes have been synthesised adapting the pathway for the synthesis of **2**. Synthetic route:



**Synthesis of P<sup>t</sup>Bu<sub>2</sub><sup>n</sup>Bu (20).** *n*-Butyllithium in hexanes (1.6 M, 3.6 mL, 5.8 mmol) was added dropwise at room-temperature to a solution of chloro-di-*t*-butylphosphine (1.0 mL, 5.3 mmol) in dry benzene (12 mL). The solution was refluxed for 17 hours. Once cooled down, the organic phase was washed with water. The organic layer was collected, dried over MgSO<sub>4</sub> and filtered. The solvent was carefully removed under reduced pressure until the solution was not freezing anymore, meaning that the benzene has been removed, in fact the benzene if put under vacuum it freezes, while the phosphine does not (b.p.<sub>benzene</sub>=80 °C, b.p.<sub>phosphine</sub>=88 °C). A colourless clear liquid was obtained. From NMR the phosphine appears to be 1:1 with benzene. Yield calculated by NMR 280.4 mg, 26%.

$^1\text{H}$  NMR (500 MHz,  $\text{CD}_2\text{Cl}_2$ )  $\delta$  1.55 – 1.33 (m, 6H, 3 $\text{CH}_2$ ), 1.12 (d,  $^3J_{\text{H-P}} = 10.7$  Hz, 18H, 2 $\text{C}(\text{CH}_3)_2$ ), 0.93 (t,  $^3J_{\text{H-H}} = 7.2$  Hz, 3H,  $\text{CH}_3$ ).  $^{31}\text{P}\{^1\text{H}\}$  NMR (202 MHz,  $\text{CD}_2\text{Cl}_2$ )  $\delta$  28.24 (s). NMR data are in accordance with the literature.<sup>136</sup>

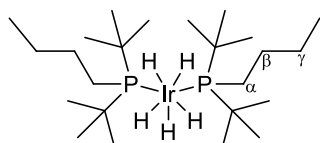


**Synthesis of  $\text{Ir}(\text{P}^t\text{Bu}_2^n\text{Bu})_2\text{H}_2\text{Cl}/\text{Ir}(\text{P}^t\text{Bu}_2^n\text{Bu})_2\text{HCl}_2$  (**21/22**).** A solution of  $\text{IrCl}_3 \cdot \text{H}_2\text{O}$  (99.7 mg, 0.3 mmol) and the solution of di-*tert*-butyl(butyl)phosphane in benzene **20** (235.6, 0.9 mmol) in degassed  $^i\text{PrOH}$  (1.5 mL) was heated to reflux for 24 hours. Over time the colour of the solution changed from green to brown. Once cooled down, the solution was concentrated under reduced pressure to yield a brown powder as a mixture of two compounds in a 6:1 ratio:  $\text{Ir}(\text{P}^t\text{Bu}_2^n\text{Bu})_2\text{H}_2\text{Cl}$  (**21**) and  $\text{Ir}(\text{P}^t\text{Bu}_2^n\text{Bu})_2\text{HCl}_2$  (**22**). Total yield 139.4 mg, approximately 77%.

$\text{Ir}(\text{P}^t\text{Bu}_2^n\text{Bu})_2\text{H}_2\text{Cl}$  (**21**):  $^1\text{H}$  NMR (500 MHz,  $\text{C}_6\text{D}_6$ )  $\delta$  2.11 – 1.40 (m, 12H, 6 $\text{CH}_2$ ), 1.33 (apparent t (dd),  $^3J_{\text{H-P}} = 6.1$  Hz, 36H, 4 $\text{CCH}_3$ ), 0.97 (t,  $^3J_{\text{H-H}} = 7.4$  Hz, 6H, 2 $\text{CH}_3$ ), -32.54 (t,  $^2J_{\text{H-P}} = 13.4$  Hz, 2H,  $\text{IrH}_2$ ).  $^{31}\text{P}\{^1\text{H}\}$  NMR (202 MHz,  $\text{C}_6\text{D}_6$ )  $\delta$  55.98 (s).  $^{13}\text{C}\{^1\text{H}\}$  NMR (101 MHz,  $\text{C}_6\text{D}_6$ )  $\delta$  35.96 (t,  $J = 11.2$  Hz, 4 $\text{CMe}_3$ ), 30.67 (s, 12 $\text{CH}_3$ ), 30.15 (s, 2 $\gamma\text{-CH}_2$ ), 25.54 (t,  $J = 6.2$  Hz, 2 $\beta\text{-CH}_2$ ), 23.75 (t,  $J = 12.4$  Hz, 2 $\alpha\text{-CH}_2$ ), 14.25 (s, 2 $\text{CH}_3$ ).

$\text{Ir}(\text{P}^t\text{Bu}_2^n\text{Bu})_2\text{HCl}_2$  (**22**):  $^1\text{H}$  NMR (500 MHz,  $\text{C}_6\text{D}_6$ )  $\delta$  2.11 – 1.40 (m, 12H, 6 $\text{CH}_2$ ), 1.33 (apparent t (dd),  $^3J_{\text{H-P}} = 6.2$  Hz, 36H, 4 $\text{CCH}_3$ ), 1.00 (t,  $^3J_{\text{H-H}} = 7.4$  Hz, 6H, 2 $\text{CH}_3$ ), -49.38 (t,  $^2J_{\text{H-P}} = 10.9$  Hz, 1H,  $\text{IrH}$ ).  $^{31}\text{P}\{^1\text{H}\}$  NMR (202 MHz,  $\text{C}_6\text{D}_6$ )  $\delta$  34.25 (s).  $^{13}\text{C}\{^1\text{H}\}$  NMR (101 MHz,  $\text{C}_6\text{D}_6$ )  $\delta$  35.96 (t,  $J = 11.2$  Hz, 4 $\text{CMe}_3$ ), 31.57 (s, 12 $\text{CH}_3$ ), 30.15 (s, 2 $\gamma\text{-CH}_2$ ), 25.54 (t,  $J = 6.2$  Hz, 2 $\beta\text{-CH}_2$ ), 23.75 (t,  $J = 12.4$  Hz, 2 $\alpha\text{-CH}_2$ ), 14.45 (s, 2 $\text{CH}_3$ ).

MS (ASAP)  $m/z$ : found 597.3342 (100%), 595.3292 (73%), 598.3366 (29%), 596.3307 (25%), 599.3432 (7%) for  $[\text{Ir}(\text{P}^t\text{Bu}_2^n\text{Bu})_2]^+$ , calculated for  $[\text{M-H}_2\text{Cl}]^+$  or  $[\text{M-HCl}_2]^+ = [\text{C}_{24}\text{H}_{54}\text{P}_2^{191}\text{Ir}]^+ = 597.3331$  (100%), 595.3307 (59%), 598.3364 (29%), 596.3341 (17%), 599.3398 (4%). HREI-MS (ASAP)  $m/z$ : found 632.33970 for  $[\text{Ir}(\text{P}^t\text{Bu}_2^n\text{Bu})_2\text{H}_2\text{Cl}]^+$ , calculated for  $[\text{M}]^+ = [\text{C}_{24}\text{H}_{56}\text{Cl}_1\text{P}_2^{191}\text{Ir}]^+ = 632.3146$ .



**Synthesis of  $\text{Ir}(\text{P}^t\text{Bu}_2^n\text{Bu})_2\text{H}_5$  (**23**).** A mixture of complexes **21** and **22** (60.7 mg, 0.1 mmol) and crushed  $\text{NaOH}$  (405.1 mg, 10.0 mmol) were dissolved in dry THF (3.6 mL). The reaction mixture was heated to 25 °C and stirred under  $\text{H}_2$  atmosphere for 3 h, during which the colour changed from brown to green to blue/grey. The solvent was removed under reduced

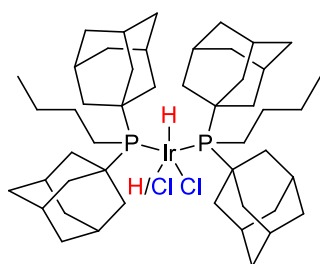
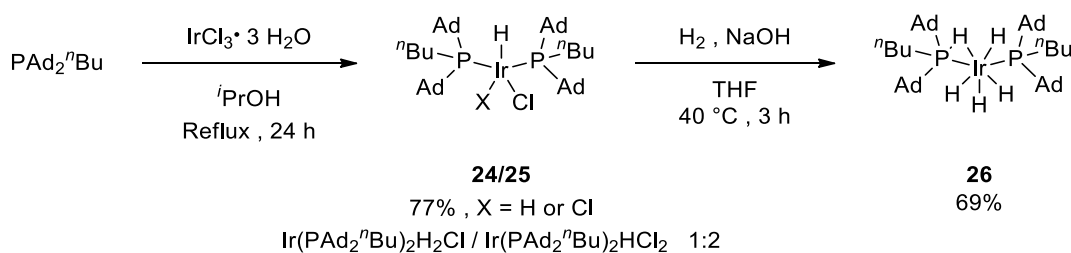
pressure and the solid was washed many times with distilled degassed water. The white solid was dried under vacuum overnight. Yield 45.3 mg, 79%.

$^1\text{H}$  NMR (500 MHz,  $\text{C}_6\text{D}_6$ )  $\delta$  1.96 – 1.82 (m, 4H,  $2\alpha\text{-CH}_2$ ), 1.74 – 1.63 (m, 4H,  $2\beta\text{-CH}_2$ ), 1.39 (q,  $^3J_{\text{H-H}} = 7.3$  Hz, 4H,  $2\gamma\text{-CH}_2$ ), 1.29 (t,  $^3J_{\text{H-P}} = 6.1$  Hz, 36H,  $4\text{CCH}_3$ ), 0.98 (t,  $^3J_{\text{H-H}} = 7.4$  Hz, 6H,  $2\text{CH}_3$ ), -10.53 (t,  $^2J_{\text{H-P}} = 12.1$  Hz, 1H, IrH).  $^{31}\text{P}\{^1\text{H}\}$  NMR (202 MHz,  $\text{C}_6\text{D}_6$ )  $\delta$  53.45 (s).  $^{13}\text{C}\{^1\text{H}\}$  NMR (101 MHz,  $\text{C}_6\text{D}_6$ )  $\delta$  33.59 (t,  $J = 12.7$  Hz,  $4\text{CMe}_3$ ), 31.53 (s,  $12\text{CH}_3$ ), 30.26 (s,  $2\alpha\text{-CH}_2$ ), 27.63 (t,  $J = 13.7$  Hz,  $2\beta\text{-CH}_2$ ), 25.28 (t,  $J = 6.3$  Hz,  $2\gamma\text{-CH}_2$ ), 14.16 (s,  $2\text{CH}_3$ ).

MS (ASAP)  $m/z$ : found 597.3357 (100%), 595.3292 (79%), 596.3290 (43%), 598.3372 (32%), 599.3422 (6%) for  $[\text{Ir}(\text{P}^t\text{Bu}_2^n\text{Bu})_2]^+$ , calculated for  $[\text{M-H}_5]^+ = [\text{C}_{24}\text{H}_{54}\text{P}_2^{191}\text{Ir}]^+ = 597.3331$  (100%), 595.3307 (59%), 598.3364 (29%), 596.3341 (17%), 599.3398 (4%).

### 2.13.3.2.2 Synthesis of $\text{Ir}(\text{PAd}_2^n\text{Bu})_2\text{H}_5$

The complex has been synthesised adapting the pathway for the synthesis of **2**. Synthetic route:



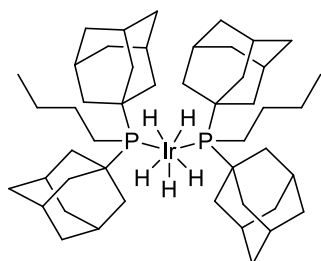
**Synthesis of  $\text{Ir}(\text{PAd}_2^n\text{Bu})_2\text{H}_2\text{Cl} / \text{Ir}(\text{PAd}_2^n\text{Bu})_2\text{HCl}_2$  (**24/25**).** A suspension of  $\text{IrCl}_3 \cdot \text{H}_2\text{O}$  (304.1 mg, 0.8 mmol) and diadamantyl(butyl)phosphine (1915.4 mg, 2.5 mmol) in degassed  $^i\text{PrOH}$  (9 mL) was heated to reflux for 24 hours. Over time the colour of the suspension changed from green to pink. Once cooled down, the solution was cannulated out and the solid

was washed with degassed  $^i\text{PrOH}$  and then dried under vacuum overnight to yield a pink powder. Yield 645.3 mg, approximately 77%.

$\text{Ir}(\text{PAd}_2^n\text{Bu})_2\text{H}_2\text{Cl}$  (**24**):  $^1\text{H}$  NMR (500 MHz,  $\text{CD}_2\text{Cl}_2$ )  $\delta$  2.64 – 1.23 (m, 72H, 4Ad and  $6\text{CH}_2$ ), 0.94 (t,  $^3J_{\text{H-H}} = 7.3$  Hz, 6H,  $2\text{CH}_3$ ), -34.16 (t,  $^2J_{\text{H-P}} = 13.7$  Hz, 2H, IrH<sub>2</sub>).  $^{31}\text{P}$  NMR (202 MHz,  $\text{CD}_2\text{Cl}_2$ )  $\delta$  50.40 (s).

$\text{Ir}(\text{PAd}_2^n\text{Bu})_2\text{HCl}_2$  (**25**):  $^1\text{H}$  NMR (500 MHz,  $\text{CD}_2\text{Cl}_2$ )  $\delta$  2.64 – 1.23 (m, 72H, 4Ad and  $6\text{CH}_2$ ), 0.90 (t,  $^3J_{\text{H-H}} = 7.3$  Hz, 6H,  $2\text{CH}_3$ ), -49.50 (m, 1/2H, IrH), -49.63 (m, 1/2H, IrH).  $^{31}\text{P}$  NMR (202 MHz,  $\text{CD}_2\text{Cl}_2$ ) 25.88 (s), 23.64 (s).

MS (ASAP) m/z: found 909.5228 (100%), 907.5156 (77%), 910.5260 (48%), 908.5187 (40%), 911.5322 (18%), 912.5375 (6%) for  $[\text{Ir}(\text{PAd}_2^{\text{nBu}})_2]^+$ , calculated for  $[\text{M}-\text{H}_2\text{Cl}]^+$  or  $[\text{M}-\text{HCl}_2]^+ = [\text{C}_{48}\text{H}_{78}\text{P}_2^{193}\text{Ir}]^+ = 909.5211$  (100%), 907.5185 (59%), 910.5243 (52%), 908.5219 (31%), 911.5276 (13%), 912.5311 (2%).



**Synthesis of  $\text{Ir}(\text{PAd}_2^{\text{nBu}})_2\text{H}_5$  (26).** A mixture of complexes **24** and **25** (49.1 mg, 0.05 mmol) and crushed NaOH (202.5 mg, 5.06 mmol) were dissolved in dry THF (5 mL). The reaction mixture was heated to 40 °C and stirred under  $\text{H}_2$  atmosphere for 3 h, during which the colour changed from purple/brown to pale yellow. The solvent was removed under reduced pressure

and the solid was washed many times with distilled degassed water. The off-white solid was dried under vacuum overnight. Yield 31.7 mg, 69%.

$^1\text{H}$  NMR (500 MHz,  $\text{C}_6\text{D}_6$ )  $\delta$  2.85 – 1.24 (m, 72H, 4Ad and 6 $\text{CH}_2$ ), 1.23 – 0.83 (m, 6H, 2 $\text{CH}_3$ ), -10.70 (t,  $^2J_{\text{H-P}} = 11.8$  Hz, 5H,  $\text{IrH}_5$ ).  $^{31}\text{P}\{^1\text{H}\}$  NMR (202 MHz,  $\text{C}_6\text{D}_6$ )  $\delta$  24.23 (s).

Pending MS data for publication.



## 2.13.4 Quantitative analysis method for sonochemical reactions

Quantitative analyses of the reaction mixtures were carried out by GC-FID technique, using the internal standard method, with isooctane or *n*-dodecane as ISTD. Each aliquot of the reaction mixture was filtered to remove any precipitate. Then to a portion of that (0.2 mL), the standard was added as a solution in ethyl acetate (0.2 mL of a 5 mM solution) and the obtained solution was correctly diluted with EtOAc (0.6 mL) in order to obtain a final standard concentration of 0.01 M for isooctane or *n*-dodecane.

### 2.13.4.1 Method development

A full method development and optimisation has been performed, in order to be able to use the same method for all different alkanes. Finding a proper column and GC method, which would allow to reliably quantify our products, proved to be quite challenging. The main reason for this was that the reaction that had to be analysed was run in neat conditions, indeed the alkane reagent was also the solvent of the reaction. Therefore, it resulted in a chromatogram where the peak of the alkane was broad and overlapped with the ones of the alkene products. For this type of transformation only a couple of analytical methods are reported in the literature,<sup>70, 151</sup> and none of them was exhaustive. The main problem has been obtaining a good separation between the peak of the alkane and the peaks of the alkenes. Indeed, different column types and conditions have been tested in order to achieve an acceptable separation. Finally, with a DB-WAX column, helium as carrier gas and an appropriate temperature program, an adequate peak separation has been achieved. Unfortunately, after a short period of time, the column stopped to give a proper retention, and GC and column type had to be switched. The second GC and temperature program, equipped with a ZB-WAX column and having also nitrogen as the carrier gas, gave much better results.

The best possible resolution among peaks has been achieved adjusting the method. However, even under the best possible conditions, the broad dodecane peak was still tailing below the following dodecene peaks. Indeed, in order to accurately quantify the alkene peaks, those have been integrated using a tangential skim integration. The new method allowed to obtain a good estimation of the area of the dodecene peaks taking into account the contribution from the partial overlap with the broad dodecane peak. The same integration method was used in every chromatogram to provide consistent results. The consumption of the hydrogen acceptor has not been calculated as TBE/TBA ratios cannot be quantified because, on these columns, these two peaks cannot be separated even running

the GC program at relatively low temperature (35 °C), probably because they are extremely volatile compounds (b.p. 40-50 °C).

#### 2.13.4.2 GC-FID Technique

A standard GC analysis involved the analysis of the sample solution prepared accordingly as described above. Then, 1 µL of this sample solution, was injected into the GC. The Agilent 6890N was equipped with a ZB-WAX column. Response factors of each analyte were determined by Multiple Point Internal Standard Quantitation Method with respect to authenticated samples of isooctane or *n*-dodecane. See the following tables for more details on the optimised instrument parameters and methods.

| <b>AGILENT 6890N INSTRUMENTS PARAMETERS</b> |                   |
|---|-------------------|
| Carrier gas                                 | N <sub>2</sub>    |
| Inlet Temperature                           | 250 °C            |
| Control Mode                                | Constant Pressure |
| Pressure                                    | 14.89 psi         |
| Injection Volume                            | 1 µL              |
| Split Ratio                                 | 100:1             |
| Detector Temperature                        | 250 °C            |
| H <sub>2</sub> Flow                         | 30 mL/min         |
| Air Flow                                    | 300 mL/min        |
| Make Up Flow (N <sub>2</sub> )              | 25 mL/min         |

| <b>ZB-WAX COLUMN PROGRAM Alkane</b> |               |                |
|-------------------------------------|---------------|----------------|
| <b>Rate (°C/min)</b>                | <b>T (°C)</b> | <b>t (min)</b> |
| -                                   | 40            | 2              |
| 40                                  | 80            | 2              |
| 40                                  | 120           | 5              |

### 2.13.5 Testing the stability of *n*-dodecane under ultrasound irradiation

In the glovebox, *n*-dodecane (5 mL) was transferred to a Schlenk tube and the sealed vessel was taken outside. The sonochemical reactor was assembled (see Figure 2.3) and evacuated completely under vacuum and backfilled with argon three times to ensure complete removal of residual air. The Schlenk tube containing the *n*-dodecane was also connected to the Schlenk line and the alkane was transferred from the Schlenk tube to the sonochemical reactor by volume. The reactor was immersed in a water-cooling bath to maintain the solution at room temperature ( $25 \pm 3$  °C). The horn and the upper part of the reactor were cooled down from the outside by a continuous stream of compressed air.

An aliquot of the solution was collected with a syringe and transferred to a 4 mL vial for analysis. This portion was quenched by exposing it to air and bubbling air through the solution. This aliquot was then properly diluted to be analysed by GC, at this stage iso-octane was also added as the internal standard. Meanwhile, the alkane solution was sonicated under a pulsing mode (amplitude 100%) for a total of 1 hour. The ultrasound was applied for 10 minutes and then stopped for another 10 minutes (total reaction time 2 h, active sonication time 1 h).

The reaction mixture was then quenched by opening it to air and bubbling air through the solution. A second aliquot of the reaction mixture was properly diluted to be analysed by GC, at this stage Iso-octane was also added as the internal standard (for details on preparation and dilution of the solution see Section 2.13.4).

The two chromatograms obtained at the beginning and at the end of the reaction were compared. No formation of dodecenes was observed, also no impurities or degradation compounds were formed after ultrasound irradiation.

### 2.13.6 Screening of complexes

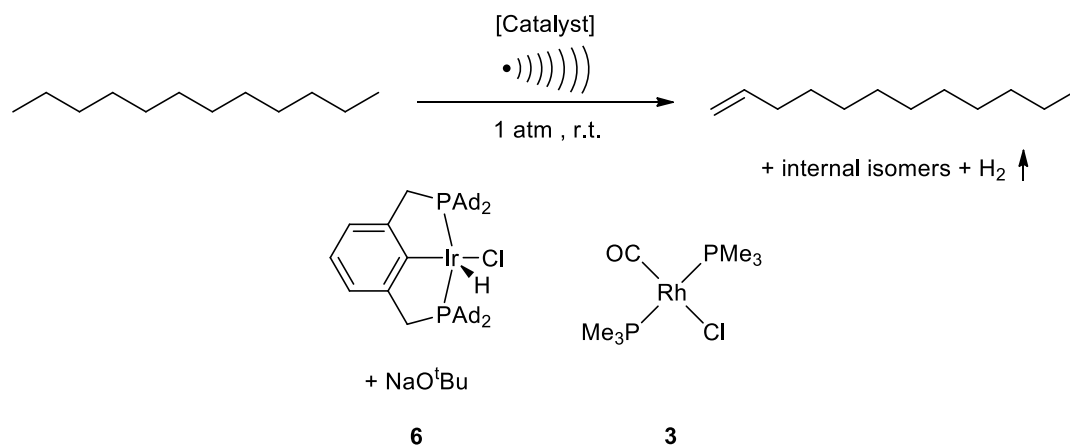
#### 2.13.6.1 Attempted sonochemical *n*-dodecane acceptorless dehydrogenation

The reagents were transferred to the vessel following always the same order as described below. In the glovebox, the complex to be tested was weighed in a Schlenk tube (0.005 mmol, specific masses in Table 2.13) (for Ir(<sup>A</sup>dPCP)HCl also NaO<sup>t</sup>Bu, 1.2 eq. with respect to the complex, was added) and solubilised in *n*-dodecane (5 mL). The sealed vessel was taken outside the glovebox and sonicated for few seconds in the ultrasonic bath in order to completely dissolve the complex. Meanwhile, the sonochemical reactor was assembled (see Figure 2.3) and evacuated completely under vacuum and backfilled with argon three times to ensure complete removal of residual air. The Schlenk tube containing the reaction mixture

was also connected to the Schlenk line and the solution was transferred from the Schlenk tube to the sonochemical reactor quantitatively with a syringe. The reactor was immersed in a water-cooling bath to maintain the solution at room temperature ( $25 \pm 3$  °C). The horn and the upper part of the reactor were cooled down from the outside by a continuous stream of compressed air. Before starting the reaction, under flow of argon, the side neck of the reaction flask was equipped with a septum. The septum was pierced with a syringe needle while a positive pressure of argon was maintained. This outlet needle on the side neck of the flask was required to perform the reaction under a stream of argon, as required for the acceptorless dehydrogenation. The reaction mixture was sonicated under a pulsing mode (amplitude 50%), irradiating with ultrasound for 10 minutes and then stopping them for another 10 minutes (specific reaction times reported in Table 2.13 and correspond to the active sonication time).

The reaction mixture was then quenched by opening it to air and bubbling air through the solution. An aliquot of the reaction mixture was properly diluted to be analysed by GC, at this stage iso-octane was also added as the internal standard (for details on preparation and dilution of the solution see Section 2.13.4)

Table 2.13 Details for the sonochemical *n*-dodecane acceptorless dehydrogenation by different complexes.



| Entry | t (min) | Catalyst              | $m_M$ (mg) | $n_M$ (mmol) | TON   |
|-------|---------|-----------------------|------------|--------------|-------|
| 1     | 10      | <b>3</b>              | 1.6        | 0.005        | < 0.1 |
| 2     | 10      | <b>6</b> <sup>a</sup> | 4.7        | 0.005        | < 0.1 |
| 3     | 20      | <b>6</b> <sup>a</sup> | 4.7        | 0.005        | < 0.1 |

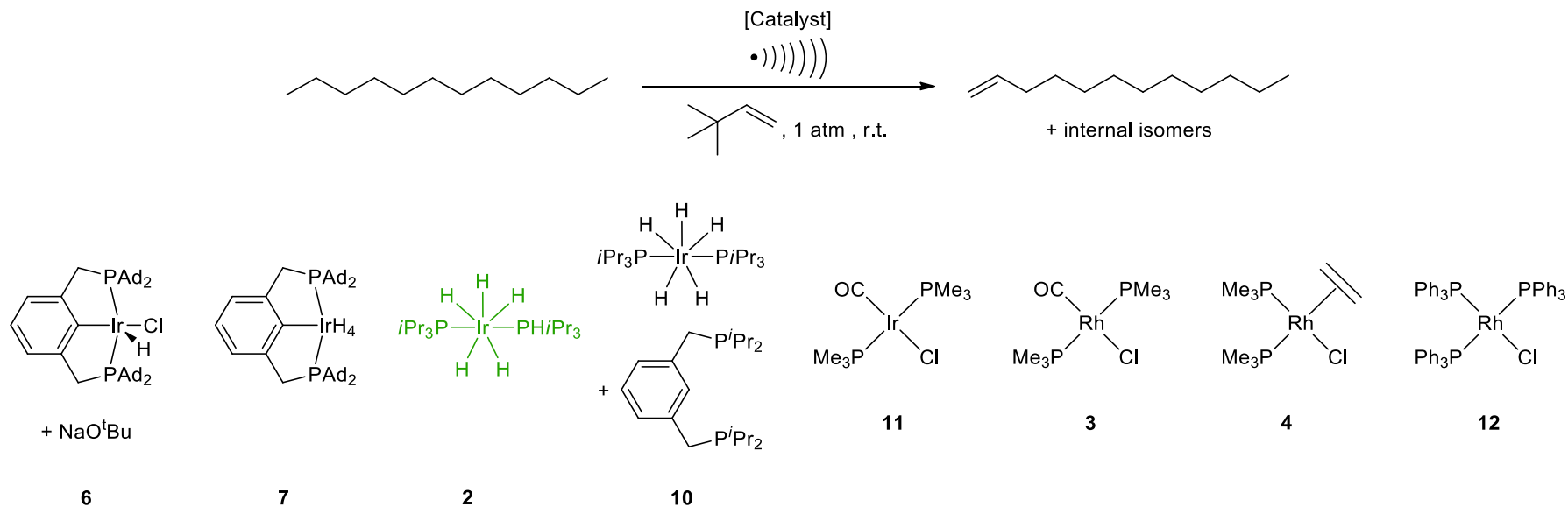
(a) 1.2 eq. of NaO<sup>t</sup>Bu also added (0.6 mg, 0.006 mmol).

### 2.13.6.2 Initial screening of complexes for the sonochemical *n*-dodecane transfer dehydrogenation

The reagents were transferred to the vessel following always the same order as described below. In the glovebox, the complex to be tested was weighed in a Schlenk tube (amounts reported in Table 2.14) (for Ir(<sup>A</sup>dPCP)HCl also NaO<sup>t</sup>Bu, 1.2 eq. with respect to the complex, was added) and solubilised in *n*-dodecane (5mL). Then TBE was added (64.4 μL, 0.50 mmol). The sealed vessel was taken outside the glovebox and sonicated for few seconds in the ultrasonic bath in order to completely dissolve the complex. Meanwhile, the sonochemical reactor was assembled (see Figure 2.3) and evacuated completely under vacuum and backfilled with argon three times to ensure complete removal of residual air. The Schlenk tube containing the reaction mixture was also connected to the Schlenk line and the solution was transferred from the Schlenk tube to the sonochemical reactor by volume. The reactor was immersed in a water-cooling bath to maintain the solution at room temperature (25 ± 3 °C). The horn and the upper part of the reactor were cooled down from the outside by a continuous stream of compressed air. The reaction mixture was sonicated with a pulse mode (amplitude 50-100%), irradiating with ultrasounds for 10 minutes and then stopping for another 10 minutes (specific amplitudes and reaction times reported in Table 2.14 and correspond to the active sonication time).

The reaction mixture was then quenched by opening it to air and bubbling air through the solution. An aliquot of the reaction mixture was properly diluted to be analysed by GC, at this stage iso-octane was also added as the internal standard (for details on preparation and dilution of the solution see Section 2.13.4).

Table 2.14 Details for the screening of complexes for the sonochemical *n*-dodecane transfer dehydrogenation.



| Entry | A (%) | t (min) | Catalyst   | $m_M$ (mg) | $n_M$ (mmol) | TBE/M | $C_{cat}$ (mM) | TON   |
|-------|-------|---------|--|------------|--------------|-------|----------------|-------|
| 1     | 50    | 10      | Rh(PMe <sub>3</sub> ) <sub>2</sub> (CO)Cl ( <b>3</b> ) | 1.6        | 0.005        | 100   | 1              | < 0.1 |
| 2     | 50    | 10      | Ir( <sup>Ad</sup> PCP)HCl ( <b>6</b> )                 | 4.7        | 0.005        | 100   | 1              | < 0.1 |
| 3     | 80    | 10      | Ir( <sup>Ad</sup> PCP)HCl ( <b>6</b> )                 | 4.7        | 0.005        | 100   | 1              | < 0.1 |
| 4     | 100   | 10      | Ir( <sup>Ad</sup> PCP)HCl ( <b>6</b> )                 | 4.7        | 0.005        | 100   | 1              | < 0.1 |
| 5     | 50    | 10      | Ir( <sup>Ad</sup> PCP)HCl ( <b>6</b> )                 | 23.4       | 0.025        | 20    | 5              | < 0.1 |

|    |     |    |  |      |        |     |   |       |
|----|-----|----|--|------|--------|-----|---|-------|
| 6  | 100 | 10 | $\text{Ir}^{\text{Ad}}\text{PCP}\text{HCl}$ ( <b>6</b> )                                     | 23.4 | 0.025  | 20  | 5 | < 0.1 |
| 7  | 100 | 20 | $\text{Ir}^{\text{Ad}}\text{PCP}\text{HCl}$ ( <b>6</b> )                                     | 23.4 | 0.025  | 20  | 5 | < 0.1 |
| 8  | 100 | 60 | $\text{Ir}^{\text{Ad}}\text{PCP}\text{HCl}$ ( <b>6</b> )                                     | 23.4 | 0.025  | 20  | 5 | < 0.1 |
| 9  | 50  | 10 | $[\text{Rh}(\text{PMe}_3)_2\text{Cl}]_2$ ( <b>9</b> ) <sup>a</sup>                           | 14.5 | 0.0025 | 100 | 1 | < 0.1 |
| 10 | 50  | 10 | $\text{Ir}(\text{PMe}_3)_2(\text{CO})\text{Cl}$ ( <b>11</b> )                                | 2.0  | 0.005  | 100 | 1 | < 0.1 |
| 11 | 50  | 10 | $\text{Ir}(\text{P}^i\text{Pr}_3)_2\text{H}_5$ ( <b>2</b> )                                  | 2.6  | 0.005  | 100 | 1 | < 0.1 |
| 12 | 50  | 10 | $\text{Ir}(\text{P}^i\text{Pr}_3)_2\text{H}_5 + {}^i\text{PrPCP}$ ( <b>10</b> ) <sup>b</sup> | 2.6  | 0.005  | 100 | 1 | < 0.1 |
| 13 | 100 | 60 | $\text{Rh}(\text{PMe}_3)_2(\text{CO})\text{Cl}$ ( <b>3</b> )                                 | 1.6  | 0.005  | 100 | 1 | < 0.1 |
| 14 | 100 | 60 | $[\text{Rh}(\text{PMe}_3)_2\text{Cl}]_2$ ( <b>9</b> ) <sup>c</sup>                           | 2.9  | 0.005  | 100 | 1 | < 0.1 |
| 15 | 100 | 60 | $\text{Ir}(\text{PMe}_3)_2(\text{CO})\text{Cl}$ ( <b>11</b> )                                | 2.0  | 0.005  | 100 | 1 | < 0.1 |
| 16 | 100 | 60 | $\text{Ir}(\text{P}^i\text{Pr}_3)_2\text{H}_5$ ( <b>2</b> )                                  | 2.6  | 0.005  | 100 | 1 | 0.9   |
| 17 | 100 | 60 | $\text{Ir}(\text{P}^i\text{Pr}_3)_2\text{H}_5 + {}^i\text{PrPCP}$ ( <b>10</b> ) <sup>d</sup> | 2.6  | 0.005  | 100 | 1 | < 0.1 |
| 18 | 100 | 60 | $\text{Ir}^{\text{Ad}}\text{PCP}\text{H}_4$ ( <b>7</b> )                                     | 4.5  | 0.005  | 100 | 1 | < 0.1 |
| 19 | 100 | 60 | $\text{Rh}(\text{PPh}_3)_3\text{Cl}$ ( <b>12</b> )   | 4.6  | 0.005  | 100 | 1 | < 0.1 |

Notes: (a) Providing the system with an inlet and outlet needle, ethylene (1 atm) is bubbled through the solution during the reaction to generate the catalytically active complex **4**, fulfilling also the role of hydrogen acceptor instead of TBE. (b) Attempt in the generation of  $\text{Ir}({}^i\text{PrPCP})\text{H}_2$  in situ from  $\text{Ir}(\text{P}^i\text{Pr}_3)_2\text{H}_5$  and the free phosphine  ${}^i\text{PrPCP}\text{-H}$  (1.5 eq. with respect to the complex).

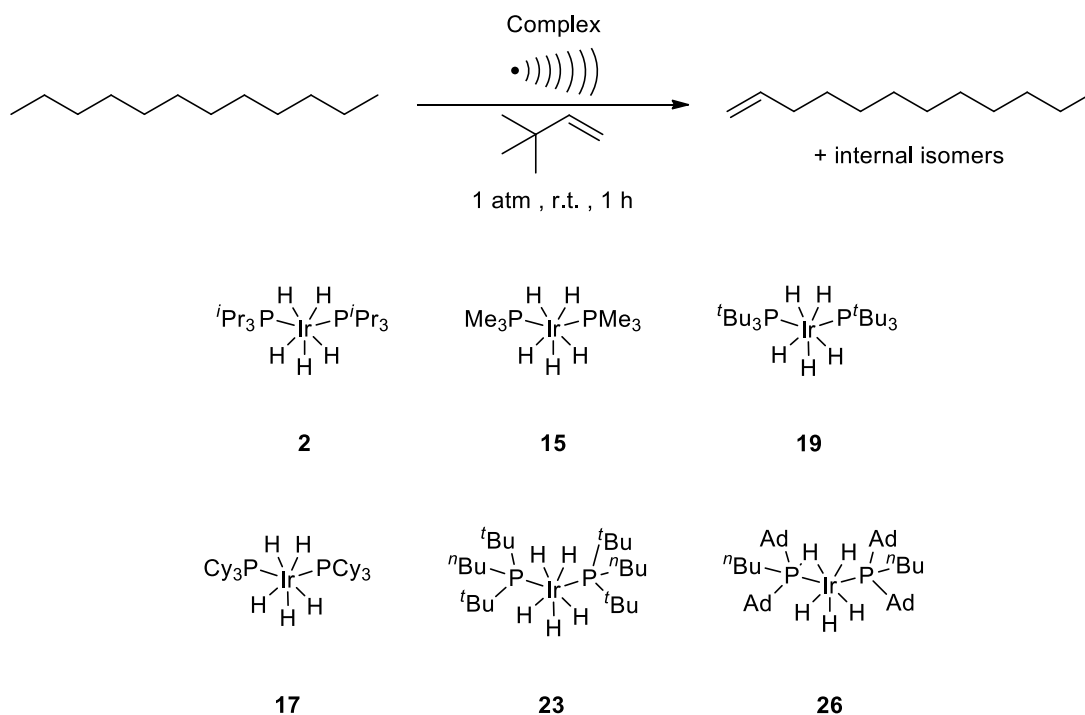
### 2.13.6.3 Screening of pentahydride analogues for the sonochemical *n*-dodecane transfer dehydrogenation

The reagents were transferred to the vessel following always the same order as described below. In the glovebox, the complex to be tested was weighed in a Schlenk tube (0.025 mmol) and solubilised in *n*-dodecane (5mL). Then TBE was added (64.4  $\mu$ L, 0.50 mmol). The sealed vessel was taken outside the glovebox and sonicated for few seconds in the ultrasonic bath in order to completely dissolve the complex. Meanwhile, the sonochemical reactor was assembled (see Figure 2.3), connected to the Schlenk line and evacuated completely under vacuum and backfilled with argon three times to ensure complete removal of residual air. The Schlenk tube containing the reaction mixture previously prepared was also connected to the Schlenk line. The solution was transferred from the Schlenk tube to the sonochemical reactor quantitatively with a syringe. The sonochemical reactor was immersed in a water-cooling bath to maintain the solution at room temperature ( $25 \pm 3$  °C). The horn and the upper part of the reactor were cooled down from the outside by a continuous stream of compressed air. The reaction mixture was sonicated with a pulse mode (amplitude 100%), irradiating with ultrasounds for 10 minutes and then stopping for another 10 minutes (specific reaction times reported in Table 2.15 and correspond to the active sonication time).

The reaction mixture was then quenched by opening it to air and bubbling air through the solution. An aliquot of the reaction mixture was properly diluted to be analysed by GC, at this stage iso-octane was also added as the internal standard (for details on preparation and dilution of the solution see Section 2.13.4).



Table 2.15 Details for the screening of pentahydride complexes for the sonochemical *n*-dodecane transfer dehydrogenation.



| Entry | Catalyst                             | $m_{Ir}$ (mg) | Time (h) | TON   |
|-------|--------------------------------------|---------------|----------|-------|
| 1     | $Ir(P^iPr_3)_2H_5$ ( <b>6</b> )      | 12.9          | 1        | 1.18  |
| 2     | $Ir(PMe_3)_2H_5$ ( <b>15</b> )       | 8.7           | 1        | < 0.1 |
| 3     | $Ir(P^tBu_3)_2H_5$ ( <b>19</b> )     | 15.0          | 1        | < 0.1 |
| 4     | $Ir(PCy_3)_2H_5$ ( <b>17</b> )       | 19.0          | 1        | < 0.1 |
| 5     | $Ir(PCy_3)_2H_5$ ( <b>17</b> )       | 19.0          | 2        | < 0.1 |
| 6     | $Ir(P^tBu_2^nBu)_2H_5$ ( <b>23</b> ) | 15.0          | 1        | < 0.1 |
| 7     | $Ir(P^tBu_2^nBu)_2H_5$ ( <b>23</b> ) | 15.0          | 2        | < 0.1 |
| 8     | $Ir(PAd_2^nBu)_2H_5$ ( <b>26</b> )   | 22.9          | 1        | < 0.1 |

### 2.13.7 Optimisation experiments for the sonochemical *n*-dodecane transfer dehydrogenation mediated by Ir(P<sup>*i*</sup>Pr<sub>3</sub>)<sub>2</sub>H<sub>5</sub>

The system optimisation has been carried out following the general procedure reported below. Amounts and conditions are modified as described in the relative following paragraphs.

#### 2.13.7.1 General procedure for the optimisation tests

For a typical sonochemical reaction the reagents were transferred to the vessel following always the same order as described below. In the glovebox, the complex Ir(P<sup>*i*</sup>Pr<sub>3</sub>)<sub>2</sub>H<sub>5</sub> was weighed in a Schlenk tube (12.9 mg, 0.025 mmol) and solubilised in *n*-dodecane (5 mL). Then TBE was added (64.4 μL, 0.50 mmol). The sealed vessel was taken outside the glovebox and sonicated for few seconds in the ultrasonic bath in order to completely dissolve the complex. Meanwhile, the sonochemical reactor was assembled (see Figure 2.3), connected to the Schlenk line and evacuated completely under vacuum and backfilled with argon three times to ensure complete removal of residual air. The Schlenk tube containing the reaction mixture previously prepared was also connected to the Schlenk line. The solution was transferred from the Schlenk tube to the sonochemical reactor quantitatively with a syringe. The flask of sonochemical reactor was immersed in a water-cooling bath to maintain the solution at room temperature (25 ± 3 °C). The horn and the upper part of the reactor were cooled down from the outside by a continuous stream of compressed air. The reaction mixture was sonicated with a pulse mode (amplitude 100%), irradiating with ultrasounds for 10 minutes and then stopping for another 10 minutes (total reaction time 2 h, active sonication time 1 h).

The reaction mixture was then quenched by opening it to air and bubbling air through the solution. An aliquot of the reaction mixture was properly diluted to be analysed by GC, at this stage iso-octane was also added as the internal standard (for details on preparation and dilution of the solution see Section 2.13.4).

#### 2.13.7.2 Optimisation of Ir(P<sup>*i*</sup>Pr<sub>3</sub>)<sub>2</sub>H<sub>5</sub> concentration

The general procedure (Section 2.13.7.1) has been followed, changing however the amounts of Ir(P<sup>*i*</sup>Pr<sub>3</sub>)<sub>2</sub>H<sub>5</sub> and TBE, which are reported below in Table 2.16. For Entry 1, when the amount of iridium complex was 2.6 mg, a stock solution of Ir(P<sup>*i*</sup>Pr<sub>3</sub>)<sub>2</sub>H<sub>5</sub> (10.4 mg, 0.020 mmol) in *n*-dodecane (20 mL) was prepared and an aliquot of 5 mL of that stock solution was used for the sonochemical reaction.

Table 2.16 Results for the optimisation of Ir(P<sup>i</sup>Pr<sub>3</sub>)<sub>2</sub>H<sub>5</sub> concentration with relative amounts of Ir(P<sup>i</sup>Pr<sub>3</sub>)<sub>2</sub>H<sub>5</sub> and TBE for each reaction.

| Entry | TBE/Ir | m <sub>Ir</sub> (mg) | n <sub>Ir</sub> (mmol) | V <sub>TBE</sub> (μL) | n <sub>TBE</sub> (mmol) | TON  |
|-------|--------|----------------------|------------------------|-----------------------|-------------------------|------|
| 1     | 100    | 2.6                  | 0.005                  | 64.4                  | 0.5                     | 0.93 |
| 2     | 20     | 12.9                 | 0.025                  | 64.4                  | 0.5                     | 1.20 |
| 3     | 2      | 129.4                | 0.250                  | 64.4                  | 0.5                     | 0.20 |
| 4     | 20     | 129.4                | 0.250                  | 644                   | 5.0                     | 0.41 |

### 2.13.7.3 Optimisation of TBE concentration

The general procedure (Section 2.13.7.1) has been followed, changing however the amount of *tert*-butylethylene, which is reported below in Table 2.17.

Table 2.17 Results for the optimisation of TBE concentration with relative amounts of TBE for each reaction.

| Entry | TBE/Ir | V <sub>TBE</sub> (μL) | n <sub>TBE</sub> (mmol) | TON  |
|-------|--------|-----------------------|-------------------------|------|
| 1     | 10     | 32.2                  | 0.25                    | 0.50 |
| 2     | 20     | 64.4                  | 0.50                    | 1.20 |
| 3     | 100    | 322                   | 2.5                     | 0.29 |
| 4     | 200    | 644                   | 5.00                    | 0.15 |

### 2.13.7.4 Amplitude optimisation

The general procedure for the sonochemical tests has been followed (Section 2.13.7.1), however the amplitude settings were varied as reported in Table 2.5 in Section 2.4.3. Ultrasound irradiation with the pulse mode was used in all cases.

### 2.13.7.5 Time optimisation and time monitoring experiments

The general procedure has been followed with few modifications as follows. For a typical time monitoring of the sonochemical reaction the reagents were transferred to the vessel following always in the same order as described below. In the glovebox, the complex Ir(P<sup>i</sup>Pr<sub>3</sub>)<sub>2</sub>H<sub>5</sub> was weighed in a Schlenk tube (20.7 mg, 0.040 mmol) and solubilised in alkane (8 mL). Then TBE was added (66.0 μL, 0.8 mmol). The sealed vessel was taken outside the glovebox, transferred to the sonochemical reactor and set up as described in the general

procedure. The reaction mixture was sonicated with a pulse mode (amplitude 100%), irradiating with ultrasounds for 10 minutes and then stopping for another 10 minutes (total reaction time 8 h, active sonication time 4 h).

At the required time points, when the ultrasound was off, an aliquot of the solution (0.5 mL) was collected with a syringe and transferred to a 4 mL vial for analysis. The time points are the processing times reported in Table 1.6 and Figure 1.5 in Section 1.4.4. Note that the processing time reported in both the table and the graph refers to the time of active sonication. Each sample of the reaction mixture was quenched by exposing it to air and bubbling air through the solution. Each aliquot was then properly diluted to be analysed by GC, at this stage iso-octane was also added as the internal standard (for details on preparation and dilution of the solution see Section 2.13.4). When *n*-hexane was used as the alkane, then *n*-dodecane was used as the internal standard for the GC analyses. After the aliquot for the last time point was collected, the remaining reaction mixture was quenched by opening it to air and bubbling air through the solution.

#### 2.13.7.6 Control experiments

Control experiments were run following the general procedure (Section 2.13.7.1), but avoiding, respectively, each time the addition of complex, TBE or without ultrasound irradiation. For the experiment with iridium chloride, no iridium pentahydride complex was added, instead,  $\text{IrCl}_3 \cdot 3\text{H}_2\text{O}$  (8.8 mg, 0.025 mmol) was added to the Schlenk tube. More details are reported in Table 2.7 in Section 2.4.5.

#### 2.13.7.7 Perfluoroalkane experiment

In the glovebox, the complex  $\text{Ir}(\text{P}^i\text{Pr}_3)_2\text{H}_5$  was weighed in a Schlenk tube (12.9 mg, 0.025 mmol) and solubilised in perfluorodecalin (5 mL). Then, *n*-dodecane (568  $\mu\text{L}$ , 2.50 mmol) and TBE were added (64.4  $\mu\text{L}$ , 0.50 mmol). The sealed vessel was taken outside the glovebox and sonicated for few seconds in the ultrasonic bath in order to completely dissolve the complex. Meanwhile, the sonochemical reactor was assembled (see Figure 2.3), connected to the Schlenk line and evacuated completely under vacuum and backfilled with argon three times to ensure complete removal of residual air. The Schlenk tube containing the reaction mixture previously prepared was also connected to the Schlenk line. The solution was transferred from the Schlenk tube to the sonochemical reactor quantitatively with a syringe. The flask of sonochemical reactor was immersed in a water-cooling bath to maintain the solution at room temperature ( $25 \pm 3$  °C). The horn and the upper part of the reactor were cooled down from

the outside by a continuous stream of compressed air. The reaction mixture was sonicated with a pulse mode (amplitude 100%), irradiating with ultrasounds for 10 minutes and then stopping for another 10 minutes (total reaction time 2 h, active sonication time 1 h).

The reaction mixture was then quenched by opening it to air and bubbling air through the solution. An aliquot of the reaction mixture was properly diluted to be analysed by GC, at this stage iso-octane was also added as the internal standard (for details on preparation and dilution of the solution see Section 2.13.4).

The perfluorodecaline phase was analysed by  $^1\text{H-NMR}$  showing still presence of *n*-dodecane and dodecenes, indeed the TON obtained was slightly lower than the actual result and the result cannot be considered quantitative.

### 2.13.8 Thermal *n*-dodecane transfer dehydrogenation mediated by ( $^{A^d}\text{PCP}$ )IrHCl with $\text{NaO}^t\text{Bu}$

In the glovebox, the catalyst ( $^{A^d}\text{PCP}$ )IrHCl (46.7 mg, 0.05 mmol) and  $\text{NaO}^t\text{Bu}$  (5.8 mg, 0.06 mmol) were weighed in a vial and 5 mL of *n*-dodecane were added. 0.5 mL of that solution were transferred to a Schlenk bomb equipped with a stirring bar. 4.5 mL of *n*-dodecane were added. At this point TBE was added (64.4  $\mu\text{L}$ , 0.50 mmol). The sealed vessel was taken outside the glovebox and sonicated for a few seconds in the ultrasonic bath in order to dissolve the catalyst and  $\text{NaO}^t\text{Bu}$ . The vessel was then immersed in a high temperature oil bath for 24 hours at high stirring rate (230  $^\circ\text{C}$ , 500 rpm).

The reaction mixture was then left to cool down, quenched by opening it to air and bubbling air through the solution. An aliquot of the reaction mixture was properly diluted to be analysed by GC, at this stage iso-octane was also added as the internal standard (for details on preparation and dilution of the solution see Section 2.13.4). A TON of 56.6 was obtained

### 2.13.9 Photochemical *n*-dodecane acceptorless dehydrogenation mediated by *trans*- $\text{Rh}(\text{PMe}_3)_2(\text{CO})\text{Cl}$

In the glovebox,  $\text{Rh}(\text{PMe}_3)_2(\text{CO})\text{Cl}$  (10.2 mg, 0.04 mmol) was weighed in a vial and 5 mL of *n*-dodecane were added. 0.5 mL of that solution were transferred to a Schlenk tube equipped with a stirring bar. 3.5 mL of *n*-dodecane were added to the Schlenk tube. The sealed vessel was taken outside and equipped with an argon filled balloon on the top. The solution was sonicated for a few seconds in the ultrasonic bath in order to dissolve the catalyst. An outlet needle was placed on the top (to facilitate removal of  $\text{H}_2$ ) and the Ar balloon refilled from

time to time. The Schlenk tube was then irradiated with light from the Xe DC ARC LAMP source for 7 hours at high stirring rate. In order to facilitate the hydrogen removal from the reaction mixture for the acceptorless AD, stirring rates of 700 rpm were maintained throughout the reaction. The reaction mixture was then left to cool down (it slightly warmed up due to the light irradiation), quenched by opening it to air and bubbling air through the solution. An aliquot of the reaction mixture was properly diluted to be analysed by GC, at this stage iso-octane was also added as the internal standard (for details on preparation and dilution of the solution see Section 2.13.4). A TON of 8.3 was obtained.

## 2.13.10 Catalyst deactivation experiments

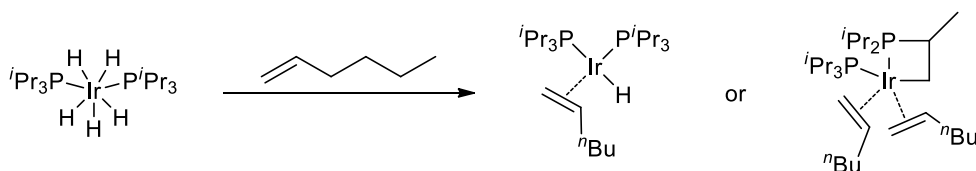
### 2.13.10.1 Isolation of the decomposed complex from the sonochemical reaction

In the glovebox, the complex  $\text{Ir}(\text{P}^i\text{Pr}_3)_2\text{H}_5$  was weighed in a Schlenk tube (12.9 mg, 0.025 mmol) and solubilised in *n*-hexane (5 mL). Then TBE was added (64.4  $\mu\text{L}$ , 0.50 mmol). The sealed vessel was taken outside the glovebox and sonicated for few seconds in the ultrasonic bath in order to completely dissolve the complex. Meanwhile, the sonochemical reactor was assembled (see Figure 2.3), connected to the Schlenk line and evacuated completely under vacuum and backfilled with argon three times to ensure complete removal of residual air. The Schlenk tube containing the reaction mixture previously prepared was also connected to the Schlenk line. The solution was transferred from the Schlenk tube to the sonochemical reactor quantitatively with a syringe. The flask of sonochemical reactor was immersed in a water-cooling bath to maintain the solution at room temperature ( $25 \pm 3$  °C). The horn and the upper part of the reactor were cooled down from the outside by a continuous stream of compressed air. The reaction mixture was sonicated with a pulse mode (amplitude 100%), irradiating with ultrasounds for 10 minutes and then stopping for another 10 minutes (total reaction time 2 h, active sonication time 1 h).

The reaction mixture was then transferred to a Schlenk flask *via* a syringe. The solution was concentrated to dryness obtaining a sticky dark green solid. The flask was transferred into the glovebox and a portion of the solid was solubilised in THF- $\text{d}^8$  and the solution analysed by proton and phosphorus NMR spectroscopy (spectra in the next Section 2.13.10.2).

### 2.13.10.2 Attempts to synthesise the decomposed cyclometalated complex *via* thermal approach

Table 2.18 Details for the various attempts in the synthesis of the deactivated complex.



| Entry | Solvent          | [Ir]/ <i>n</i> -hexene | T (°C) | t (h) |
|-------|------------------|------------------------|--------|-------|
| 1     | <i>n</i> -Hexane | 01:10                  | 100    | 5     |
| 2     | 1-Hexene         | Excess                 | 100    | 5     |
| 3     | 1-Hexene         | Excess                 | r.t.   | 5     |
| 4     | 1-Hexene         | Excess                 | r.t.   | 0     |

**Entry 1:** In the glovebox, the complex Ir(P<sup>*i*</sup>Pr<sub>3</sub>)<sub>2</sub>H<sub>5</sub> was weighed in a Schlenk bomb (20.3 mg, 0.04 mmol) and solubilised in *n*-hexane (1 mL). Then 1-hexene was added (47.5 μL, 0.4 mmol) followed by a stirring bar. The sealed vessel was taken outside the glovebox and placed in an oil bath at 100 °C for 5 hours. The pale-yellow solution turned red after 5 minutes and dark red after 5 hours. The homogeneous solution was then dried under vacuum to obtain a brown oily residue. A portion of the isolated oil was analysed by proton and phosphorus NMR in d<sup>8</sup>-THF in a J-Young NMR tube.

**Entries 2-4:** In the glovebox, the complex Ir(P<sup>*i*</sup>Pr<sub>3</sub>)<sub>2</sub>H<sub>5</sub> was weighed in a Schlenk bomb (20.6 mg, 0.04 mmol) and solubilised in 1-hexene (0.8 mL). Then, a stirring bar was added. The sealed vessel was taken outside the glovebox and placed in an oil bath (see Table 2.18 for temperatures and reaction times). The solution appeared green at the beginning, turned red after 5 minutes and dark red after 5 hours. The homogeneous solution was then concentrated under reduced pressure to obtain a brown oily residue. A portion of the isolated oil was analysed by proton and phosphorus NMR in d<sup>8</sup>-THF in a J-Young NMR tube.

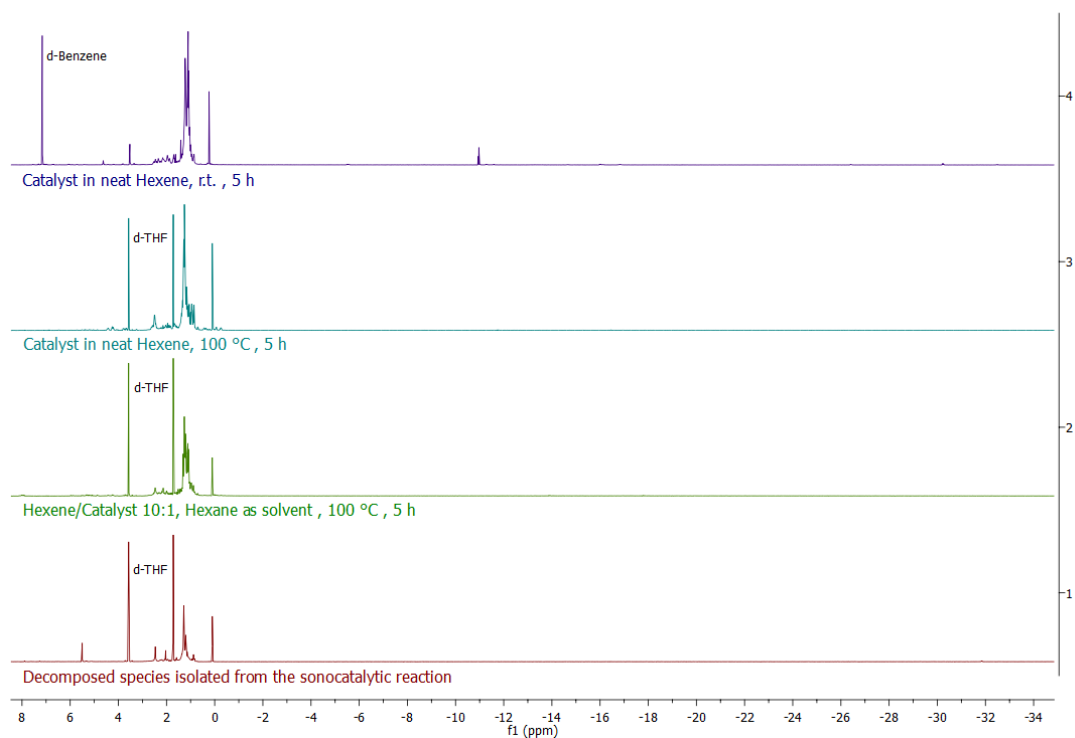


Figure 2.17 Stacked  $^1\text{H}$ -NMR spectra (298 K, 500 MHz) for the different attempts in the synthesis of the deactivated catalyst. (1) Attempt in synthesising the deactivated catalyst species by reaction of the  $\text{Ir}(\text{P}^i\text{Pr}_3)_2\text{H}_5$  and 1-hexene (1-Hexene/Ir 10:1) in a *n*-hexane solution at 100 °C for 5 hours. (2) Attempt in synthesising the deactivated catalyst species by reaction of the  $\text{Ir}(\text{P}^i\text{Pr}_3)_2\text{H}_5$  in neat 1-hexene at 100 °C for 5 hours. (3) Attempt in synthesising the deactivated catalyst species by reaction of the  $\text{Ir}(\text{P}^i\text{Pr}_3)_2\text{H}_5$  in neat Hexene at room temperature for 5 hours. (4) Attempt in synthesising the deactivated catalyst species by reaction of the  $\text{Ir}(\text{P}^i\text{Pr}_3)_2\text{H}_5$  in neat Hexene at room temperature immediately after mixing.



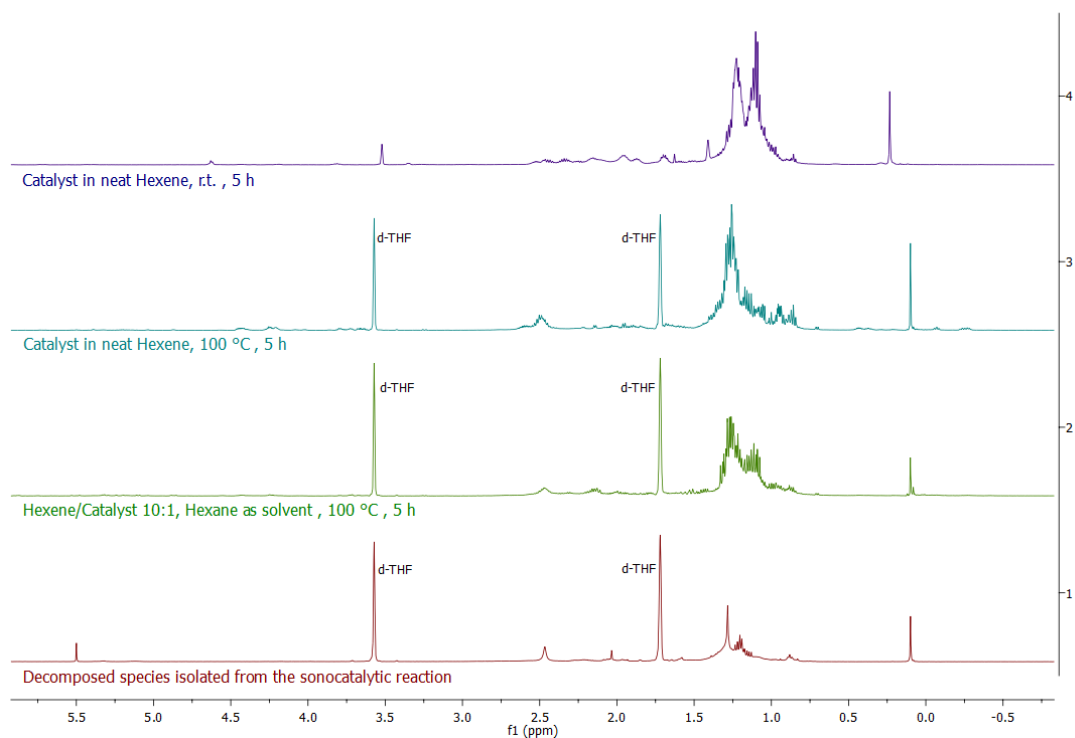


Figure 2.18 Stacked  $^1\text{H}$ -NMR spectra (298 K, 500 MHz), aliphatic region, for the different attempts in the synthesis of the deactivated catalyst. Details of the different attempts as in the caption of Figure 2.17.

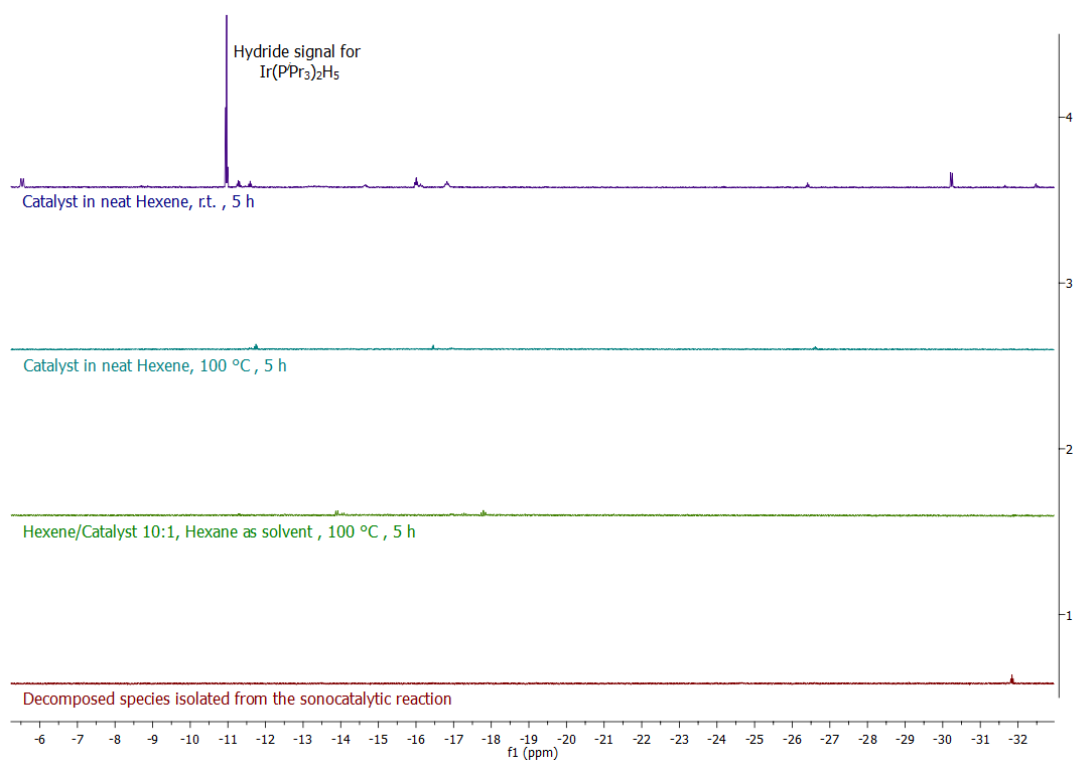


Figure 2.19 Stacked  $^1\text{H}$ -NMR spectra (298 K, 500 MHz), hydride region, for the different attempts in the synthesis of the deactivated catalyst. Details of the different attempts as in the caption of Figure 2.17.

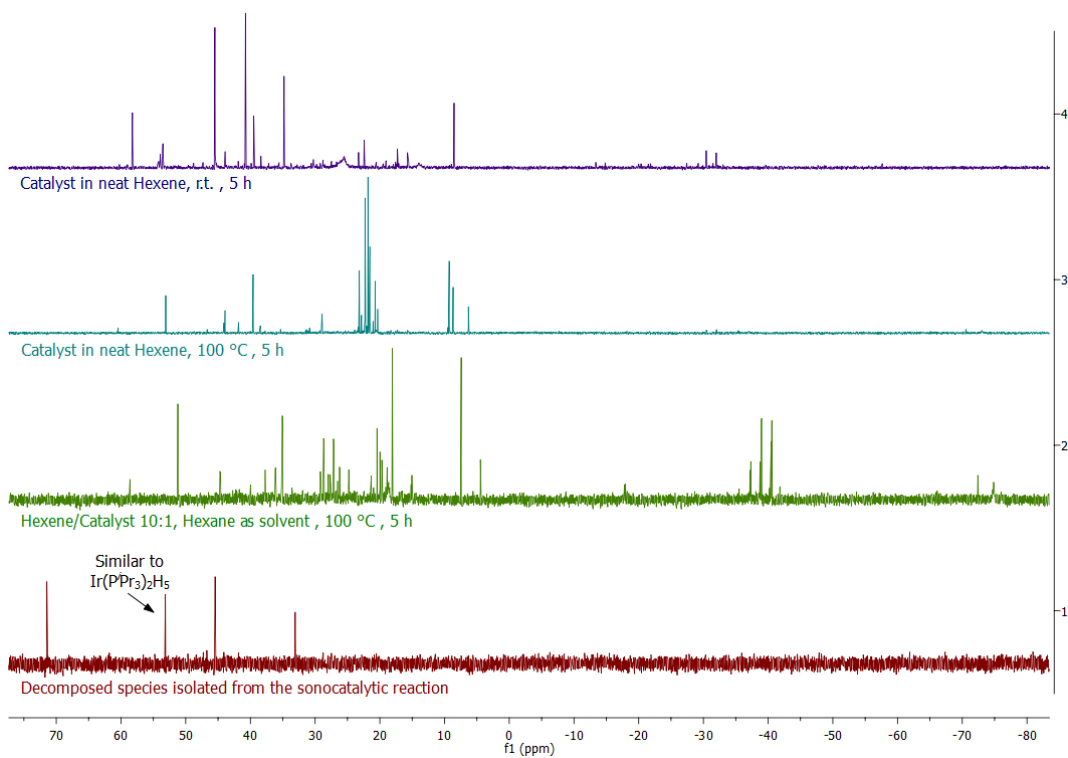


Figure 2.20 Stacked  $^{31}\text{P}\{^1\text{H}\}$ -NMR spectra (298 K, 202 MHz) for the different attempts in the synthesis of the deactivated catalyst. Details of the different attempts as in the caption of Figure 2.17.

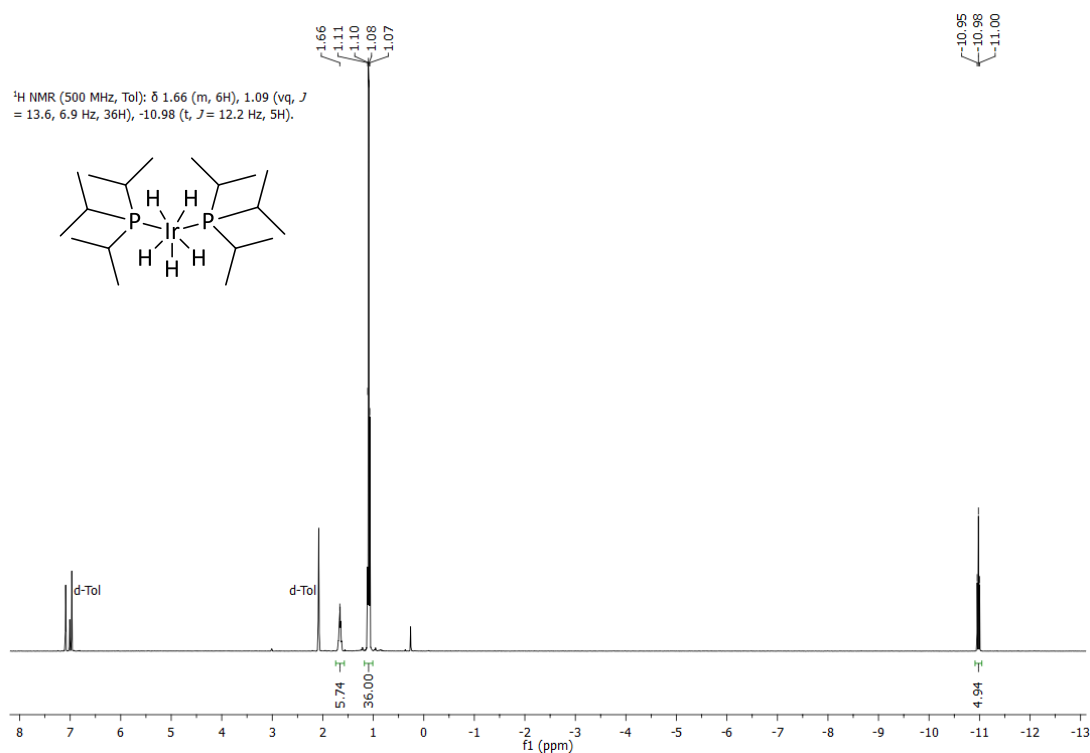


Figure 2.21  $^1\text{H}$ -NMR (298 K, 500 MHz) of  $\text{Ir}(\text{P}^i\text{Pr}_3)_2\text{H}_5$  (**2**) for reference.

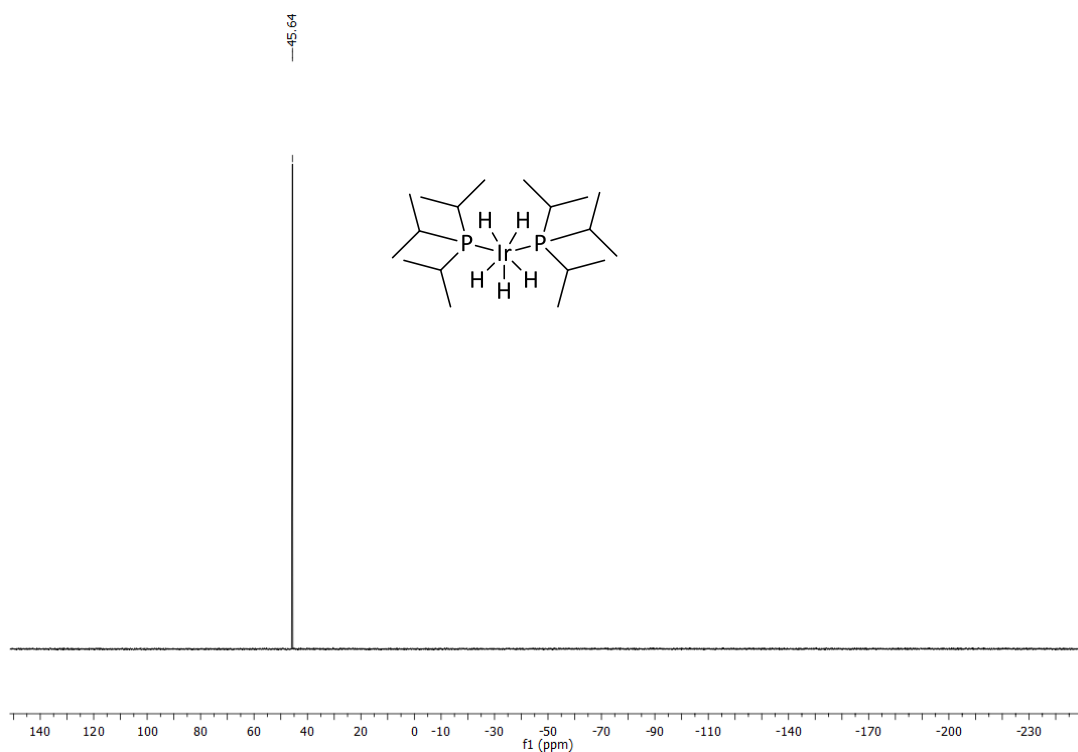


Figure 2.22  $^{31}\text{P}\{^1\text{H}\}$ -NMR spectra (298 K, 202 MHz) of  $\text{Ir}(\text{P}^i\text{Pr}_3)_2\text{H}_5$  (2) for reference.

### 2.13.10.3 Product inhibition experiments

The general procedure reported in Section 2.13.7.5 has been followed with few modifications as below.

#### 2.13.10.3.1 Sonochemical *n*-dodecane transfer dehydrogenation mediated by $\text{Ir}(\text{P}^i\text{Pr}_3)_2\text{H}_5$ with addition of a second aliquot of $\text{Ir}(\text{P}^i\text{Pr}_3)_2\text{H}_5$ after 1 hour

After 1 hour of processing time a second aliquot of complex  $\text{Ir}(\text{P}^i\text{Pr}_3)_2\text{H}_5$  (14.2 mg, 0.028 mmol) was quantitatively transferred to the reaction mixture *via* the side neck of the flask. This aliquot has been pre-weighted in the glovebox in a 4 mL vial sealed with a Teflon lined screw cap. Then, the experiment was carried on and more aliquots of the solution were collected and analysed accordingly to the general method. The time points were the processing times reported in Figure 2.10 in Section 2.7.1.3. Note that the processing time reported in the graph refers to the time of active sonication.

#### 2.13.10.3.2 Sonochemical *n*-dodecane transfer dehydrogenation mediated by $\text{Ir}(\text{P}^i\text{Pr}_3)_2\text{H}_5$ with addition of 1-dodecene

In the glovebox, when the Schlenk tube was charged with the required reagents, 1-dodecene was also added (8.7  $\mu\text{L}$ , 0.040 mmol, 1 equivalent compared to the complex). The time points were the processing times reported in Figure 2.11 in Section 2.7.1.3. Note that the processing time reported in the graph refers to the time of active sonication.

#### 2.13.10.4 TGA analysis of $\text{Ir}(\text{P}^i\text{Pr}_3)_2\text{H}_5$ (2)

In the glovebox, 17.8 mg of  $\text{Ir}(\text{P}^i\text{Pr}_3)_2\text{H}_5$  (colourless transparent crystals) were weighed in the crucible. The sample was placed in a vial, sealed with a Teflon cap and taken out the glovebox for the analysis. The instrument was set, and the background was recorded. Once the background was collected the vial with the sample was opened and the crucible with the sample quickly transferred to the instrument using a pair of tweezers. The analysis was run heating the sample from room temperature to 700 °C at 5 °C/min. Once cooled down, the resulting decomposed sample was observed as a black residue.

#### 2.13.10.5 DSC analysis of $\text{Ir}(\text{P}^i\text{Pr}_3)_2\text{H}_5$ (2)

In the glovebox, 15.2 mg of  $\text{Ir}(\text{P}^i\text{Pr}_3)_2\text{H}_5$  (colourless transparent crystals) were weighed in the pan. The pan with the sample was sealed and placed in a vial, closed with a Teflon cap and taken out the glovebox for the analysis. Once the instrument was set, the vial with the sample was opened and the pan with the sample quickly transferred to the instrument using a pair of tweezers. The analysis was run following the method in Table 2.9.

### 2.13.11 Sonochemical transfer dehydrogenation of different alkanes mediated by $\text{Ir}(\text{P}^i\text{Pr}_3)_2\text{H}_5$

Alkanes tested are listed in Table 2.12 of Section 2.9. The reagents were transferred to the vessel following always the same order as described below. In the glovebox, the complex  $\text{Ir}(\text{P}^i\text{Pr}_3)_2\text{H}_5$  was weighed in a Schlenk tube (12.9 mg, 0.025 mmol) and solubilised in alkane (5 mL). Then TBE was added (64.4  $\mu\text{L}$ , 0.50 mmol). The sealed vessel was taken outside the glovebox and sonicated for few seconds in the ultrasonic bath in order to completely dissolve the complex. Meanwhile, the sonochemical reactor was assembled (see Figure 2.3), connected to the Schlenk line and evacuated completely under vacuum and backfilled with argon three times to ensure complete removal of residual air. The Schlenk tube containing

the reaction mixture previously prepared was also connected to the Schlenk line. The solution was transferred from the Schlenk tube to the sonochemical reactor quantitatively with a syringe. The flask of sonochemical reactor was immersed in a water-cooling bath to maintain the solution at room temperature ( $25 \pm 3$  °C). The horn and the upper part of the reactor were cooled down from the outside by a continuous stream of compressed air. The reaction mixture was sonicated with a pulse mode (amplitude 100%), irradiating with ultrasounds for 10 minutes and then stopping for another 10 minutes (total reaction time 2 h, active sonication time 1 h).

The reaction mixture was then quenched by opening it to air and bubbling air through the solution. An aliquot of the reaction mixture was properly diluted to be analysed by GC, at this stage iso-octane was also added as the internal standard in most cases (for details on preparation and dilution of the solution see Section 2.13.4). Exceptions were the tests for the *n*-hexane and *n*-heptane dehydrogenation, where *n*-dodecane was used as the internal standard for the GC analyses.

## 2.13.12 Dct and Hg tests

### 2.13.12.1 Protocol for the dct experiment

The general procedure (Section 2.13.7.1) has been followed and modified as follows. The system was set up as usual and the active species was generated by subjecting the reaction mixture to ultrasound for 10 minutes. An aliquot of the reaction mixture was analysed by GC. The required amount of dct (commercially available) has been pre-weighed (Table 2.19) in a Schlenk tube equipped with a stirring bar. A portion of the reaction mixture was transferred to the Schlenk tube and stirred until all the dct was in solution. Then, the mixture was transferred back to the sonochemical reactor. The solution was sonicated again for 50 minutes (total reaction time of 1 hour and 50 minutes). The activity at the end of the reaction was determined by GC analysis using the standard protocol. The influence of the dct on the activity of the system was calculated by comparison between the TON calculated after 10 minutes, before the addition of dct, and the TON at the end of the reaction. Aliquots of the reaction mixture were analysed for the time points reported in Figure 2.16 in Section 2.10. Note that the processing time reported in both the table and the graph refers to the time of active sonication.

Table 2.19 Details for the sonochemical alkane dehydrogenation experiments with dct.

| Entry | Ir (mg) | dct (mg) | [Ir]/dct | TON (10 min) | TON (1 h) |
|-------|---------|----------|----------|--------------|-----------|
| 1     | 12.3    | 6.4      | 1:1      | 0.37         | 0.90      |
| 2     | 12.9    | 52.9     | 1:10     | 0.26         | 0.27      |
| 3     | 13.4    | 50.2     | 1:10     | 0.38         | 0.45      |

#### 2.13.12.2 Protocol for the Hg experiment

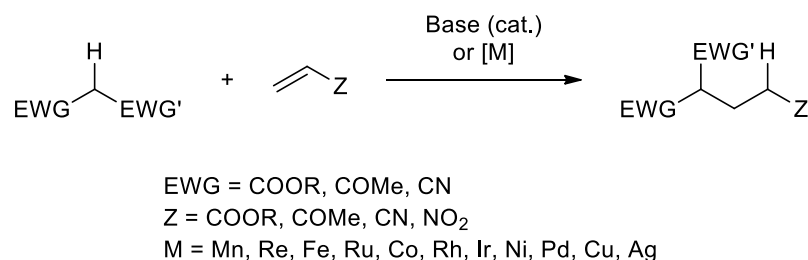
The general procedure (Section 2.13.7.1) has been followed and modified as follows. The system was set up as usual and equipped with a secondary container between the water bath containing the flask and the sound enclosure (two plastic boxes with proper holes to allow the passage of the different hoses and the ultrasound probe). Mercury (0.2 mL, 13.5 mmol) was then added with a syringe *via* the side neck of the flask. The mixture was subjected to sonication for 1 hour (total reaction time of 1 hour and 50 minutes). At the end of this time the solution was worked up by filtration and the activity of the iridium complex was measured by GC using the standard analysis procedure. A TON of 0.7 was obtained.

3

Iridium-catalysed Michael-type  
hydroalkylation of cyclohexenone  
with alkyl-aryl-nitriles

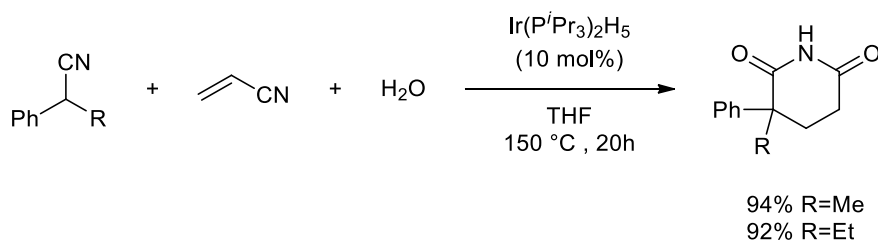
## 3.1 Introduction

### 3.1.1 Background on Michael additions



Scheme 3.1 Michael addition of C-H activated nucleophiles.

Michael addition reactions are a powerful synthetic method for constructing new aliphatic C-C bonds and they are widely used in organic synthesis. They require a nucleophile bearing functional groups (EWG) and a base, such as alkali hydroxides and alkoxides (Scheme 3.1). The functional groups are required to increase the nucleophile acidity and to effectively stabilise the charge. The presence of the base is very important to generate the “active nucleophile”, that will attack the double bond. However, the strong basic conditions also favour the formation of undesired side-products. To solve this issue many transition-metal catalysts, which are able to perform this addition *via* C-H activation, have been developed and are now commonly used. The alternative mechanism, through which they operate, allows the nucleophile scope to be expanded to less acidic substrates. Many examples are reported in the literature of activated nucleophiles bearing two EWGs. Fewer examples are present for transition-metal-catalysed Michael additions of weakly acidic C-H nucleophiles with primary or secondary  $\alpha$ -C-H bonds. But there is only one example, reported by Murahashi, where an iridium complex catalyses the Michael addition of a nucleophile bearing a weakly acidic tertiary C-H bond (Scheme 3.2).<sup>96</sup>



Scheme 3.2 Michael addition of a weakly acidic tertiary C-H bond.

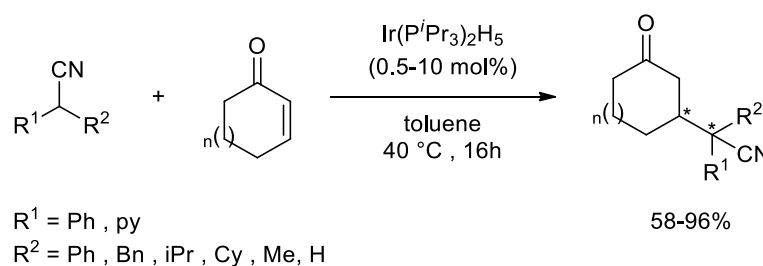
As described, the alkylation of activated and non-activated C-H bonds *via* transition-metal catalysis is one of the most common synthetic approaches to form new C-C bonds in organic



compounds. However, despite the significant progress made in the past two decades, to date Michael additions of non-activated tertiary C-H bonds have not yet been investigated. This is because the Michael addition of weakly acidic tertiary C-H bonds is very challenging, however it is also highly desirable from a synthetic point of view because they provide access to compounds bearing a quaternary carbon centre which is of high synthetic interest. This specific type of Michael addition reaction will be discussed in this chapter.

### 3.1.2 Previous work carried out by the group on the Michael-type hydroalkylation reaction

Aiming to expand the scope of nucleophiles to non-activated tertiary C-H bonds, previously in Sergeev's laboratories a novel iridium-catalysed Michael-type hydroalkylation of cyclic  $\alpha,\beta$ -unsaturated ketones with non-activated alkyl-aryl-nitriles has been developed by Marta Fernandez-Gimenez (Scheme 3.3).<sup>152</sup> Weakly acidic nitriles react with a cyclic ketone to give access to substituted cyclohexanones with a quaternary centre. These are interesting products because  $\beta$ -substituted cyclic ketone derivatives are important building blocks in the synthesis of pharmaceuticals and natural products.<sup>153-155</sup>



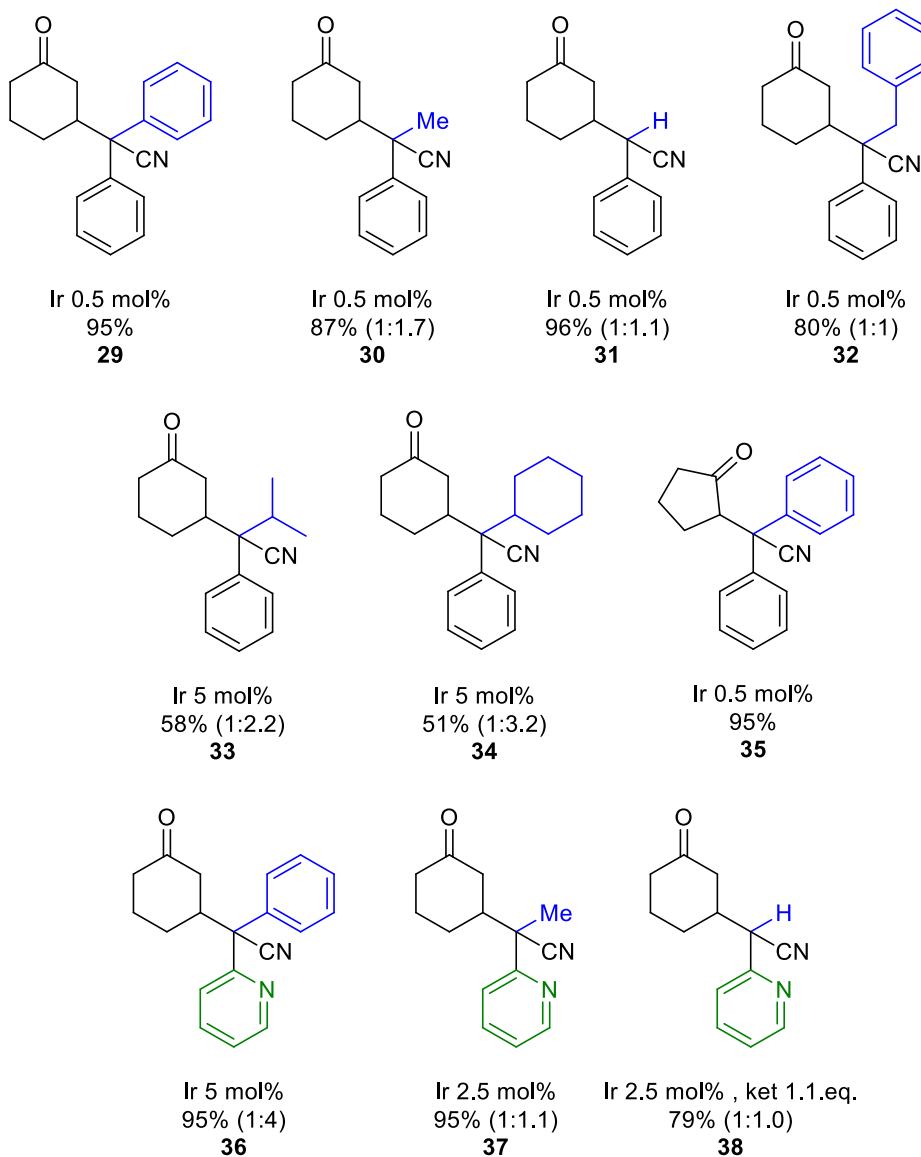
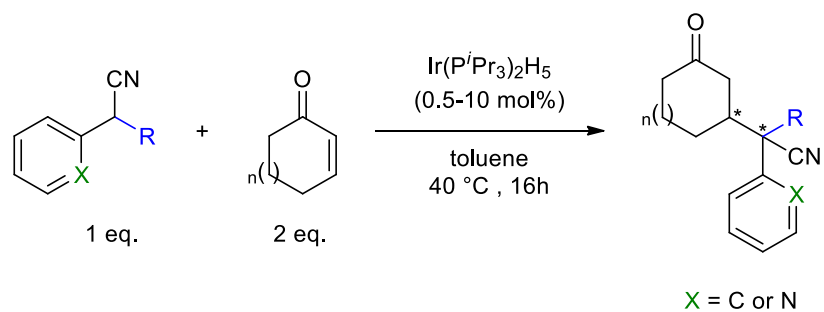
Scheme 3.3 Iridium-catalysed Michael-type hydroalkylation of cyclic  $\alpha,\beta$ -unsaturated ketones with non-activated alkyl-aryl-nitriles.

Previously in the group, the reaction conditions have been optimised by investigating different reaction temperatures, the amount of ketone and the catalyst loading using diphenylacetonitrile and 2-cyclohexen-1-one as the model substrates. The optimal reaction conditions have been identified to be 0.5 mol% of iridium catalyst loading, 40 °C for 16 hours with 2 equivalents of 2-cyclohexen-1-one, leading to an isolated yield of 94% for the hydroalkylation product (Scheme 3.4).<sup>152</sup> Indeed, very mild reaction conditions have been achieved, together with a remarkably low catalyst loading.



Under the newly optimised conditions, good to excellent yields were obtained (products **36**, **37** and **38**).

To summarise, a novel iridium-catalysed Michael-type hydroalkylation of cyclic  $\alpha,\beta$ -unsaturated ketones with non-activated alkyl-aryl-nitriles under mild conditions has been previously developed in Sergeev's laboratories. Some preliminary studies on the system allowed also to optimise the reaction conditions and investigate the scope of ketones and nitriles.



Scheme 3.5 Substrate scope for the iridium-catalysed Michael-type hydroalkylation of cyclic  $\alpha,\beta$ -unsaturated ketones with alkyl aryl nitriles. Yields reported are isolated yields (dr determined by GC). Reaction conditions: Nitrile (0.8 mmol), 2-cyclohexen-1-one (1.60 mmol, 2 equiv),  $\text{Ir}(\text{P}^i\text{Pr}_3)_2\text{H}_5$  (as reported) in toluene (4 ml) under argon atmosphere, at 40 °C for 16 h.

### 3.1.3 Summary and objectives

The Michael addition of acidic carbon nucleophiles to activated olefins is one of the most common methods to form new C-C bonds. However, the use of basic catalysis leads to the formation of undesired side-products. For this reason, alternative transition-metal catalysed approaches have been developed. Many examples are reported in the literature of activated C-H bonds bearing two EWGs, few are for transition-metal-catalysed Michael additions of weakly acidic C-H nucleophiles with primary or secondary  $\alpha$ -C-H bonds and there is only one example of a nucleophile bearing a weakly acidic tertiary C-H bond. Aiming to expand the scope of nucleophiles, previously in Sergeev's laboratories a novel iridium-catalysed Michael-type hydroalkylation of cyclic  $\alpha,\beta$ -unsaturated ketones with non-activated alkyl-aryl-nitriles has been developed by Marta Fernandez-Gimenez.<sup>152</sup>

In the present chapter, this Michael-type hydroalkylation reaction will be further investigated to develop a more general hydroalkylation reaction. A series of iridium-pentahydride catalysts with different steric and electronic properties will be tested against the most difficult substrates previously identified. The substrate scope will be expanded to include differently substituted pyridylacetonitriles. In the desire to make this hydroalkylation reaction even milder, the use of ultrasound will be investigated. The mechanism of this process will be investigated by conducting the various steps of the previously proposed catalytic cycle with stoichiometric amounts of well-defined iridium species with the hope to identify and isolate the intermediate complexes. Finally, some investigations will be carried out to improve the dehydrogenation process of the Michael addition products to obtain *meta*-substituted phenols.

## 3.2 Hydroalkylation of 2-cyclohexen-1-ones with di-substituted acetonitriles

In this section will be outlined the various developments on the Michael-type addition reaction previously reported by Marta Fernandez-Gimenez<sup>152</sup> which have been further investigated.

First the pentahydride catalysts synthesised for the sonochemical dehydrogenation project (*see* previous chapter) were also tested for the hydroalkylation reaction aiming to improve the yields of difficult substrates, such as *iso*-propyl- and cyclohexyl-substituted phenylacetonitriles.

Then, the acetonitrile scope initially investigated was expanded with more pyridyl-substituted acetonitriles. The weakly C-H acidic substrates were first synthesised and then tested for the catalytic Michael-type hydroalkylation reaction.

Finally, as the Ir(P<sup>*i*</sup>Pr<sub>3</sub>)<sub>2</sub>H<sub>5</sub> catalyst was the same complex able to promote the sonochemical alkane dehydrogenation (as described in the previous chapter), the ultrasound-mediated Michael-type addition was also investigated, to understand if this transformation could be performed even under milder conditions.

### 3.2.1 Catalyst screening for difficult substrates

Analysing the preliminary substrate scope for the Michael-type hydroalkylation reaction developed in Sergeev's laboratories, some difficult substrates could be identified. Specifically, as stated in Section 3.1.2, the results with the poorest yields have been obtained when an *iso*-propyl or cyclohexyl group was present.

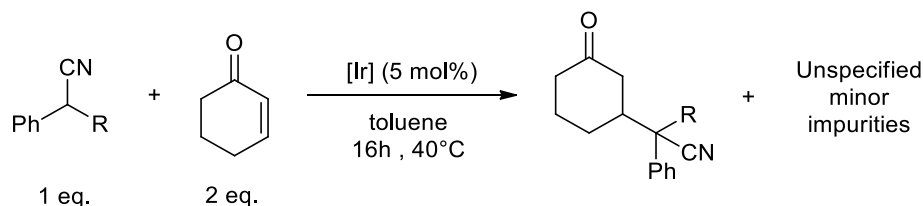
Trying to improve the results for those substrates, different catalysts have been tested with the aim to increase the yield. As the Ir(P<sup>*i*</sup>Pr<sub>3</sub>)<sub>2</sub>H<sub>5</sub> catalyst has been shown to be the best one, other iridium bisphosphine-pentahydride complexes have been tested. The synthesis of those complexes has been reported in the previous chapter. The outcome of the screening can be found in Table 3.1. For the purpose of comparison, the results of the standard hydroalkylation reaction catalysed by Ir(P<sup>*i*</sup>Pr<sub>3</sub>)<sub>2</sub>H<sub>5</sub> are also reported for the phenyl, *iso*-propyl and cyclohexyl-substituted phenylacetonitriles (Entries 1-2 and 8). The screening was carried out using *iso*-propyl-phenylacetonitrile as the benchmark substrate, under the optimised reaction conditions developed for this substrate: 2 equivalents of cyclohexenone, 5 mol% of catalyst loading, at 40 °C for 16 hours. The *iso*-propylbenzyl nitrile **39** has been synthesised following the synthetic procedure optimised by Marta Fernandez-Gimenez<sup>152</sup> reported in



To check whether the reactivity pattern was the same for the cyclohexyl-substituted acetonitrile, the Ir(P<sup>t</sup>Bu<sub>3</sub>)<sub>2</sub>H<sub>5</sub> (**19**) and Ir(P<sup>t</sup>Bu<sub>2</sub><sup>n</sup>Bu)<sub>2</sub>H<sub>5</sub> (**23**) catalysts were tested also for this substrate and comparable results were obtained (Entries 9 and 10).

To summarise, complex **2** is confirmed to be the best catalyst for the Michael addition of *iso*-propyl or cyclohexyl-substituted phenylacetonitriles to cyclohexenones.

Table 3.1 Catalyst screening for the Michael addition of *i*Pr- and Cy-substituted phenylacetonitriles to cyclohexenone.



| Entry | R           | Catalyst   | Cyclohexenone Conv (%) | Nitrile Conv (%) | Product Yield (%) |
|-------|-------------|--|------------------------|------------------|-------------------|
| 1     | Ph          | Ir(P <sup>i</sup> Pr <sub>3</sub> ) <sub>2</sub> H <sub>5</sub> ( <b>2</b> )                 | 57                     | 97               | 95                |
| 2     | <i>i</i> Pr | Ir(P <sup>i</sup> Pr <sub>3</sub> ) <sub>2</sub> H <sub>5</sub> ( <b>2</b> )                 | 61                     | 70               | 58                |
| 3     | <i>i</i> Pr | Ir(PMe <sub>3</sub> ) <sub>2</sub> H <sub>5</sub> ( <b>15</b> )                              | 6                      | 32               | -                 |
| 4     | <i>i</i> Pr | Ir(P <sup>t</sup> Bu <sub>3</sub> ) <sub>2</sub> H <sub>5</sub> ( <b>19</b> )                | 11                     | 22               | -                 |
| 5     | <i>i</i> Pr | Ir(PCy <sub>3</sub> ) <sub>2</sub> H <sub>5</sub> ( <b>17</b> )                              | 61                     | 64               | 28                |
| 6     | <i>i</i> Pr | Ir(P <sup>t</sup> Bu <sub>2</sub> <sup>n</sup> Bu) <sub>2</sub> H <sub>5</sub> ( <b>23</b> ) | 100                    | 36               | 9                 |
| 7     | <i>i</i> Pr | Ir( <sup>ad</sup> PCP)H <sub>4</sub> ( <b>7</b> )  | 98                     | 37               | -                 |
| 8     | Cy          | Ir(P <sup>i</sup> Pr <sub>3</sub> ) <sub>2</sub> H <sub>5</sub> ( <b>2</b> )                 | 44                     | 59               | 51                |
| 9     | Cy          | Ir(P <sup>t</sup> Bu <sub>3</sub> ) <sub>2</sub> H <sub>5</sub> ( <b>19</b> )                | 14                     | 14               | -                 |
| 10    | Cy          | Ir(P <sup>t</sup> Bu <sub>2</sub> <sup>n</sup> Bu) <sub>2</sub> H <sub>5</sub> ( <b>23</b> ) | 100                    | 23               | 1                 |

Experimental conditions: reactions were carried out in toluene (2 mL) at 40 °C for 16 hours, under argon atmosphere. Iridium catalyst loading was 5 mol% (except for entry 1, which was 0.5 mol%). All conversions and yields are based on quantitative GC analysis using n-dodecane as the internal standard.



### 3.2.2 Scope of pyridyl-substituted acetonitriles

After the catalyst screening for difficult substrates, the scope of different pyridyl-substituted acetonitriles was investigated. Many phenyl-substituted acetonitriles, bearing different substituents at the  $\alpha$ -carbon atom of the nitrile, have been previously synthesised and tested, together with few pyridyl-substituted ones (Section 3.1.2). Therefore, the aim was to complete the pyridylacetonitrile scope for the hydroalkylation reaction, by synthesising and testing the benzyl-, *iso*-propyl- and cyclohexyl-substituted pyridylacetonitriles. The interest in the 2-pyridyl moiety is supported by its wide use as a directing group in various C-H activation reactions,<sup>163</sup> meaning that the introduction of this functional group in the Michael addition product would make it more suitable for further functionalisation reactions. In particular, the use of pyridines as directing groups enables the alkylation of C-H bonds of benzylamines,<sup>164</sup>  $\alpha$ -alkylation of cyclic amines<sup>165-166</sup> and alkylation of aromatic C-H bonds.<sup>167</sup> Moreover, no examples are reported in the literature on the use of substituted 2-pyridylacetonitriles with a non-activated C(sp<sup>3</sup>)-H bond as the Michael-donors in such hydroalkylation reaction. Finally, pyridines are recurrent moieties in compounds of pharmaceutical interest.<sup>163</sup>

#### 3.2.2.1 Syntheses of the substrates

First, 2-pyridylacetonitrile substrates had to be synthesised as they are not commercially available. The target substituted compounds are shown in Figure 3.1 and have been synthesised *via* different methods as described below. Those synthesis have been carried out by Rhiannon Davies, as part of her Master project.

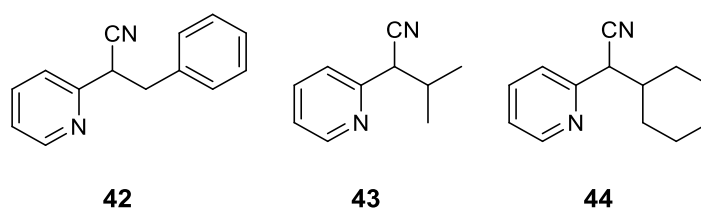
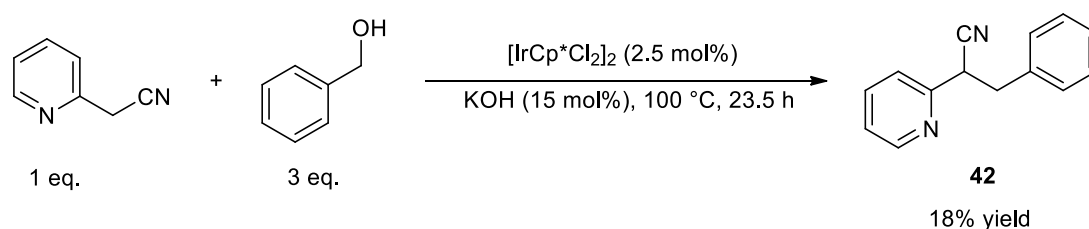


Figure 3.1 Alkyl pyridyl-acetonitrile synthesised to be tested as substrates for the iridium-catalysed Michael-type hydroalkylation.

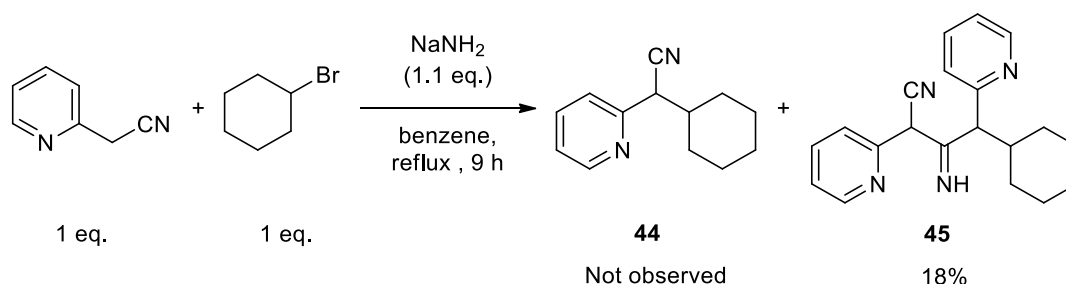
The 3-phenyl-2-(pyridin-2-yl)propanenitrile **42** was obtained, as reported in the literature,<sup>168</sup> from the reaction of 2-pyridylacetonitrile with benzyl alcohol catalysed by the iridium dimer [IrCp\*Cl<sub>2</sub>]<sub>2</sub> in the presence of 15 mol% of KOH (Scheme 3.8). Although full conversion of the 2-pyridylacetonitrile was observed, the desired product **42** was isolated

only in 18% yield, mainly due to difficulties in the purification step with the separation of the product from the benzyl alcohol reagent used in excess.



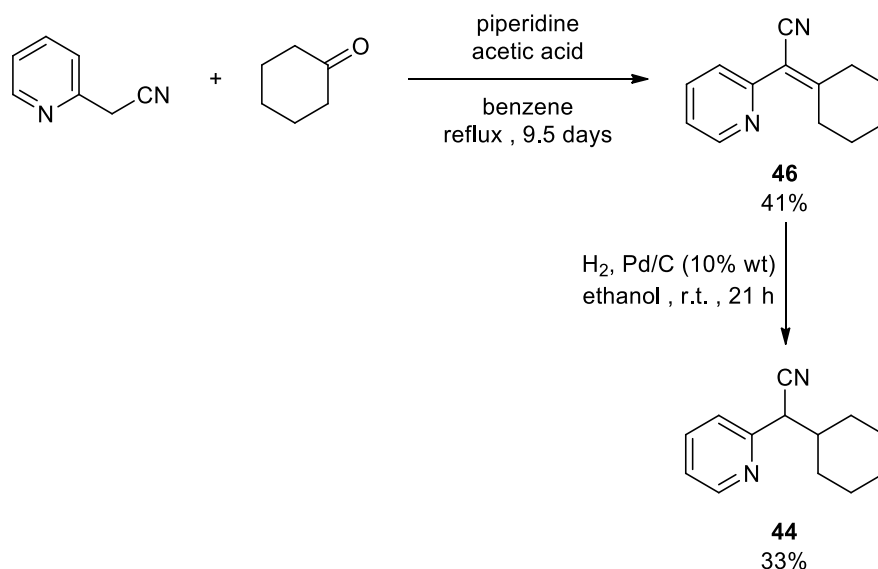
Scheme 3.8 Iridium-catalysed reaction of 2-pyridylacetonitrile with benzyl alcohol to afford 3-phenyl-2-(pyridin-2-yl)propanenitrile **42**.

Preparation of cyclohexyl-2-pyridylacetonitrile **44** was at first attempted by the reaction of 2-pyridylacetonitrile and bromocyclohexane in the presence of a base (Scheme 3.9). Unfortunately, formation of the desired product **44** was not observed, although the formation of a side-product was detected. The side-product **45**, which has been isolated and fully characterised, probably arose from desired product **44**, which underwent further addition of the 2-pyridylacetonitrile yielding **45** in 18% yield.



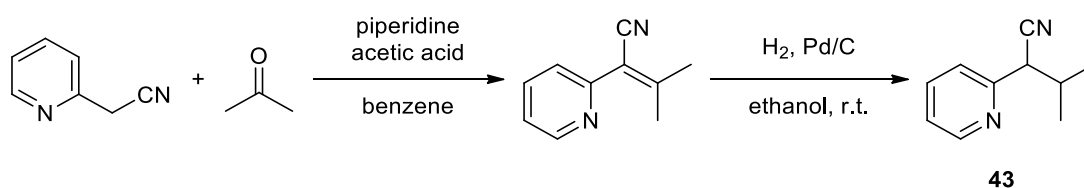
Scheme 3.9 Attempted synthesis of cyclohexyl-2-pyridylacetonitrile **44**, yielding the side-product **45**.

Another approach for the synthesis of cyclohexyl-2-pyridylacetonitrile **44** was tested. This consisted of a two steps route starting always from 2-pyridylacetonitrile. First, the nitrile reacted with cyclohexanone in a reaction catalysed by piperidine and acetic acid, yielding the alkene **46** which was further hydrogenated to obtain the desired product **44** in 33% overall isolated yield (Scheme 3.10). This bespoke synthesis has been adapted from the literature<sup>169</sup> where less hindered ketones are used instead of cyclohexanone; this explains the long reaction time needed to reach full conversion of the 2-pyridylacetonitrile reagent. Although the starting nitrile was fully consumed and not present in the alkene intermediate **46**, it was observed again at the end of the second step, meaning the cleavage of the intermediate **46** or the product **44** was also taking place during the hydrogenation step.



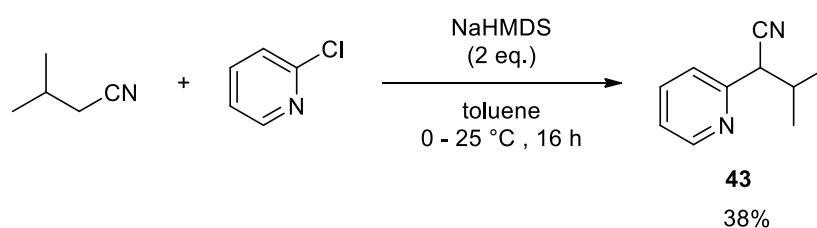
Scheme 3.10 Synthesis of cyclohexyl-2-pyridylacetonitrile **44**.

The  $\alpha$ -*iso*-propyl-2-pyridylacetonitrile **43** could also be synthesised catalytically by reaction of 2-pyridylacetonitrile with acetone in the presence of piperidine and acetic acid as reported in the literature,<sup>169</sup> followed by hydrogenation of the double bond as reported in Scheme 3.11.



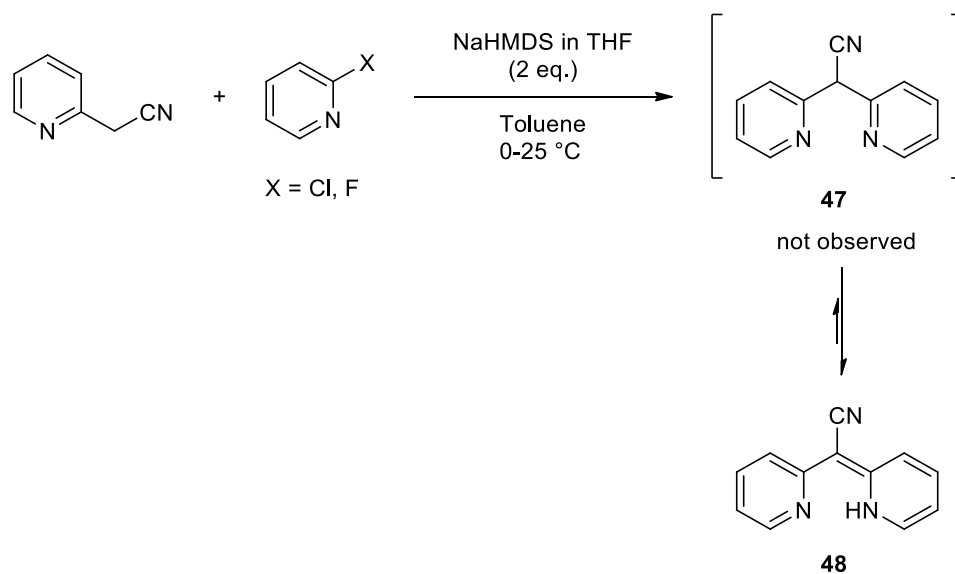
Scheme 3.11 Literature 2-steps reaction for the synthesis of  $\alpha$ -*iso*-propyl-2-pyridylacetonitrile **43**.

However, due to the long reaction time with cyclohexanone (Scheme 3.10), an alternative approach was adopted exploiting a base-mediated nucleophilic substitution reaction (Scheme 3.12). The reaction of 2-chloropyridine with *iso*-valeronitrile has been previously reported in the literature.<sup>170</sup> The desired compound **43** was isolated in only 38% yield. The lower result with respect to the literature data was caused by solubilisation issues during the work-up, resulting in loss of product.



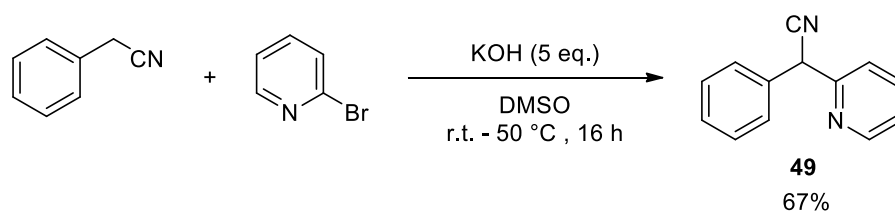
Scheme 3.12 Adopted approach for the synthesis of  $\alpha$ -*iso*-propyl-2pyridylacetonitrile **43**.

The synthesis of the symmetric 2,2-bis-(pyridin-2-yl)-acetonitrile **47** has also been attempted using the same successful approach as for the synthesis of **43**, indeed by reacting 2-pyridylacetonitrile with 2-bromopyridine or 2-fluoropyridine under basic conditions (Scheme 3.13). Unfortunately, formation of the desired nitrile **47** was not observed in both cases (X = Cl or F), but the reagents were fully consumed. Further investigation coupled with literature research<sup>171</sup> highlighted that the desired product **47** cannot be isolated. Once formed, it immediately and fully rearranged into the corresponding tautomer **48**, more stable form due to the higher degree of conjugation (Scheme 3.13).



Scheme 3.13 Attempted reaction for the synthesis of 2,2-bis-(pyridin-2-yl)-acetonitrile **47** and corresponding tautomeric form **48**.

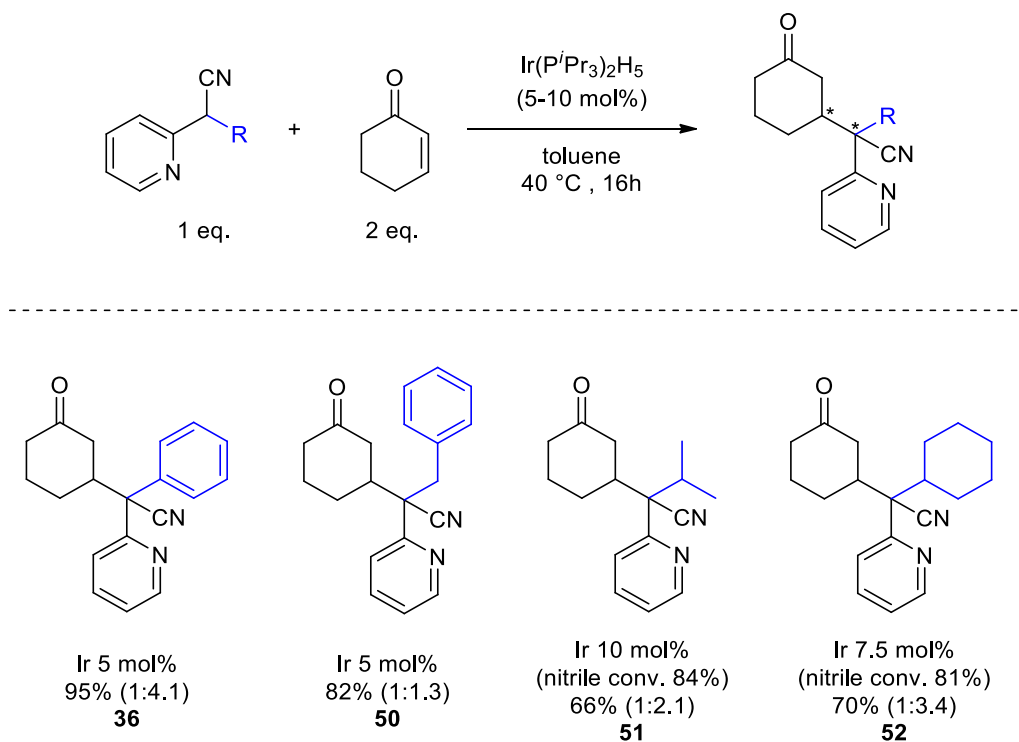
Finally, also the classic base-mediated nucleophilic substitution reaction was used to synthesise the 2-phenyl-2-(2-pyridyl)acetonitrile **49**. The synthesis has been previously optimised by the group<sup>152, 172</sup> and the product has already been tested for the hydroalkylation reaction. However, it was synthesised again and the hydroalkylation reaction repeated to use it as a comparison and to check for reproducibility of the hydroalkylation procedure and consistency of results. Compound **49** was prepared from benzylnitrile and 2-bromopyridine in the presence of KOH obtaining an improved yield of 67%, compared to the previous 60% (Scheme 3.14).



Scheme 3.14 Synthesis of 2-phenyl-2-(2-pyridyl)acetonitrile **49**.

### 3.2.2.2 Catalytic tests

The synthesised pyridyl-substituted acetonitriles have then been tested for the Michael-type hydroalkylation reaction. To explore the scope of those substrates, initially the reproducibility of the catalytic tests had to be checked, validating the synthetic and isolation procedures. The phenylpyridylacetonitrile **49** was tested under the previously optimised reaction conditions, which were found to be 5 mol% of  $\text{Ir}(\text{P}^i\text{Pr}_3)_2\text{H}_5$  catalyst loading, 2 equivalents of cyclohexenone, at 40 °C for 16 hours.<sup>152</sup> Under those conditions and after product isolation *via* flash chromatography, the desired 2-(3-oxocyclohexyl)-2-phenyl-2-(pyridin-2-yl)acetonitrile **36** was obtained in 95% isolated yield (Scheme 3.15), with full conversion of the nitrile substrate, in accordance with the previous results. The optimal catalyst loading for the pyridylphenylacetonitrile substrate **49** was found to be 5 mol%, against the 0.5 mol% for the diphenylacetonitrile **27** as the Michael-donor. Similar pyridyl-substituted acetonitriles were tested, 5 mol% was the starting catalyst loading used for the optimisation of the reaction conditions for each substrate. For the benzyl-substituted pyridylacetonitrile **42** the use of 5 mol% of iridium catalyst loading yielded the desired product **50** in 82% isolated yield. However, with this catalyst loading, products **51** and **52** were obtained only in 44 and 65% yield, respectively. Therefore, for those compounds the catalyst loading had to be increased to improve the yield. A catalyst loading of 7.5 mol% allowed to obtain product **52** in 70% yield. With the *iso*-propyl-substituted pyridylacetonitrile **43** the catalyst loading had to be increased again to obtain a comparable result. Finally, with 10 mol% of iridium catalyst, the desired product **51** could be isolated in 66% yield. It is worth to mention that when the *iso*-propyl- or cyclohexyl-substituted pyridylacetonitrile were employed as substrates, complete nitrile conversion could not be achieved over 16 hours. Longer reaction times did not improve the conversion; an equilibrium was likely to be formed, which hampered the formation of the desired products in higher yields. As observed from the work of Marta Fernanzed-Gimenez, the hydroalkylation reaction can be a reversible process.<sup>152</sup> Moreover, from the diastereomeric ratios it can be observed that the bigger the substituents, the more pronounced the ratio of a diastereomer over the other.



Scheme 3.15 Substrate scope for the iridium catalysed Michael-type hydroalkylation of cyclic 2-cyclohexen-1-one with alkyl-pyridyl-acetonitriles. Yields reported are isolated yields (dr determined by  $^{13}\text{C}$ -NMR). Reaction conditions: nitrile (0.4 mmol), 2-cyclohexen-1-one (0.8 mmol, 2 eq.),  $\text{Ir}(\text{P}^i\text{Pr}_3)_2\text{H}_5$  (as reported) in toluene (2 mL) under argon atmosphere, at 40 °C for 16 h.

By comparing the scope of the phenyl- and pyridyl-substituted acetonitriles, a similar reactivity pattern between the two series of pyridyl- and phenyl-alkyl-substituted acetonitriles can be observed, with the *iso*-propyl- (**43** and starting material for the synthesis of **33**) and cyclohexyl-substituted ones (**44** and starting material for the synthesis of **34**) being the poorest Michael-donors, where the catalyst loading had to be increased the most to achieve acceptable yields (Scheme 3.5 and Scheme 3.15).

In summary, the scope of the iridium-catalysed Michael-type hydroalkylation of  $\alpha,\beta$ -unsaturated cyclohexenone with non-activated alkyl-aryl-nitriles has been completed with the pyridyl-substituted series. The reaction occurs under mild conditions, 40 °C, with catalyst loadings of 5-10 mol% for bulky 2-pyridyl analogues such as benzyl, *iso*-propyl and cyclohexyl groups. It is worth to note the similar reactivity pattern for the two series of phenyl- and pyridyl-substituted alkyl acetonitriles.

### 3.2.3 Attempts for the ultrasound-promoted hydroalkylation

To try to further improve the Michael-type hydroalkylation reaction, the aim was to facilitate the reaction using ultrasounds irradiation, following a similar approach as described in the previous chapter. Moreover, the hydroalkylation reaction investigated uses as catalysts the same  $\text{Ir}(\text{P}^i\text{Pr}_3)_2\text{H}_5$  complex that has been demonstrated to promote the sonochemical alkane transfer dehydrogenation (see previous chapter). Indeed, it was already shown that this specific iridium-pentahydride complex is active under ultrasound irradiation. Aiming to further improve the reaction conditions of this Michael-type hydroalkylation reaction, it was worth investigating whether this reaction could be performed under even milder reaction conditions, replacing the thermal activation with a sonochemical one. The activity of the Michael addition system was investigated by subjecting the reaction mixture to ultrasound irradiation.

As the thermal hydroalkylation reaction has already been developed under relatively mild conditions (40 °C), for every ultrasound mediated reaction, a similar one was run in parallel under the exact same conditions, but with the set-up of the classic thermally mediated reactions and without ultrasound irradiation, at room temperature: this was done to check if the ultrasound irradiation could have any additional benefit to the reaction. The results of this investigation are reported in Table 3.2. The time reported for the ultrasound mediated reaction is the time of active sonication, the actual total reaction time is double as the ultrasound was delivered using a pulse mode (the ultrasound was switched on and off every 10 min). Summarising, the reaction was subjected to one hour of ultrasound irradiation and to another hour of only thermal activation (room temperature). Hence, it is explained the comparison with the corresponding room temperature reaction. Diphenylacetonitrile and 2-cyclohexen-1-one have been chosen as the benchmark substrates for the investigation.

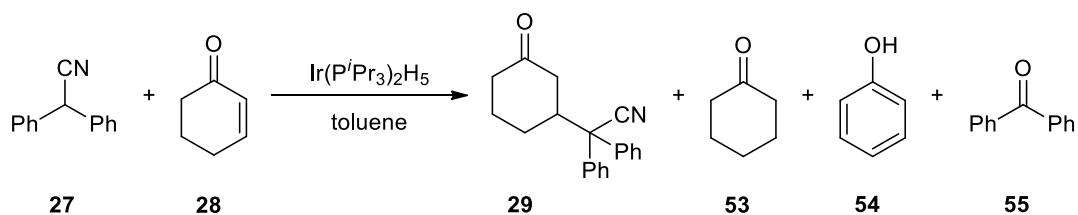
At first, the reaction mixture has been subjected to ultrasound irradiation for 1 hour, with the optimised catalyst loading of 5 mol% (Entry 2) and no formation of the desired Michael addition product **29** was observed. Indeed, the catalyst loading was increased to 10 mol% and under these conditions, a yield of 12% was observed for the desired product **29** (Entry 4). Together with the desired product, also cyclohexanone **53** was formed in 13% yield as a side-product. Moreover, by comparing the same reaction carried out without the ultrasound irradiation, but only stirring the reaction mixture at room temperature for 2 hours (Entry 3), a much better yield of 44% of the desired product was obtained, even if with formation of a small amount of cyclohexanone. To check whether the lower results under sonochemical conditions were due to the presence of a possible induction period, a subsequent test has

been done irradiating with ultrasound for 2 hours (Entry 6). With this longer reaction time, the yield of **29** was improved to 23%, almost double compared to entry 4. Interestingly, the amount of cyclohexanone formed was comparable for both one- and two-hours reactions. However, looking at the same reaction performed under thermal conditions (Entry 5) the yield of the desired product **29** was increased to 70%, with a small increase also in the cyclohexanone **53** yield. Indeed, it was confirmed that the system worked better under thermal conditions than under ultrasound irradiation. Finally, it is interesting to note how under thermal conditions another side-product was formed in small amount, phenol **54** (Entry 3 and 5). On the other hand, under sonochemical conditions **54** was not observed, while another side-product, benzophenone **55**, was formed in small amounts (Entry 4 and 6). **55** can be formed by oxidation of diphenylacetonitrile **27**.

To conclude, unfortunately, it has been shown that under these conditions, the Michael-type hydroalkylation reaction was much more efficient under thermal conditions than under sonochemical conditions. Indeed, the ultrasound irradiation seems to have a detrimental effect on this reaction, possibly because the ultrasound is converting the catalyst into another inactive species as widely discussed in Chapter 2. This could explain the diminished yield between the thermal and ultrasound-mediated reaction. Moreover, the increase in catalyst loading favours also the formations of different side-products. For those reasons the idea of an ultrasound promoted Michael-type hydroalkylation was not further investigated.



Table 3.2 Attempts for the ultrasound-mediated Michael-type hydroalkylation of cyclohexenone with diphenylacetonitrile.



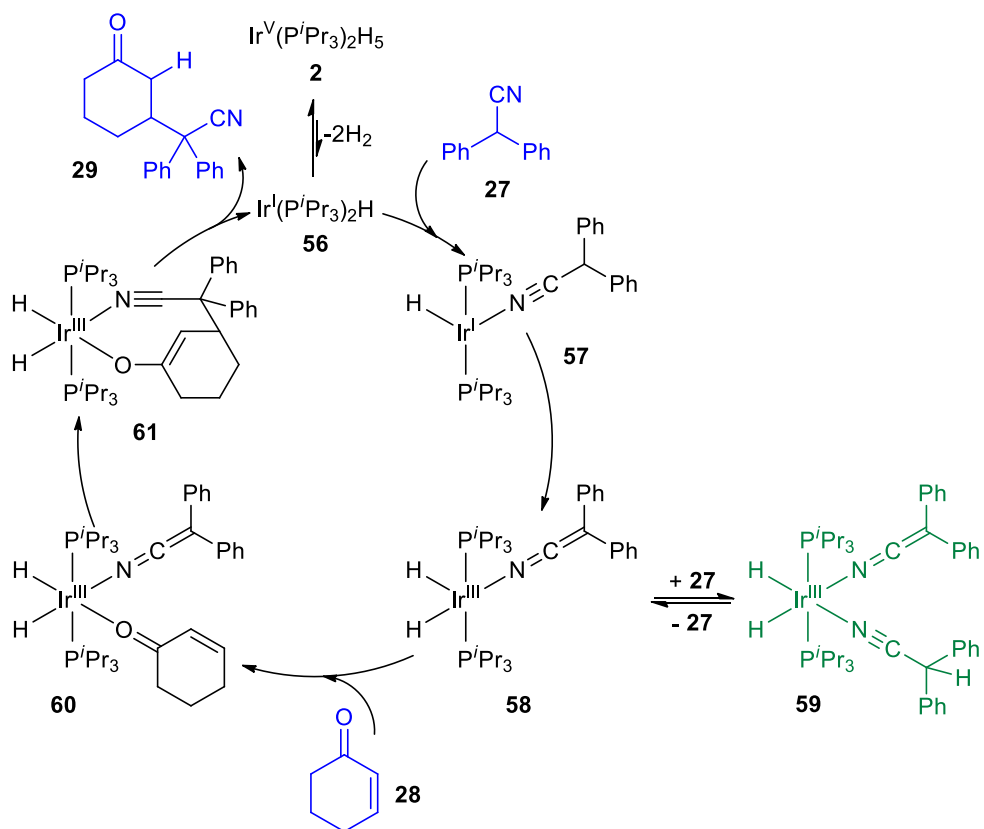
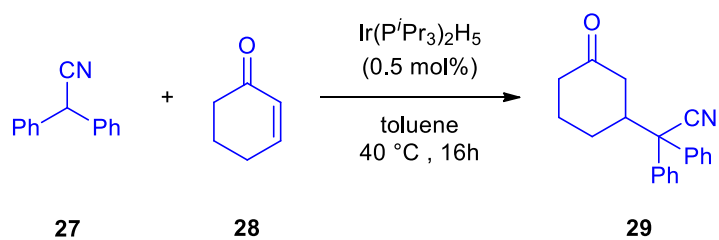
| Entry | t (h) | Activation mode | Ir (mol%) | 27 Conv. (%) | 28 Conv. (%) | 29 Yield (%) | 53 Yield (%) | 54 Yield (%) | 55 Yield (%) |
|-------|-------|-----------------|-----------|--------------|--------------|--------------|--------------|--------------|--------------|
| 1     | 2     | thermal         | 0.5       | 5            | 5            | 2            | 0            | 0            | 0            |
| 2     | 1     | US              | 0.5       | 1            | 2            | 0            | 5            | 0            | 0            |
| 3     | 2     | thermal         | 10.0      | 45           | 26           | 44           | 15           | 6            | 0            |
| 4     | 1     | US              | 10.0      | 16           | 11           | 12           | 13           | 0            | 9            |
| 5     | 4     | thermal         | 10.0      | 80           | 43           | 70           | 21           | 6            | 0            |
| 6     | 2     | US              | 10.0      | 15           | 17           | 23           | 14           | 0            | 10           |

Experimental conditions: sonochemical reactions are carried out in toluene (5 mL) at room temperature ( $25 \pm 3$  °C), under argon atmosphere, with a water cooling bath and with the microtip being cooled by a continuous stream of compressed air. Amplitude is 100%. Thermal reactions are carried out in toluene (10 mL) at 25 °C under argon atmosphere. All conversions and yields are based on quantitative GC analysis using n-dodecane as the internal standard.

### 3.3 Insights into the catalytic cycle of the iridium-catalysed Michael-type hydroalkylation of 2-cyclohexen-1-one with diphenylacetonitrile

#### 3.3.1 Previously proposed catalytic cycle

To further understand and improve this Michael-type hydroalkylation reaction, the mechanism had to be investigated with the aim to identify and isolate the intermediate complexes. A general catalytic cycle for this hydroalkylation reaction was proposed by Marta Fernandez-Gimenez based on previous mechanistic studies on the C-C cleavage of dinitriles and the principle of microscopic reversibility. The proposed catalytic cycle is reported in Scheme 3.16.<sup>152</sup> The cycle starts with the generation of the catalytically active species  $\text{Ir}(\text{P}^i\text{Pr}_3)_2\text{H}$  **56**, by dihydrogen release from the starting iridium-pentahydride complex as described in the literature.<sup>39</sup> The next step is the coordination of a molecule of diphenylacetonitrile **27** to the iridium centre *via* the nitrogen atom to form intermediate **57**, followed by C-H activation of the nitrile ligand by the iridium centre with formation of intermediate **58**. Complex **58** is hypothesised to exist in equilibrium with complex **59** by coordination of a second nitrile molecule **27**. Complex **59** has been previously isolated.<sup>152</sup> Subsequently, a molecule of cyclohexenone **28** coordinates to the iridium centre *via* the oxygen atom of the carbonyl<sup>173-174</sup> forming intermediate **60**. The following step is an intramolecular nucleophilic attack of the  $\alpha$ -deprotonated nitrile to the conjugated double bond of the ketone with formation of a new C-C bond of complex **61**. Intermediate **61** is a N- and  $\eta^1$ -O-bonded enolate complex and similar O-coordinated ligands have been reported previously in the literature.<sup>175-176</sup> The desired Michael addition product **29** is finally released *via* reductive elimination with regeneration of the catalytically active species **56**.

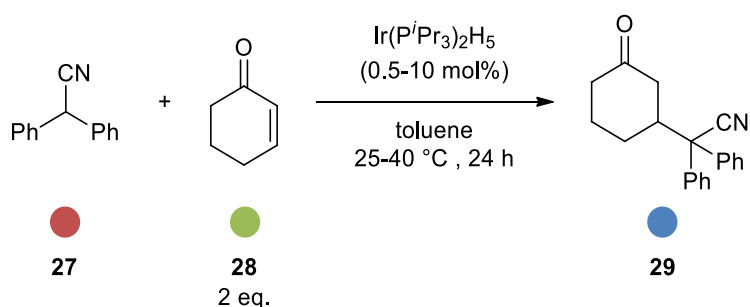


Scheme 3.16 Previously proposed mechanism of the catalytic cycle for the iridium-catalysed Michael-type hydroalkylation of 2-cyclohexen-1-one with alkyl-aryl-nitriles.

### 3.3.2 Time monitoring experiments of the hydroalkylation reaction by GC

Some mechanistic studies have been undertaken to investigate the reaction mechanism and prove the previously proposed catalytic cycle. To achieve this, the aim was to reproduce stoichiometrically every major step in the catalytic cycle and isolate the intermediates where possible. To gain an insight of the reaction mechanism, the GC has been identified as the preferred method to monitor the conversions and yields. This method was then combined with proton and phosphorus NMR spectroscopy to identify the various complexes involved in the reaction. In order to be able to monitor the reaction by GC and NMR, the reaction conditions had to be slightly modified. To identify the best reaction conditions that would allow an optimal monitoring by NMR spectroscopy, at first the classic hydroalkylation reaction had to be repeated and time monitored by GC.

Indeed, as a starting point, the hydroalkylation of cyclohexenone with diphenylacetonitrile has been chosen as the model reaction using the previously optimised conditions (Scheme 3.17). With this aim, two equivalents of 2-cyclohexen-1-one **28** and diphenylacetonitrile **27** were allowed to react in the presence of 0.5 mol% of  $\text{Ir}(\text{P}^i\text{Pr}_3)_2\text{H}_5$  **2** in toluene at 40 °C. This reaction was time monitored up to 24 hours by analysing an aliquot of the reaction mixture at specific time points by GC analysis. The results are expressed as a function of the concentration over time for the reagents and the product (Figure 3.2). From the graph below it can be observed that after 16 hours the nitrile was almost fully consumed and consequently the concentration of the product **29** reached a plateau corresponding to a final yield of 95%.



Scheme 3.17 Reaction scheme for the model hydroalkylation reaction for the time monitoring experiments by GC.

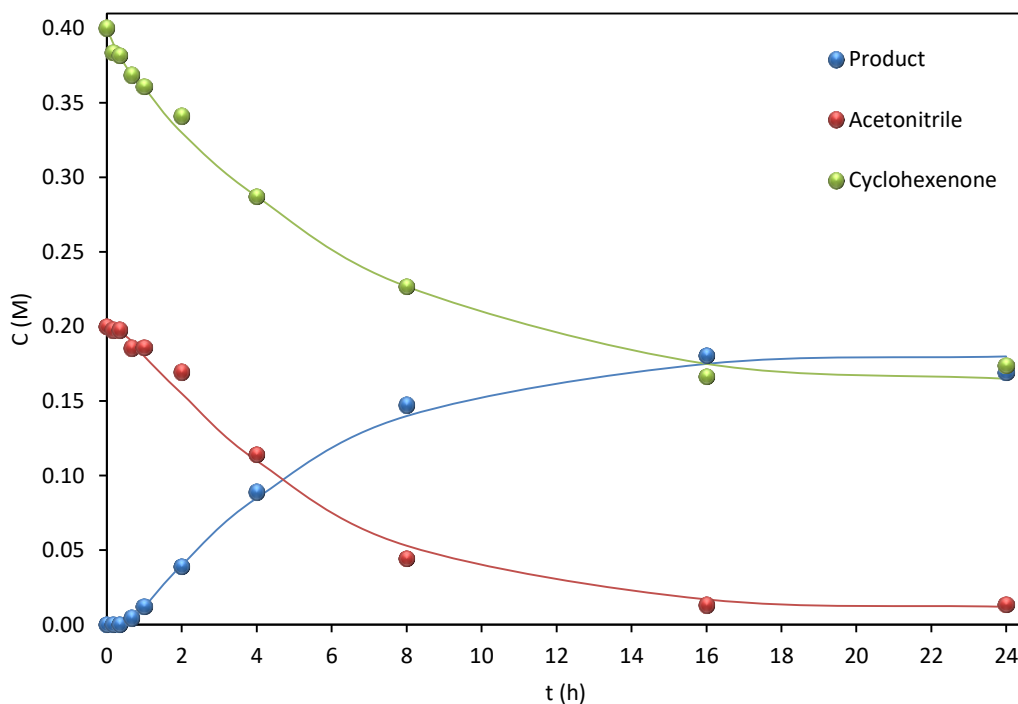


Figure 3.2 Time monitoring by GC of the hydroalkylation reaction at 40 °C (Ir 0.5 mol%) (standard reaction conditions).

Next, it was investigated whether the reaction could be performed at milder temperatures. Previously, during the process for optimising the reaction conditions, the hydroalkylation was already tested at room-temperature, however with 10 mol% of catalyst loading and in the presence of 10 equivalents of ketone.<sup>152</sup> Under those conditions the yields were low due to the formation of many side-products. Once the reaction conditions have been optimised to 0.5 mol% of catalyst loading and 2 equivalents of ketone, the lower temperature has not been tested anymore. Therefore, the time monitoring experiment was performed at room-temperature with the optimised reaction conditions, also with the aim of slowing down the kinetics and obtaining more insights into the process. Initially, the model reaction has been tested at 40 °C, which afforded product **29** in 95% yield. Decreasing the temperature to 25 °C also allowed to obtain the desired hydroalkylation product in 94% yield after 24 hours. The results of the time monitoring experiment at 25 °C are reported in Figure 3.3. As it can be clearly observed from the graph, there is an induction period of 2 hour before any product formation can be detected. Moreover, for the first 2 hours also the consumption of the nitrile reagent was minimal. This can be explained by the fact that the iridium-pentahydride catalyst **2** needs to be converted into the catalytically active species **56**, *via* loss of hydrides, before the reaction can take place. Looking more closely at the graph in Figure 3.2, an induction time of around 20 minutes can also be observed. However, at lower

temperatures this reaction is much slower, i.e. at 25 °C compared to 40 °C, and the induction period can be clearly observed (Figure 3.3).

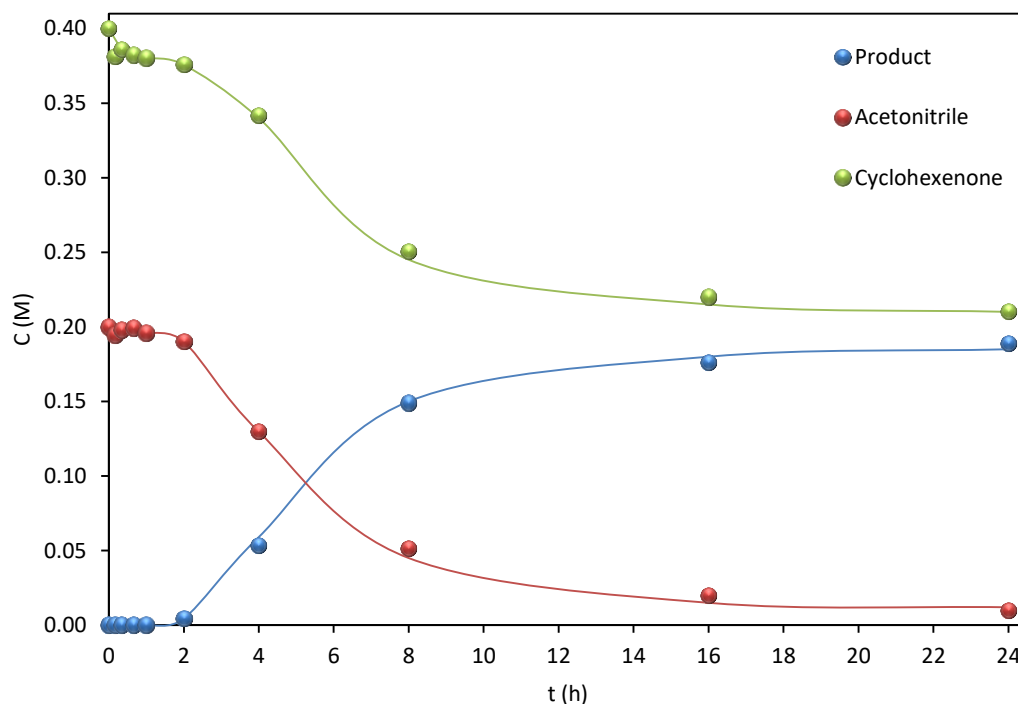


Figure 3.3 Time monitoring by GC of the hydroalkylation reaction at 25 °C (Ir 0.5 mol%).

Then, because the aim was to monitor the reaction by NMR spectroscopy in order to get more information on the different metallic species involved in the reaction, a further GC monitoring test has been performed to reach reaction condition suitable for NMR monitoring experiments. The reaction temperature was kept at 25 °C to guarantee a slow reaction rate in order to be able to clearly monitor the different steps of the reaction. However, the catalyst loading was increased to 10 mol%, to increase the iridium concentration and therefore to be able to observe the complexes by NMR spectroscopy. Results of this time monitoring experiment are reported in Figure 3.4. With the increased catalyst loading, the induction period cannot be observed anymore, even though the operating temperature was still 25 °C. Moreover, due to the higher catalyst loading, formation of by-products can be observed, in particular cyclohexanone and benzophenone (in trace amounts). This resulted also in a decreased yield of 73% for the desired product **29**. It is worth to mention that cyclohexanone formed corresponded to 3 equivalents compared to the iridium. This is an important information and the reason for that will be disclosed and explained later in the text (see Section 3.3.5.1), but as already mentioned, cyclohexenone can be formed by the hydrogenation of cyclohexenone promoted by the iridium-pentahydride complex.

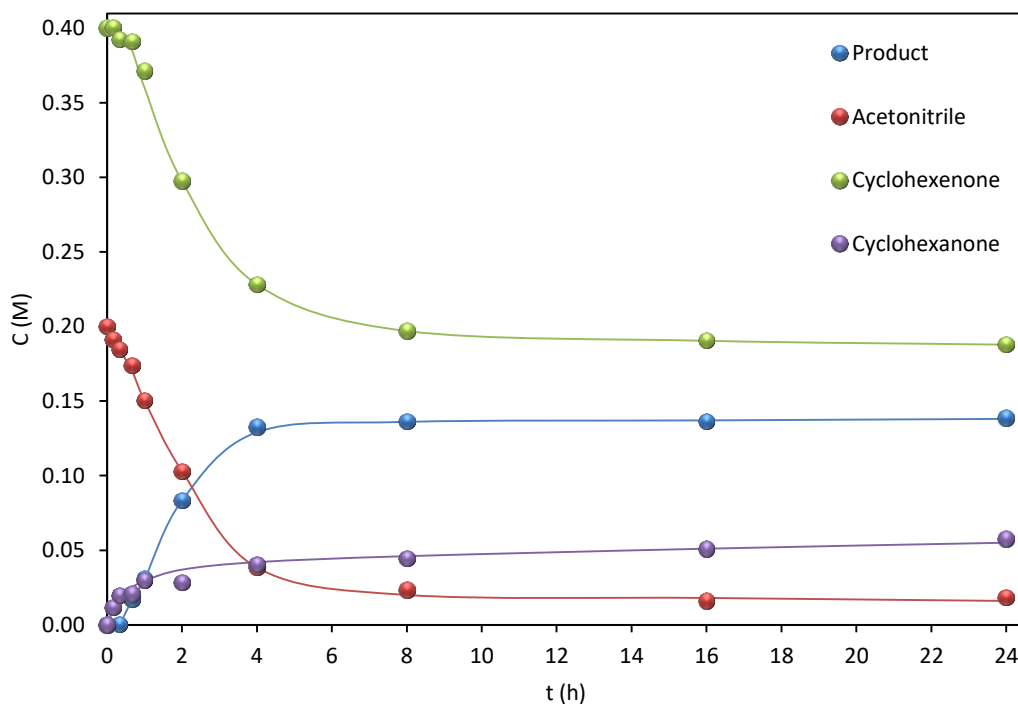


Figure 3.4 Time monitoring by GC of the hydroalkylation reaction at 25 °C with increased iridium catalyst loading of 10 mol%.

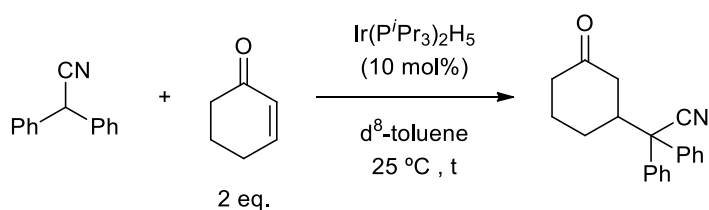
To summarise, with these time monitoring experiments, an induction time of 2 hours was observed when the iridium-pentahydride **2** was used as catalyst at 25 °C in 0.5 mol% catalyst loading. This induction time corresponds, most probably, to the time required to convert the complex in the catalytically active species by loss of hydrides under the operating conditions. Once this first activation step is concluded, then the catalytic cycle can start and the formation of the desired product can be observed. Also, the reaction conditions have been modified in order to allow the analysis by NMR of the reaction mixture. These conditions will be used as the standard ones in the following NMR monitoring experiments.

### 3.3.3 Time monitoring experiment of the hydroalkylation reaction by NMR spectroscopy

The aim was then to perform stoichiometrically every step of the previously proposed catalytic cycle and observe potential intermediates and/or resting states, following the reaction by NMR spectroscopy. With the increased catalyst loading and by swapping toluene for  $d^8$ -toluene, the reaction mixture could be directly analysed by NMR spectroscopy, without the need of any further manipulation. To do this, the reaction mixture was prepared in a J-Young NMR tube and  $^1\text{H}$ - and  $^{31}\text{P}$ -NMR spectra were acquired at the desired time points, by

leaving the sample inside the spectrometer for the overall time of the experiment at a controlled temperature of 25 °C.

First, to verify the conditions were fitting for purpose, the reactivity of diphenylacetonitrile with cyclohexenone in the presence of the iridium catalyst was monitored by NMR spectroscopy over 48 hours. From the  $^{31}\text{P}$ -NMR, over time, the formation of a new peak, a singlet at *ca.* 32 ppm, was observed. This peak matched with the chemical shifts of the previously reported iridium-ylide-nitrile complex **59**. This complex has been already fully characterised and therefore the chemical shifts are known.<sup>152</sup> As it can be observed from the stacked phosphorus spectra in Figure 3.5, the iridium pentahydride was gradually converted into the iridium-dinitrile intermediate, although the formation of the intermediate seemed to be very slow. Nevertheless, complex **2** was fully converted into the intermediate **59** after 24 hours. Peaks were visible and well defined also in the hydride regions of the  $^1\text{H}$ -NMR spectra (Figure 3.6, peak at *ca.* -11 ppm disappearing, while peak at *ca.* -22 ppm appearing). Therefore, this reaction conditions were chosen as benchmark for the mechanistic studies by NMR. From the  $^1\text{H}$ -NMR spectra, the diphenylacetonitrile seemed to be fully consumed after 4 hours, because the signal relative to the acidic proton at *ca.* 4.5 ppm decreases until fully disappearing after only 4 hours (Figure 3.7). However, as shown from the GC data (see Figure 3.4) full conversion was not reached, therefore the disappearance of this peak in the NMR spectra was most probably due to the H/D exchange. The small shift in ppm after 4 hours, observable from both the proton and phosphorus NMR spectra if zooming in, was probably due to H/D exchange in the ligands of the complexes.



Scheme 3.18 Model iridium-catalysed hydroalkylation reaction screened with the time monitoring experiments by NMR.



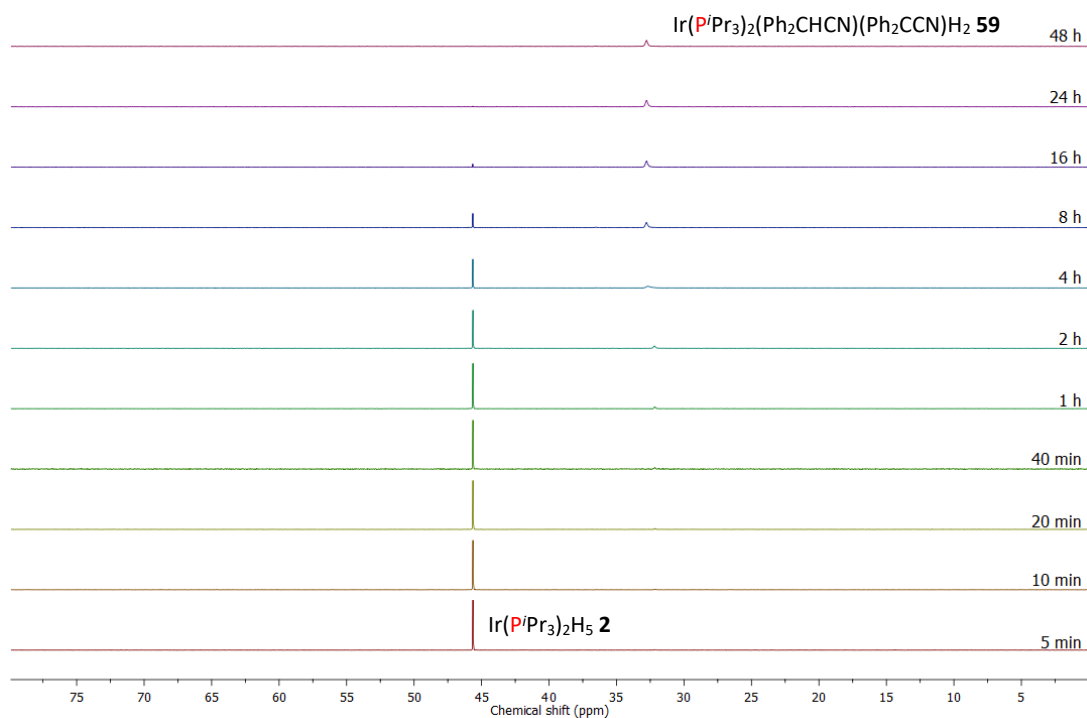


Figure 3.5 Stacked  $^{31}\text{P}\{^1\text{H}\}$ -NMR spectra (298 K,  $d^8$ -toluene, 202 MHz) of the time monitoring experiment of the model hydroalkylation reaction.

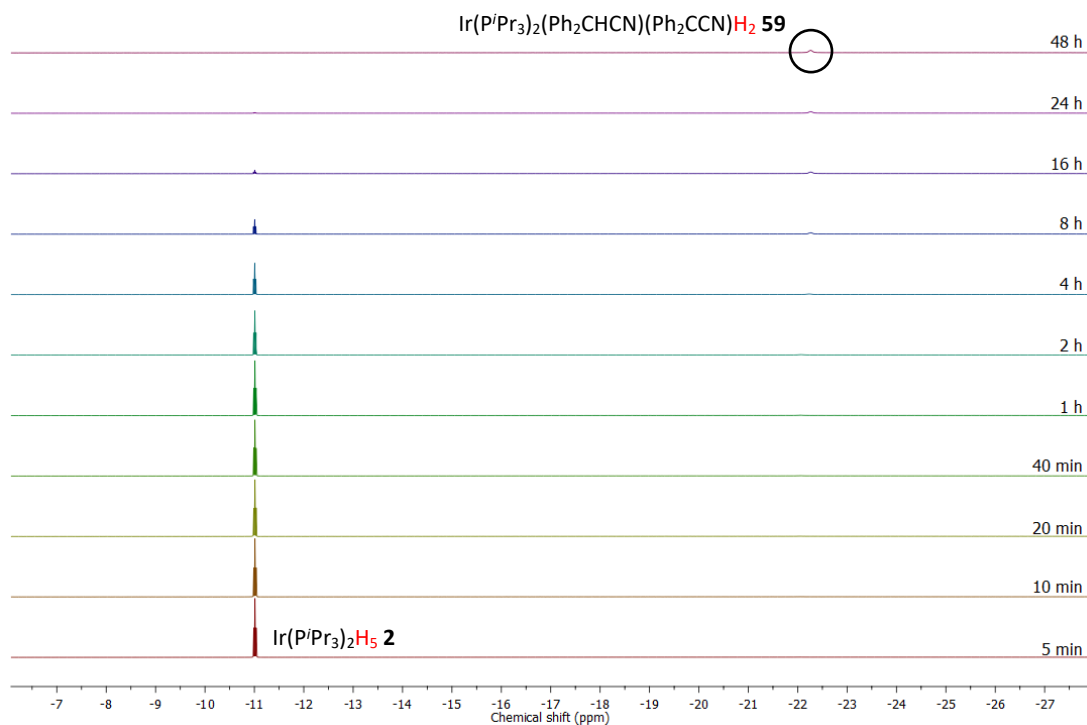


Figure 3.6 Stacked  $^1\text{H}$ -NMR spectra (298 k,  $d^8$ -toluene, 500 MHz), hydride region, of the time monitoring experiment of the model hydroalkylation reaction.

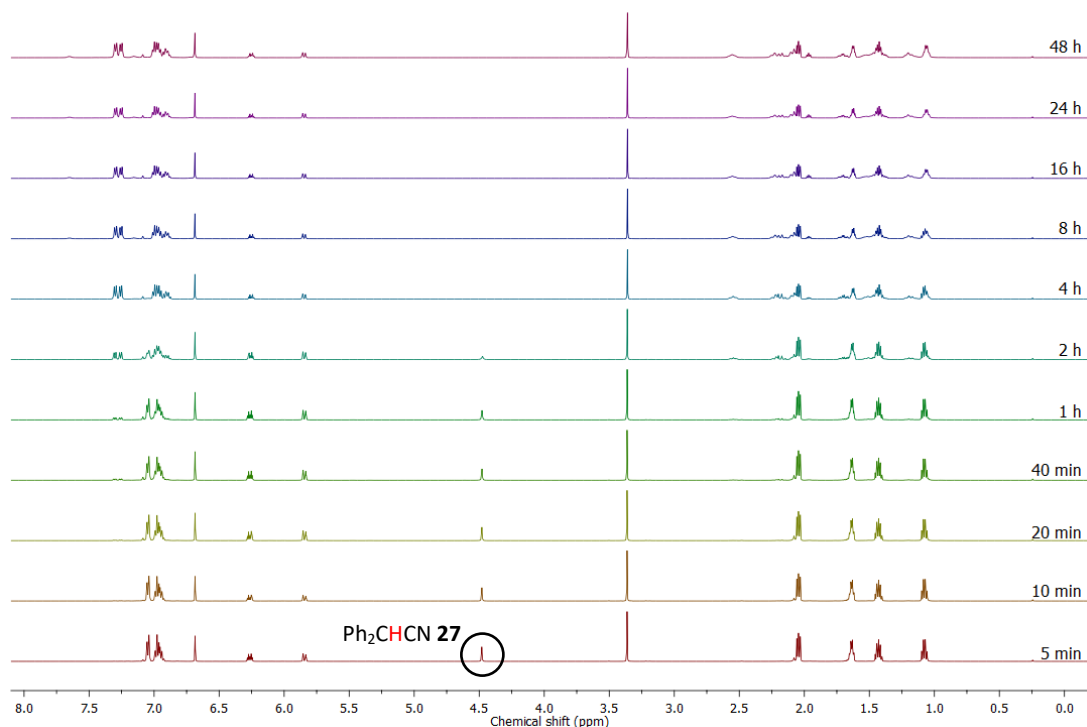


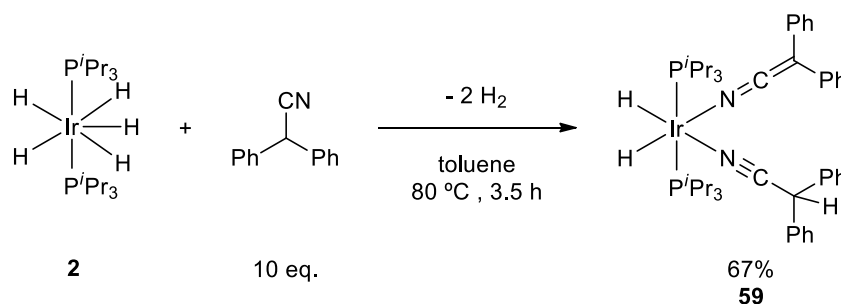
Figure 3.7 Stacked  $^1\text{H}$ -NMR spectra (298 K,  $d^8$ -toluene, 500 MHz), aliphatic and aromatic region, of the time monitoring experiment of the model hydroalkylation reaction.

With this NMR monitoring experiment, the iridium-ylide-nitrile complex **59** was confirmed to be a reaction intermediate, as hypothesised in the previously proposed catalytic cycle. The developed conditions were also found to be suitable for the investigation of the reaction by NMR spectroscopy. The next step was to investigate more closely the different stages of the catalytic cycle and to confirm them, possibly identifying more intermediates.

### 3.3.4 Investigation of C-H activation step: reactivity of the iridium-pentahydride catalyst with diphenylacetonitrile

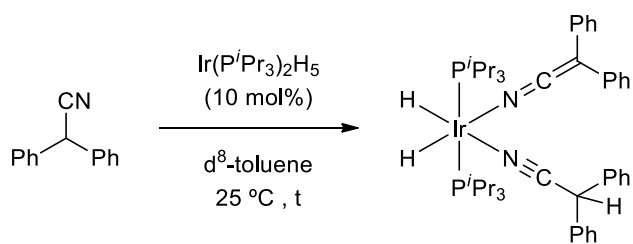
According to the proposed catalytic cycle (see Scheme 3.16), after the conversion of the iridium pentahydride catalyst into the catalytically active species, the first steps of the catalytic cycle are the coordination of the diphenylacetonitrile substrate to the iridium centre, followed by intramolecular C-H activation to yield complex **58**. Further coordination of another nitrile molecule would yield complex **59**. This first section of the catalytic cycle could be studied by observing the reactivity of the diphenylacetonitrile with the iridium catalyst; indeed, using the optimised reaction conditions, except the addition of cyclohexenone.

First of all, it is already known from previous work in the research group that, by reacting the diphenylacetonitrile substrate with the iridium-pentahydride complex **2**, the iridium-ylide-nitrile intermediate **59** is formed when the reaction is performed at 80 °C.<sup>152</sup> The synthesis of the intermediate has been improved compared to previous work and the desired complex has been isolated improving the yield from 56 to 67% (Scheme 3.19). Specifically, this could be achieved by releasing the build-up of hydrogen pressure after 1 hour of reaction and therefore shifting the equilibrium towards the desired product **59**.



Scheme 3.19 Synthesis of the iridium-ylide-nitrile complex **59** by reaction of the iridium-pentahydride complex **2** with the diphenylacetonitrile substrate.

To confirm that the iridium intermediate **59** can be formed by reaction of the diphenylacetonitrile with the iridium-pentahydride catalyst, not only at 80 °C but also at the lower operating temperature, the reactivity of the of diphenylacetonitrile with complex **2** at 25 °C was time monitored by <sup>1</sup>H- and <sup>31</sup>P-NMR spectroscopy (Scheme 3.20). The pentahydride complex **2** was reacted with diphenylacetonitrile in the same ratio and concentration as per the standard catalytic reaction to make the reaction conditions as similar as possible. Therefore, if the proposed catalytic cycle was correct, by monitoring the reactivity of diphenylacetonitrile with the iridium-pentahydride catalyst **2** at 25 °C, a similar reactivity pattern to the catalytic reaction monitoring should be observed. By comparing the results with the previous experiment (Section 3.3.3), it is clear that the formation of the iridium-ylide-nitrile intermediate **59** was much slower in comparison to what happened in the catalytic reaction. In fact, after 48 hours, looking at the peaks from the <sup>31</sup>P-NMR spectra, the percentages of the integrations are: 85% for the iridium-pentahydride (peak at *ca.* 45 ppm) and only 15% for the iridium-dinitrile complex (peak at *ca.* 32 ppm, Figure 3.8). On the other hand, in the catalytic reaction full conversion was observed. This means that something else is involved in the catalytic reaction leading to the formation of intermediate **59**. The same considerations are supported by the hydride region of the proton spectra (Figure 3.9).



Scheme 3.20 Reactivity of diphenylacetonitrile with the iridium-pentahydride catalyst under model reaction conditions screened with the time monitoring experiments by NMR.

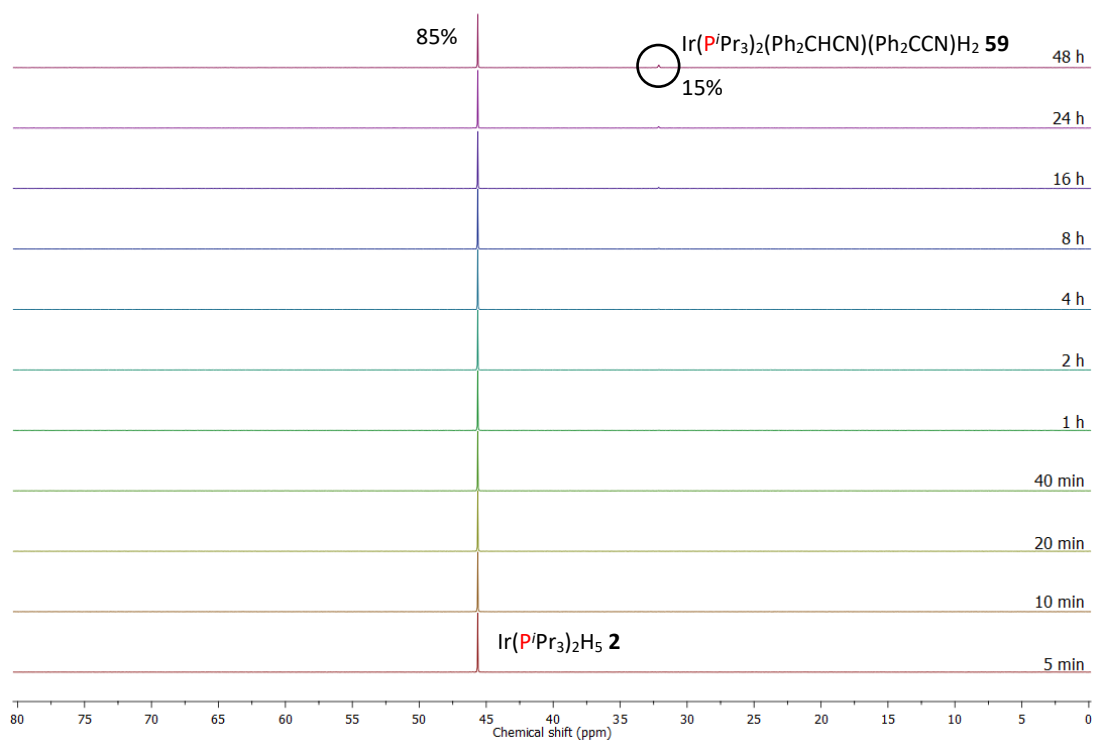


Figure 3.8 Stacked  $^{31}\text{P}\{^1\text{H}\}$ -NMR spectra (298 K,  $\text{d}^8\text{-toluene}$ , 202 MHz) of the time monitoring experiment of the reactivity of diphenylacetonitrile with the iridium-pentahydride catalyst under model reaction conditions.

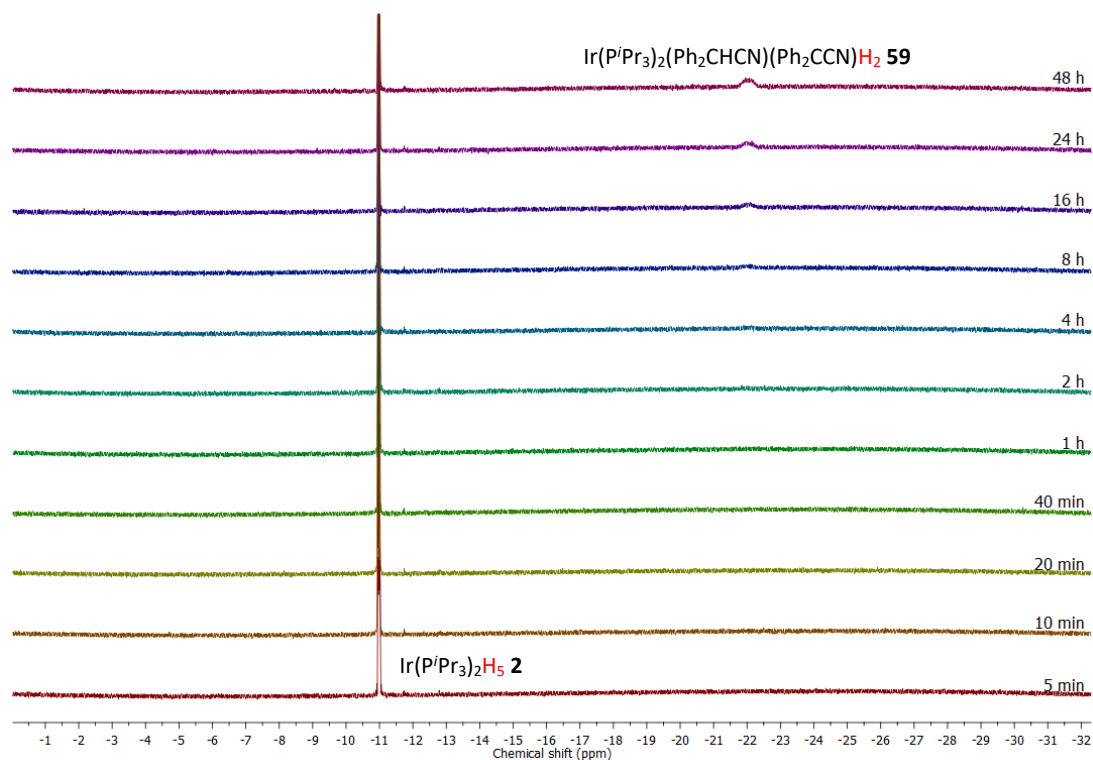


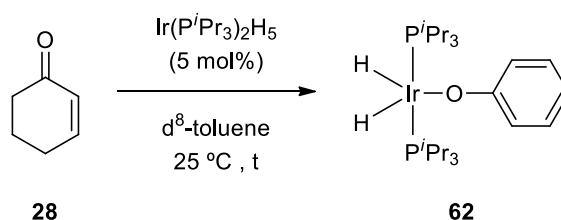
Figure 3.9 Stacked  $^1\text{H-NMR}$  spectra (298 K,  $d^8$ -toluene, 500 MHz), hydride region, of the time monitoring experiment of the reactivity of diphenylacetonitrile with the iridium-pentahydride catalyst under model reaction conditions.

To summarise, with this experiment the formation of intermediate **59** by reaction of diphenylacetonitrile with the iridium catalyst was confirmed also at lower temperature. Although, the oxidative addition leading to its formation was much slower compared to the same reaction at 80 °C, where the energy provided with the heating was crucial for the fast formation of the desired complex **59**. This unusual fact needed further investigation. Comparing those results with the ones obtained from the time monitoring of the catalytic reaction at 25 °C, the only difference in the experimental set up between the two tests was the absence of cyclohexenone in the former one. As already hypothesised earlier on, cyclohexenone could facilitate the formation of the catalytically active species **56** (Scheme 3.16), favouring the loss of hydrides *via* its hydrogenation to cyclohexanone. Indeed, the reactivity of cyclohexenone with the iridium catalyst is explained in the following paragraph.

### 3.3.5 Reactivity of iridium-pentahydride catalyst with cyclohexenone

#### 3.3.5.1 A new iridium-phenoxide complex and cyclohexenone disproportionation reaction

To investigate the unusual fact that at room temperature the oxidative addition of diphenylacetonitrile appeared to be slower, the reactivity of the iridium-pentahydride complex with cyclohexenone was investigated to verify whether cyclohexenone could have a role in this step of the transformation. To achieve that, the reaction between the two compounds was time monitored by NMR spectroscopy under the same optimised reaction conditions, except for the addition of diphenylacetonitrile. As it can be observed from Scheme 3.21, complex **2** was reacted with 20 equivalents of cyclohexenone, the same ratio used in the catalytic reaction at 25 °C. The stacked spectra obtained from the reaction monitoring are reported in Figure 3.10 and Figure 3.11. As it can be clearly seen from both the proton and phosphorus spectra, the iridium pentahydride is fully consumed and the clean formation of another species is observed since the first few hours of reaction, to reach full conversion after 24 hours. Specifically, from the proton spectra the Ir(P<sup>i</sup>Pr<sub>3</sub>)<sub>2</sub>H<sub>5</sub> triplet at -11 ppm disappears over time, while another peak at -32 ppm forms. From the phosphorus spectra instead, the iridium-pentahydride peak at 45 ppm disappears for the formation of the other peak at 52 ppm.



Scheme 3.21 Reactivity of cyclohexenone with the iridium-pentahydride catalyst under model reaction conditions screened with the time monitoring experiments by NMR.

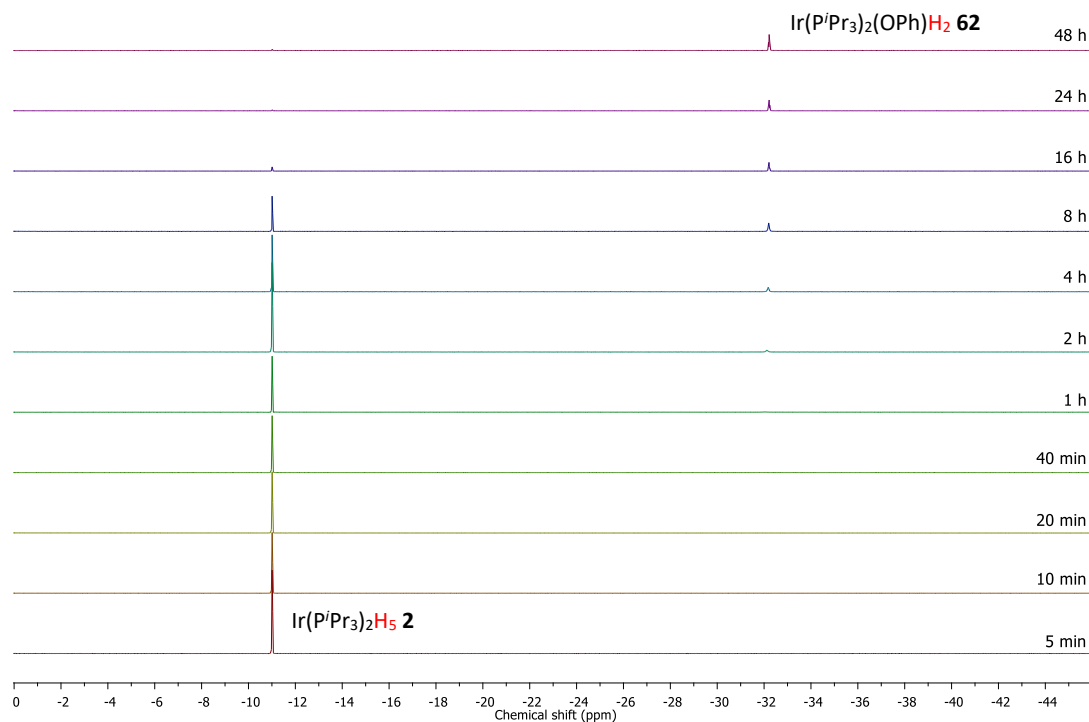


Figure 3.10 Stacked  $^1\text{H-NMR}$  spectra (298 K,  $d^8$ -toluene, 500 MHz), hydride region, of the time monitoring experiment of the reactivity of cyclohexenone with the iridium-pentahydride catalyst under model reaction conditions.

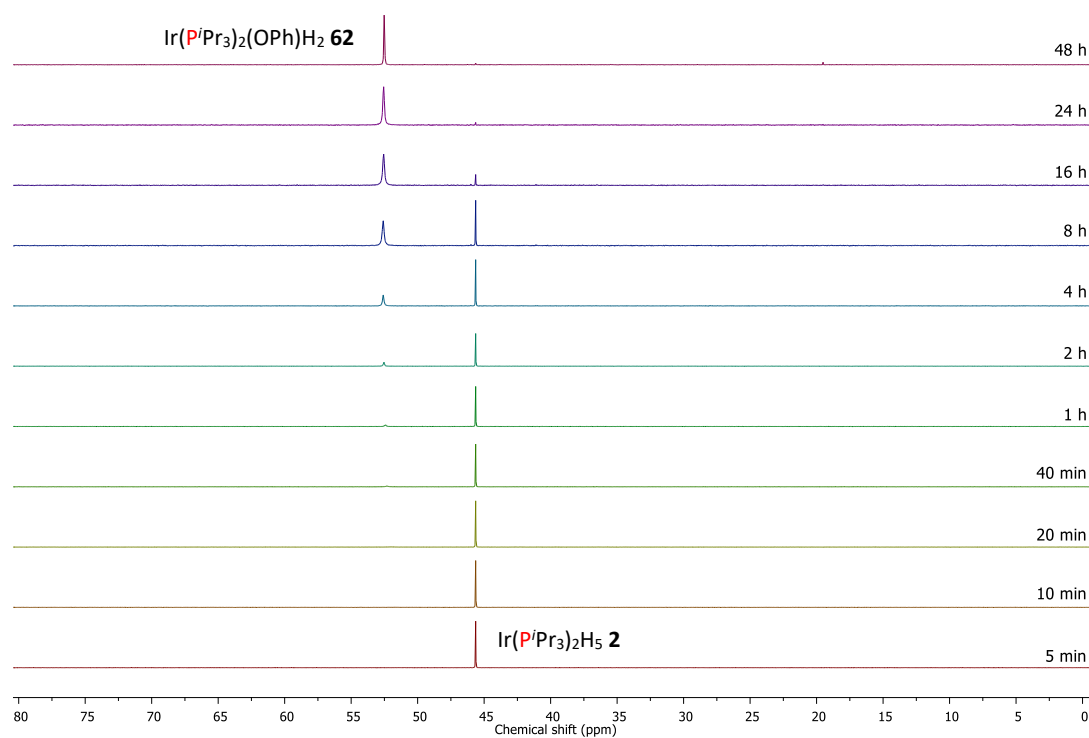
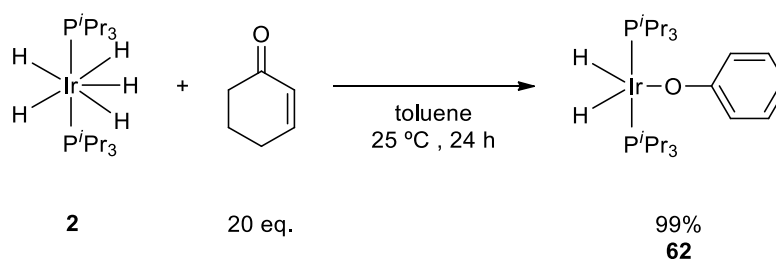


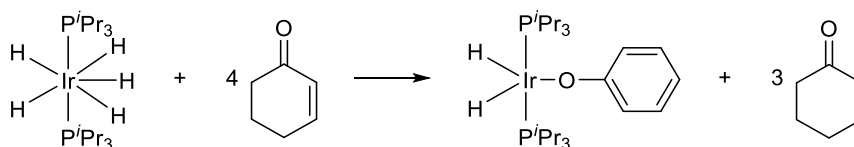
Figure 3.11 Stacked  $^{31}\text{P}\{^1\text{H}\}$ -NMR spectra (298 K,  $d^8$ -toluene, 202 MHz) of the time monitoring experiment of the reactivity of cyclohexenone with the iridium-pentahydride catalyst under model reaction conditions.

To find out the identity of this complex the same reaction was scaled-up and repeated under the same conditions to try and isolate this new compound. The interpretation of the NMR spectra (assignment in Section 3.7.9.2) was consistent with the formation of the iridium-phenoxide complex **62** reported in Scheme 3.22. The characterisation of this complex will be discussed later on in this section. The new complex can be quantitatively synthesised from the reaction of iridium-pentahydride **2** with cyclohexenone in toluene. Once the reaction was complete, both the solvent and cyclohexenone could be removed at reduced pressure to obtain the clean phenoxide complex in quantitative yield. During this reaction cyclohexenone was probably being hydrogenated as well, facilitating the conversion of complex **2** into the catalytically active species *via* loss of hydrides. This would also explain why in the catalytic reaction cyclohexenone was needed in excess compared to the nitrile.



Scheme 3.22 Synthesis of the iridium-phenoxide complex **62** by reaction of the iridium-pentahydride complex **2** with the cyclohexenone substrate.

To fully understand the reactivity of the iridium species with cyclohexenone the reaction mixture at the end of the reaction, after work-up, was also analysed by GC and GC-MS trying to detect, quantify and identify the different species formed in the transformation, in particular to verify if cyclohexanone was also formed. From the GC-MS analysis of the reaction mixture at the end of the 24 hours, after all the iridium pentahydride was converted into the iridium-phenoxide complex, the formation of cyclohexanone and phenol was observed. From the quantitative GC analysis, the Ir/cyclohexenone/cyclohexanone/phenol ratio was 1:16:3:1 which means that 3 equivalents of cyclohexanone were formed per mole of iridium. This led to the following balanced cyclohexenone disproportionation equation (Scheme 3.23).

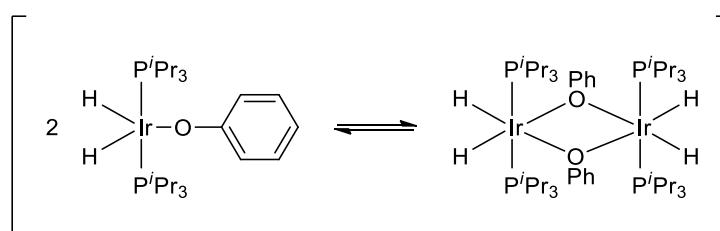


Scheme 3.23 Balanced equation for the synthesis of the iridium-phenoxide complex **62** highlighting the disproportionation reaction of cyclohexenone.



Free phenol was observed because the work-up of the reaction mixture caused the iridium complex to decompose, and indeed the free ligands could be observed by GC. Moreover, the observed ratio of products also means that overall no hydrogen was released in the form of molecular hydrogen. Indeed, the cyclohexenone seemed to be facilitating the conversion of the pentahydride complex into the Ir(III) catalytically active species. This was achieved *via* partial hydrogenation of the cyclohexenone into cyclohexanone, favouring the loss of protons from the iridium centre. At the same time, one equivalent of cyclohexenone was dehydrogenated into the corresponding phenol, which binds to the metal centre, yielding the observed iridium-phenoxide complex.

For simplicity, the complex **62** has been so far depicted as a monomer, but further considerations on the nature of the complex should be made. From the NMR data it cannot be said if the complex exists as a monomer or as a dimer shown in Scheme 3.24. In fact, as a monomer the Ir(III) centre, as implied by the 18 electron rule, is two electrons short of the rare gas configuration and is thus coordinatively unsaturated. In the dimeric structure, the free coordination space would be occupied by the bridging phenoxide ligand and the rare gas configuration would be filled by the free doublet from the oxygen atom.



Scheme 3.24 Possible equilibrium between the monomeric and dimeric structure of the iridium-phenoxide complex **62**.

To shed light on the monomeric or dimeric nature of the complex, x-ray crystallography data were collected. Suitable crystals for x-ray were obtained from pentane. The x-ray data were consistent with a monomeric structure of the complex and confirmed that the compound was an iridium-phenoxide complex with two phosphine ligands (Figure 3.12). As happens in most XRD structures of hydride complexes, the position of the two hydrides could not be adequately model around the metal centre. However, the presence of the two hydrides was confirmed by the peak at -32 ppm in the proton NMR spectrum, which integrates two protons. The x-ray diffraction analysis of complex **62** showed a trigonal bipyramidal configuration ( $D_{3h}$ ) for the Ir(III) centre. The equatorial plane is occupied by the oxygen of the phenoxide ligand and ideally by the two *cis*-hydrides. The O-deprotonated phenol ligand is coordinated via the oxygen atom and exists as a phenoxide ligand (PhO<sup>-</sup>).

This ligand has a shorter C-O bond (1.330 Å) compared to the corresponding bond length in the free phenol (1.372 Å),<sup>177</sup> which means that in complex **62**, the C-O bond has an increased double bond character on account of the conjugation of unshared electron pair of oxygen with the aromatic ring. The Ir-O distance is 2.067 Å, comparable to other Ir-O complexes characterised by x-ray crystallography.<sup>178-179</sup> Also, the C-O-Ir angle is 130.4 °, considerably larger compared to the 108 ° of the free phenol,<sup>177</sup> probably due to steric reasons the phenyl ring is pushed further away from the metal centre to accommodate the different ligands. Interesting to note is that the two O-Ir-P angles are considerably different, O-Ir-P2 = 99.87 ° and O-Ir-P1 = 87.17 °, this is because the phenyl ring is oriented towards the P2 phosphine, resulting in an increase of the O-Ir-P2 angle due to steric repulsion. Consequently, the O-Ir-P1 angle is smaller as the only repulsion between the phosphine and the phenoxide ligand comes from the free doublets of the oxygen atom. The asymmetry of the ligands on the equatorial plane makes the trigonal bipyramidal structure slightly distorted, with the two *trans*-propyl-phosphines in axial position with a P-Ir-P angle of 172.9 °, slightly distorted from linearity. This can be explained with the presence of the bulky phenoxide ligand, which sterically repulses the two phosphine ligands, pushing them closer to the smaller hydrides. Moreover, the high bulkiness of the phosphine ligands blocks them in the *trans*-arrangement, impeding Berry's pseudo-rotation,<sup>180</sup> classic for trigonal bipyramidal structures. Indeed, from the crystalline structure, it appears that at least in the solid-state complex **62** exists in its monomeric form.

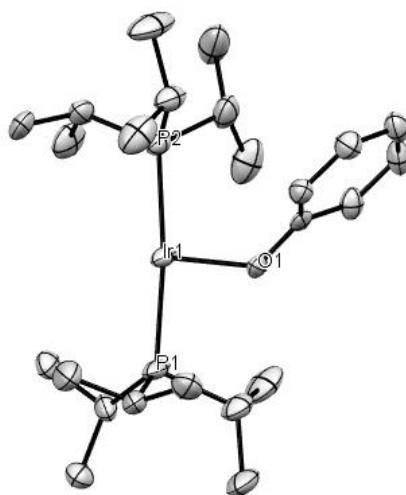


Figure 3.12 ORTEP crystal structure of the iridium-phenoxide complex **62**. All hydrogen atoms have been omitted for clarity.

As mentioned, from the characterisation of the isolated complex **62** by NMR spectroscopy, the presence of the two hydrides was hypothesised in the structure of complex

based on the presence of the triplet in the hydride region of the proton NMR spectrum of the compound. Because the crystal structure elucidation performed was not able to identify the position of the two hydride atoms in the  $\text{Ir}(\text{OPh})(\text{P}^i\text{Pr}_3)_2\text{H}_2$  complex **62**, additional experiments were required to confirm the structure has two hydrides. The experiments performed involved the use of different NMR spectroscopy techniques. The VT NMR experiments were performed with the goal to show the non-equivalency of the two hydrides. Unfortunately, even at  $-60^\circ\text{C}$ , the rotation of the molecule is too fast in order to distinguish the two hydrides. From the  $^1\text{H}$ - $^{31}\text{P}$ -HMBC 2D-NMR experiment the long-range coupling between the hydride and the phosphorus signal can be observed, confirming the hypothesised position of the two atoms in the complex (Figure 3.13). Nuclear Overhauser effect (NOE) experiments of the  $\text{Ir}(\text{OPh})(\text{P}^i\text{Pr}_3)_2\text{H}_2$  complex **62** have also been run (Figure 3.14). From those spectra it can be observed a polarisation transfer to the hydrides when irradiating at the frequency of the methyl group in the phosphine (bottom spectrum). And vice-versa, it can be observed a polarisation transfer to the  $\text{CH}_3$  protons of the tri-*iso*-propylphosphines after irradiation at the hydride frequency (middle spectrum). This result, confirms that a through-space correlation exists between these protons, ultimately confirming the position of the two hydrides in the complex.

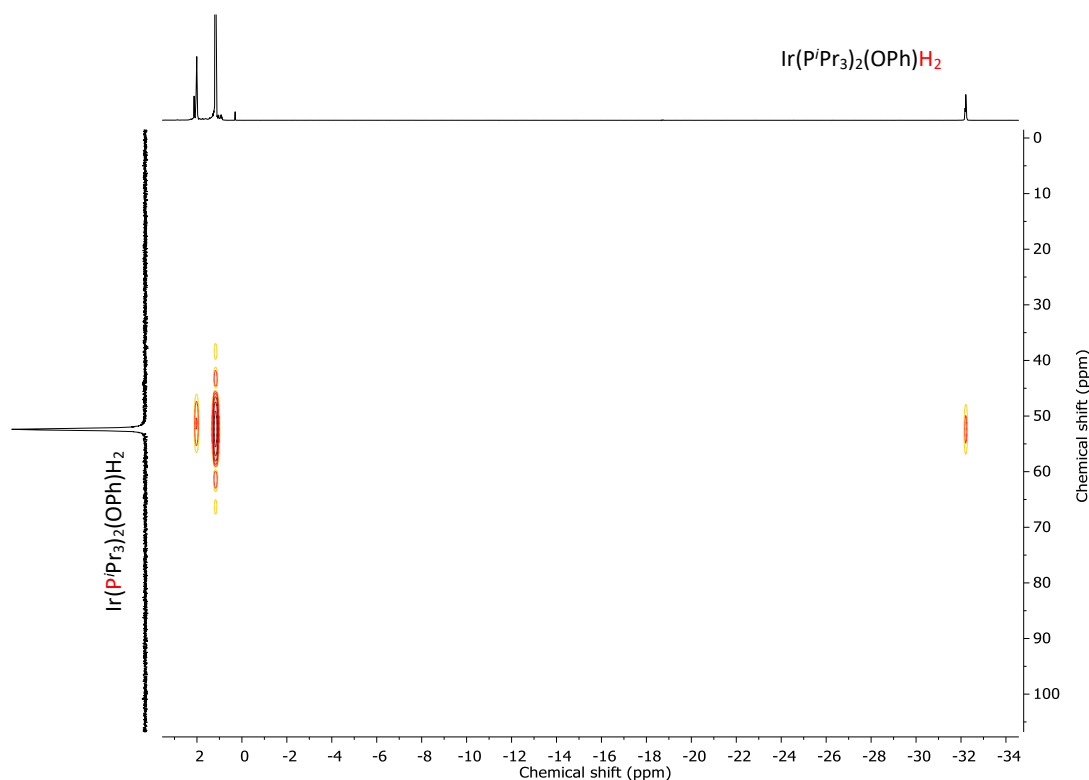


Figure 3.13  $^1\text{H}$ - $^{31}\text{P}$ -HMBC 2D-NMR spectrum (298 K,  $d^8$ -toluene, 500MHz and 202 MHz) of  $\text{Ir}(\text{P}^i\text{Pr}_3)_2(\text{OPh})\text{H}_2$  complex **62**.

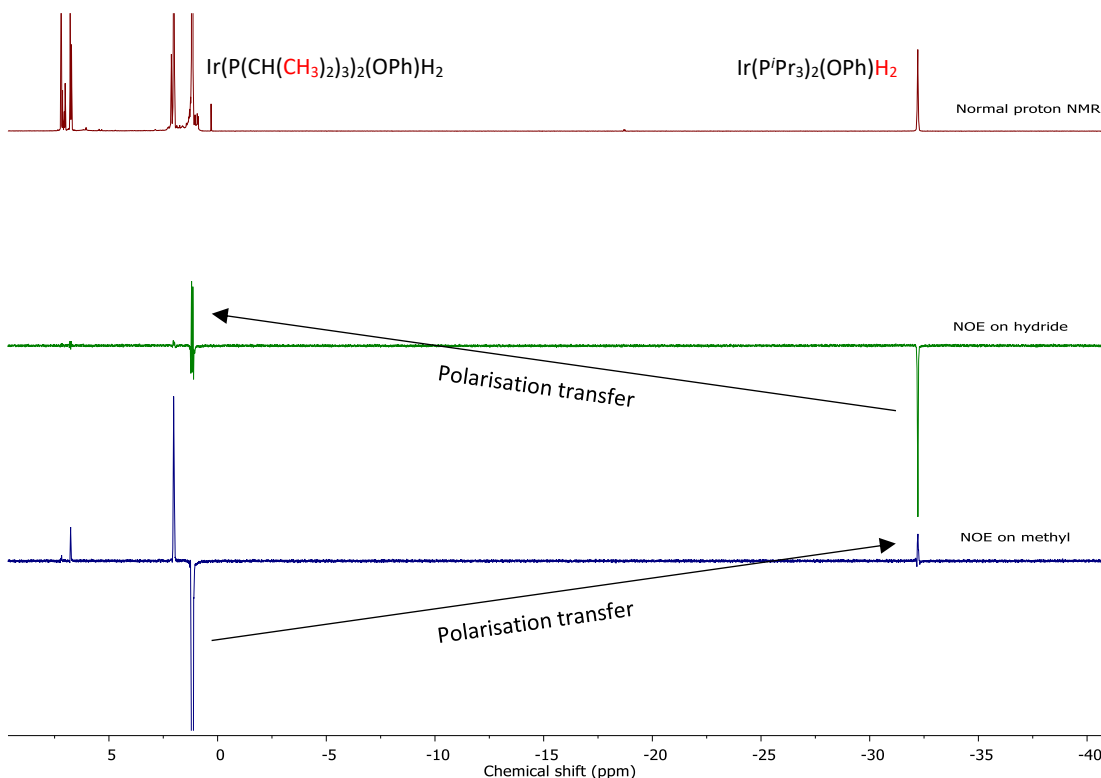


Figure 3.14  $^1\text{H-NMR}$  spectra (298 K,  $\text{d}^8$ -toluene, 500MHz) of  $\text{Ir}(\text{P}^i\text{Pr}_3)_2(\text{OPh})\text{H}_2$  complex **62** with nuclear Overhauser effect (NOE) irradiation on frequency of hydride signal (middle spectrum) and irradiation on frequency of phosphine methyl group signal (bottom spectrum).

Indeed, although the position of the hydrides could not be confirmed by x-ray data, the results of further NMR experiments all supports the proposed structure for the isolated complex **62**, which is confirmed to be a phenoxide complex bearing two hydrides and two phosphines with formula  $\text{Ir}(\text{OPh})(\text{P}^i\text{Pr}_3)_2\text{H}_2$ .

Several examples of iridium-phenoxide complexes are reported in the literature with various geometries. In the dimer  $[\text{Ir}(\mu\text{-OPh})(\text{COD})]_2$ , which has been first reported by Platzer and co-workers together with other dimers bearing different  $\mu$ -alkoxide groups, the phenoxide ligands are bridging between two iridium metal centers.<sup>181</sup> Oro and co-workers reported that the dimer  $[\text{Ir}(\mu\text{-OPh})(\text{COD})]_2$  can react in the presence of tri-cyclohexylphosphine to yield the monomer  $\text{Ir}(\text{OPh})(\text{COD})\text{PCy}_3$ .<sup>182</sup> Another example is the *mer*-( $\text{Me}_3\text{P}$ )<sub>3</sub> $\text{Ir}(\text{OPh})\text{HCl}$  complex reported by Merola and co-workers. This hexa-coordinated iridium species can be synthesised by oxidative addition of phenol to the  $[\text{Ir}(\text{COD})(\text{PMe}_3)_3]\text{Cl}$  complex. However, the most relevant and interesting example is  $^t\text{BuPCPIr}(\text{OPh})\text{H}$  complex reported by Goldman and co-workers.<sup>179, 183</sup> This complex has been characterised by NMR spectroscopy and the hydride signal in the  $^1\text{H-NMR}$  can be found at -39 ppm, close to the -32 ppm of our  $\text{Ir}(\text{OPh})(\text{P}^i\text{Pr}_3)_2\text{H}_2$  complex **62**. To the best of our knowledge, complex **62** is the

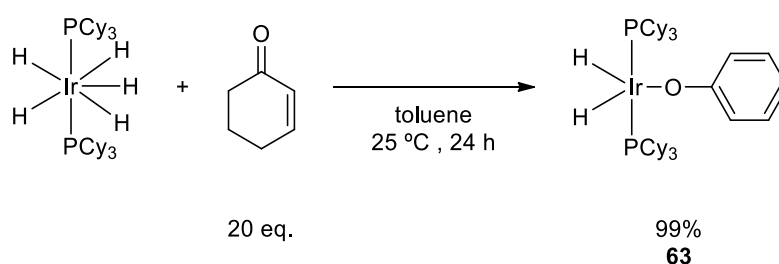
first reported example of a well-defined iridium-phenoxide complex bearing two tri-*iso*-propyl-phosphines and two hydrides.

To summarise, it has been shown that by reacting the pentahydride catalyst **2** with cyclohexenone in the same ratio and concentration as for the catalytic reaction, the clean formation of the new unexpected iridium-phenoxide complex **62** could be observed. After 24 hours at room temperature, the pentahydride was fully converted into the iridium-phenoxide complex **62**. From those experiments it can also be concluded that the cyclohexenone not only had the role of reagent for the hydroalkylation reaction, but also the role to convert iridium-pentahydride catalyst into the iridium-phenoxide complex *via* a disproportionation reaction to phenol and cyclohexanone. The novel Ir(OPh)(P<sup>*i*</sup>Pr<sub>3</sub>)<sub>2</sub>H<sub>2</sub> complex **62** has been isolated and fully characterised by NMR spectroscopy and x-ray crystallography.

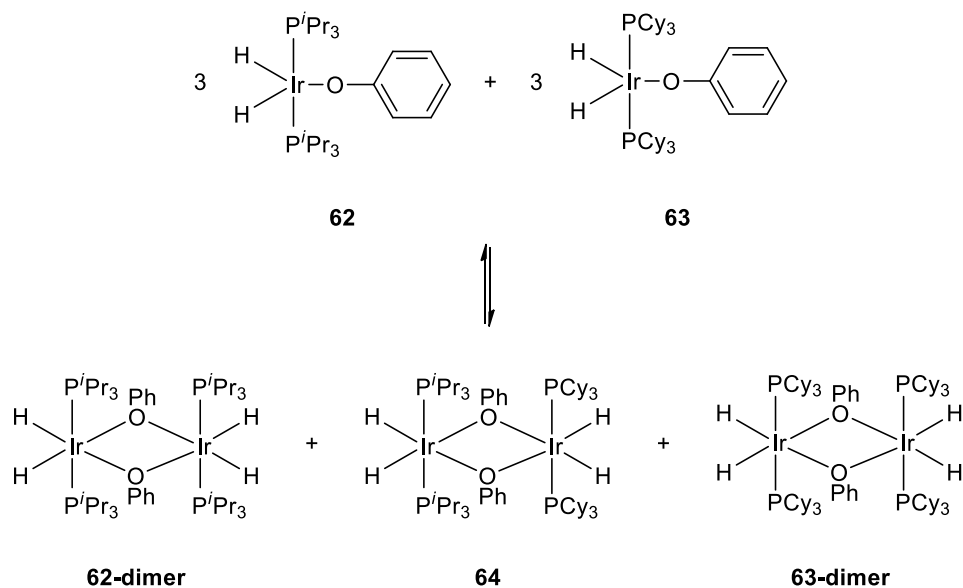
### 3.3.5.2 Synthesis and characterisation of the PCy<sub>3</sub> analogue of the iridium-phenoxide intermediate and mixing experiment

From the x-ray data appeared clear that complex **62** in solid state existed as a monomer. To check whether the same behaviour was adopted in solution a mixing experiment was designed. An analogue of complex **62** was synthesised under the same conditions, bearing two cyclohexyl-phosphines instead of *iso*-propyl ones (Scheme 3.25). Complex **63** was characterised by NMR spectroscopy, showing a well-defined singlet in the phosphorus spectrum at 42 ppm. The obtained cyclohexyl-substituted iridium-phenoxide complex **63** was assumed to be a monomer in solid state, by analogy with the *iso*-propyl-substituted complex **62**. When the complexes were dissolved in solution, they can maintain the monomeric form or they can aggregate forming dimeric species as highlighted in Scheme 3.24. If they were forming dimeric species, by mixing equimolar amounts of complexes **62** and **63** in the same solution, it is likely that mixed dimeric species might be formed. As depicted in Scheme 3.26 three different dimeric species can be present: **62-dimer**, **63-dimer** and also the mixed dimer **64** formed by the interaction between the two monomers **62** and **63**. If the dimer is the preferred structure in solution, following the mixing experiment by phosphorus NMR spectroscopy, formation of a third and fourth signal should be observed in the spectrum, with chemical shifts between the ones of complexes **62** and **63**. Those two new signals, in fact, would belong to the two tri-*iso*-propyl-phosphines and the two tri-cyclohexyl-phosphines in the **64** dimer. However, when the described experiment was performed, in the phosphorus spectrum no additional signals could be observed (Figure 3.15). The reaction mixture was

also heated to higher temperatures for longer time to favour the mixing between the two species, however NMR spectra have been recorded after every heating cycle without observing any differences. Moreover, the shapes and chemical shifts of peaks from complexes **62** and **63** remained unchanged, excluding the possibility that the additional signals were not observed because of a fast equilibrium between the three different dimeric forms. Indeed, with a discreet degree of confidence, it can be concluded that even in solution, the iridium-phenoxide complexes exist as monomers. In solution, the free coordination space could be occupied by a solvent molecule, increasing the steric stability of the overall compound.



Scheme 3.25 Synthesis of the iridium-phenoxide complex **63**.



Scheme 3.26 Reaction scheme for the mixing experiment between complexes **62** and **63** with formation of the three possible dimeric species.

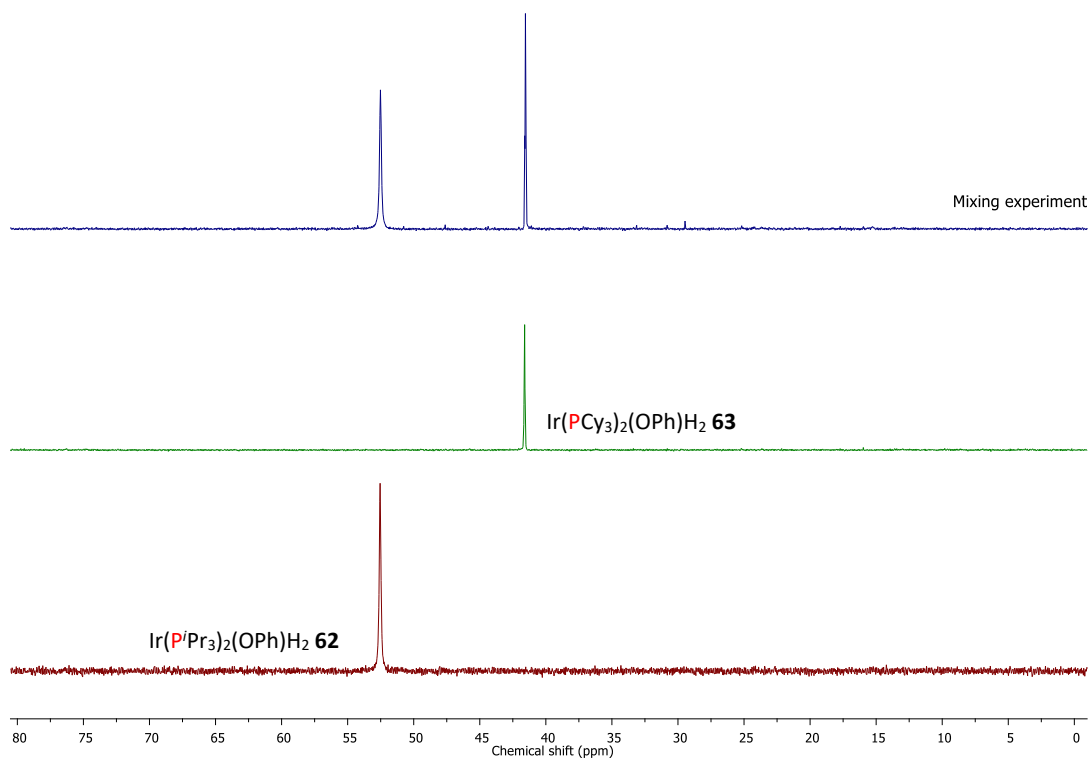


Figure 3.15 Stacked  $^{31}\text{P}\{^1\text{H}\}$ -NMR spectra (298 K,  $d^8$ -toluene, 202 MHz) of the isolated complexes **62** (bottom spectrum) and **63** (middle spectrum) with the spectrum from the monitoring of the mixing experiment (top spectrum).

### 3.3.6 Test of the isolated intermediates as catalysts

After the two reaction intermediates **59** and **62** were identified and isolated, to verify if they were kinetically competitive, their reactivity has been studied. At first, they were tested as catalysts themselves for the iridium-catalysed Michael-type hydroalkylation reaction under exam. They should be at least as active as the original catalyst and give comparable yields of the product. The reaction was monitored both by GC and NMR spectroscopy.

#### 3.3.6.1 Time monitoring by GC

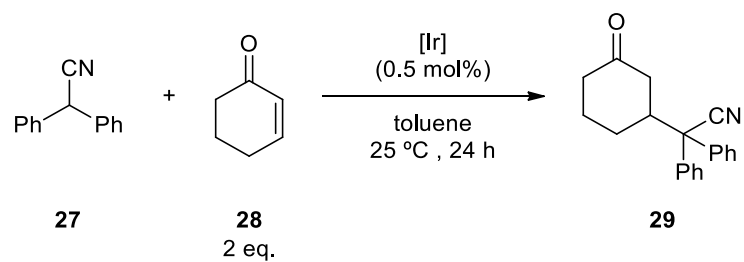
The reaction of cyclohexenone with diphenylacetonitrile was monitored by GC using the previously optimised conditions for the time-monitoring by GC, i.e. two equivalents of cyclohexenone, with 0.5 mol% of iridium catalyst, at 25 °C up to 24 h (Scheme 3.27). The activity of the complexes **59** and **62** is reported and compared to the results obtained when the iridium-pentahydride **2** was used as catalyst under the same conditions. The results of the study are reported in the plot of Figure 3.16.

As it can be observed from the graph, intermediate **59** has a much shorter induction time compared to the iridium-pentahydride catalyst **2**. This is because complex **59** was already in the catalytically active form and did not need to be activated as catalyst **2**, which needed to lose the hydrides. However, it is important to note that complex **59** over time seemed to work less efficiently: the formation of product can be observed almost since the beginning, however over time the reaction slowed down considerably compared to the reaction with the iridium-pentahydride catalyst. The final yield for the hydroalkylation product with the intermediate **59** was 77% against the 94% yield achieved when the classic iridium catalyst **2** was catalysing the same reaction. This observation will be explained and supported with experimental data later in the chapter (Section 3.3.10).

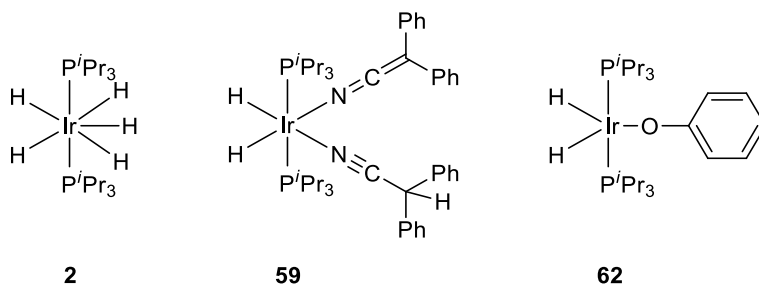
When the hydroalkylation reaction was catalysed by the **62** intermediate, it did not show any induction time and the initial rate appeared to be fastest one compared with both complexes **2** and **59**. Over time the yield levels off comparably to the iridium-pentahydride catalyst **2**, achieving a slightly lower yield of 85%.

The intermediate **62** was the most active towards the hydroalkylation reaction under standard conditions, at least in the first 8 hours of reaction. This is because no induction time was required as the iridium complex added was already in the catalytically active form. Indeed, complex **62** could be efficiently used as an alternative catalyst for the Michael-type hydroalkylation reaction of cyclohexenone with diphenylacetonitrile.





Iridium complexes:



Scheme 3.27 Reaction scheme for the hydroalkylation reaction catalysed by different iridium species ([Ir] 0.5 mol%, iridium complexes **2**, **59** and **62**) and screened by time monitoring by GC.

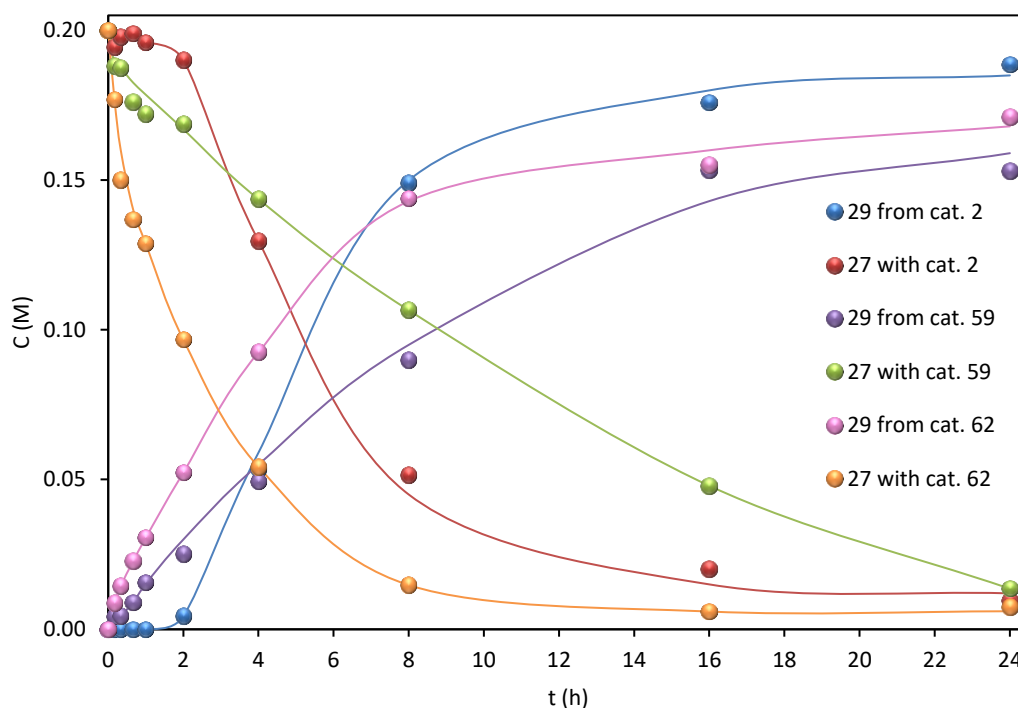
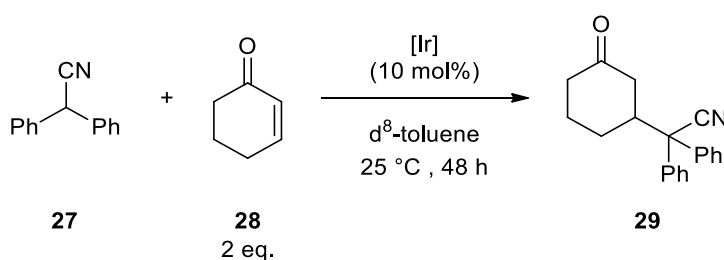


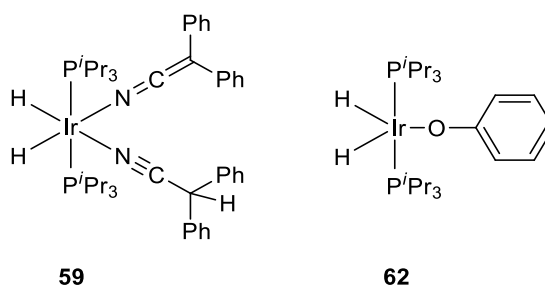
Figure 3.16 Time monitoring by GC of the hydroalkylation reaction at 25 °C catalysed by different iridium species ([Ir] 0.5 mol%). The plot shows the hydroalkylation product formation and diphenylacetonitrile consumption for all the three different iridium species tested as catalysts (iridium complexes **2**, **59** and **62**).

### 3.3.6.2 Time monitoring by NMR spectroscopy

The same hydroalkylation reaction monitored by GC was then time monitored by NMR spectroscopy, with the only differences of using 10 mol% of iridium catalyst and monitoring the reaction up to 48 hours (Scheme 3.28). The monitoring by NMR spectroscopy was performed to check whether the iridium-ylide-nitrile intermediate **59** was effectively the catalyst resting state. If so, regardless of the intermediate tested as catalyst, all in solution should be converted into the intermediate **59** and this can be confirmed by observing the NMR spectra.



Iridium complexes:



Scheme 3.28 Reaction scheme for the model hydroalkylation reaction catalysed by different iridium species ([Ir] 10 mol%, iridium complexes **59** and **62**) and screened by time monitoring by NMR.

At first, the behaviour of the iridium-ylide-nitrile intermediate **59** was monitored for the hydroalkylation reaction and the results were compared against what it was observed when the iridium-pentahydride catalyst **2** was used as catalyst under the same conditions (Section 3.3.3). The reaction was monitored throughout the entire time and the peaks characteristic of the iridium intermediate complex **59** can be observed from both the proton (-22 ppm) and phosphorus NMR spectra (32 ppm) reported in Figure 3.17 and Figure 3.18 respectively. This is in agreement with what has been observed with the iridium-pentahydride catalyst time monitoring experiment by NMR spectroscopy (Section 3.3.3). There, the intensity of the peaks belonging to catalyst **2** ( $^1H$ -NMR -11 ppm,  $^{31}P$ -NMR 45 ppm) was decreasing over time as the formation of the peaks belonging to intermediate **59** were observed ( $^1H$ -NMR -22 ppm,  $^{31}P$ -NMR 32 ppm) (previous Figure 3.5 and Figure 3.6 from Section 3.3.3). Intermediate **59**

was also proposed to be the resting state of the catalyst in the catalytic cycle. In this experiment, the complex **59** was added as catalyst since the beginning and, because it is the resting state of the catalyst, its concentration remained constant throughout the entire reaction time as supported by the constant intensity of the corresponding peaks ( $^1\text{H-NMR}$  - 22 ppm,  $^{31}\text{P-NMR}$  32 ppm).

Over time, formation of a small amount of another unknown species (called unknown hydride species A) was observed as a triplet at -32 ppm in the proton spectra. In the phosphorus spectra this unknown species corresponded most likely to the small broad peak around 45 ppm. However, the peak of this unknown species has an integral value which is negligible compared to the peak of interest of complex **59**.

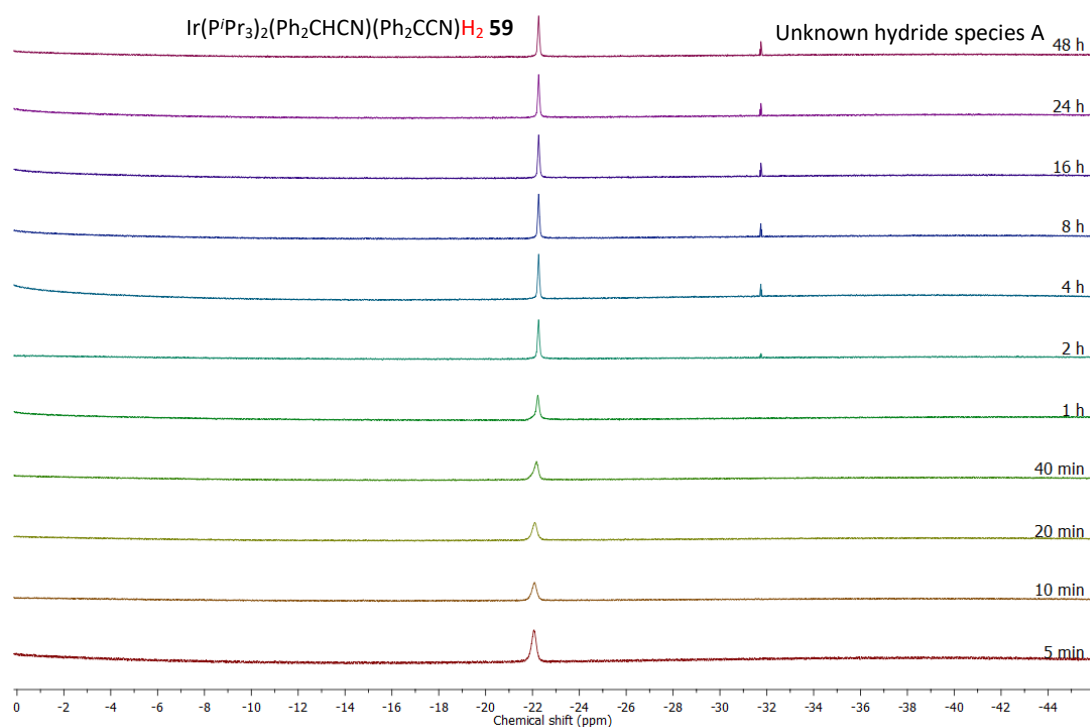


Figure 3.17 Stacked  $^1\text{H-NMR}$  spectra (298 K,  $d^8$ -toluene, 500 MHz), hydride region, of the time monitoring experiment of the model hydroalkylation reaction catalysed by iridium-ylide-nitrile intermediate **59** (Ir 10 mol%, 25 °C).

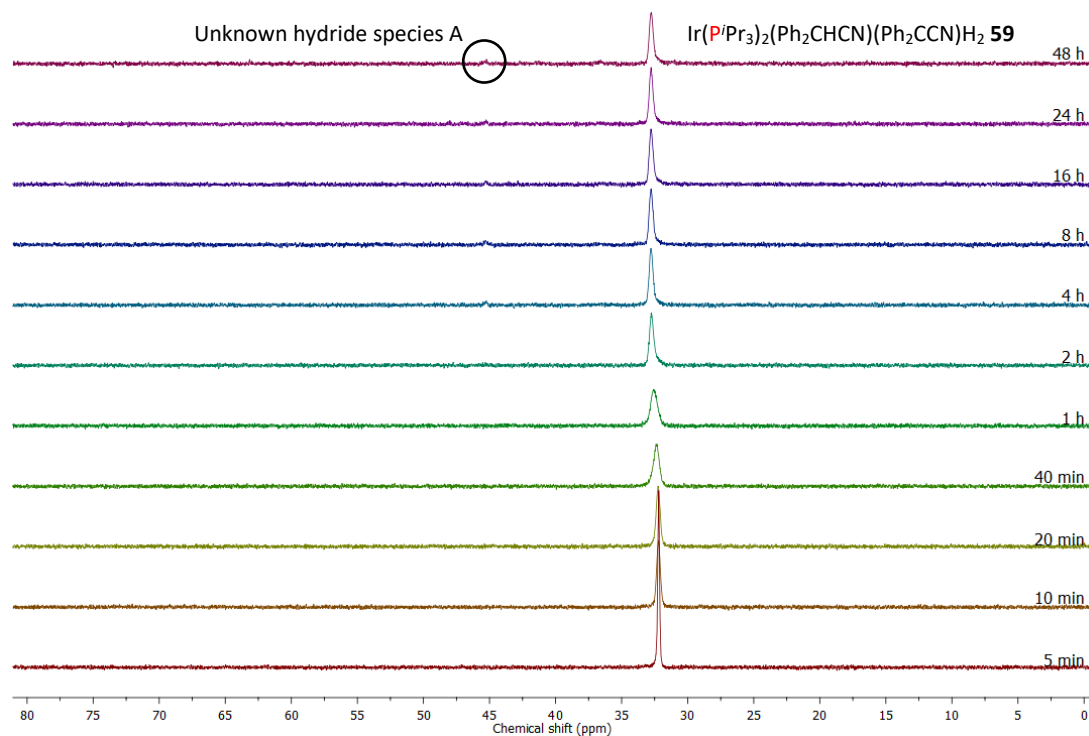


Figure 3.18 Stacked  $^{31}\text{P}\{^1\text{H}\}$ -NMR spectra (298 K,  $d^8$ -toluene, 202 MHz) of the time monitoring experiment of the model hydroalkylation reaction catalysed by iridium-ylide-nitrile intermediate **59** (Ir 10 mol%, 25 °C).

The behaviour of the iridium-phenoxide intermediate **62** in the hydroalkylation reaction was also investigated, once again by monitoring the reactivity by  $^1\text{H}$ - and  $^{31}\text{P}$ -NMR spectroscopy. From the spectra reported in Figure 3.19 and Figure 3.20 it can be concluded that the iridium-phenoxide intermediate **62** was instantaneously converted into the iridium-ylide-nitrile intermediate **59**, which is the main peak in both the proton and phosphorus NMR spectra after 5 minutes of reaction time ( $^1\text{H}$ -NMR -22 ppm,  $^{31}\text{P}$ -NMR 32 ppm). Over time, the initially formed intermediate **59** was converted into two other hydride species, called unknown hydride species A and B. Looking at the phosphorus spectra, the formation of a major peak can be observed over time at 37 ppm, belonging to the unknown hydride species B. The intensity of this peak increases as the peak belonging to intermediate **59** decreases. Because of this observation, it can be hypothesised that the two small peaks of equal intensity, at -22 and -26 ppm in the hydride region of the proton spectra, belong to the same unknown hydride species B, which is likely to be another reaction intermediate. This experiment shows also the presence of the previously observed unknown hydride species A, with a triplet at -32 ppm and a phosphorus peak around 45 ppm. Again, the value of the integration for this unknown hydride species A is fairly low and can be considered negligible compared to the other peaks.

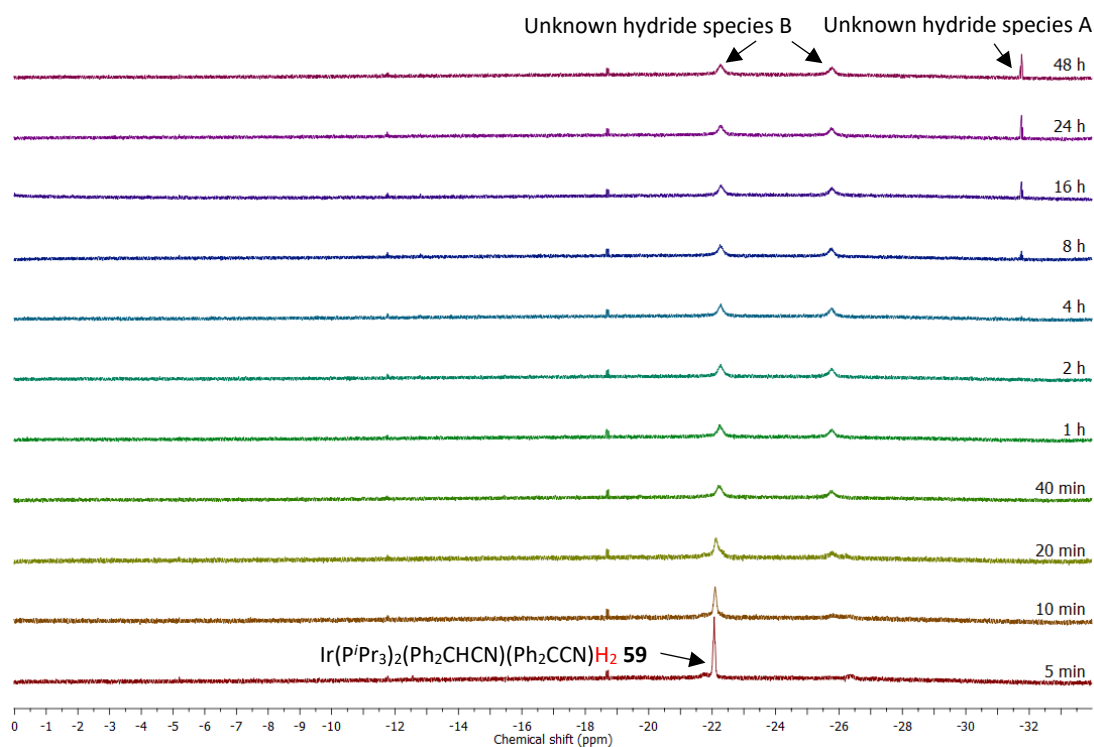


Figure 3.19 Stacked  $^1\text{H-NMR}$  spectra (298 K,  $d^8$ -toluene, 500 MHz), hydride region, of the time monitoring experiment of the model hydroalkylation reaction catalysed by iridium-phenoxide intermediate **62** (Ir 10 mol%, 25 °C).

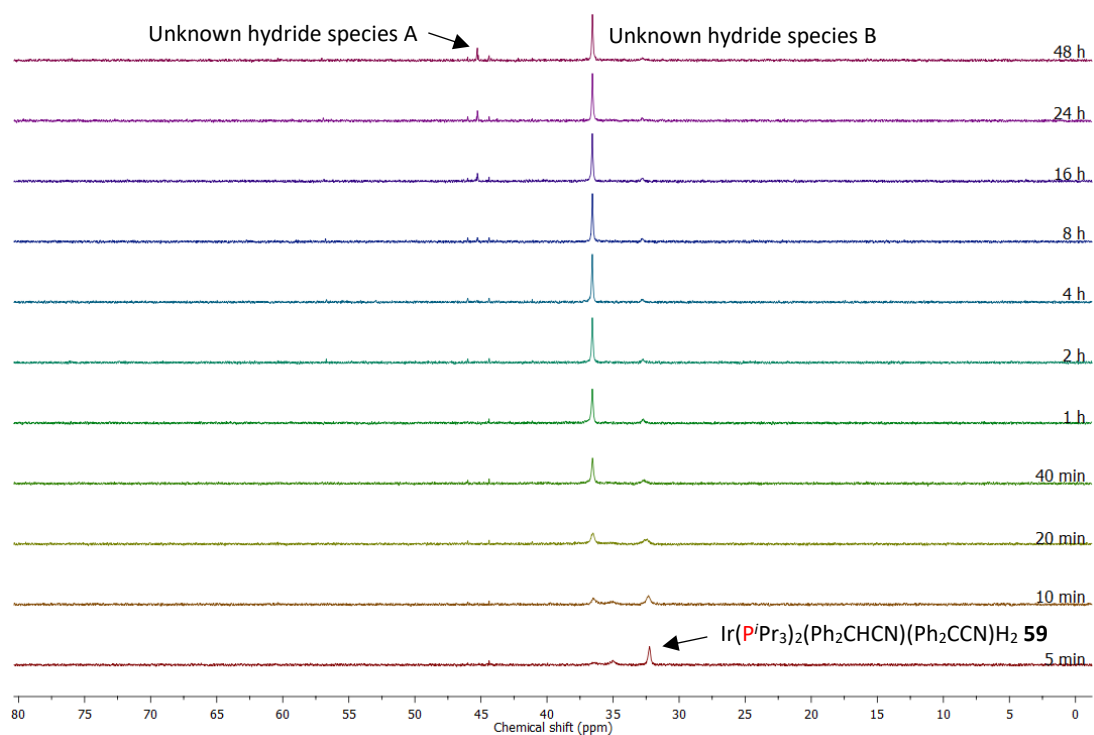


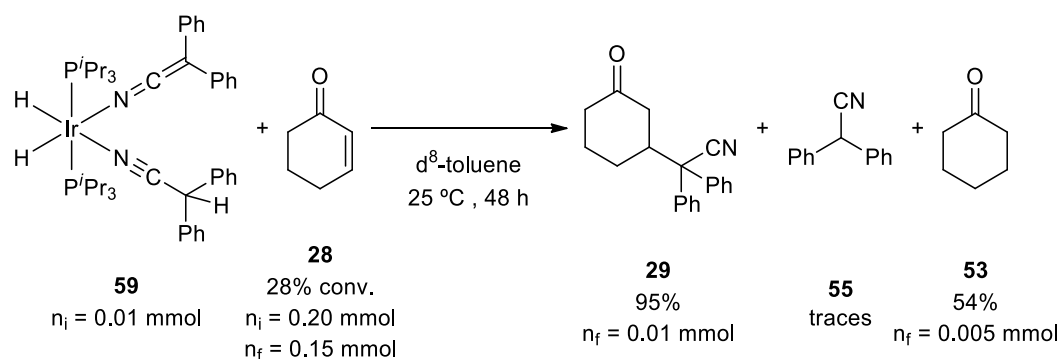
Figure 3.20 Stacked  $^{31}\text{P}\{^1\text{H}\}$ -NMR spectra (298 K,  $d^8$ -toluene, 202 MHz) of the time monitoring experiment of the model hydroalkylation reaction catalysed by iridium-phenoxide intermediate **62** (Ir 10 mol%, 25 °C).

To summarise, the most relevant findings from the above monitoring experiments by NMR spectroscopy are that the iridium-ylide-nitrile complex **59** is confirmed to be the resting state of the catalytic cycle. The iridium-phenoxide complex **62** is highly reactive and it is immediately converted into complex **59** under the standard reaction conditions. However, when the iridium-phenoxide complex **62** is used as the catalyst, after being converted into complex **59**, over time it is further converted into a possible new intermediate, here identified as unknown hydride species B. The identity of this complex will be further investigated later in the chapter. Over time, other species are also formed and they are most likely decomposition products of the complexes (i.e. the unknown hydride species A). However, their amount is always marginal compared to the main complexes observed, indeed their identity is not further investigated.

### 3.3.7 Investigation of C-C bond formation step: reactivity of the iridium-ylide-nitrile intermediate with cyclohexenone

Moving on to the mechanistic studies to prove the various steps of the previously proposed catalytic cycle, the reactivity of the iridium-ylide-nitrile intermediate **59** with cyclohexenone was investigated. According to the proposed catalytic cycle from Scheme 3.16, by reacting complex **59** with the ketone, the C-C bond formation step should take place, to finally released the desired Michael addition product **29**.

Indeed, complex **59** was reacted at room temperature with 20 equivalents of cyclohexenone, the same iridium/ketone ratio, concentration and reaction temperature used to test the standard hydroalkylation reaction (Scheme 3.29). The reaction was time monitored by NMR spectroscopy up to 48 hours to investigate the different iridium species that might be formed. Then after the 48 hours the reaction mixture after work-up was also analysed by GC to quantify the amount of hydroalkylation product formed.



Scheme 3.29 Reactivity of cyclohexenone with the iridium-ylide-nitrile complex **59** under model reaction conditions screened with the time monitoring experiments by NMR and quantified by GC. Yields are calculated with respect to the starting complex **59**.

Results from the GC analysis showed that a product yield of 95% was achieved for the desired hydroalkylation product **29**, with respect to the iridium complex **59**, as cyclohexenone was used in excess. Formation of the desired hydroalkylation product from the reaction of intermediate **59** with cyclohexenone confirms the C-C bond formation step followed by reductive elimination of the product as proposed in the catalytic cycle (see Scheme 3.16). The iridium-ylide-nitrile complex bears two ligands which can potentially be released as a molecule of diphenylacetonitrile. The yield obtained corresponds to the formation of one equivalent of product per mole of iridium and it suggests that only one of the two nitrogen ligands can react with cyclohexenone, while the second one remains bonded to the iridium centre. Traces of free diphenylacetonitrile have also been observed. The GC analysis also revealed the formation of 54% yield of cyclohexanone, again with respect to the iridium complex, meaning that the iridium intermediate **59** was also able to hydrogenate the cyclohexenone.

As mentioned, the reaction was also monitored by NMR spectroscopy. The proton and phosphorus stacked spectra of the time monitoring experiment are reported in Figure 3.21 and Figure 3.22. From the NMR spectra is clear that over time the iridium intermediate **59** is gradually converted into another species. The chemical shift of this species matches with the previously observed unknown hydride species B (Figure 3.19 and Figure 3.20): a singlet at -37 ppm in the phosphorus spectra and 2 broad singlets at -22 and -26 ppm in the proton spectra, when the iridium-phenoxide intermediate **62** was tested as catalyst for the hydroalkylation reaction.

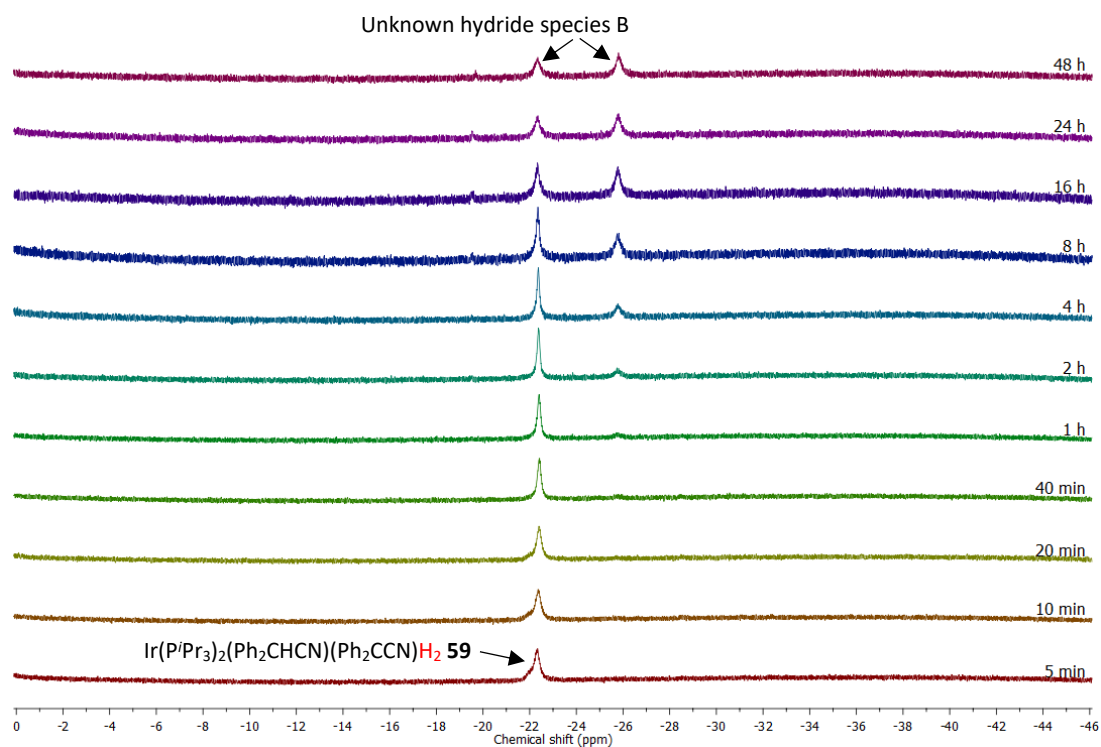


Figure 3.21 Stacked  $^1\text{H-NMR}$  spectra (298 K,  $d^8$ -toluene, 500 MHz), hydride region, of the time monitoring experiment of the reactivity of the iridium-ylide-nitrile intermediate **59** with cyclohexenone under the model reaction conditions.

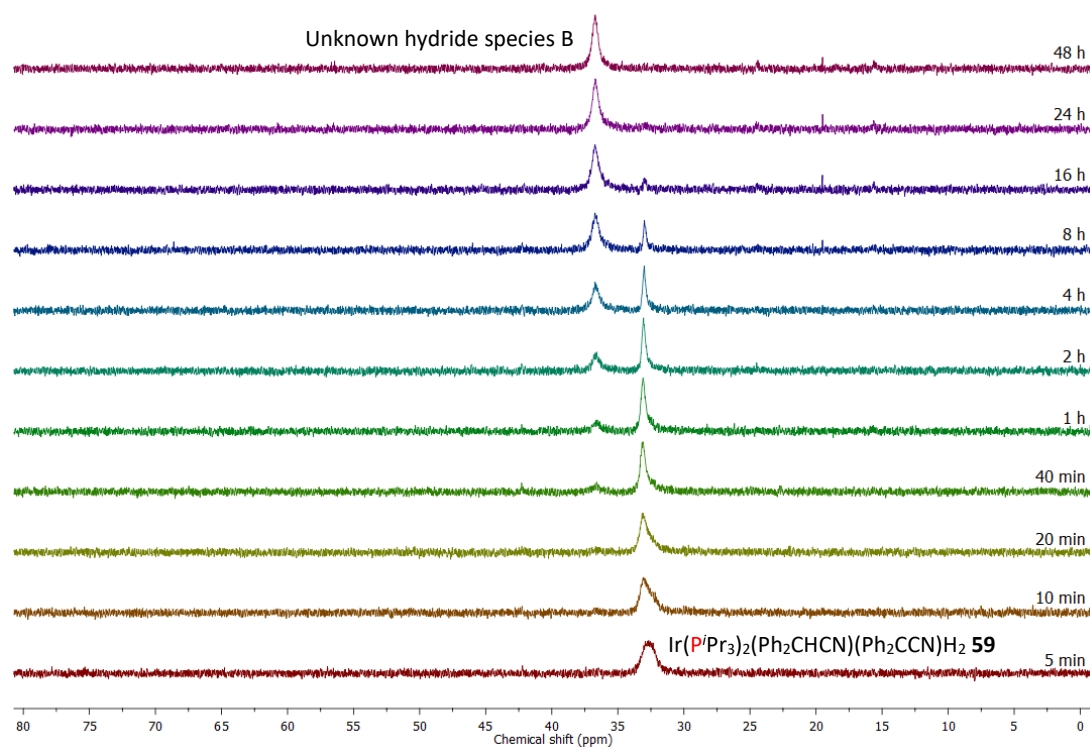


Figure 3.22 Stacked  $^{31}\text{P}\{^1\text{H}\}$ -NMR spectra (298 K,  $d^8$ -toluene, 202 MHz) of the time monitoring experiment of the reactivity of the iridium-ylide-nitrile intermediate **59** with cyclohexenone under the model reaction conditions.



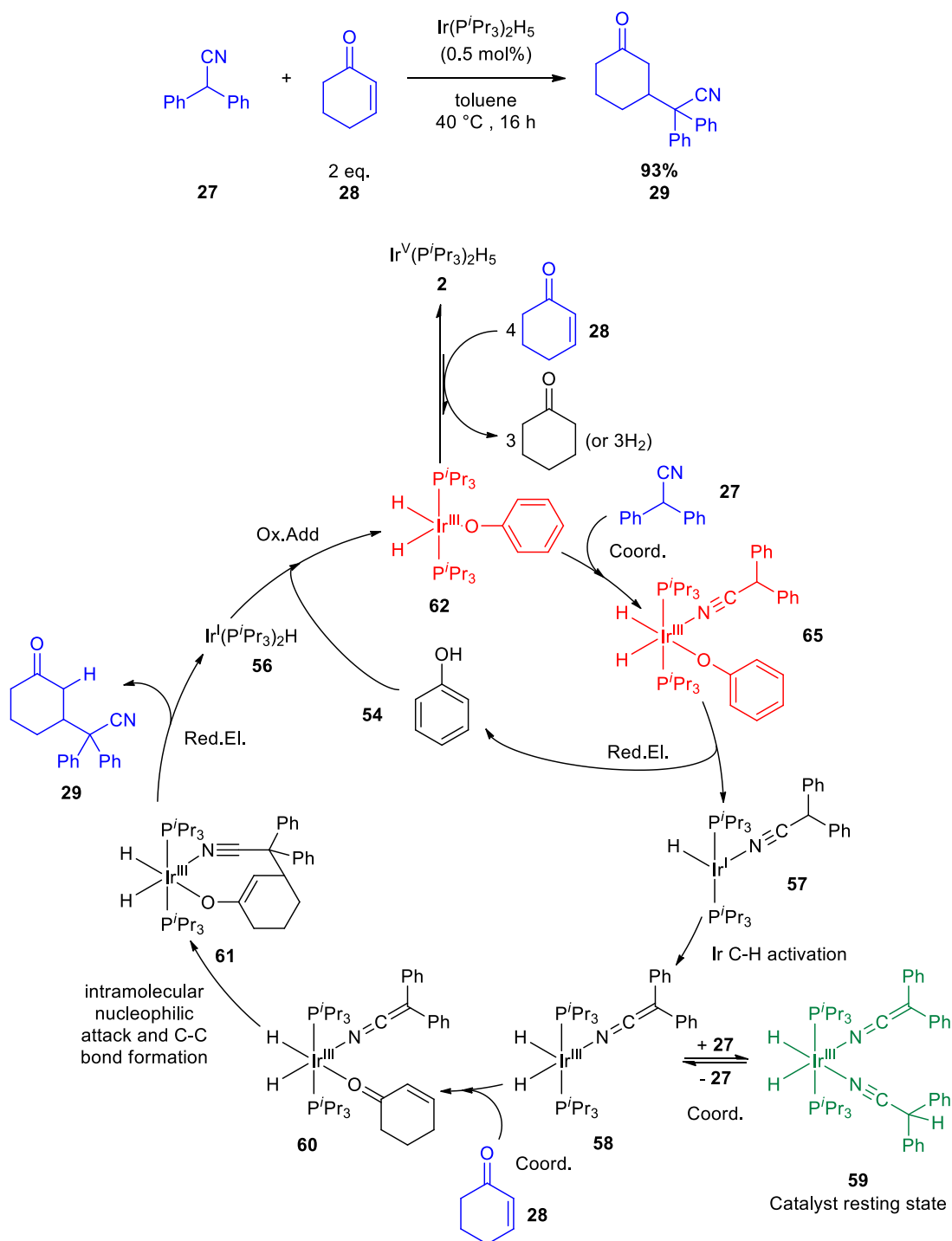
To summarise, this experiment further confirms that the iridium-ylide-nitrile intermediate **59** is definitely part of the catalytic cycle of the Michael-type hydroalkylation reaction under exam. By reacting the iridium intermediate **59** with cyclohexenone, the formation of the desired hydroalkylation product is observed, supporting the intramolecular nucleophilic addition and C-C bond formation step of the proposed catalytic cycle (Section 3.3.1). Interestingly, the iridium complex can transfer only one equivalent of nitrile.

### 3.3.8 Revised catalytic cycle

After both the C-H activation and the C-C-bond formation step have been investigated, a revised catalytic cycle can be proposed taking into consideration the new findings.

By monitoring the reaction by GC at 25 °C an induction period was observed, this is because the iridium-pentahydride catalyst **2** needs to be converted into the catalytically active species by loss of hydrides. Investigation of the reactivity of the iridium-pentahydride catalyst with diphenylacetonitrile and then with cyclohexenone showed that the loss of hydrides is facilitated by a cyclohexenone disproportionation reaction, where four molecules of cyclohexenone reacts with catalyst **2** to yield the iridium-phenoxide intermediate **62** and three molecules of cyclohexanone. Intermediate **62** was hypothesised to be the catalytically active species, which having a free coordination space, can easily coordinate a diphenylacetonitrile molecule to yield complex **65**. This is in line with the previously proposed catalytic cycle or literature data, where after the formation of the catalytically active species, the first step of the catalytic cycle is the coordination of the nitrile compound.<sup>96, 152</sup> Phenol is then released *via* reductive elimination to obtain the iridium (I) complex **57**. Reductive elimination reactions to form a C-O bond have been widely studied during the mechanistic investigations on transition-metal-catalysed reactions.<sup>184</sup> The cycle then proceeds as previously hypothesised with the C-H activation step yielding complex **58** which is in equilibrium with complex **59** by coordination of a second diphenylacetonitrile molecule. The iridium-ylide-nitrile complex **59** is confirmed to be an intermediate in the catalytic cycle and possibly the resting state of the catalyst as it is the complex present in major amount as long as free diphenylacetonitrile is present in large amount. Complex **58** however could also be obtained directly from complex **65** *via* C-H activation of the nitrile ligand mediated by the phenoxy ligand. From complex **58** on, the catalytic cycle is demonstrated to proceed as previously hypothesised in Scheme 3.16, with the binding of a molecule of cyclohexenone to the free coordination space of complex **58**, yielding complex **60**. Then, an intramolecular nucleophilic attack and C-C bond formation takes place and the desired product is released

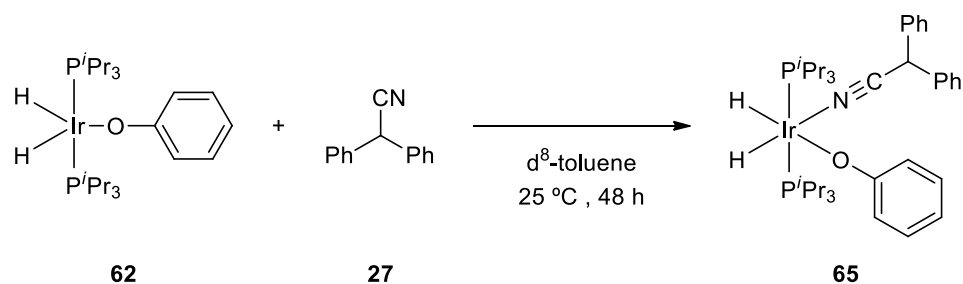
via reductive elimination. After the product is released the remaining iridium species **56** can close the catalytic cycle by oxidatively adding the phenol eliminated at the beginning of the cycle, regenerating the iridium-phenoxide complex **62**. More experiments were performed based on and to further support the revised catalytic cycle.



Scheme 3.30 Revised mechanism of the catalytic cycle for the iridium-catalysed Michael-type hydroalkylation of 2-cyclohexen-1-one with alkyl-aryl-nitriles based on the new findings.

### 3.3.9 Reactivity of iridium-phenoxide intermediate with diphenylacetonitrile

To support the revisions to the catalytic cycle, the diphenylacetonitrile coordination step was investigated in more detail. According to the first step of the revised catalytic cycle reported in Scheme 3.30, the iridium-phenoxide complex **62** coordinates a molecule of diphenylacetonitrile to form the iridium-nitrile-phenoxide intermediate **65**. The formation of this iridium-nitrile-phenoxide complex could be proven by reacting the iridium-phenoxide complex **62** with diphenylacetonitrile in equimolar amount (Scheme 3.31).



Scheme 3.31 Reactivity of the iridium-phenoxide complex **62** with diphenylacetonitrile in equimolar amount under model reaction conditions screened with the time monitoring experiments by NMR.

The reaction reported in Scheme 3.31 was time monitored by proton and phosphorus NMR spectroscopy. From the NMR spectra reported in Figure 3.23 and Figure 3.24 it can be observed that the reaction is completed after only 5 minutes. The iridium-phenoxide intermediate **62** reacts with the diphenylacetonitrile almost instantaneously and it is fully consumed to obtain a new clean compound which does not change over the 48 hour of reaction monitoring. This fast reaction supports the high reactivity hypothesised for the iridium-phenoxide intermediate **62**, due to its free coordination space. The NMR patterns of this new species are in agreement with the proposed structure of intermediate **65** with two hydride signals in the proton spectra at -22 and -26 ppm, which appear as broad singlets. The two hydrides are in fact non-equivalents due to different ligands in *trans* position. The phosphorus spectra, instead, show a sharp singlet at 35 ppm. Considering the NMR patterns, the new species observed seems to match with the previously observed unknown hydride species B. This species was previously observed in the NMR monitoring experiments where the iridium-phenoxide intermediate was used as a catalyst (Figure 3.19 and Figure 3.20) and when the reactivity of iridium-ylide-nitrile complex with cyclohexenone was investigated (Figure 3.21 and Figure 3.22). In both cases, the iridium-ylide-nitrile complex **59** is formed at first and over time it is converted into another species, identified as complex **65**. This is

because as more hydroalkylation product is formed, the less diphenylacetonitrile is available to coordinate to the iridium centre, therefore the free phenol is coordinated.

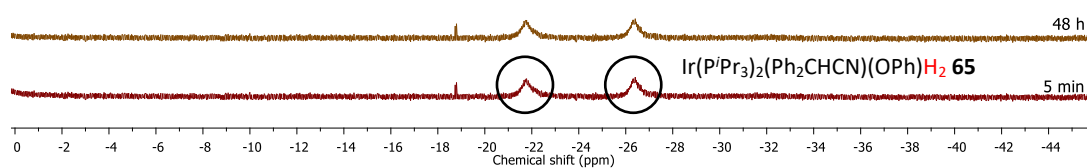


Figure 3.23 Stacked  $^1\text{H}$ -NMR spectra (298 K,  $d^8$ -toluene, 500MHz), hydride region, of the time monitoring experiment of the reactivity of the iridium-phenoxide intermediate **62** with diphenylacetonitrile in equimolar amount.

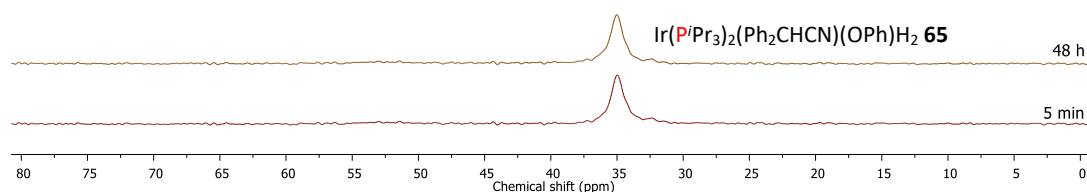
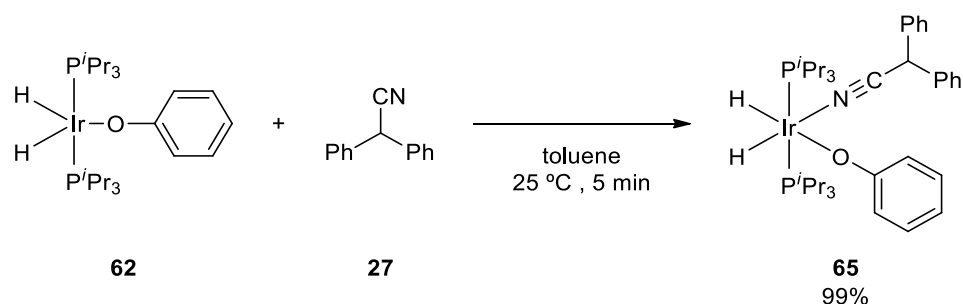


Figure 3.24 Stacked  $^{31}\text{P}\{^1\text{H}\}$ -NMR spectra (298 K,  $d^8$ -toluene, 202 MHz) of the time monitoring experiment of the reactivity of the iridium-phenoxide intermediate **62** with diphenylacetonitrile in equimolar amount.

The new iridium-nitrile-phenoxide intermediate **65** can indeed be quantitatively synthesised by reacting the iridium-phenoxide complex and diphenylacetonitrile in equimolar amount in an easy and clean reaction which takes place at room temperature in less than 5 minutes (Scheme 3.32). Indeed, the new complex **65** was isolated and characterised.



Scheme 3.32 Synthesis of proposed iridium-nitrile-phenoxide intermediate **65** from the reaction of intermediate **62** with diphenylacetonitrile.

As already mentioned, the NMR spectra at room temperature of complex **65** present two hydride signals as the two hydrides are non-equivalent, however those hydride signals are broad and their multiplicity is not resolved because of a fast ligands exchange which takes place in solution at room temperature. Indeed, some variable temperature NMR experiments have been performed to get more resolved signals and assign more accurately the structure. At lower temperature in fact any equilibrium should slow down, including the ligand

exchange. Complex **65** was dissolved in *d*<sup>8</sup>-toluene and the low temperature NMR spectra were recorded from room temperature down to -80 °C, spectra are reported below only down to -40 °C as lowering the temperature further caused the complex to precipitate. Again, as usual proton and phosphorus NMRs were recorded. From the hydride region of the proton spectra (Figure 3.25) it can be noted that as the temperature was lowered both the hydride signals become sharper, with the signal at -22 ppm even splitting in a triplet of doublets at -20 °C because of the coupling with the two phosphorus atoms and the other hydride. From both the aliphatic region of the proton spectra (Figure 3.26) and the phosphorus spectra (Figure 3.27) it can be observed that lowering the temperature also caused the signals belonging to the phosphines to split into two separate peaks. This is a classic behaviour for this type of complexes, which present coalescing signals with the increasing temperature.<sup>185</sup> This is consistent with what found from the crystal structure of the related complex **62** and **59** where the two phosphines form an angle <180 ° with the iridium metal centre. Indeed, it can be assumed that the same happens in the **65** complex and this is supported by the findings from the NMR spectra showing non-equivalent phosphines as the ligand rotation and exchange is slowed down. From both the proton and phosphorus spectra it can be also noted that at -20 °C formation of a small amount of iridium-phenoxy species **62** can be observed, this can be attributed to the diphenylacetonitrile starting to partially de-coordinate the iridium and precipitate from the solution.

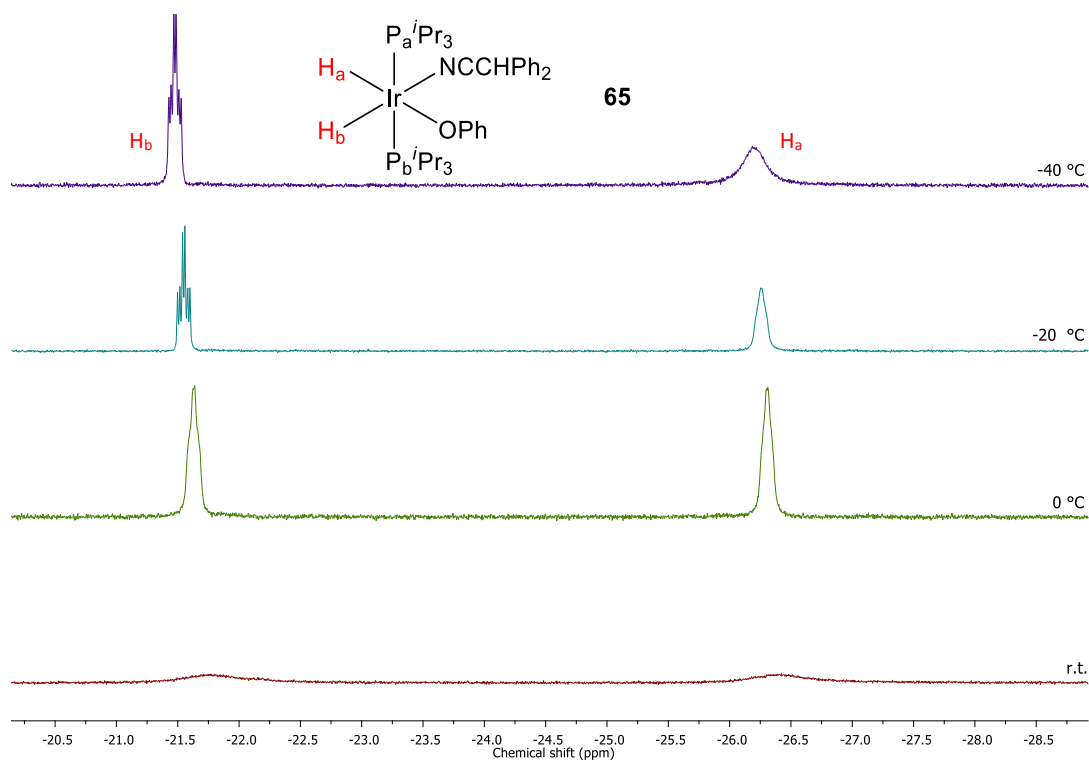


Figure 3.25 Stacked  $^1\text{H}$ -NMR spectra ( $d^8$ -toluene, 400 MHz), hydride region, of the VT NMR experiment for the iridium-nitrile-phenoxide intermediate **65**.

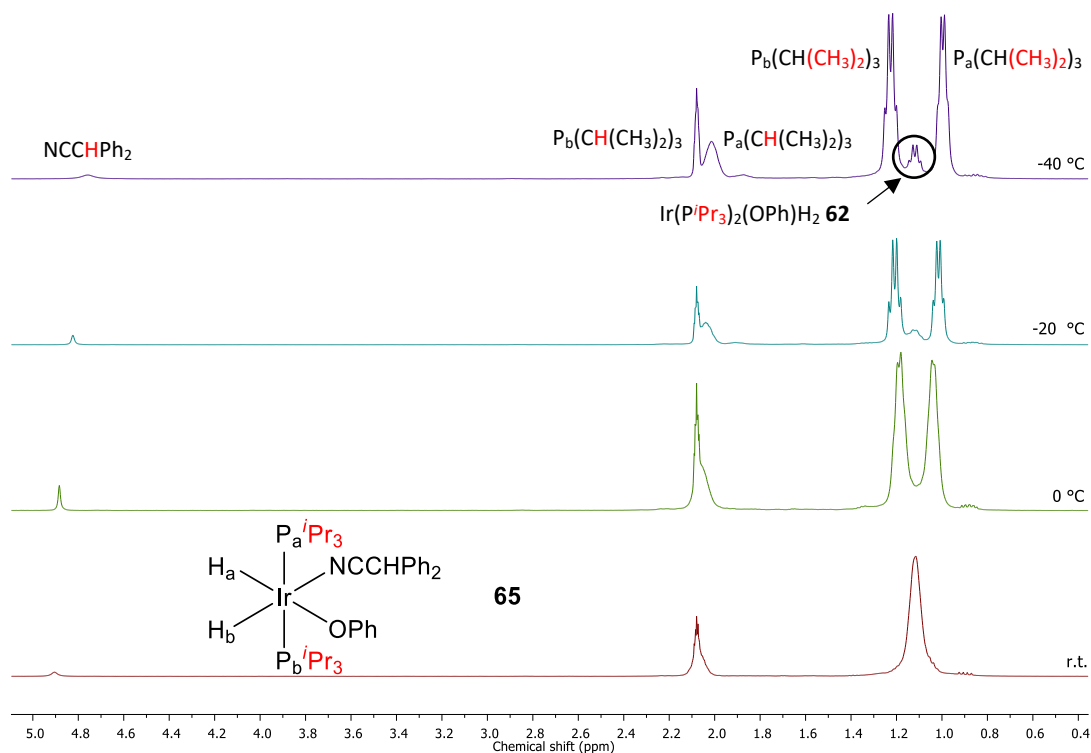


Figure 3.26 Stacked  $^1\text{H}$ -NMR spectra ( $d^8$ -toluene, 400 MHz), aliphatic region, of the VT NMR experiment for the iridium-nitrile-phenoxide intermediate **65**.

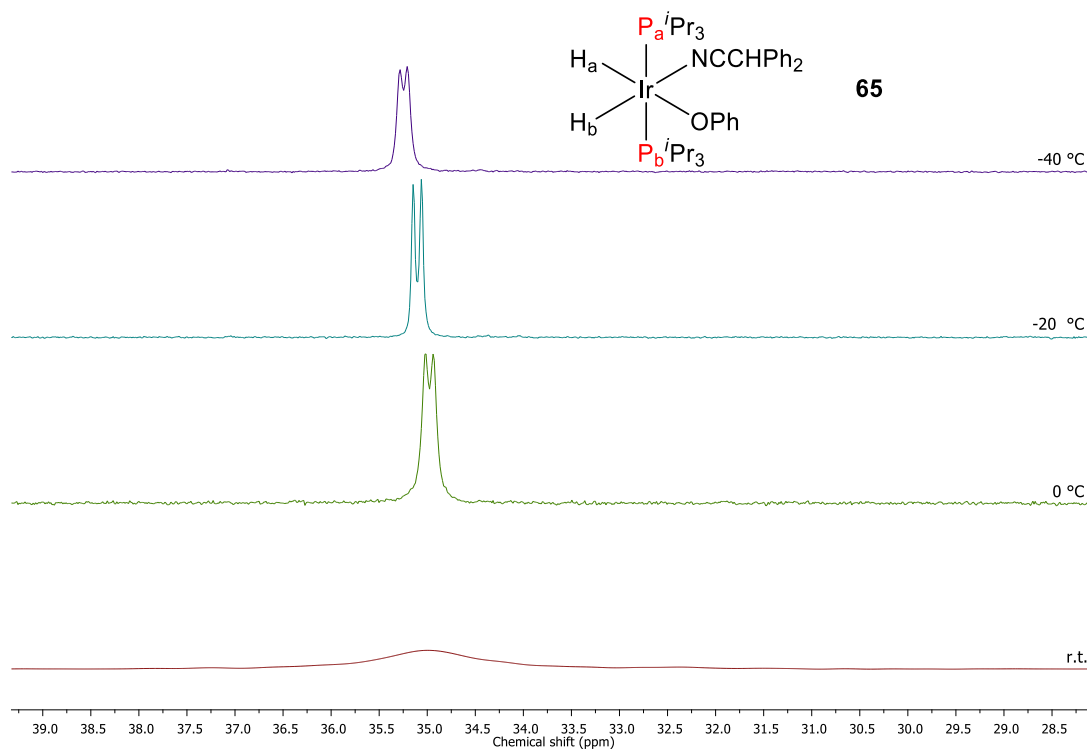
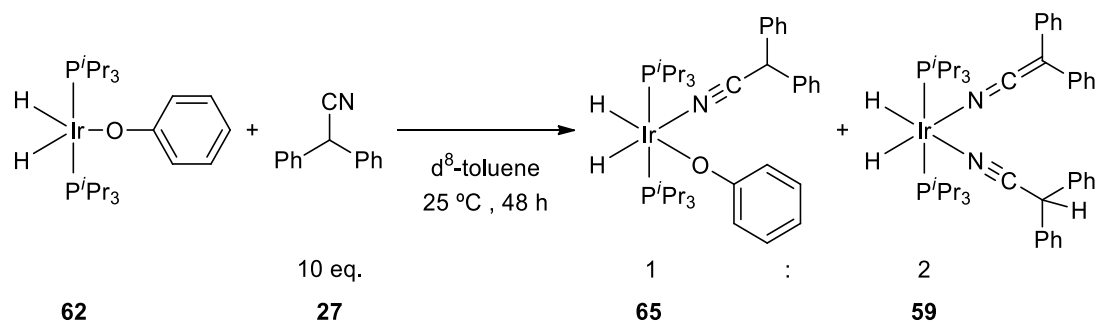


Figure 3.27 Stacked  $^{31}\text{P}\{^1\text{H}\}$ -NMR spectra ( $d^8$ -toluene, 162 MHz), of the VT NMR experiment for the iridium-nitrile-phenoxide intermediate **65**.

Now, it has been shown that complex **65** is formed when the iridium-phenoxide complex **62** and diphenylacetone nitrile react together in a 1:1 ratio, but what really happens when the diphenylacetone nitrile is present in excess as in the classic catalytic reaction? The monitoring experiments were indeed repeated with an iridium/diphenylacetone nitrile ratio of 1:10, as it would be in a catalytic reaction with an iridium catalyst loading of 10 mol% (Scheme 3.33). As it can be observed from the NMR spectra in Figure 3.28 and Figure 3.29, when the diphenylacetone nitrile was added in excess compared to the iridium, the iridium-phenoxide complex **62** was immediately fully consumed and the reaction was pushed all the way towards the formation of complex **59** and complex **65** in minor amount. The two complexes are in equilibrium and, as no hydroalkylation product could be formed due to the absence of cyclohexenone, the ratio of the two iridium species stayed constant throughout the entire monitoring time of the reaction. From the proton spectra the signals for the complex **65** are too broad to be able to reliably measure their integration value, but from the phosphorus NMR spectra in Figure 3.29, the two signals have a relative integration of 1:2, which remains constant throughout all the reaction time.



Scheme 3.33 Monitoring experiment of the reactivity of the iridium-phenoxide complex **62** with di[phenylacetonitrile] under the model reaction conditions and ratios.

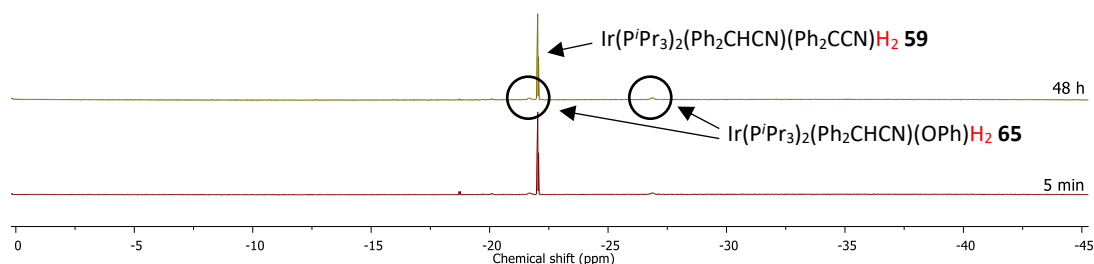


Figure 3.28 Stacked  $^1H$ -NMR spectra (298 K,  $d^8$ -toluene, 500 MHz), hydride region, of the time monitoring experiment of the reactivity of the iridium-phenoxide intermediate **62** with diphenylacetonitrile under the model reaction conditions.

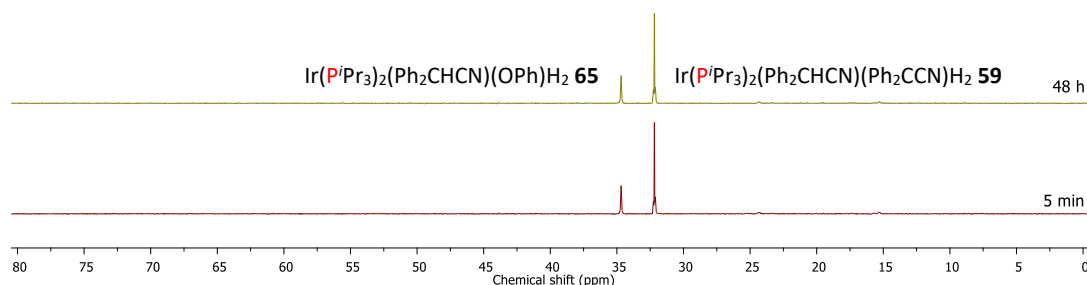


Figure 3.29 Stacked  $^{31}P\{^1H\}$ -NMR spectra (298 K,  $d^8$ -toluene, 202 MHz) of the time monitoring experiment of the reactivity of the iridium-phenoxide intermediate **62** with diphenylacetonitrile under the model reaction conditions.

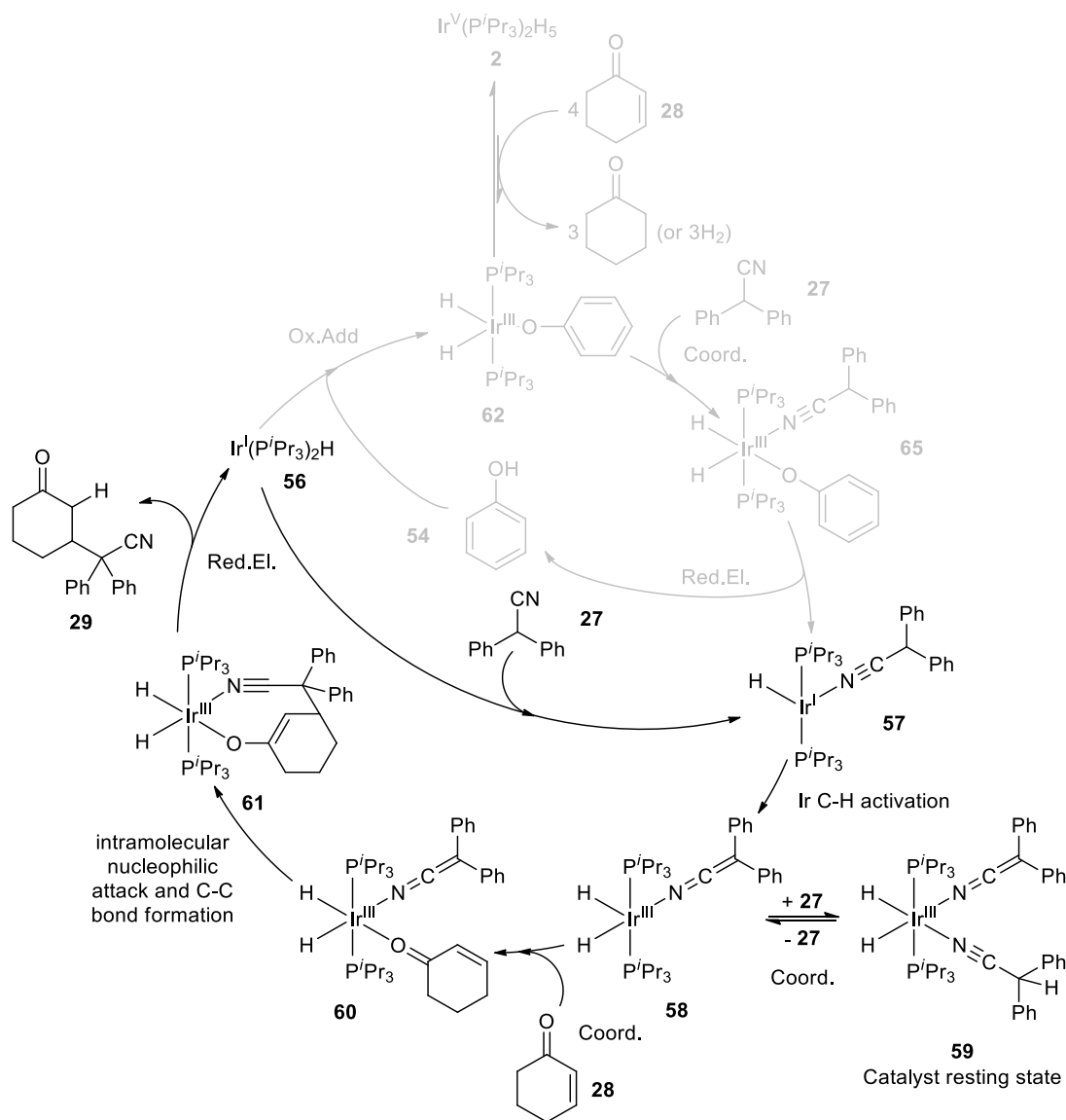
To summarise, from these experiments on the reactivity of the iridium-phenoxide intermediate **62** with diphenylacetonitrile, it has been confirmed that when the two compounds are mixed in a 1:1 ratio, the iridium-nitrile-phenoxide complex **65** is formed in quantitative amount. X-ray data for this complex are yet to be obtained, however all the findings from the NMR experiments are consistent with the proposed structure for complex **65** and support the revised catalytic cycle. Hence, the new intermediate **65** has been identified, isolated and characterised to the best of our capabilities. When the iridium-phenoxide intermediate **62** reacts with an excess amount of diphenylacetonitrile, both



complex **65** and **59** are formed in a 1:2 ration, meaning that the excess nitrile pushed the reaction towards the formation of the iridium-ylide-nitrile complex **59**. This results further supports the hypothesis that complex **59** is the catalyst resting state.

### 3.3.10 Reactivity of iridium-ylide-nitrile with phenol

Another observation that could not be explained with the previously proposed catalytic cycle (Scheme 3.16), was that when the iridium-ylide-nitrile intermediate **59** was tested as a catalyst, it showed a lower catalytic activity compared to both the iridium-pentahydride catalyst and iridium-phenoxide intermediate. According to the new revised catalytic cycle (Scheme 3.30), this fact has a simple explanation: when the intermediate **59** is the sole catalysts, phenol formation has not been observed, indeed the catalytic reaction can only take place *via* an alternative pathway, which does not imply the use of phenol. This alternative pathway is shown in Scheme 3.34 and it essentially corresponds to the previously proposed catalytic cycle (Scheme 3.16).



Scheme 3.34 In black, the mechanism of the catalytic cycle for the iridium-catalysed Michael-type hydroalkylation of 2-cyclohexen-1-one with alkyl-aryl-nitriles when the iridium-ylide-nitrile intermediate **59** is used as the catalyst. In grey the proposed pathway that would normally take place in the presence of phenol.

To further support this explanation, few experiments were carried out to investigate the reactivity of the iridium-ylide-nitrile intermediate in the presence of phenol.

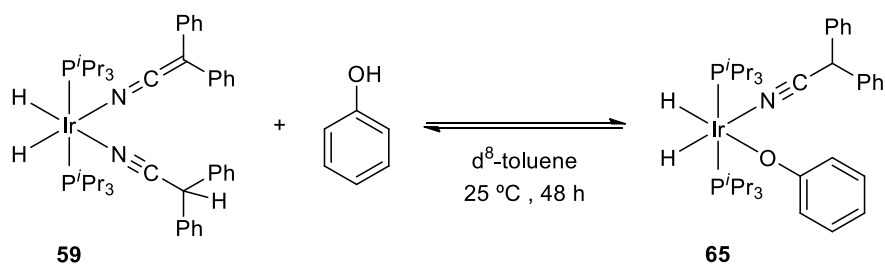
### 3.3.10.1 Equimolar amount: observation of the same equilibrium between iridium-ylide-nitrile and iridium-nitrile-phenoxide

As previously observed, when the iridium-ylide-nitrile intermediate is used as a catalyst it is the least active among the iridium-complexes tested (Figure 3.16). This is because when the catalyst is the iridium-ylide-nitrile intermediate **59**, the catalytic cycle occurs via an

alternative pathway as the phenol is not present and cannot be generated in situ as it happens with the iridium-pentahydride catalyst.

The reaction was investigated with the addition of phenol to the catalytic reaction mixture in order to test its ability to favour the catalytic cycle *via* the iridium-phenoxide intermediates **62** and **65**. When the iridium-ylide-nitrile complex **59** is used as the catalyst and phenol is added in equimolar amount to the iridium, the reaction should occur *via* the standard catalytic cycle (pathway reported in grey in Scheme 3.34) and the catalytic activity should be similar to when the iridium-phenoxide complex **62** is used as catalyst.

First, the reactivity of the iridium-ylide-nitrile complex **59** with phenol in equimolar amount was investigated by reaction monitoring *via* NMR spectroscopy (Scheme 3.35). As it can be observed from the proton and phosphorus NMR spectra in Figure 3.30 and Figure 3.31, in the presence of phenol, the iridium-ylide-nitrile intermediate **59** exists in equilibrium with the iridium-nitrile-phenoxide intermediate **65**. From the NMR spectra it can also be observed that this equilibrium between the two iridium species was immediately attained after 5 minutes of reaction and it was maintained constant throughout the entire monitoring time. The small changes in chemical shifts, especially from the proton spectra, compared with the classic chemical shifts of the isolated complexes, can be explained with the fact that in this experiment complexes **59** and **65** are in a fast equilibrium and this causes their chemical shifts to partially move closer to one another in an attempt to merge together. Finally, the fact that the complex **59** in the presence of phenol could be converted into complex **65** is also an evidence that the C-H activation and the phenol reductive elimination are reversible steps of the catalytic cycle.



Scheme 3.35 Monitoring experiment of the reactivity of the iridium-ylide-nitrile complex **59** with phenol in equimolar ratio under the model reaction conditions.

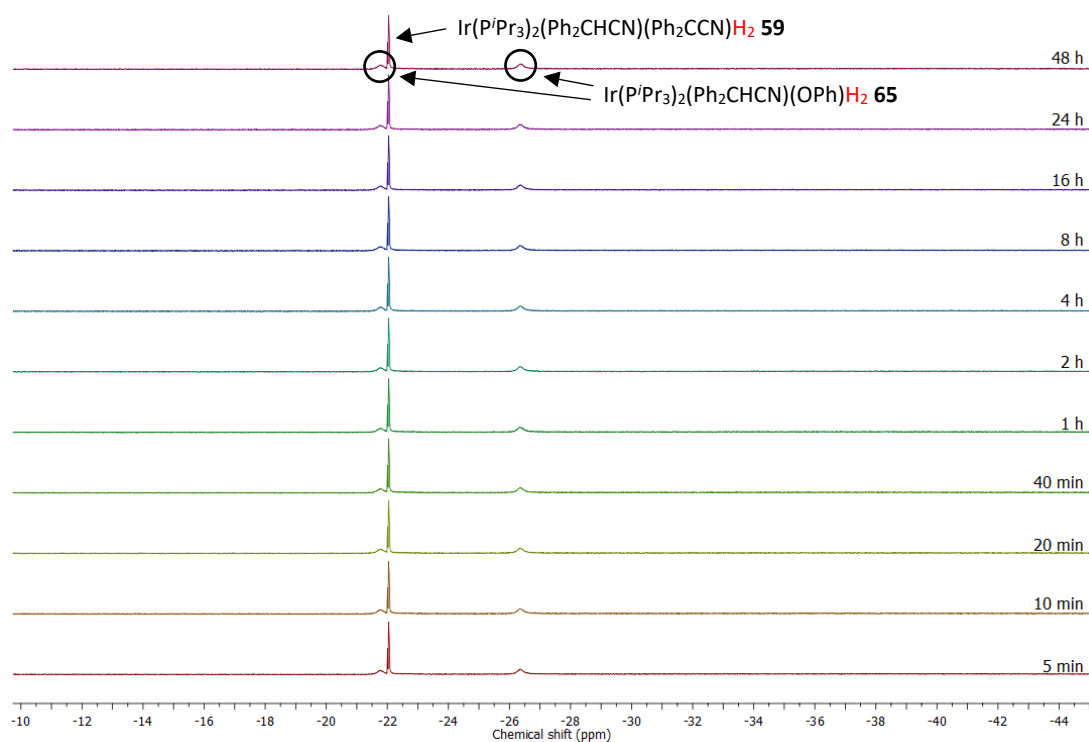


Figure 3.30 Stacked  $^1\text{H}$ -NMR spectra (298 K,  $d^8$ -toluene, 500 MHz), hydride region, of the time monitoring experiment of the reactivity of the iridium-ylide-nitrile intermediate **59** with phenol under the model reaction conditions.

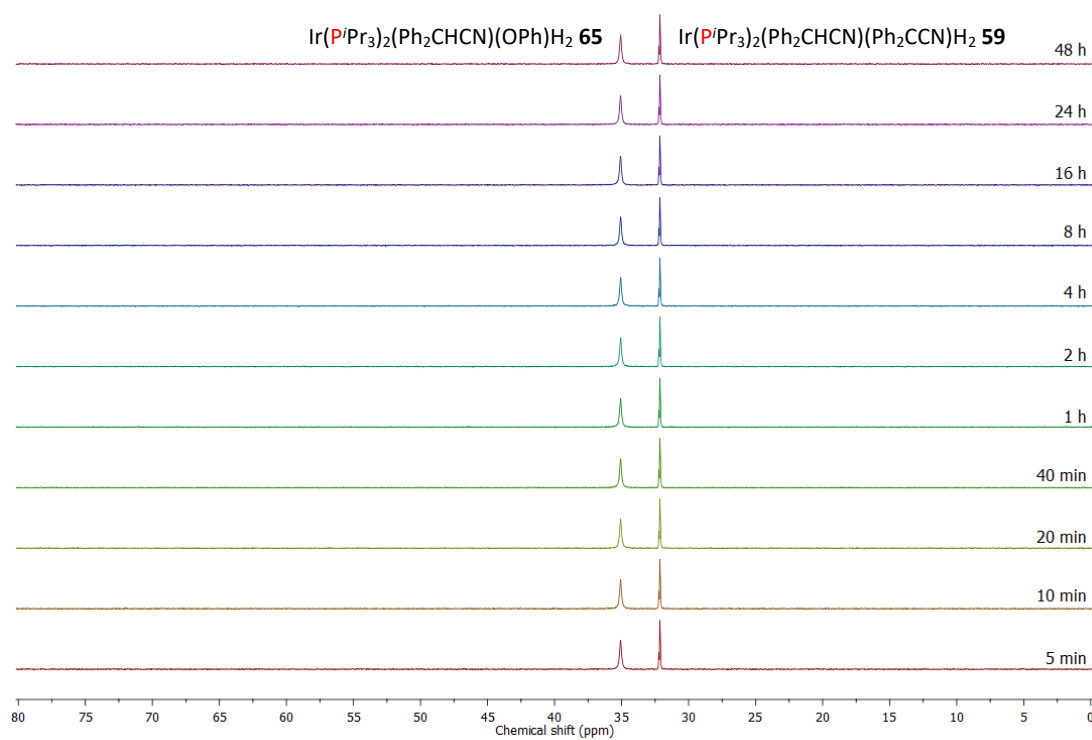
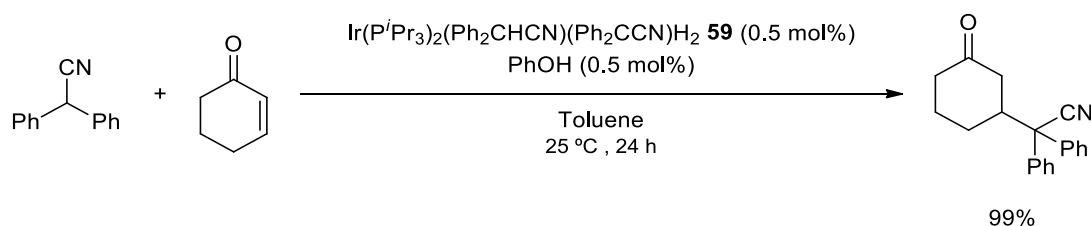


Figure 3.31 Stacked  $^{31}\text{P}\{^1\text{H}\}$ -NMR spectra (298 K,  $d^8$ -toluene, 202 MHz) of the time monitoring experiment of the reactivity of the iridium-ylide-nitrile intermediate **59** with phenol under the model reaction conditions.

After the proof that in the presence of phenol the iridium-ylide-nitrile complex **59** can be converted into the iridium-nitrile-phenoxide complex **65**, the catalytic activity of complex **59** in the presence of phenol was investigated. By performing the classic hydroalkylation reaction using complex **59** as the catalyst, the addition of phenol to the reaction mixture should improve the catalyst activity towards higher yields comparable to the ones obtained when the iridium-phenoxide complex **62** is employed as the catalyst. Indeed, the catalytic reaction reported in Scheme 3.36 was time monitored by GC over 24 hour, after which time the diphenylacetonitrile was fully converted into the product which was detected in a remarkable 99% yield. The results are presented in Figure 3.32 and the graph from the hydroalkylation reaction catalysed by iridium-phenoxide complex under the same reaction conditions is also reported for comparison. By comparing the two iridium catalysts reported in the graph below, a similar activity trend can be observed, with the activity of the iridium-ylide-nitrile complex **59** in the presence of phenol additive which is even higher than that with the iridium-phenoxide complex **62** (yield 85%).



Scheme 3.36 Monitoring experiment of the model Michael-type hydroalkylation reaction catalysed by the iridium-ylide-nitrile complex **59** with phenol in equimolar ratio to the iridium complex and under the model reaction conditions.

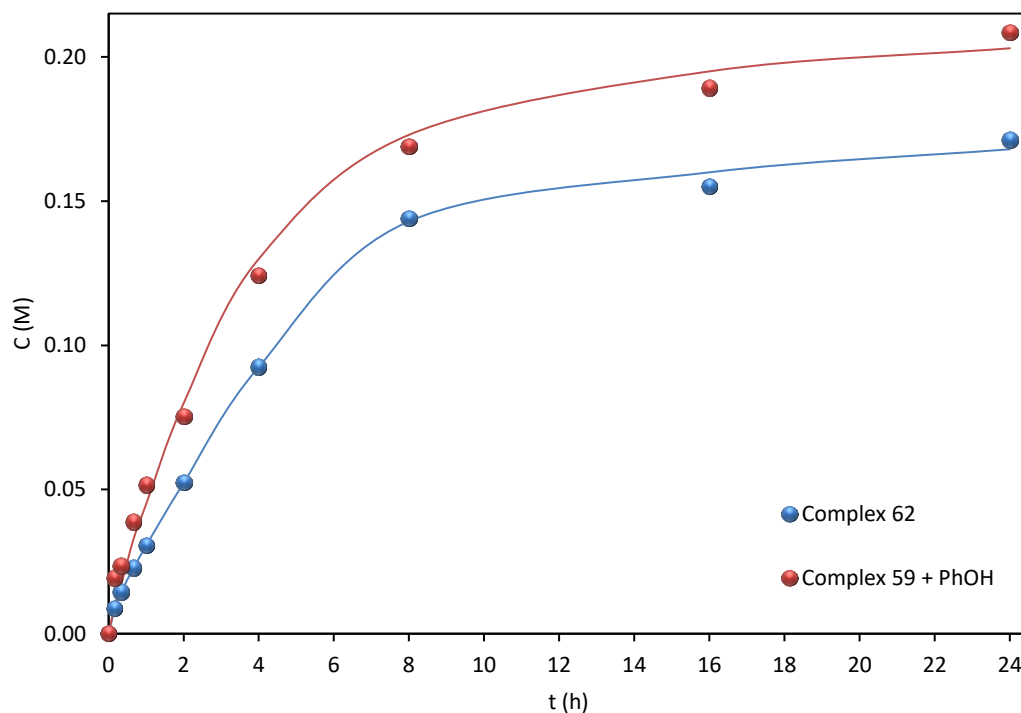
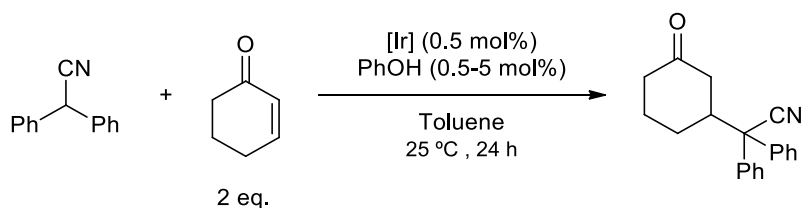


Figure 3.32 Comparison of the time monitoring by GC of the hydroalkylation reaction catalysed by the iridium-phenoxide complex **62** and the iridium-ylide-nitrile complex **59** with phenol in equimolar ratio to the iridium complex and under the model reaction conditions ( $[Ir] = 0.5 \text{ mol\%}$ ,  $25 \text{ }^\circ\text{C}$ ). The plot shows the hydroalkylation product formation over time for the two different iridium species.

These results, from both the NMR and GC monitoring experiments, support the proposed catalytic cycle and show the reversibility of the phenol reductive-elimination and successive C-H activation steps. Moreover, it can be observed that complete conversion with subsequent remarkably higher yields can be achieved when the phenol is used as an additive in the hydroalkylation reaction catalysed by the iridium-ylide-nitrile intermediate.

### 3.3.11 Phenol as an additive to the Michael addition reaction

Building on the positive results obtained using phenol in conjunction with complex **59**, the effect of the phenol was more thoroughly investigated because its use as an additive could improve the activity of the system. Indeed, the effect of a higher amount of phenol was tested by using 10 equivalents compared to the iridium-ylide-nitrile complex. The phenol additive test was also performed with the iridium-pentahydride catalyst **2**, with an iridium/phenol ratio of 1:1 and 1:10. The reaction scheme for the catalytic reactions is reported below (Scheme 3.37).



Scheme 3.37 Monitoring experiments for the use of phenol as an additive for the model Michael-type hydroalkylation reaction catalysed by the iridium-ylide-nitrile complex **59** or the iridium-pentahydride catalyst **2** under the model reaction conditions.

### 3.3.11.1 With the iridium-ylide-nitrile complex as catalyst

In the graph from Figure 3.33 are reported the results of the reaction monitoring by GC when the iridium-ylide-nitrile complex **59** was used as catalyst together with phenol in a 1:10 ratio. For completeness and comparison, also the previous results are reported, which have been obtained in the absence of phenol and when phenol has been used in equimolar amount to the iridium complex. As it can be observed from the graph, higher yields were achieved in the presence of phenol. In particular, the best results were obtained when the phenol was used in excess compared to the iridium, with the fastest initial reaction rate. This is probably because the catalytic cycle could be closed much faster due to the higher concentration of phenol which could undergo oxidative addition and indeed regenerate the catalytically active species **62**.

The reaction was so instantaneous that, as soon as the phenol was added to the reaction mixture, product formation could be detected already from the first timepoint (at  $t = 0$ ). For this reason, the product concentration at  $t = 0$  for the reaction with complex **59** was obtained by analysing the reaction mixture before the addition of phenol.

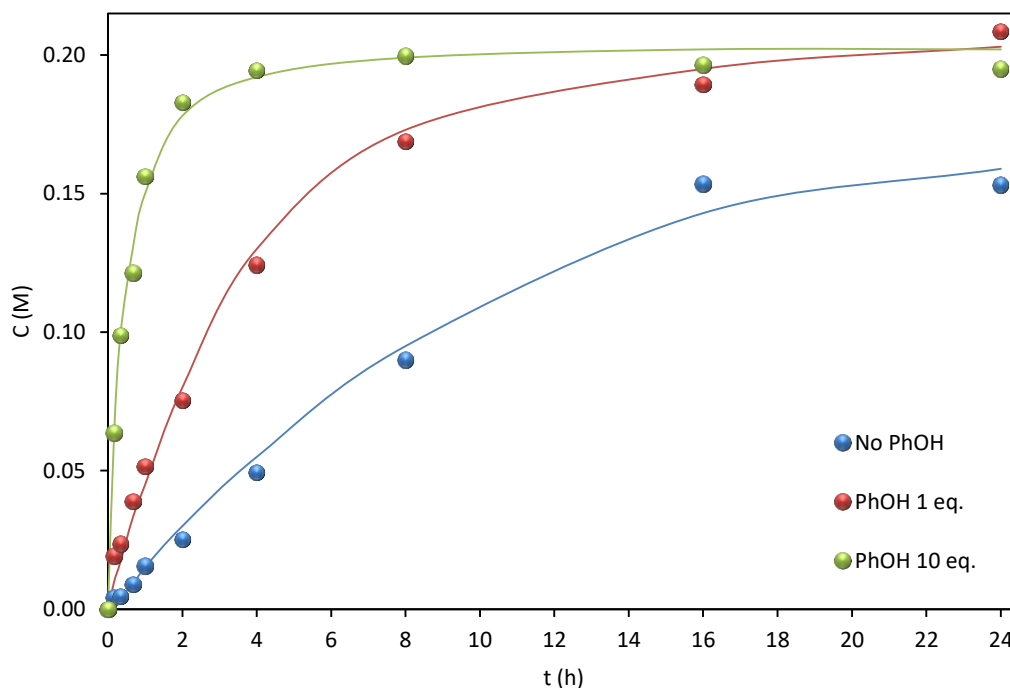


Figure 3.33 Comparison of the time monitoring by GC of the hydroalkylation reaction catalysed by iridium-ylide-nitrile complex **59** with phenol in different ratios and under the model reaction conditions ( $[\text{Ir}] = 0.5 \text{ mol\%}$ ,  $25 \text{ }^\circ\text{C}$ , phenol = 0, 1 or 10 eq. compared to the Ir). The plot shows the hydroalkylation product formation over time with different amounts of phenol. (Note: the product concentration at  $t = 0$  for the reaction with complex **59** was obtained by analysing the reaction mixture before the addition of phenol. In fact, the reaction was so fast under these conditions that formation of product appeared almost instantaneously as the phenol was added to the reaction).

Also, during the catalytic hydroalkylation reaction reported in Scheme 3.36, the concentration of the phenol stayed constant throughout the reaction as it can be observed from the graph below (Figure 3.34). This confirms that the phenol is not consumed during the reaction, but it is regenerated in the catalytic cycle; indeed, its sole role is only to promote the reaction catalytically, in agreement with the proposed catalytic cycle. In the presence of phenol, the initial reaction rate increases with increase in the concentration of phenol. This is because in the presence of phenol the concentration of the highly active iridium-phenoxide complex **62** increases at the expenses of the catalyst resting state **59**, which is in equilibrium with **62**. Therefore, the higher the concentration of phenol, the larger portion of complex **59** is converted into **62**.



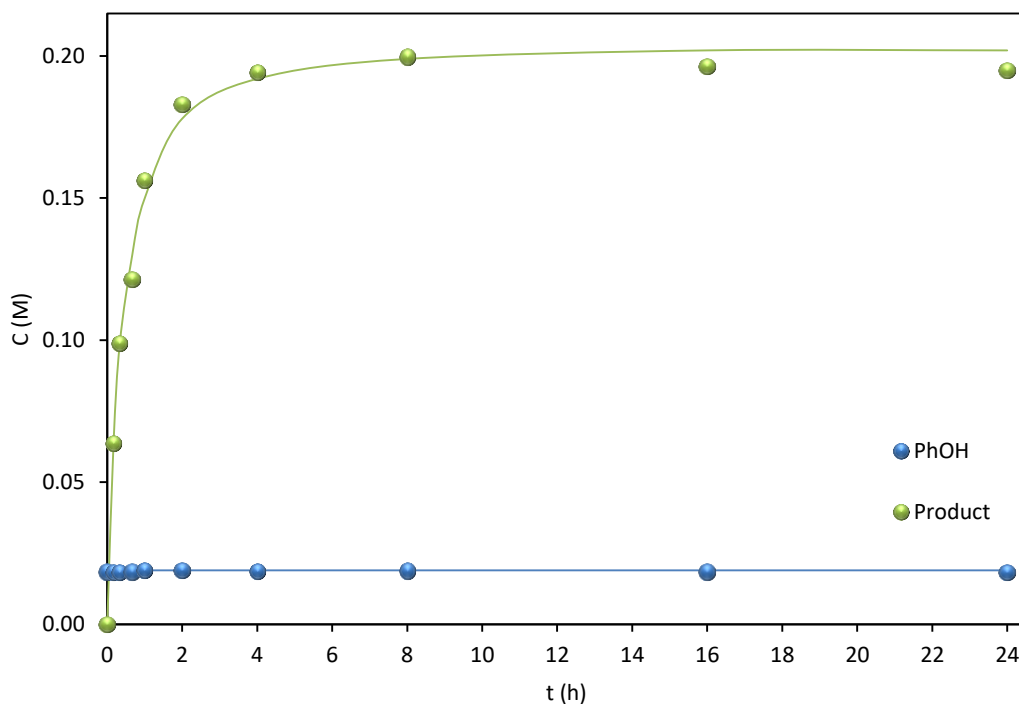


Figure 3.34 Time monitoring by GC of the hydroalkylation reaction catalysed by iridium-ylide-nitrile complex **59** with phenol in a 1:10 ratio under the model reaction conditions ( $[Ir] = 0.5 \text{ mol\%}$ ,  $25 \text{ }^\circ\text{C}$ ). The plot shows the formation of hydroalkylation product over time and the amount of phenol remains constant at any time. (Note: the product concentration at  $t = 0$  was obtained by analysing the reaction mixture before the addition of phenol.)

### 3.3.11.2 With the classic iridium-pentahydride catalyst

Next, the effect of the phenol addition to the classic Michael-type hydroalkylation reaction was investigated to probe whether phenol additives could also improve the catalytic activity of the pentahydride catalyst. The same time monitoring tests were repeated this time using the classic iridium-pentahydride complex **2** as the catalyst in the presence of 1 and 10 equivalents of phenol.

The results are shown in Figure 3.35, together with the results from the same hydroalkylation reaction in the absence of phenol for comparison. Adding one equivalent of phenol seems to have the only effect of shortening the initial induction time, however the overall yield achieved overtime, compared to the standard reaction, does not change.

Using the phenol in excess, 10 equivalents compared to the iridium, notably increases the reaction rate, with the reaction reaching a steady state already after 10 hours.

Although the yields were not drastically improved as with the iridium-ylide-nitrile complex, still the addition of phenol increased the reaction rate. This is because, as before,

the higher the concentration of the phenol, the larger the portion of iridium complex which is converted into the highly active iridium-phenoxide complex **62**. Once again, this result supports the proposed catalytic cycle.

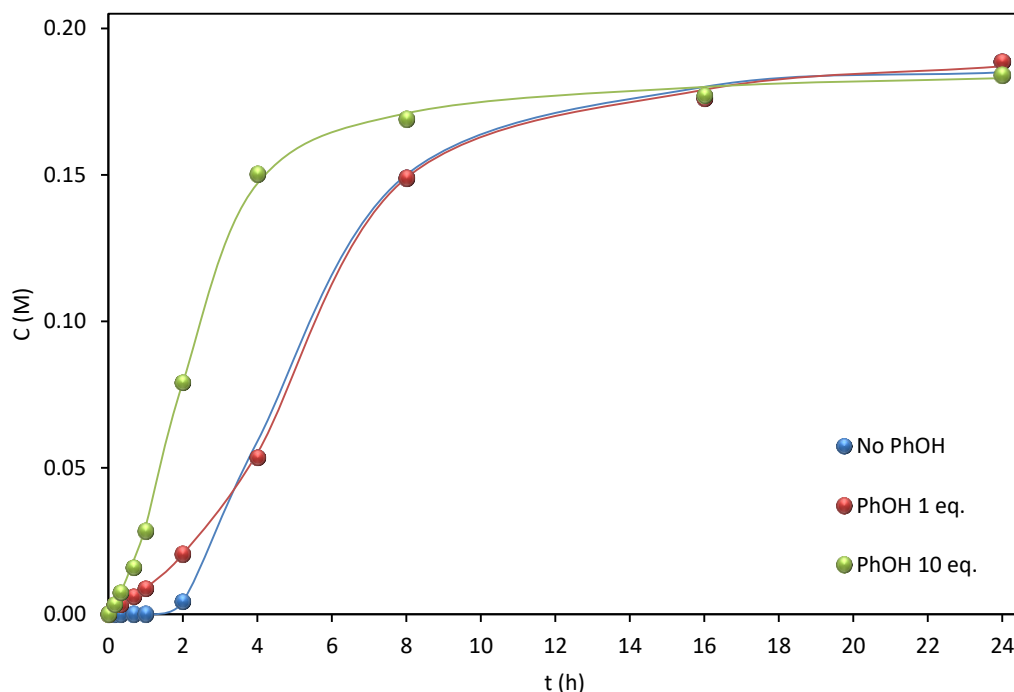


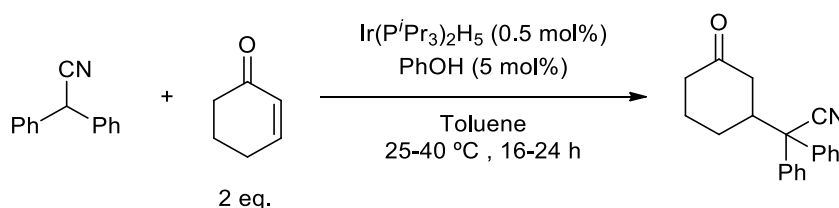
Figure 3.35 Comparison of the time monitoring by GC of the hydroalkylation reaction catalysed by iridium-pentahydride catalyst **2** with phenol in different ratios and under the model reaction conditions ( $[\text{Ir}] = 0.5 \text{ mol\%}$ ,  $25 \text{ }^\circ\text{C}$ , phenol = 0, 1 or 10 eq. compared to the Ir). The plot shows the hydroalkylation product formation over time with different amounts of phenol.

A control experiment was performed to verify that the phenol is not capable of catalysing the reaction by itself. Indeed, the classic hydroalkylation reaction was conducted in the absence of iridium catalyst, but with 5 mol% of phenol (Table 3.3 Entry 1) and the product was formed only in trace amount.

It needs also to be reminded that the standard hydroalkylation reaction is performed at  $40 \text{ }^\circ\text{C}$ , few tests were carried out to investigate whether the addition of phenol could improve the yields at this higher temperature. This might be useful to improve the results for difficult substrates, like for *iso*-propyl- or cyclohexyl-substituted aryl-nitriles. The results are reported in Table 3.3 (Entries 4 and 5) together with the results of the corresponding reaction carried out at  $25 \text{ }^\circ\text{C}$ , from the graph above (Entries 2 and 3, results from Figure 3.35) and again the same reactions performed in the absence of phenol (last column from Table 3.3 and results from Figure 3.2 and Figure 3.3), all for comparison.

From the analysis of the results reported in Table 3.3 can be concluded that the use of excess of phenol additives increases the reaction rate, but do not affect the already high reaction yields, even increasing the reaction temperature. Small changes in the reported yield could be attributed to variability of the quantification procedure.

Table 3.3 Michael-type hydroalkylation reaction of 2-cyclohexen-1-one with diphenylacetonitrile catalysed by  $\text{Ir}(\text{P}^i\text{Pr}_3)_2\text{H}_5$  in the presence of 10 equivalents of phenol as an additive.



| Entry | T (°C) | t (h) | Ir (mol%) | Yield (%)<br>with PhOH | Yield (%)<br>without PhOH* |
|-------|--------|-------|-----------|------------------------|----------------------------|
| 1     | 25     | 24    | -         | traces                 | -                          |
| 2     | 25     | 16    | 0.5       | 88                     | 87                         |
| 3     | 25     | 24    | 0.5       | 91                     | 94                         |
| 4     | 40     | 16    | 0.5       | 85                     | 91                         |
| 5     | 40     | 24    | 0.5       | 87                     | 84                         |

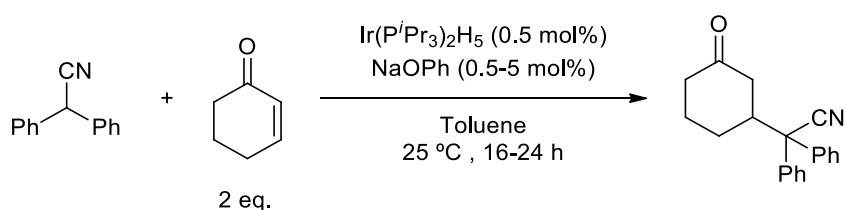
Experimental conditions: reactions were carried out in toluene (1 mL), under argon atmosphere with the  $\text{Ir}(\text{P}^i\text{Pr}_3)_2\text{H}_5$  catalyst and 10 equivalents of PhOH (5 mol%). Yields are based on quantitative GC analysis using *n*-dodecane as the internal standard. (\*) Yield for the same reaction performed in the absence of PhOH.

### 3.3.11.3 NaOPh as an additive

According to the proposed catalytic cycle, phenol binds the iridium centre as a phenoxy ligand. Indeed, alternative sources of phenoxy ligand could ideally be used as additives for the reaction. To verify this, the use of NaOPh additive was investigated. Michael-type hydroalkylation of cyclohexenone with diphenylacetonitrile at 25 °C with 0.5 mol% of  $\text{Ir}(\text{P}^i\text{Pr}_3)_2\text{H}_5$  catalyst loading was performed in the presence of NaOPh. NaOPh was used as an additive in 1:1 and 1:10 ratio with the iridium catalyst. The reaction mixture was analysed to quantify the product after 16 and 24 hours. Results are reported in Table 3.4 together with the results of the same reaction performed using phenol as an additive instead of NaOPh (last column of Table 3.4). First the reaction was performed in the absence of iridium catalyst,

to verify that NaOPh was not able to act as a catalyst and this was confirmed as the desired product was obtained only in trace amount (Entry 1). The results reported in the table confirm the idea that NaOPh can be used as the source of phenoxide. However, by comparing the product yields obtained after 16 and 24 hours with NaOPh or PhOH, it appears that with NaOPh the reaction is slower. This is particularly true with low concentrations of the additive (Entries 2 and 3). These experiments confirm the phenol to be the best option as an additive.

Table 3.4 Michael-type hydroalkylation reaction of 2-cyclohexen-1-one with diphenylacetonitrile catalysed by  $\text{Ir}(\text{P}^i\text{Pr}_3)_2\text{H}_5$  in the presence of NaOPh as an additive.



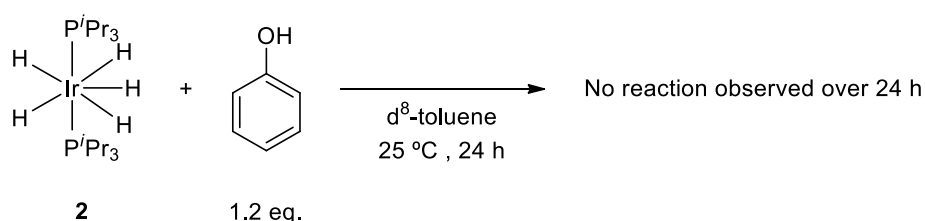
| Entry | t (h) | Ir (mol%) | NaOPh (mol%) | Yield (%) | Yield (%)<br>with PhOH* |
|-------|-------|-----------|--------------|-----------|-------------------------|
| 1     | 24    | -         | 0.5          | traces    | -                       |
| 2     | 16    | 0.5       | 0.5          | 59        | 87                      |
| 3     | 24    | 0.5       | 0.5          | 92        | 94                      |
| 4     | 16    | 0.5       | 5.0          | 76        | 88                      |
| 5     | 24    | 0.5       | 5.0          | 94        | 91                      |

Experimental conditions: reactions were carried out in toluene (1 mL), under argon atmosphere with the  $\text{Ir}(\text{P}^i\text{Pr}_3)_2\text{H}_5$  catalyst and NaOPh at 25 °C. Yields are based on quantitative GC analysis using *n*-dodecane as the internal standard. (\*) Yield for the same reaction performed using PhOH as the additive instead than NaOPh.

#### 3.3.11.4 Reactivity of iridium-pentahydride complex with phenol: no reaction, cyclohexenone is still needed

It has been demonstrated how cyclohexenone promotes the activation of the iridium-pentahydride catalyst **2** via a disproportionation reaction, yielding the iridium-phenoxide complex **62**. However ideally this complex could also be obtained by reaction of the phenol directly with the iridium-pentahydride complex, which would spontaneously loose the hydrides in the form of molecular hydrogen. If this is the case, then the addition of phenol improved the reaction not only facilitating the closure of the catalytic cycle, but also promoting the activation of the catalyst into the catalytically active species.

Indeed, to test this hypothesis, the reactivity of the iridium-pentahydride catalyst **2** with 1.2 equivalents of phenol was monitored over time by NMR spectroscopy at 25 °C to evaluate the formation of the iridium-phenoxide complex **62** (Scheme 3.38). However, from both the proton and phosphorus NMR spectra, no formation of the iridium-phenoxide complex **62** can be observed and the initial reaction mixture is comparable to the one after 24 hours (Figure 3.36 and Figure 3.37). To check whether the loss of hydrides and the subsequent formation of the desired phenoxide complex could be triggered by heating, the reaction mixture was heated up to 40 °C for 16 hours and then to 80 °C for an additional 4 hours, however at any time the result did not change. More prolonged heating led to complex decomposition.



Scheme 3.38 Reactivity of the iridium-pentahydride catalyst **2** with phenol (Ir:PhOH 1:1.2) under model reaction conditions screened with the time monitoring experiments by NMR spectroscopy.

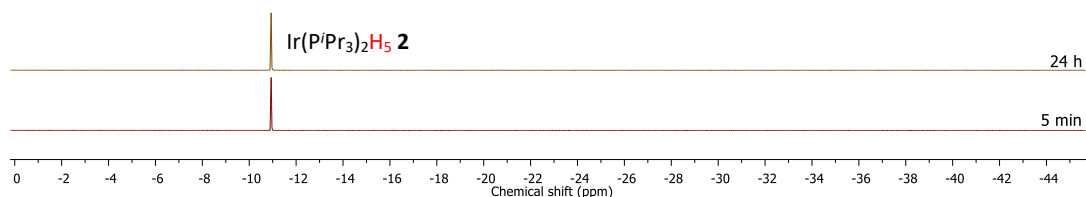


Figure 3.36 Stacked  $^1\text{H}$ -NMR spectra (298 K,  $\text{d}^8$ -toluene, 500 MHz), hydride region, of the time monitoring experiment of the reactivity of the iridium-pentahydride catalyst **2** with phenol (Ir:PhOH 1:1.2) under the model reaction conditions.

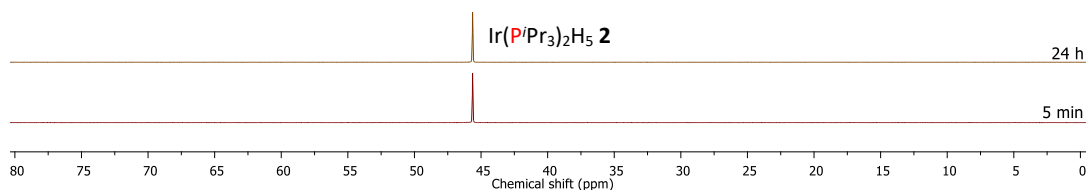


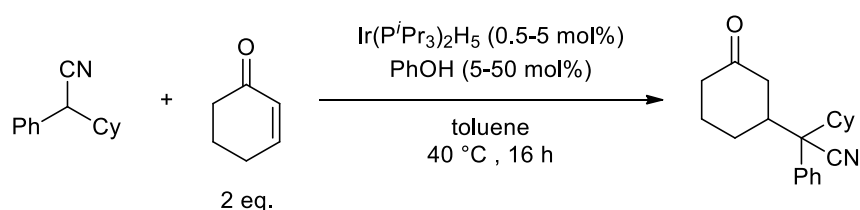
Figure 3.37 Stacked  $^{31}\text{P}\{^1\text{H}\}$ -NMR spectra (298 K,  $\text{d}^8$ -toluene, 202 MHz) of the time monitoring experiment of the reactivity of the iridium-pentahydride catalyst **2** with phenol (Ir:PhOH 1:1.2) under the model reaction conditions.

### 3.3.11.5 Use of phenol as an additive to improve the results for the hydroalkylation of difficult acetonitrile substrates

It has been demonstrated how the use of phenol as an additive can be beneficial for the Michael-type hydroalkylation of cyclohexenone with diphenylacetonitrile. The use of the phenol additive was investigated also with the cyclohexyl-phenyl-acetonitrile substrate, which has been previously identified as a difficult substrate together with the *iso*-propyl-substituted analogue. The cyclohexyl-phenyl-acetonitrile substrate gives a product yield of 58% with an increased catalyst loading of 10 mol%.<sup>152</sup> Therefore, the use of phenol additive has been investigated under the same reaction conditions, but varying the catalyst loading to see if a similar yield could be achieved using a lower amount of catalyst.

The cyclohexyl-phenyl-acetonitrile substrate was subjected to reaction with two equivalents cyclohexenone at 40 °C for 16 hours. Different loadings of Ir(P<sup>*i*</sup>Pr<sub>3</sub>)<sub>2</sub>H<sub>5</sub> were used together with the phenol additive, always in a 1:10 ratio with the iridium catalyst. The results are reported in Table 3.5 and as a comparison in brackets are the yields for the same reaction performed in the absence of phenol.<sup>152</sup> As it can be observed from Entry 3, when an iridium catalyst loading of 5 mol% was used in the presence of the phenol additive, the desired hydroalkylation product was isolated in 57% yield. In the absence of phenol with 5 mol% of catalyst loading, a yield of 51% was obtained. For the cyclohexyl-phenyl-acetonitrile substrate the use of phenol as an additive allowed to obtain similar yields using half of the catalyst loading.

Table 3.5 Results for the optimisation of the Michael addition of Cy-substituted phenylacetonitriles to cyclohexenone with phenol as an additive.



| Entry | Ir (mol%) | PhOH (mol%) | Yield (%) |
|-------|-----------|-------------|-----------|
| 1     | 0.5       | 5           | 21 (14)   |
| 2     | 2.5       | 25          | 43        |
| 3     | 5.0       | 50          | 57 (51)   |

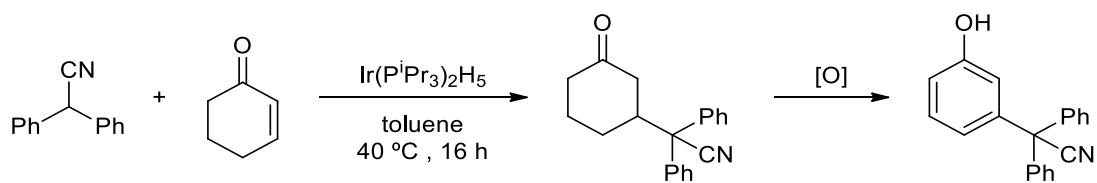
Experimental conditions: reactions were carried out in toluene (1 mL), under argon atmosphere with the Ir(P<sup>*i*</sup>Pr<sub>3</sub>)<sub>2</sub>H<sub>5</sub> catalyst and PhOH (10 eq. with respect to the iridium). Reported are isolated yields after chromatography and in brackets are the yields from the same reaction performed in the absence of phenol.<sup>152</sup>

To summarise the findings on the use of additives for the Michael-type hydroalkylation reaction of cyclohexenone with diphenylacetonitrile, it has been demonstrated how both the phenol and NaOPh can serve as additives and phenol has shown the fastest reaction rates. The effect of the use of the phenol additive, is more marked if the iridium-ylide-nitrile intermediate is used as the catalyst as higher yields and complete conversion were achieved compared to the classic iridium-pentahydride complex. Last, if a more difficult substrate is used, such as the cyclohexyl-substituted phenylacetonitrile, the presence of phenol additive allows to achieve similar yield with lower iridium catalyst loadings.

## 3.4 Towards the dehydrogenation of 3-substituted cyclohexanones to *meta*-substituted phenols

### 3.4.1 Introduction and background

To highlight the synthetic utility of the 3-substituted cyclohexanones product of the Michael-type hydroalkylation reaction, they can be subjected to subsequent dehydrogenation reaction to achieve *meta*-substituted phenols (Scheme 3.39).



Scheme 3.39 Dehydrogenation of substituted cyclohexanones to *meta*-substituted phenols.

Phenols are widely used in the chemical industry<sup>186-187</sup> and a common motif of drugs and natural products (Figure 3.38).<sup>188</sup> Therefore, the development of a simple approach to substituted phenols is highly desirable.

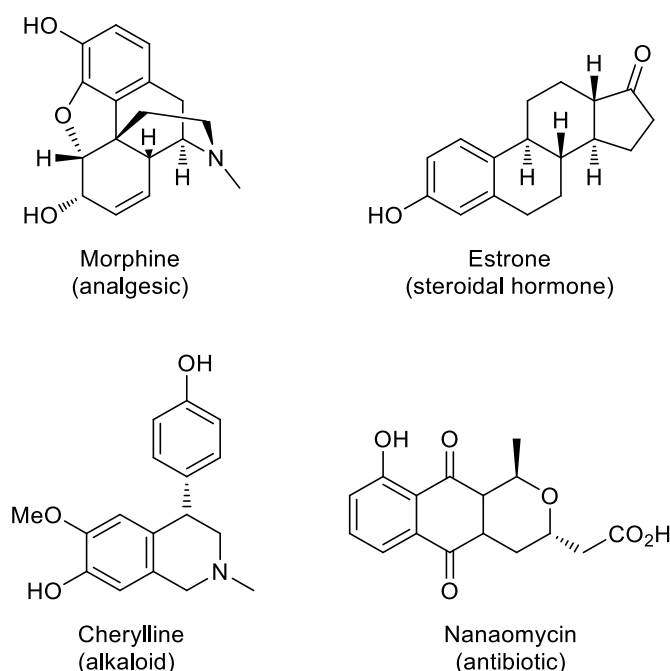
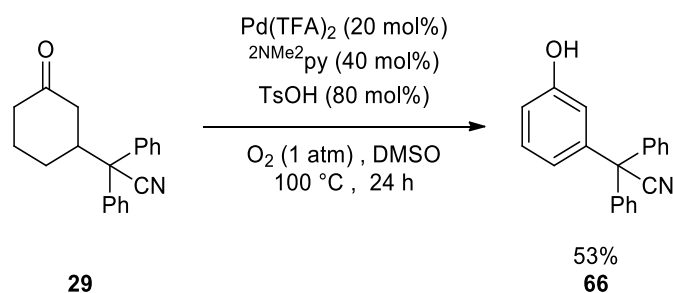


Figure 3.38 Drugs and natural products with phenolic structure.

The most common synthetic strategy to obtain substituted phenols is the electrophilic aromatic substitution on the phenolic ring. However, this approach gives access only to *ortho*- and *para*-substituted phenols due to the electronic directing effect of the hydroxyl group.<sup>188</sup> To access *meta*-substituted phenols is much more challenging and cannot be done



*via* common synthetic methodologies, however the use of long and complex multi-step syntheses is required.<sup>189</sup> In the past decades, alternative methods to obtain these highly desirable substrates have been developed, which involve the synthesis of substituted phenols from the corresponding cyclohexanones *via* catalytic dehydrogenation reactions.<sup>190-194</sup> Starting from the literature precedents, Marta Fernandez-Gimenez, optimised a catalytic dehydrogenation method based on the palladium-catalysed dehydrogenation of cyclohexanones to phenols reported by Stahl and co-workers.<sup>190</sup> This method, has been applied to synthesise *meta*-substituted phenols from the products of the Michael-type hydroalkylation reaction investigated.<sup>152</sup> The feasibility of this approach has been demonstrated with the dehydrogenation of cyclohexanone **29** catalysed by Pd(TFA)<sub>2</sub> in combination with 2-(N,N-dimethylamino)pyridine and *p*-toluensulfonic acid in the presence of molecular oxygen yielding the desired *meta*-substituted phenol **66** in 53 % yield (Scheme 3.40). However, the approach suffers from the formation of various side-products which impede to reach high product yields.



Scheme 3.40 Dehydrogenation of cyclohexanone **29** under the optimised Stahl conditions.

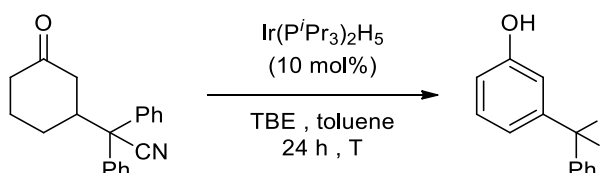
### 3.4.2 Attempts for the iridium-catalysed transfer dehydrogenation

With the aim of developing a general method for the synthesis of *meta*-substituted phenols, we decided to test the Ir(P<sup>*i*</sup>Pr<sub>3</sub>)<sub>2</sub>H<sub>5</sub> catalyst, which has not been tested before for this dehydrogenation reaction. This was the catalyst of choice for many different reasons. This catalyst has been reported to catalyse the dehydrogenation of various compounds, *in primis* alkane substrates (see previous chapter). Moreover, the iridium-pentahydride complex also catalyses the Michael-type hydroalkylation of cyclic  $\alpha,\beta$ -unsaturated ketones with alkyl aryl nitriles and indeed ideally a highly desirable one-pot hydroalkylation-dehydrogenation reaction could be achieved. Last, it has been demonstrated how the Ir(P<sup>*i*</sup>Pr<sub>3</sub>)<sub>2</sub>H<sub>5</sub> catalyst is able to dehydrogenate cyclohexenone to phenol *via* a disproportionation reaction (see Section 3.3.5.1).

### 3.4.2.1 Screening of temperatures

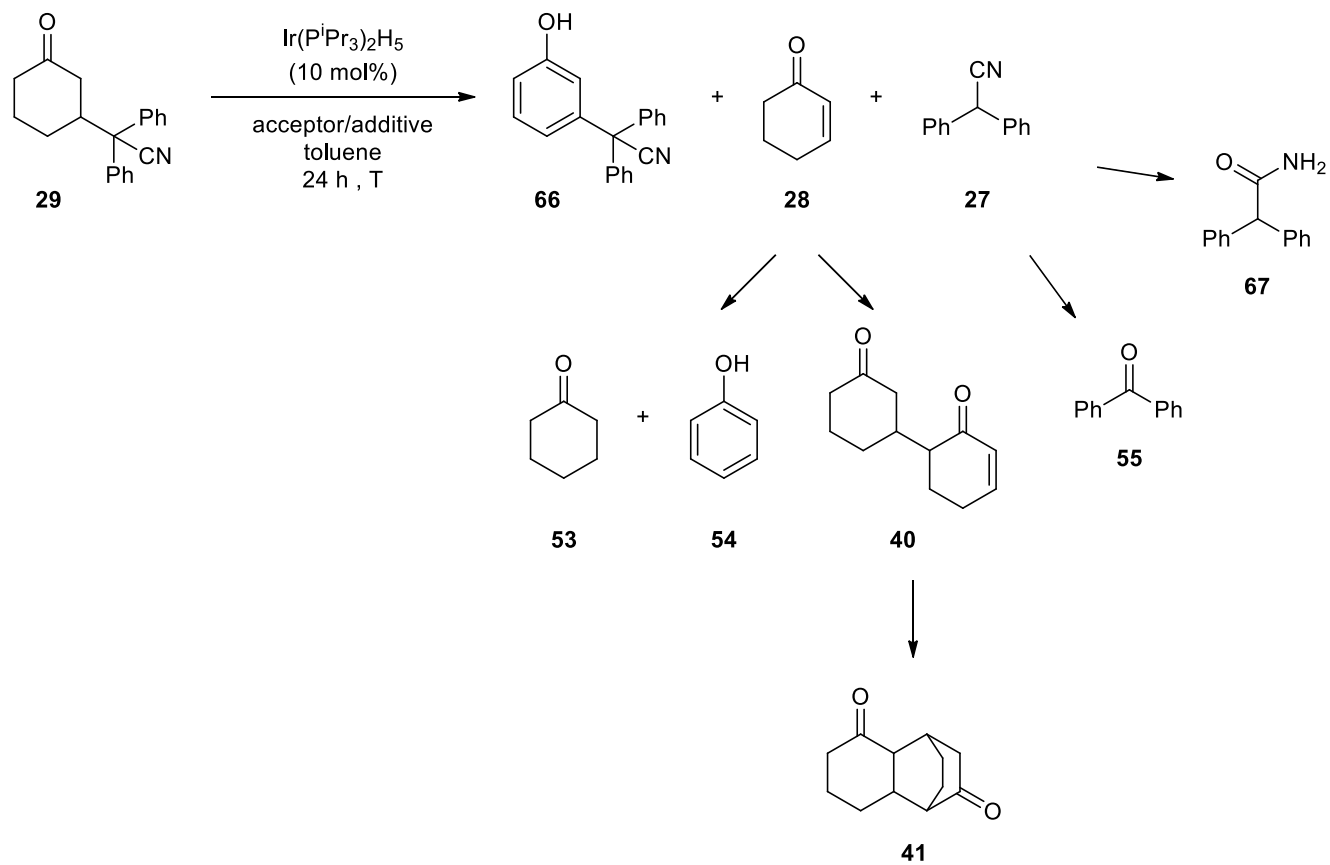
As a starting point  $\text{Ir}(\text{P}^i\text{Pr}_3)_2\text{H}_5$  was tested under the classic conditions used for the transfer alkane dehydrogenation, i.e. using TBE as the hydrogen acceptor. The choice of this hydrogen acceptor is also supported by literature data, in fact a similar complex,  $^t\text{BuPCPIrH}_2$ , has been reported to promote the dehydrogenation of cyclohexanone and 3-methyl-cyclohexanone to the corresponding phenols in the presence of TBE, although not catalytically.<sup>183</sup> Toluene is also chosen as the solvent as it has been previously used in the hydroalkylation reaction.

The first attempts for the dehydrogenation to *meta*-substituted phenol **66** were performed by reacting cyclohexanone **29** with  $\text{Ir}(\text{P}^i\text{Pr}_3)_2\text{H}_5$  catalyst, in the presence of TBE as the hydrogen acceptor for 24 hours at various temperatures starting from reflux conditions (120 °C) (Scheme 3.41).



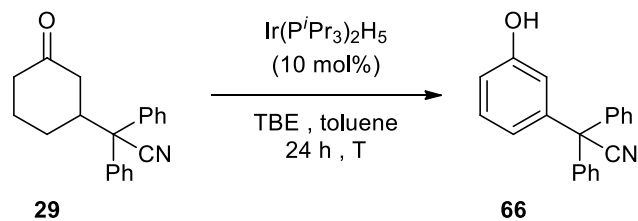
Scheme 3.41 Reaction scheme for the transfer dehydrogenation of cyclohexanone **29** to *meta*-substituted phenol **66** using  $\text{Ir}(\text{P}^i\text{Pr}_3)_2\text{H}_5$  as the catalyst and TBE as the hydrogen acceptor.

Unfortunately, after the experiments, the desired *meta*-substituted phenol **66** was not formed under any of the temperatures tested (Table 3.6). At first, the reaction was tested under reflux conditions at 120 °C, however formation of diphenylacetone, cyclohexenone, cyclohexanone and phenol side-products was observed (Entry 1). The formation of all the possible side-products is shown in Scheme 3.42. The formation of those side-products is not surprising, cyclohexenone **28** and diphenylacetone **27** are formed *via* a C-C bond cleavage of ketone **29** in a retro-Michael addition reaction. Previously has also been demonstrated how the  $\text{Ir}(\text{P}^i\text{Pr}_3)_2\text{H}_5$  catalyst promotes a cyclohexenone disproportionation reaction to yield cyclohexanone **53** and phenol **54** (see Section 3.3.5.1). With the aim of reducing the formation of side-products the reaction was performed at lower temperatures: 80 and 40 °C (Entries 2 and 3 respectively). At 40 °C, secondary reactions as the formation of cyclohexanone and phenol were suppressed, however also the conversion was dramatically decreased and the desired product **66** still could not be formed. Formation of trace amounts of benzophenone **55** are also observed.



Scheme 3.42 Possible side-products formed during the iridium-catalysed transfer dehydrogenation of ketone **29** to *meta*-substituted phenol **66**.

Table 3.6 Screening of temperatures for the the iridium-catalysed transfer dehydrogenation of ketone **29** to *meta*-substituted phenol **66** (see Scheme 3.42 for formation of side-products).



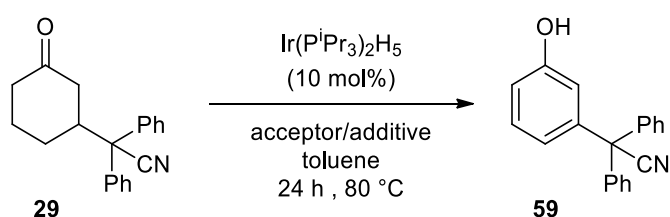
| Entry | T (°C) | <b>29</b><br>Conv. (%) | <b>66</b><br>Yield (%) | <b>28</b><br>Yield (%) | <b>27</b><br>Yield (%) | <b>53</b><br>Yield (%) | <b>54</b><br>Yield (%) | <b>55</b><br>Yield (%) |
|-------|--------|------------------------|------------------------|------------------------|------------------------|------------------------|------------------------|------------------------|
| 1     | 120    | 100                    | -                      | 0                      | 88                     | 24                     | 40                     | -                      |
| 2     | 80     | 97                     | -                      | 13                     | 70                     | 27                     | 40                     | traces                 |
| 3     | 40     | 36                     | -                      | 23                     | 25                     | -                      | -                      | traces                 |

Conversions and yields are based on the quantitative analysis by GC using *n*-dodecane as the internal standard. Compounds have been confirmed by analysis by GC-MS and matching with the mass spec database.

### 3.4.2.2 Screening of hydrogen acceptor and additives

The temperature screening reaction have shown that the Michael-type hydroalkylation is a reversible reaction as the  $\text{Ir}(\text{P}^i\text{Pr}_3)_2\text{H}_5$  catalyst is also able to catalyse the retro- Michael addition, releasing back the starting cyclohexenone and diphenylacetonitrile. As this is an equilibrium reaction, the addition of reagents should shift the equilibrium towards the products, i.e. cyclohexanone **29**. If the product formation is favoured, it is also made available to undergo further reaction, i.e. our desired dehydrogenation to *meta*-substituted phenols.

To test this idea, the same reaction was performed using cyclohexenone **28** or diphenylacetonitrile **27** in conjunction with or instead of TBE (Scheme 3.43).

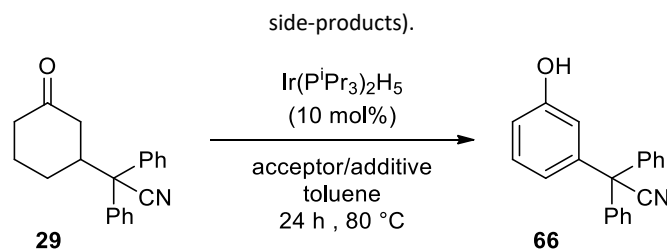


Scheme 3.43 Reaction scheme for the transfer dehydrogenation of cyclohexanone **29** to *meta*-substituted phenol **59** using  $\text{Ir}(\text{P}^i\text{Pr}_3)_2\text{H}_5$  as the catalyst with various additives with or without hydrogen acceptor.

The tests were performed with 10 equivalents of the different additives, with and without the same amount of TBE. The results are reported in Table 3.7, but unfortunately, in any case the desired dehydrogenated product **66** was not observed. Instead, many side-products were formed in variable amounts, such as diphenylacetonitrile, benzophenone, cyclohexenone, cyclohexanone and phenol as before, together with the double-Michael addition product **41** and the amide **67** (Scheme 3.42). Formation of the cyclohexenone dimer **41** has been described previously (Section 3.2.1); amide **67** instead can be formed *via* an hydration reaction of the nitrile group of the diphenylacetonitrile by some moisture present in the system.

Due to the lack of encouraging results for the dehydrogenation of cyclohexanone **29** to *meta*-substituted phenol **66** catalysed by  $\text{Ir}(\text{P}^i\text{Pr}_3)_2\text{H}_5$  catalyst, the focus has been redirected towards other experiments.

Table 3.7 Screening of hydrogen acceptor and additives for the the iridium-catalysed transfer dehydrogenation of ketone **29** to *meta*-substituted phenol **66** (see Scheme 3.42 for formation of



| Entry | TBE<br>(eq.) | (eq.) | <b>28</b><br>Conv. (%) | Yield (%) | (eq.) | <b>27</b><br>Conv. (%) | Yield (%) | <b>29</b><br>Conv. (%) | <b>66</b><br>Yield (%) | <b>53</b><br>Yield (%) | <b>54</b><br>Yield (%) | <b>55</b><br>Yield (%) | <b>41</b><br>Yield (%) | <b>67</b><br>Yield (%) |
|-------|--------------|-------|------------------------|-----------|-------|------------------------|-----------|------------------------|------------------------|------------------------|------------------------|------------------------|------------------------|------------------------|
| 1     | -            | 10    | 45                     | n.a.      | -     | n.a.                   | 18        | 58                     | -                      | 179*                   | 151*                   | traces                 | 18                     | traces                 |
| 2     | 10           | 10    | 36                     | n.a.      | -     | n.a.                   | 17        | 58                     | -                      | 213*                   | 197*                   | traces                 | 15                     | traces                 |
| 3     | -            | -     | n.a.                   | 18        | 10    | 17                     | n.a.      | 43                     | -                      | -                      | -                      | traces                 | -                      | traces                 |
| 4     | 10           | -     | n.a.                   | 9         | 10    | 20                     | n.a.      | 43                     | -                      | traces                 | traces                 | traces                 | -                      | traces                 |

Conversions and yields are based on the quantitative analysis by GC using *n*-dodecane as the internal standard. Compounds have been confirmed by analysis by GC-MS and matching with the mass spec database. (\*) for consistency those yields, as all the others, have been calculated with respect to reagent **29**; however, those numbers look so high because in those two experiments 10 eq. of ketone **28** have also been used.

### 3.4.3 Attempts for the ultrasound-promoted Stahl dehydrogenation

The dehydrogenation of cyclohexanone **29** to *meta*-substituted phenol **66** has been previously achieved by Marta Fernandez-Gimenez in 53 % yield by optimising for this specific substrate the conditions reported by Stahl and co-workers.<sup>152, 190</sup> However as discussed, this approach requires a reaction temperature of 100 °C (Scheme 3.40). With the aim to perform this transformation under milder reaction conditions, this reaction has been tested *via* ultrasound activation, rather than thermal.

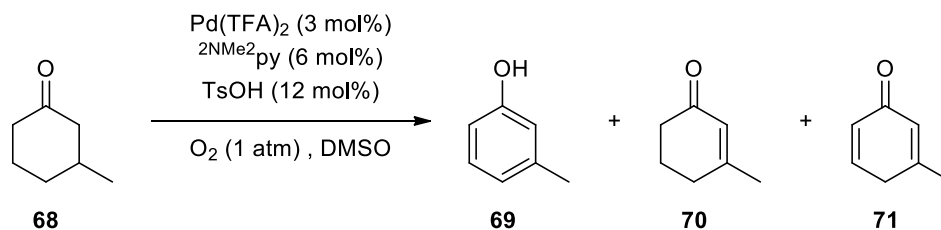
To exemplify the system, 3-methyl-cyclohexanone **68** was chosen as the benchmark substrate, with the idea to possibly in the future further extend the reaction to the hydroalkylation product **29**. Also, the reaction conditions reported by Stahl have been chosen as a starting point, i.e. 3 mol% of Pd(TFA)<sub>2</sub> catalyst in combination with 6 mol% of 2-(N,N-dimethylamino)pyridine and 12 mol% of *p*-toluensulfonic acid in the presence of molecular oxygen.<sup>190</sup> By reproducing the literature reaction at 80 °C for 24 hours (Table 3.8, Entry 2), a product yield of 20% was obtained. The lower yield obtained compared to the literature can be due to the different system used. In our case in fact the reaction was performed in a 4 mL vial equipped with a stirring bar and inserted in a heating block over a classic stirring plate, with the oxygen supplied *via* a balloon piercing the septa of the vial lid. In the literature instead they used a fit for purpose system, a large capacity mixer (Glas-Col) which guaranteed the delivery of a constant pressure of 1 atm of molecular oxygen, controlled temperature and orbital agitation.<sup>190</sup> Together with the desired dehydrogenation product **69**, also mono- and di-dehydrogenation products were detected. Formation of cyclohexenones **70** and **71** can be explained by the palladium catalysed dehydrogenation of cyclohexanones proposed by Stahl (Scheme 3.44).<sup>195</sup> The ultrasound-mediated dehydrogenation reaction was run in the same reactor which have been developed for the sonochemical transfer alkane dehydrogenation (*see* Figure 2.3 in the previous chapter), with the only difference that the reactor was not connected to the Schlenk line, but the side-arm of the system was sealed with a septum to which the oxygen balloon was fitted. To use this reactor, the reaction volume had to be increased from 0.36 ml to 5 mL, the same scaled-up reaction has been also performed under thermal activation for reliable comparison (Entries 3 and 4). Then, as the ultrasound-promoted reaction would have been performed at room temperature, a final control experiment was run without heating (Entry 5), which confirms that the desired dehydrogenation product **69** cannot be obtained without heating. The ultrasound-promoted cyclohexanone dehydrogenation was performed and products analysed after 1 hour of active sonication (Entry 6). The desired phenol **69** was detected only in 1% yield, while the mono-

and di-dehydrogenation product in 14% and 16% yield respectively. Clearly those yields are very low, however dehydrogenation products were detected in higher amounts compared to the same reaction performed without ultrasound irradiation (Entry 5). Ultrasound irradiation seems to favour the formation of cyclohexenone **70** over the desired phenol, however cyclohexenone **70** is just an intermediate for the formation of phenol **69** as described in Scheme 3.44. Indeed, encouraged by those results, the ultrasound mediated dehydrogenation was performed for longer times, hoping that cyclohexenone **70** could be converted into phenol **69** over time. Unfortunately, after both 2 and 3 hours of active sonication, yields of the dehydrogenation products did not increase (Entries 6 and 7) and were comparable to what has been obtained after 1 hour. The fact that the amounts of products remained the same at all times, suggests that the catalyst was not active anymore, probably decomposed under ultrasound irradiation.

Although ultrasound do not seem to promote the dehydrogenation of cyclohexanone **29** to *meta*-substituted phenol **66**, once again this result can be imputed to the catalyst stability under ultrasound irradiation. However, the formation of dehydrogenation products such as cyclohexenone **70** and **71** confirmed that the catalyst can be activated *via* the ultrasound method.

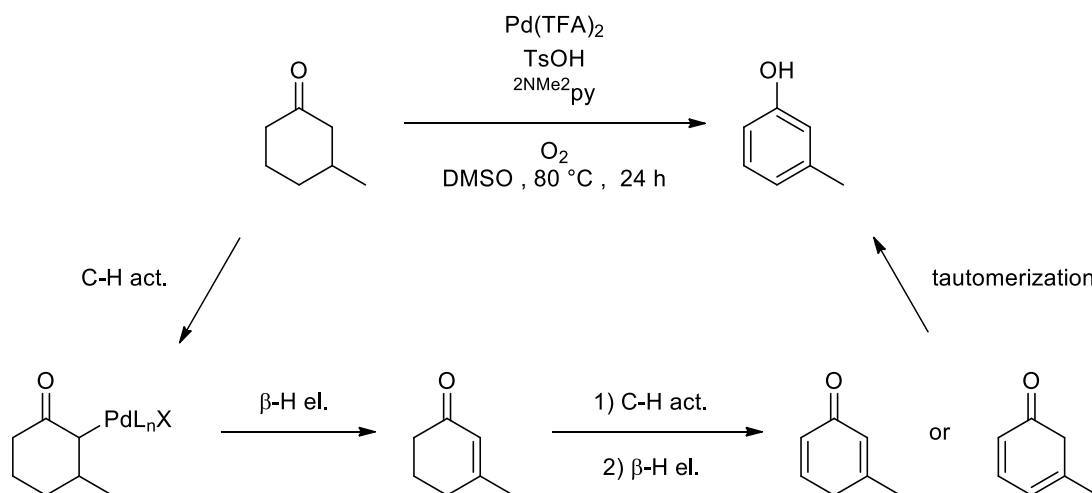


Table 3.8 Attempts for the ultrasound-promoted dehydrogenation of cyclohexanone **68** to phenol **69** catalysed by Pd(TFA)<sub>2</sub> and reference reaction under thermal activation.



| Entry | T (°C) | V (mL) | t (h) | <b>68</b><br>Conv. (%) | <b>69</b><br>Yield (%) | <b>70</b><br>Yield (%) | <b>71</b><br>Yield (%) |
|-------|--------|--------|-------|------------------------|------------------------|------------------------|------------------------|
| 1     | 80     | 0.36   | 1     | 20                     | 4                      | 11                     | 2                      |
| 2     | 80     | 0.36   | 24    | 29                     | 20                     | 3                      | 1                      |
| 3     | 80     | 5      | 1     | 12                     | 1                      | 3                      | 1                      |
| 4     | 80     | 5      | 24    | 46                     | 26                     | 2                      | 1                      |
| 5     | r.t.   | 0.36   | 2     | 19                     | 0                      | 7                      | 3                      |
| 6     | US     | 5      | 1*    | 32                     | 1                      | 14                     | 6                      |
| 7     | US     | 5      | 2*    | 32                     | 2                      | 14                     | 6                      |
| 8     | US     | 5      | 3*    | 30                     | 2                      | 15                     | 6                      |

Conversions and yields are based on the quantitative analysis by GC using *n*-dodecane as the internal standard. Compounds have been confirmed by analysis by GC-MS and matching with the mass spec database. (\*) The time reported in the table refers to the time of active sonication, the total reaction time is two times this amount.



Scheme 3.44 Mechanism for the Pd-catalysed dehydrogenation of cyclohexanones to phenols proposed by Stahl.

### 3.5 Conclusions

In the present chapter, the developments on a novel iridium-catalysed Michael-type hydroalkylation reaction of cyclic  $\alpha,\beta$ -unsaturated ketones with non-activated nitriles have been presented. This Michael-type hydroalkylation occurs under mild conditions and provides a straightforward access to new substituted cyclohexanones containing a quaternary centre, starting from non-activated nitriles as Michael-donors. These products could be used as building blocks in the chemical industry for the production of pharmaceuticals.<sup>154-155</sup>

The acetonitrile scope of the iridium-catalysed Michael-type hydroalkylation of  $\alpha,\beta$ -unsaturated cyclohexenone with non-activated alkyl-aryl-nitriles has been completed with the pyridyl-substituted series. Despite these starting materials all contained a 2-pyridylacetonitrile moiety with an additional electron donating group attached to the central carbon atom (R = Cy, <sup>i</sup>Pr, Bn), which makes them extremely weakly acidic substrates, the reaction occurs under mild conditions (40 °C), with catalyst loadings of 5-10 mol% for bulky 2-pyridyl analogues such as with benzyl, *iso*-propyl and cyclohexyl groups. Three novel compounds, benzyl-, *iso*-propyl- and cyclohexyl-substituted oxocyclohexyl-pyridinyl-acetonitriles (compounds **50**, **51** and **52**), have been isolated and fully characterised. These are interesting compounds because of the pyridyl moiety on the 3-substituted cyclohexanone, that makes them viable for post-functionalisation reactions.

The mechanistic investigation of this Michael-type hydroalkylation, undertaken to confirm the reaction mechanism and to identify possible intermediate complexes, lead to some interesting findings. Based on that, a revised catalytic cycle has been proposed. The iridium-pentahydride catalyst **2** is converted into the catalytically active species *via* a cyclohexenone disproportionation reaction, where four molecules of cyclohexenone react with catalyst **2** to yield the iridium-phenoxide intermediate **62** and three molecules of cyclohexanone. Then, coordination of a molecule of diphenylacetonitrile lead to the formation of the isolated iridium-nitrile-phenoxide intermediate **65**. Subsequent C-H activation and coordination of another molecule of nitrile yield the iridium-ylide-nitrile complex **59**, which has been confirmed to be an intermediate of the hydroalkylation reaction and possible catalyst resting state. Coordination of cyclohexenone and intramolecular nucleophilic attack releases the desire hydroalkylation product. Oxidative addition of a phenol molecule then closes the catalytic cycle, regenerating the catalytically active iridium-phenoxide intermediate **62**. The mechanistic investigation allowed to identify three complexes to be reaction intermediates (**62**, **65** and **59**). Two have been isolated and

characterised as novel complexes, the iridium-phenoxide intermediate **62** and the iridium-nitrile-phenoxide intermediate **65**. An analogue of the iridium-phenoxide intermediate bearing cyclohexyl-phosphines (complex **63**) has also been synthesised and characterised. The iridium-phenoxide **62** and iridium-ylide-nitrile **59** complexes have also been tested as catalyst for the hydroalkylation reaction, showing higher activity compared to the classic iridium-pentahydride complex. The use of phenol as an additive to the Michael-type hydroalkylation reaction was found to increase the reaction rate. When the complex **59** was used as catalyst, the use of phenol can remarkably improve the yield. With a difficult substrate, such as the cyclohexyl-substituted phenylacetonitrile, comparable yields were achieved in the presence of phenol and with lower iridium catalyst loadings.

### 3.6 Possible future plans

First, the proposed mechanism needs to be further investigated by conducting kinetic and DFT studies to support the proposed catalytic cycle. Furthermore, the identified iridium-nitrile-phenoxide intermediate **65** and the iridium-phenoxide complex bearing cyclohexylphosphines (complex **63**) needs to be further characterised by other characterisation methods, other than NMR spectroscopy. Ideally *via* x-ray crystallography and mass spectrometry under inert atmosphere, however accessibility issues to the facilities impeded to obtain the desired data on time.

The iridium-phenoxide intermediate **65** has been identified to be the best catalyst for the Michael-type hydroalkylation of cyclohexenone with diphenylacetonitrile. At this time the complex is synthesised starting from the iridium-pentahydride catalyst **2**, which is a time consuming and expensive approach. Indeed, an alternative synthetic pathway to obtain this complex is desirable. An easier access to this complex will also allow to test it more thoroughly for the Michael-type hydroalkylation of cyclohexenone with other alkyl-aryl-acetonitrile substrates, hopefully increasing the yields of the most difficult ones.

The novel iridium-phenoxide complex **62** could also be tested as catalyst in other iridium-catalysed reactions with C-H acidic substrates.

The development of a method for the one-pot hydroalkylation-dehydrogenation to synthesise *meta*-substituted phenols starting from cyclohexenones and alkyl-aryl-substituted acetonitriles needs to be further investigated. A more extensive screening of catalysts, hydrogen acceptors and reaction conditions is required to try to decrease the formation of side-products in favour of the desired *meta*-substituted phenol.

## 3.7 Experimental section

### 3.7.1 Materials and general procedures

All reactions and manipulations were performed under argon atmosphere either in a glovebox or using standard Schlenk techniques and apparatus. All glassware and magnetic stirring bars were kept in an oven at 120 °C for at least two hours and let to cool down under vacuum before use.

Solvents used in the syntheses were dried and distilled under argon by standard procedures<sup>148</sup> and stored under an Argon atmosphere. THF, Et<sub>2</sub>O, toluene, hexane, and chloroform were dried by distillation over Na-benzophenone ketyl. MeOH was distilled over CaH<sub>2</sub>. Anhydrous benzene was purchased from Alfa Aesar and stored under argon in the glovebox. All distilled solvents were stored either in Sure/Stor™ flasks under argon or in the glovebox. Acetone and *i*-PrOH were degassed by several freeze-pump-thaw cycles, stored in Sure/Stor™ flasks under argon and used fresh.

2-Cyclohexen-1-one was purified by passing through basic aluminium oxide and stored in an argon-atmosphere glovebox. n-Dodecane, used as GC standard, was dried over 4 Å molecular sieves, degassed by several freeze-pump-thaw cycles and stored in an argon-atmosphere glovebox or Sure/Stor™ flasks under argon.

Deuterated solvents were purchased from Cambridge Isotopes; they were degassed by several freeze-pump-thaw cycles and stored over 4 Å molecular sieves under an argon atmosphere in Sure/Stor™ flasks.

All other reagents were used as received without any further purification. All chemicals were purchased from commercial suppliers (Merck Sigma-Aldrich, Alfa Aesar, Strem Chemicals, Pressure Chemicals, Cambridge Isotopes, TCI, VWR or Fisher chemical companies).

### 3.7.2 Equipment and methods

For catalytic reactions, quantitative analyses were performed by gas chromatography on an Agilent 7890A GC system equipped with a HP-5 column (Fused Silica Capillary Column 30 m x 0.32 mm ID x 0.25 µm film thickness). The GC was equipped with an FID detector. For details on instruments parameters see Section 3.7.3.

GC-MS analyses were performed on a Thermo Scientific GC directly interfaced to an ISQ Single Quadrupole equipped with an HP-1 column (Fused Silica Capillary Column 30 m x 0.25 mm ID x 0.25 µm film thickness). For details on instruments parameters see Section 3.7.3.

Mass spectrometry analyses were conducted by the EPSRC UK National Mass Spectrometry Facility at Swansea University. Samples of compounds were sent to Swansea University in sealed ampullas under argon. Spectra were acquired under argon on an Agilent QTOF 6540 using EI and ASAP ionisation methods.

Elemental analyses were performed by the departmental Microanalysis Laboratory on a Thermo Flash EA 112 Series instrument.

Nuclear Magnetic Resonance (NMR) spectra were acquired on a Bruker Avance III 500 MHz, Bruker 400 MHz and Bruker DPX 400 MHz spectrometers. Chemical shifts for  $^1\text{H}$ -NMR and  $^{13}\text{C}$ -NMR are reported in ppm relative to a peak of residual solvent with ppm as reported in the literature,<sup>149</sup> for  $^{31}\text{P}$ -NMR relative to  $\text{H}_3\text{PO}_4$ . The data are reported as follows: chemical shift in ppm ( $\delta$ ); multiplicity; coupling constants in Hz (J); integration, assignment. The splitting patterns are designated as follows: s (singlet), d (doublet), t (triplet), q (quartet), m (multiplet), dd (doublet of doublets), dt (doublet of triplets), br (broad).

IR spectra were acquired on a Perkin Elmer FT-IR Spectrum 100 spectrometer and on a Bruker alpha FT-IR platinum ATR spectrometer.

Analytical thin-layer chromatography (TLC) was performed on Whatman F254 precoated silica gel plates (250  $\mu\text{m}$  thickness) visualizing with UV light (254 nm). Column chromatography was performed using Whatman Silica Gel 60 Å (230-400 mesh).

The glovebox used was argon filled Innovative Technologies PureLab HE cp-1.

Sonochemical experiments were performed using a Sonic Dismembrator Ultrasonic Processor (Fisher Scientific™, Model 705, 50/60 Hz, 700 W): equipped with a 1/8" Microtip (Fisher Scientific™, Catalog n. F6318); inside a Sound Enclosure (Fisher Scientific™, Catalog n. F622B).

Crystal data were collected on a Rigaku Oxford Diffraction SuperNova diffractometer using Cu K $\alpha$  radiation; the structures were solved by direct methods using ShelXT and refined by least squares using ShelXL. Metal bound hydrogen atoms were located in the difference map and refined isotropically. Single crystals were mounted on Mitegen using Paratone-N oil and cooled under a stream of nitrogen.

### 3.7.3 Quantitative analysis methods for the catalytic experiments

Quantitative analyses of the reaction mixtures were carried out by GC using the internal standard method, with *n*-dodecane as ISTD. Each aliquot of the reaction mixture was filtered by passing through a short silica gel column (a glass Pasteur pipette filled with 2 cm of silica

gel) and eluted with the required amount of EtOAc (10.5 mL of EtOAc per mL of reaction mixture) in order to obtain a final standard concentration of 0.01 M for *n*-dodecane.

### 3.7.3.1 GC-FID technique

A standard GC analysis involved the analysis of the sample solution prepared accordingly as described above. Then, 1  $\mu$ L of this sample solution, was injected into the GC. The Agilent 7890A GC system was equipped with a HP-5 column. Response factors of each analyte were determined by Multiple Point Internal Standard Quantitation Method with respect to authenticated samples of *n*-dodecane. See the following tables for more details on the instrument parameters and methods.

| <b>AGILENT 7890A INSTRUMENTS PARAMETERS</b> |                   |
|---|-------------------|
| Carrier gas                                 | He                |
| Inlet Temperature                           | 250 °C            |
| Control Mode                                | Constant Pressure |
| Pressure                                    | 14.89 psi         |
| Injection Volume                            | 1 $\mu$ L         |
| Split Ratio                                 | 50:1              |
| Detector Temperature                        | 250 °C            |
| H <sub>2</sub> Flow                         | 35 mL/min         |
| Air Flow                                    | 300 mL/min        |
| Make Up Flow (N <sub>2</sub> )              | 20 mL/min         |

| <b>HP-5 COLUMN PROGRAM</b> |               |                |
|----------------------------|---------------|----------------|
| <b>Rate (°C/min)</b>       | <b>T (°C)</b> | <b>t (min)</b> |
| -                          | 50            | 5              |
| 5                          | 80            | 5              |
| 40                         | 250           | 10             |

### 3.7.3.2 GC-MS technique

A standard GC-MS analysis involved the analysis of the sample solution prepared accordingly as described above. Then, 1  $\mu\text{L}$  of this sample solution, was injected into the GC-MS system. The Thermo Scientific GC system was equipped with a HP-1 column. The GC was directly interfaced to an ISQ Single Quadrupole system. The compounds were identified against the database. See the following tables for more details on the instrument parameters and methods.

---

#### Thermo Scientific GC with ISQ Single Quadrupole INSTRUMENTS PARAMETERS

---

|                                |                   |
|--------------------------------|-------------------|
| Carrier gas                    | He                |
| Inlet Temperature              | 250 °C            |
| Control Mode                   | Constant Pressure |
| Pressure                       | 14.89 psi         |
| Injection Volume               | 1 $\mu\text{L}$   |
| Split Ratio                    | 50:1              |
| Detector Temperature           | 250 °C            |
| H <sub>2</sub> Flow            | 35 mL/min         |
| Air Flow                       | 300 mL/min        |
| Make Up Flow (N <sub>2</sub> ) | 20 mL/min         |
| MS Transfer Line Temperature   | 250 °C            |
| Ion Source Temperature         | 200 °C            |
| Ionisation mode                | EI                |

---

---

#### HP-1 COLUMN PROGRAM

---

| Rate (°C/min) | T (°C) | t (min) |
|---------------|--------|---------|
| -             | 50     | 2       |
| 20            | 250    | 10      |
| -             | 250    | 7       |

---



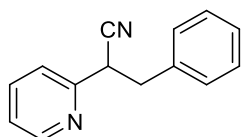
### 3.7.4 Synthesis of the catalysts

See the experimental section of the previous chapter (Section 2.13.3).

### 3.7.5 Synthesis of the substrates

#### 3.7.5.1 Synthesis of 3-phenyl-2-(pyridin-2-yl)propanenitrile (42)

Synthesised according to literature procedure.<sup>169</sup>



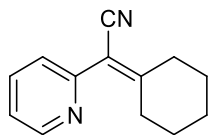
A Schlenk bomb equipped with magnetic stirring was charged with potassium hydroxide (0.16 g, 2.90 mmol) and  $[\text{IrCp}^*\text{Cl}_2]_2$  (0.42 g, 0.528 mmol). Benzyl alcohol (7.22 g, 66.7 mmol) was then added together with 2-pyridylacetonitrile (2.58 g, 21.8 mmol) in one portion, obtaining a dark brown solution. The reaction mixture was heated to 100 °C for 23.5 hours, with no colour change observed. The reaction mixture was purified *via* flash chromatography (silica gel, eluent: DCM/methanol, 95:5) without previous manipulation. The purified product was obtained as a yellow oil (0.83 g) in 18% yield.

<sup>1</sup>H-NMR (400 MHz,  $\text{CDCl}_3$ )  $\delta$  8.63 (d,  $J$  = 5.0 Hz, 1H, Py-H), 7.65 (td,  $J$  = 1.9, 7.8 Hz, 1H, Py-H), 7.28-7.23 (m, 5H, aromatic Ph-H), 7.15 (m, 2H, Py-H), 4.21 (dd,  $J$  = 5.8, 8.6 Hz, 1H, NC-CH), 3.36 (dd,  $J$  = 5.8, 13.6 Hz, 1H,  $\text{CH}_2$ ), 3.26 (dd,  $J$  = 8.6, 13.6 Hz, 1H,  $\text{CH}_2$ ). <sup>13</sup>C{<sup>1</sup>H} NMR (101 MHz,  $\text{CDCl}_3$ )  $\delta$  155.5 (C), 149.9 (C), 136.9 (CH), 134.7 (CH), 129.2 (CH), 128.4 (CH), 127.7 (CH), 123.1 (CH), 121.9 (CH), 119.0 (CN), 46.4 (CH), 36.4 ( $\text{CH}_2$ ).

IR (FTIR)  $\nu_{\text{max}}/\text{cm}^{-1}$  3054 w (aromatic C-H stretch), 2941 s (alkyl C-H stretch), 2239 w (CN), 1495 s (aromatic C=C bending), 1453 s (aromatic C=C stretch).

#### 3.7.5.2 Synthesis of cyclohexyl-2-pyridylacetonitrile (44)

##### 3.7.5.2.1 Synthesis of 2-cyclohexylidene-2-(pyridin-2-yl)acetonitrile (46)



To 250 ml 2-neck round bottom flask equipped with magnetic stirring 2-pyridylacetonitrile (3.05 g, 25.8 mmol) was added, followed by piperidine (0.0833 g, 0.978 mmol), benzene (100 mL) and cyclohexanone (8.35 g, 85.1 mmol). Acetic acid (0.085 g, 1.41 mmol) was then added, turning the solution dark brown. The flask was fitted with a Dean Stark condenser and the reaction was heated to 90 °C. The reaction progression was monitored with TLC at time-points: 3 h, 4 h, 10 h, 14 h, 38 h, 109 h, 179 h, and 228 h. The reaction was stopped after 228 h (9.5 days). The reaction mixture was filtered by gravity and water (15 mL) was added. The organic layer was separated and washed with water (2 x 50 mL), and the combined aqueous layer was re-extracted with

hexane (2 x 30 mL). The combined dark brown organic phase was dried over Na<sub>2</sub>SO<sub>4</sub> and filtered by gravity. The solvent was concentrated under reduced pressure, yielding the crude product as a yellow oil (7.54 g), purified by vacuum distillation: the first fraction (clear oil) was collected at 108 °C oil bath, 35 °C vapour pressure and 180 mbar. The second fraction (yellow oil) was collected at 135 °C oil bath, 65 °C vapour pressure and 60 mbar. The third fraction (bright orange/red) was collected at 165 °C oil bath, 130 °C vapour pressure and 4.3 x 10<sup>-1</sup> mbar. The third fraction crystallised upon standing yielding the product as orange crystals (2.08 g) in 41% yield.

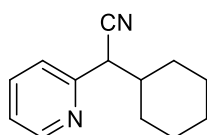
<sup>1</sup>H NMR (400 MHz, CDCl<sub>3</sub>) δ 8.60 (d, J = 4.7 Hz, 1H, Py-H), 7.72 (td, J = 1.6, 7.7 Hz, 1H, Py-H), 7.42 (d, J = 7.8 Hz, 1H, Py-H), 7.24 (m, 1H, Py-H), 3.87 (d, J = 6.1 Hz, 1H, NC-CH), 2.05 (m, 1H, NC-CH-CH-), 1.72 (m, 5H, cyclohexyl-H), 1.24 (m, 5H, cyclohexyl-H). <sup>13</sup>C{<sup>1</sup>H} NMR (101 MHz, CDCl<sub>3</sub>) δ 153.4 (C), 149.2 (CH), 136.4 (CH), 130.8 (C), 129.2 (C), 123.8 (CH), 123.4 (CH), 115.9 (CN), 30.1 (2CH<sub>2</sub>), 27.5 (CH<sub>2</sub>), 26.6 (2CH<sub>2</sub>).

Elemental analysis: calculated for C<sub>13</sub>H<sub>14</sub>N<sub>2</sub>: C 78.75; H 7.12; N 14.13; found C: 78.18; H 7.02; N 14.23.

IR (FTIR) ν<sub>max</sub>/cm<sup>-1</sup> 2931 s (sp<sup>3</sup> C-H), 2857 w (sp<sup>2</sup> C-H), 2213 w (CN).

HRMS (CI<sup>+</sup>) m/z 199.1226 (M+H)<sup>+</sup> (199.123 calculated for C<sub>13</sub>H<sub>14</sub>N<sub>2</sub> (M+H)<sup>+</sup>).

### 3.7.5.2.2 Synthesis of 2-cyclohexyl-2-(pyridin-2-yl)acetonitrile (44)



To a 100 ml Schlenk flask equipped with magnetic stirrer the orange crystals previously obtained (2.08 g, 10.5 mmol) were charged followed by EtOH (25 ml). The system was evacuated and refilled with argon three times. 10% Pd/C (207 mg, 10% w/w) was added, and the system was again evacuated and refilled with argon three times. The reaction mixture (black suspension) was then left stirring under an H<sub>2</sub> atmosphere at room temperature for 4 h. The reaction mixture was filtered through Celite<sup>®</sup> to remove Pd/C, and the solvent was removed under reduced pressure, yielding a dark green oil, purified *via* flash chromatography (silica gel, eluent: DCM:EtOAc 95:5). The fractions containing homogeneous spot were concentrated under reduced pressure yielding a yellow/orange oil which crystallised upon standing. The final product was obtained upon filtration as a white powder (0.684 g) in 33% yield.

<sup>1</sup>H NMR (400 MHz, CDCl<sub>3</sub>) δ 8.60 (d, J = 4.7 Hz, 1H, Py-H), 7.72 (td, J = 1.6, 7.7 Hz, 1H, Py-H), 7.42 (d, J = 7.8 Hz, 1H, Py-H), 7.24 (m, 1H, Py-H), 3.87 (d, J = 6.1 Hz, 1H, NC-CH), 2.05 (m, 1H, NC-CH-CH-), 1.72 (m, 5H, cyclohexyl-H), 1.24 (m, 5H, cyclohexyl-H). <sup>13</sup>C{<sup>1</sup>H} NMR (101

MHz, CDCl<sub>3</sub>)  $\delta$  162.4 (C), 149.3 (CH), 136.8 (CH), 123.4 (CH), 118.4 (CH), 117.1 (CN), 41.0 (CH), 38.8 (CH), 30.6 (2CH<sub>2</sub>), 26.3 (CH<sub>2</sub>), 26.0 (2CH<sub>2</sub>).

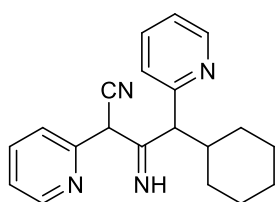
Elemental analysis: calculated for C<sub>13</sub>H<sub>16</sub>N<sub>2</sub>: C 77.96; H 8.05; N 13.99; found C: 78.08; H 8.08; N 14.01.

HRMS (Cl<sup>+</sup>) m/z 01.1394 (M+H)<sup>+</sup> 201.1386 calculated for C<sub>13</sub>H<sub>16</sub>N<sub>2</sub> (M+H)<sup>+</sup>.

IR (FTIR)  $\nu_{\max}$ /cm<sup>-1</sup> 2943 s (alkyl C-H stretch), 2212 w (CN).

### 3.7.5.2.3 Synthesis of 4-cyclohexyl-3-imino-2,4-di(pyridin-2-yl)butanenitrile (45)

A literature procedure for the synthesis of cyclohexyl-pyridylacetonitrile (**44**) has been followed.<sup>169-170</sup>



To a 50 ml 3-neck round bottom flask equipped with condenser, magnetic stirring and previously evacuated and refilled with argon, sodium amide (1.79 g, 45.9 mmol) was added followed by benzene (6 mL). A solution of 2-pyridylacetonitrile (4.84 g, 40.9 mmol) in benzene (4 mL) was charged to a dropping funnel and slowly added to the reaction mixture. The reaction was heated at 90 °C and stirred for 2 h 45 min. Degassed bromocyclohexane (6.72 g, 41.2 mmol) was added dropwise to the dark brown reaction mixture, with no colour change observed. The reaction mixture was left stirring for 9 h at room temperature, and then it was slowly quenched with water (5 mL). The organic phase was washed with water (3 x 15 mL), dried over Na<sub>2</sub>SO<sub>4</sub>, filtered and the cake was washed with EtOAc (5 mL). The solvent was removed under reduced pressure and the crude product was purified *via* flash chromatography (silica gel, eluent: hexane:EtOAc 60:40). The fractions containing homogeneous spot were collected together and the solvent was removed under reduced pressure, yielding a clear orange/pink oil. The material was dissolved in the minimum amount of EtOAc and crystallisation happened upon addition of cold hexane. The final product was obtained upon filtration as white solid (1.135 g) in 18% yield.

<sup>1</sup>H NMR (400 MHz, CDCl<sub>3</sub>)  $\delta$  10.78 (s, 1H, =NH), 8.58 (d, J = 4.5 Hz, 1H, Py-H), 8.34 (d, J = 4.5 Hz, 1H, Py-H), 7.63 (m, 1H, Py-H), 7.62 (m, 1H, Py-H), 7.54 (m, 1H, Py-H), 7.53 (m, 1H, CN-CH), 7.33 (m, 1H, Py-H), 7.20 (m, 1H, Py-H), 6.92 (m, 1H, Py-H), 4.05 (d, J = 10.5 Hz, 1H, Py-CH-Cy), 2.27 (m, 1H, Cy-H), 1.94 (m, 1H, Cy-H), 1.78 (m, 1H, Cy-H), 1.63 (m, 2H, Cy-H), 1.26 (m, 5H, Cy-H), 0.93 (m, 1H, Cy-H). <sup>13</sup>C{<sup>1</sup>H} NMR (101 MHz, CDCl<sub>3</sub>)  $\delta$  165.3 (HN=C), 159.1 (CH), 156.8 (CH), 149.4 (CH), 146.7 (CH), 137.0 (CH), 136.6 (CH), 125.5 (CH), 122.5 (CH), 122.4 (CH), 120.3 (CH), 118.4 (CN), 78.2 (CH), 57.8 (CH<sub>2</sub>), 43.0 (CH<sub>2</sub>), 31.5 (CH<sub>2</sub>), 30.5 (CH<sub>2</sub>), 26.3 (CH<sub>2</sub>), 26.3 (CH<sub>2</sub>), 26.2 (CH<sub>2</sub>).

Elemental analysis: calculated for C<sub>20</sub>H<sub>22</sub>N<sub>4</sub>: C 75.44; H 6.96; N 17.60; found: C 75.27; H 6.83; N 17.33.

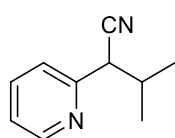
IR (FTIR)  $\nu_{\text{max}}/\text{cm}^{-1}$  3338 w (secondary amine stretch), 3053 w (aromatic C-H stretch), 2915 w (alkyl C-H stretch), 2191 m (CN), 1567 s (aromatic C=C bending), 1465 s (aromatic C=C stretch).

HRMS (Cl<sup>+</sup>) m/z 201.1392 (M+H)<sup>+</sup> (201.1386 calculated for C<sub>20</sub>H<sub>22</sub>N<sub>4</sub> (M+H)<sup>+</sup>).

Following these analyses, it was determined that 4-cyclohexyl-3-imino-2,4-di(pyridin-2-yl)butanenitrile **45** had been synthesised.

### 3.7.5.3 Synthesis of 3-methyl-2-(pyridin-2-yl)butanenitrile (43)

Synthesised according to literature procedure.<sup>170</sup>



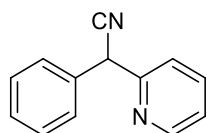
To a 500 mL round bottom flask equipped with magnetic stirring, *iso*-valonitrile (3.0042 g, 36.14 mmol) was added along with 2-chloropyridine (4.3107 g, 37.97 mmol) and dry toluene (95 ml). The mixture was cooled to 0 °C and NaHMDS (70.5 ml, 70.5 mmol) was added dropwise over 1.5 hours while stirring. The colour of the reaction mixture turned from brown to bright yellow and then to bright orange towards the end of addition. The reaction mixture was stirred for 2 hours at 0 °C and then allowed to warm-up to room temperature for 16 hours, with the colour turning darker. The reaction was stopped, and the solvent was removed under reduced pressure. The obtained bright orange slurry was filtered through Celite<sup>®</sup> and washed with hexane, resulting in an orange solution. The final product was obtained after purification *via* flash chromatography (silica gel, hexane/EtOAc 65:35) as an orange oil (1.53 g) in 26% yield.

<sup>1</sup>H NMR (400 MHz, CDCl<sub>3</sub>)  $\delta$  8.56 (d, J = 4.8 Hz, 1H, Py-H), 7.69 (t, J = 7.8 Hz, 1H, Py-H), 7.39 (d, J = 7.8 Hz, 1H, Py-H), 7.22 (m, 1H, Py-H), 3.85 (d, J = 5.8 Hz, 1H, NC-CH), 2.37 (octet, J = 6.6 Hz, 1H, CH-CH-(Me<sub>2</sub>)), 1.07 (d, J = 6.8 Hz, 3H, CH-(CH<sub>3</sub>)<sub>2</sub>), 0.97 (d, J = 6.8 Hz, 3H, CH-(CH<sub>3</sub>)<sub>2</sub>).  
<sup>13</sup>C{<sup>1</sup>H} NMR (101 MHz, CDCl<sub>3</sub>)  $\delta$  141.1 (CH), 139.8 (CH), 139.5 (CH), 125.9 (CH), 124.2 (CH), 119.3 (CN), 43.6 (CH), 33.7 (CH), 20.3 (CH<sub>3</sub>), 19.2 (CH<sub>3</sub>).

IR (FTIR)  $\nu_{\text{max}}/\text{cm}^{-1}$  3050 w (aromatic C-H stretch), 2949 w (alkyl C-H stretch), 2238 w (CN).

### 3.7.5.4 Synthesis of 2-phenyl-2-(pyridin-2-yl)acetonitrile (49)

Synthesised according to literature procedure.<sup>172</sup>



In a 100 ml Schlenk flask equipped with magnetic stirring bar and previously evacuated and refilled with Ar, KOH (9.65 g, 172.0 mmol) was charged followed by dry DMSO (18 mL). Benzyl cyanide (5.89 g, 50.30

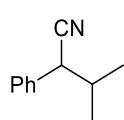
mmol) was added dropwise over 30 minutes at room temperature while stirring. 2-bromopyridine (5.76 g, 36.40 mmol) was then slowly added, turning the reaction from bright yellow to bright orange. The reaction was heated to 50 °C for 16 h. The reaction mixture was then carefully poured into cold water (45 mL) and it was extracted with CHCl<sub>3</sub> (3 x 30 mL). The combined organic layers were washed with water (3 x 15 mL), dried over MgSO<sub>4</sub>, filtered and the solvent was removed under reduced pressure yielding an orange oil. The crude product was purified *via* flash chromatography (silica gel, eluent: hexane:EtOAc 95:5). The collected fractions were concentrated under reduced pressure yielding an orange oil, which was dissolved in DCM and crystallisation was induced upon addition of cold hexane and standing at -20 °C for 48 h. The purified product was obtained as a white solid (4.73 g) in 67% yield.

<sup>1</sup>H NMR (400 MHz, CDCl<sub>3</sub>) δ 8.61 (d, J = 4.5 Hz, 1H, Py-H), 7.70 (td, J = 1.2, 7.8 Hz, 1H, Py-H), 7.46 (s, 1H, Py-H), 7.44 (s, 1H, Py-H), 7.40-7.33 (m, 4H, Ph-H), 7.25-7.23 (m, 1H, Ph-H), 5.32 (s, 1H, NC-CH). <sup>13</sup>C{<sup>1</sup>H} NMR (101 MHz, CDCl<sub>3</sub>) δ 155.5 (C), 149.9 (C), 137.5 (CH), 134.7 (CH), 129.2 (CH), 128.4 (CH), 127.7 (CH), 123.1 (CH), 121.9 (CH), 119.0 (CN), 45.4 (CH).

IR (FTIR)  $\nu_{\max}/\text{cm}^{-1}$  3057 w (aromatic C-H stretch), 2939 s (alkyl C-H stretch), 2242 m (CN), 1587 s (aromatic C=C bending), 1454 s (aromatic C=C stretch).

### 3.7.5.5 Synthesis of 3-methyl-2-phenylbutanenitrile (39)

Synthesised according to literature procedure.<sup>196</sup>

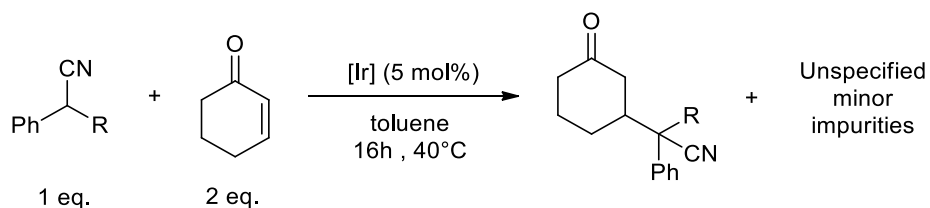


In a 50 mL round bottom flask equipped with magnetic stirring benzyl nitrile (8.07 g, 68.9 mmol), iodopropane (12.78 g, 75.2 mmol) and tetrabutylammonium bromide (0.24 g, 0.74 mmol) were added sequentially, followed by a dropwise addition of a 60% w/w aqueous solution of KOH (32 mL). The reaction mixture was heated for 22 h at 50 °C with vigorous stirring. The solution turned first dark red over the first 5 h, to become almost black the following day. The reaction mixture was then diluted with water (30 mL) and extracted with EtOAc (3 x 30 mL). The combined organic layers were washed with brine (30 mL) before being dried over MgSO<sub>4</sub>. The solvent was removed under reduced pressure and the crude product (10.4 g) was purified *via* flash chromatography (silica gel, hexane:EtOAc, 10:1). The purified product was obtained as a colourless oil (2.26 g) in 21% yield.

<sup>1</sup>H NMR (400 MHz, CDCl<sub>3</sub>) δ 7.39-7.29 (m, 5H, Ph-H), 3.66 (d, J = 6.3 Hz, 1H, CH), 2.13 (sept, 1H, CH), 1.04 (dd, J = 6.3, 11.38 Hz, 6H, CH<sub>3</sub>). <sup>13</sup>C{<sup>1</sup>H} NMR (101 MHz, CDCl<sub>3</sub>) δ 134.9 (C), 128.8 (CH), 127.9 (CH), 127.8 (CH), 119.8 (CN), 45.1 (CH), 33.8 (CH), 20.8 (CH<sub>3</sub>), 18.82 (CH<sub>3</sub>).

IR (FTIR)  $\nu_{\text{max}}/\text{cm}^{-1}$  3032 w (aromatic C-H stretch), 2965-2931 s (alkyl C-H stretch), 2236 m (CN), 1492 s (aromatic C=C bending), 1465 s (aromatic C=C stretch).

### 3.7.6 Catalyst screening for the iridium-catalysed hydroalkylation of 2-cyclohexen-1-one with *i*Pr- and Cy-substituted phenylacetonitriles



In a glovebox, the desired iridium-catalyst (0.02 mmol, except Entry 1: 0.002 mmol), substituted acetonitrile (0.40 mmol) and *n*-dodecane (53.3  $\mu\text{L}$ , 0.23 mmol, GC standard) were dissolved in toluene (2 mL) in a glass 4 mL vial. Then, 2-cyclohexen-1-one (77.4  $\mu\text{L}$ , 0.8 mmol) was added and the vial equipped with a stirring bar sealed with a Teflon lined cap. Once outside the glovebox, the reaction was heated at 40 °C for 16 h. The reaction was quenched by cooling in an ice-bath and bubbling air through the solution. The reaction mixture was passed through a short pad of silica gel (a glass Pasteur pipette filled with 2 cm of silica gel) eluting with EtOAc (21 mL). The obtained solution was analysed by GC.

Results and amounts of reagents are reported in the table below (Table 3.9).

Table 3.9 Exact amounts and results for the catalyst screening for the Michael addition of *i*Pr- and Cy-substituted phenylacetonitriles to cyclohexenone.

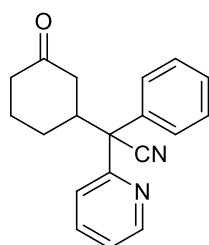
| Entry | R           | Catalyst   | Catalyst mass (mg) | Cyclohexenone mass (mg) | Nitrile mass (mg) | <i>n</i> -Dodecane mass (mg) | Cyclohexenone Conv (%) | Nitrile Conv (%) | Product Yield (%) |
|-------|-------------|--|--------------------|-------------------------|-------------------|------------------------------|------------------------|------------------|-------------------|
| 1     | Ph          | Ir(P <sup><i>i</i></sup> Pr <sub>3</sub> ) <sub>2</sub> H <sub>5</sub>                       | 1.2                | 78.5                    | 77.3              | 37.1                         | 57                     | 97               | 95                |
| 2     | <i>i</i> Pr | Ir(P <sup><i>i</i></sup> Pr <sub>3</sub> ) <sub>2</sub> H <sub>5</sub>                       | 10.7               | 78.9                    | 64.5              | 41.8                         | 61                     | 70               | 58                |
| 4     | <i>i</i> Pr | Ir(PMe <sub>3</sub> ) <sub>2</sub> H <sub>5</sub>  | 7.2                | 77.8                    | 68.8              | 42.0                         | 6                      | 32               | -                 |
| 4     | <i>i</i> Pr | Ir(P <sup><i>t</i></sup> Bu <sub>3</sub> ) <sub>2</sub> H <sub>5</sub>                       | 12.0               | 76.8                    | 63.5              | 41.5                         | 11                     | 22               | -                 |
| 5     | <i>i</i> Pr | Ir(PCy <sub>3</sub> ) <sub>2</sub> H <sub>5</sub>  | 15.2               | 77.8                    | 62.0              | 42.2                         | 61                     | 64               | 28                |
| 6     | <i>i</i> Pr | Ir(P <sup><i>t</i></sup> Bu <sub>2</sub> <sup><i>n</i></sup> Bu) <sub>2</sub> H <sub>5</sub> | 12.5               | 80.1                    | 67.9              | 41.3                         | 100                    | 36               | 9                 |
| 7     | <i>i</i> Pr | Ir( <sup><i>ad</i></sup> PCP)H <sub>4</sub>  | 19.8               | 78.6                    | 74.8              | 41.6                         | 98                     | 37               | -                 |
| 8     | Cy          | Ir(P <sup><i>i</i></sup> Pr <sub>3</sub> ) <sub>2</sub> H <sub>5</sub>                       | 10.4               | 74.3                    | 77.3              | 40.6                         | 44                     | 59               | 51                |
| 9     | Cy          | Ir(P <sup><i>t</i></sup> Bu <sub>3</sub> ) <sub>2</sub> H <sub>5</sub>                       | 12.1               | 78.2                    | 85.5              | 40.7                         | 14                     | 14               | -                 |
| 10    | Cy          | Ir(P <sup><i>t</i></sup> Bu <sub>2</sub> <sup><i>n</i></sup> Bu) <sub>2</sub> H <sub>5</sub> | 11.9               | 77.0                    | 80.7              | 41.2                         | 100                    | 23               | 1                 |

### 3.7.7 Scope of the pyridyl-substituted acetonitrile substrates

#### 3.7.7.1 General procedure for iridium-catalysed hydroalkylation of pyridyl-substituted acetonitriles with 2-cyclohexen-1-one

In a glovebox, Ir(P<sup>i</sup>Pr<sub>3</sub>)<sub>2</sub>H<sub>5</sub> catalyst (10.4-20.7 mg, 0.02-0.04 mmol), alkyl-pyridyl-nitrile (0.40 mmol) and *n*-dodecane (53.3 μL, 40 mg, 0.23 mmol, GC standard) were dissolved in toluene (2 mL) in a glass 4 mL vial. Then, 2-cyclohexen-1-one (77.4 μL, 0.8 mmol) was added and the vial, previously equipped with a stirring bar, was sealed with a Teflon lined cap. Once outside the glovebox, the reaction was heated at 40 °C for 16 h. The reaction was quenched by cooling in an ice-bath and bubbling air through the solution. The reaction mixture was passed through a short pad of silica gel (a glass Pasteur pipette filled with 2 cm of silica gel) eluting with EtOAc (21 mL). The obtained solution was analysed by GC, however instrument errors did not allow to reliably use the GC for the quantification of the reaction mixture. The products were, indeed, quantified after being isolated by column chromatography as described below.

#### 3.7.7.2 Synthesis of 2-(3-oxocyclohexyl)-2-phenyl-2-(pyridin-2-yl)acetonitrile (36)



Prepared according to the general procedure in Section 3.7.7.1 using Ir(P<sup>i</sup>Pr<sub>3</sub>)<sub>2</sub>H<sub>5</sub> catalyst (10.8 mg, 0.02 mmol, 5 mol%), 2-phenyl-2-(pyridin-2-yl)acetonitrile (78.9 mg, 0.40 mmol), *n*-dodecane (41.5 mg, 0.23 mmol, GC standard) and 2-cyclohexen-1-one (79.4 mg, 0.80 mmol) in toluene (2 mL) at 40 °C for 16 h. The crude product was purified *via* flash chromatography (silica gel, eluting with 4:1, hexane:EtOAc) to give 2-(3-oxocyclohexyl)-2-phenyl-2-(pyridin-2-yl)acetonitrile as a mixture of two diastereomers as a white solid (113 mg) in 95% yield, dr = 1:4.1 (determined by <sup>13</sup>C NMR).

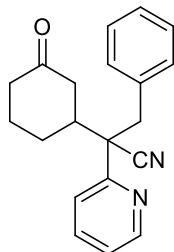
<sup>1</sup>H NMR (400 MHz, CDCl<sub>3</sub>) δ 8.64 (t, J = 4.6 Hz, 1H, aromatic-H), 7.80-7.54 (m, 4H, aromatic-H), 7.45 – 7.11 (m, 4H, aromatic-H), 3.52 (dtd, J = 3.7, 7.3, 14.5 Hz, 1H, CH), 2.58 – 2.23 (m, 3H, CH<sub>2</sub>), 2.21 – 1.99 (m, 2H, CH<sub>2</sub>), 1.98 – 1.52 (m, 3H, CH<sub>2</sub>). <sup>13</sup>C {<sup>1</sup>H} NMR (101 MHz, CDCl<sub>3</sub>) δ 209.9 (CO), 209.7 (CO), 156.8 (C), 156.1 (C), 149.6 (CH), 149.5 (CH), 137.4 (C), 137.4 (CH), 137.3 (CH), 136.7 (C), 129.0 (CH), 128.9 (CH), 128.2 (CH), 128.1 (CH), 126.5 (CH), 126.3 (CH), 122.8 (CH), 122.8 (CH), 122.6 (CH), 122.4 (CH), 120.1 (CN), 120.1 (CN), 59.8 (C), 59.8 (C), 45.1 (CH<sub>2</sub>), 44.9 (CH<sub>2</sub>), 44.5 (CH<sub>2</sub>), 43.5 (CH<sub>2</sub>), 41.1 (CH), 40.9 (CH), 27.8 (CH<sub>2</sub>), 26.6 (CH<sub>2</sub>), 24.3 (CH<sub>2</sub>), 24.3 (CH<sub>2</sub>).

HRMS (ES<sup>+</sup>) m/z 313.1323 (M+Na)<sup>+</sup> (313.1317 calculated for C<sub>19</sub>H<sub>18</sub>N<sub>2</sub>ONa (M+Na)<sup>+</sup>).



IR (FTIR)  $\nu_{\max}/\text{cm}^{-1}$  2961 w (sp<sup>2</sup> C-H), 1707 w (R(C=O)R'), 1495 w (C=N).

### 3.7.7.3 Synthesis of 2-(3-oxocyclohexyl)-3-phenyl-2-(pyridin-2-yl)propanenitrile (50)



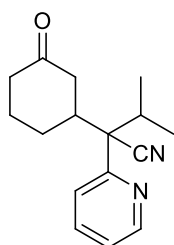
Prepared according to the general procedure in Section 3.7.7.1 using Ir(P<sup>i</sup>Pr<sub>3</sub>)<sub>2</sub>H<sub>5</sub> catalyst (10.5 mg, 0.02 mmol, 5 mol%), 3-phenyl-2-(pyridin-2-yl)propanenitrile (88.6 mg, 0.40 mmol), *n*-dodecane (41.4 mg, 0.23 mmol, GC standard) and 2-cyclohexen-1-one (76.0 mg, 0.80 mmol) in toluene (2 mL) at 40 °C for 16 h. The crude product was purified *via* flash chromatography (silica gel, eluting with 3:1, hexane:EtOAc) to give 2-(3-oxocyclohexyl)-2-phenyl-2-(pyridin-2-yl)acetone nitrile as a mixture of two diastereomers as a white solid (106.5 mg) in 82% yield, dr = 1:1.3 (determined by <sup>13</sup>C NMR).

<sup>1</sup>H NMR (400 MHz, CDCl<sub>3</sub>)  $\delta$  8.66 (t, J = 5.0 Hz, 1H, aromatic-H), 7.48 (qd, J = 1.9, 7.7 Hz, 1H, aromatic-H), 7.18 (m, 1H, aromatic-H), 7.09 (m, 4H, aromatic-H), 6.79 (m, 2H, aromatic-H), 3.38 (aq, J = 8.0, 12.0 Hz, 1H, CH<sub>2</sub>), 3.26 (aq, J = 8.0, 12.0 Hz, 1H, CH<sub>2</sub>), 2.92 (m, 2H, CH<sub>2</sub>), 2.60-2.14 (m, 4H, 2CH<sub>2</sub>), 2.01-1.66 (m, 2H, CH<sub>2</sub>), 1.65-1.42 (m, 1H, CH). <sup>13</sup>C {<sup>1</sup>H} NMR (101 MHz, CDCl<sub>3</sub>)  $\delta$  209.6 (CO), 209.5 (CO), 155.8 (CH), 155.2 (CH), 150.0 (CH), 149.8 (CH), 136.8 (CH), 136.7 (CH), 135.3 (CH), 135.2 (CH), 130.0 (CH), 128.1 (CH), 127.2 (CH), 127.2 (CH), 123.5 (CH), 123.4 (CH), 123.0 (CH), 122.9 (CH), 120.4 (CN), 120.3 (CN), 56.6 (C), 56.5 (C), 45.7 (CH<sub>2</sub>), 45.7 (CH<sub>2</sub>), 44.3 (CH), 43.9 (CH), 43.2 (CH), 42.8 (CH), 41.2 (CH), 41.0 (CH), 27.7 (CH), 26.9 (CH), 24.5 (CH), 24.4 (CH).

HRMS (Cl<sup>+</sup>) *m/z* 327.1471 (M+Na)<sup>+</sup> (327.1468 calculated for C<sub>20</sub>H<sub>20</sub>N<sub>2</sub>NaO (M+Na)<sup>+</sup>).

IR (FTIR)  $\nu_{\max}/\text{cm}^{-1}$  2950 w (sp<sup>2</sup> C-H), 1708 w (R(C=O)R'), 1588 w (CN).

### 3.7.7.4 Synthesis of 3-methyl-2-(3-oxocyclohexyl)-2-(pyridin-2-yl)butanenitrile (51)



Prepared according to the general procedure in Section 3.7.7.1 using Ir(P<sup>i</sup>Pr<sub>3</sub>)<sub>2</sub>H<sub>5</sub> catalyst (21.3 mg, 0.04 mmol, 10 mol%), 3-methyl-2-(pyridin-2-yl)butanenitrile (77.9 mg, 0.40 mmol), *n*-dodecane (42.2 mg, 0.23 mmol, GC standard) and 2-cyclohexen-1-one (78.6 mg, 0.80 mmol) in toluene (2 mL) at 40 °C for 16 h. The crude product was purified *via* flash chromatography (silica gel, eluting with 4:1, hexane:EtOAc) to give 2-(3-oxocyclohexyl)-2-phenyl-2-(pyridin-2-yl)acetone nitrile as a mixture of two diastereomers as white solid (82.6 mg) in 66% yield, dr = 1:2.1 (determined by <sup>13</sup>C NMR). (With [Ir] = 5 mol%, isolated yield = 44%)

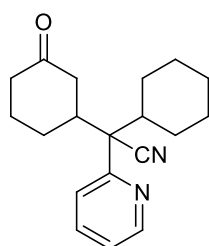
$^1\text{H}$  NMR (400 MHz,  $\text{CDCl}_3$ )  $\delta$  8.61 (m, 1H, Py-H), 7.72 (td,  $J = 1.9, 7.8$  Hz, 1H, Py-H), 7.60 (m, 1H, Py-H), 7.25 (m, 1H, Py-H), 2.37 (m, 7H,  $\text{CH}_2$ ), 1.63 (m, 2H,  $\text{CH}_2$ ), 1.25 (m, 1H,  $\text{CH}_2$ ), 0.94 (m, 6H,  $(\text{CH}_3)_2$ ).  $^{13}\text{C}$   $\{^1\text{H}\}$  NMR (101 MHz,  $\text{CDCl}_3$ )  $\delta$  210.1 (CO), 209.9 (CO), 154.9 (C), 154.6 (C), 149.4 (CH), 149.4 (CH), 136.6 (CH), 136.6 (CH), 124.1 (CH), 123.9 (CH), 122.9 (CH), 121.5 (CN), 121.4 (CN), 158.5 ( $\text{CH}_2$ ), 158.4 ( $\text{CH}_2$ ), 44.1 ( $\text{CH}_2$ ), 43.2 ( $\text{CH}_2$ ), 42.8 ( $\text{CH}_2$ ), 42.4 ( $\text{CH}_2$ ), 41.3 ( $\text{CH}_2$ ), 41.1 ( $\text{CH}_2$ ), 32.9 ( $\text{CH}_2$ ), 32.4 ( $\text{CH}_2$ ), 27.6 ( $\text{CH}_2\text{O}$ ), 26.9 ( $\text{CH}_2$ ), 24.6 ( $\text{CH}_2$ ), 24.6 ( $\text{CH}_2$ ), 19.0 ( $\text{CH}_3$ ), 18.6 ( $\text{CH}_3$ ), 17.9 ( $\text{CH}_3$ ), 17.3 ( $\text{CH}_3$ ).

HRMS ( $\text{Cl}^+$ )  $m/z$  279.147 ( $\text{M}+\text{Na}^+$ ) (279.1468 calculated for  $\text{C}_{16}\text{H}_{20}\text{N}_2\text{NaO}$  ( $\text{M}+\text{Na}^+$ ))

Elemental analysis: calculated for  $\text{C}_{16}\text{H}_{20}\text{N}_2\text{O}$ : C 74.97; H 7.86; N 10.93; found: C 73.80; H 8.04; N 10.29.

IR (FTIR)  $\nu_{\text{max}}/\text{cm}^{-1}$  2967 w ( $\text{sp}^2$  C-H), 1710 s ( $\text{R}(\text{C}=\text{O})\text{R}'$ ), 1587 w (CN).

### 3.7.7.5 Synthesis of 2-cyclohexyl-2-(3-oxocyclohexyl)-2-(pyridin-2-yl)acetonitrile (52)



Prepared according to the general procedure in Section 3.7.7.1 using  $\text{Ir}(\text{P}^i\text{Pr}_3)_2\text{H}_5$  catalyst (16.0 mg, 0.03 mmol, 7.5 mol%), cyclohexyl-2-pyridylacetonitrile (85.3 mg, 0.40 mmol), *n*-dodecane (42.4 mg, 0.23 mmol, GC standard) and 2-cyclohexen-1-one (81.3 mg, 0.80 mmol) in toluene (2 mL) at 40 °C for 16 h. The crude product was purified *via* flash chromatography (silica gel, eluting with 4:1, hexane:EtOAc) to give 2-(3-oxocyclohexyl)-2-phenyl-2-(pyridin-2-yl)acetonitrile as a mixture of two diastereomers as white solid (88.7 mg) in 70% yield, *dr* = 1:3.4 (determined by  $^{13}\text{C}$  NMR). (With  $[\text{Ir}] = 5$  mol%, isolated yield = 65%)

$^1\text{H}$  NMR (400 MHz,  $\text{CDCl}_3$ )  $\delta$  8.61 (m, 1H, Py-H), 7.71 (td,  $J = 2.0, 7.7$  Hz, 1H, PyH), 7.58 (m, 1H, Py-H), 7.24 (m, 1H, Py-H), 2.95 (m, 1H, CH), 2.70 (m, 1H, CH), 2.23 (m, 6H,  $\text{CH}_2$ ), 1.68 (m, 6H,  $\text{CH}_2$ ), 1.03 (m, 6H,  $\text{CH}_2$ ).  $^{13}\text{C}$   $\{^1\text{H}\}$  NMR (101 MHz,  $\text{CDCl}_3$ )  $\delta$  210.2 (CO), 210.1 (CO), 155.0 (C), 149.5 (C), 149.4 (C), 136.6 (CH), 124.1 (CH), 122.9 (CN), 121.6 (CN), 58.5 (C), 44.0 ( $\text{CH}_2$ ), 43.2 ( $\text{CH}_2$ ), 42.7 ( $\text{CH}_2$ ), 42.0 ( $\text{CH}_2$ ), 41.5 ( $\text{CH}_2$ ), 41.1 ( $\text{CH}_2$ ), 29.5 ( $\text{CH}_2$ ), 28.9 ( $\text{CH}_2$ ), 28.0 ( $\text{CH}_2$ ), 27.5 ( $\text{CH}_2$ ), 27.0 ( $\text{CH}_2$ ), 26.5 ( $\text{CH}_2$ ), 26.4 ( $\text{CH}_2$ ), 26.1 ( $\text{CH}_2$ ), 24.7 ( $\text{CH}_2$ ).

HRMS ( $\text{Cl}^+$ )  $m/z$  319.1782 ( $\text{M}+\text{Na}^+$ ) (319.1781 calculated for  $\text{C}_{19}\text{H}_{24}\text{N}_2\text{NaO}$  ( $\text{M}+\text{Na}^+$ )).

Elemental analysis: calculated for  $\text{C}_{19}\text{H}_{24}\text{N}_2\text{O}$ : C 76.99; H 8.16; N 9.45; found: C 75.87; H 7.98; N 8.13.

IR (FTIR) 2924 w ( $\text{sp}^2$  C-H), 1709 w ( $\text{R}(\text{C}=\text{O})\text{R}'$ ), 1586 w (CN).

### 3.7.8 Attempted ultrasound-mediated Michael-type hydroalkylation of cyclohexenone with diphenylacetonitrile

#### 3.7.8.1 General procedure for the ultrasound-mediated iridium-catalysed hydroalkylation of 2-cyclohexen-1-one with diphenylacetonitrile

In a glovebox, Ir(P<sup>*i*</sup>Pr<sub>3</sub>)<sub>2</sub>H<sub>5</sub> catalyst (2.6-51.8 mg, 0.005-0.1 mmol), diphenylacetonitrile (193.3 mg, 1.0 mmol) and *n*-dodecane (133.3 μL, 100.0 mg, 0.59 mmol, GC standard) were weighted in a 10 mL Schlenk tube equipped with a stirring bar. Then, 2-cyclohexen-1-one (193.6 μL, 2.0 mmol) was dissolved in toluene (5 mL) in a second 10 mL Schlenk tube. The sealed vessels were taken outside the glovebox and connected to the Schlenk line. Meanwhile, the sonochemical reactor was assembled (see Figure 2.3 in the previous chapter) and evacuated completely under vacuum and backfilled with argon three times to ensure complete removal of residual air. At this point, the solution of cyclohexenone in toluene was quantitatively transferred with a syringe in the Schlenk tube containing the other reagents. After complete solubilisation of all the reagents, the reaction mixture was quantitatively transferred with a syringe from the Schlenk tube to the sonochemical reactor. The reactor was immersed in a water-cooling bath to maintain the solution at room temperature (25 ± 3 °C). The horn and the upper part of the reactor were cooled down from the outside by a continuous stream of compressed air. The reaction mixture was sonicated under a pulse mode (amplitude 100%). The ultrasound was applied for 10 minutes and then stopped for another 10 minutes (specific reaction times reported in Table 3.2 and correspond to the active sonication time). The reaction was quenched by cooling in an ice-bath and bubbling air through the solution. 1 mL of the reaction mixture was passed through a short pad of silica gel (a glass Pasteur pipette filled with 2 cm of silica gel) eluting with EtOAc (10.5 mL). The obtained solution was analysed by GC.

#### 3.7.8.2 Thermal iridium-catalysed hydroalkylation of diphenylacetonitrile with 2-cyclohexen-1-one

The thermal control experiments reported in Table 3.2 refer to the results of the corresponding GC time monitoring experiments reported in Section 3.7.10.3 and Section 3.7.10.4.

### 3.7.8.3 Ultrasound-mediated iridium-catalysed hydroalkylation of 2-cyclohexen-1-one with diphenylacetonitrile with 0.5 mol% catalyst loading for 1 hour of sonication

The general procedure described in Section 3.7.8.1 was followed using Ir(*P*<sup>*i*</sup>Pr<sub>3</sub>)<sub>2</sub>H<sub>5</sub> catalyst (3.8 mg, 0.005 mmol), diphenylacetonitrile (191.7 mg, 1.0 mmol) and *n*-dodecane (99.2 mg, 0.59 mmol, GC standard) and 2-cyclohexen-1-one (195.1 mg, 2.0 mmol) in toluene (5 mL) at 25 °C for a total of 2 h (1 h sonication). The results are reported in Table 3.2 Figure 3.2.

### 3.7.8.4 Ultrasound-mediated iridium-catalysed hydroalkylation of 2-cyclohexen-1-one with diphenylacetonitrile with 10 mol% catalyst loading for 1 hour of sonication

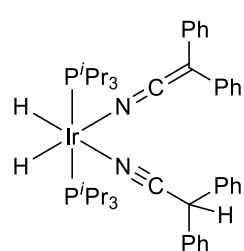
The general procedure described in Section 3.7.8.1 was followed using Ir(*P*<sup>*i*</sup>Pr<sub>3</sub>)<sub>2</sub>H<sub>5</sub> catalyst (52.3 mg, 0.1 mmol), diphenylacetonitrile (193.1 mg, 1.0 mmol) and *n*-dodecane (104.9 mg, 0.59 mmol, GC standard) and 2-cyclohexen-1-one (197.5 mg, 2.0 mmol) in toluene (5 mL) at 25 °C for a total of 2 h (1 h sonication). The results are reported in Table 3.2 Figure 3.2.

### 3.7.8.5 Ultrasound-mediated iridium-catalysed hydroalkylation of 2-cyclohexen-1-one with diphenylacetonitrile with 10 mol% catalyst loading for 2 hours of sonication

The general procedure described in Section 3.7.8.1 was followed using Ir(*P*<sup>*i*</sup>Pr<sub>3</sub>)<sub>2</sub>H<sub>5</sub> catalyst (52.3 mg, 0.1 mmol), diphenylacetonitrile (193.1 mg, 1.0 mmol) and *n*-dodecane (104.9 mg, 0.59 mmol, GC standard) and 2-cyclohexen-1-one (197.5 mg, 2.0 mmol) in toluene (5 mL) at 25 °C for a total of 4 h (2 h sonication). The results are reported in Table 3.2 Figure 3.2.

## 3.7.9 Independent synthesis and isolation of the intermediate complexes

### 3.7.9.1 Synthesis of the iridium-ylide-nitrile intermediate 59



In a glovebox, a 50 mL Schlenk bomb equipped with magnetic stirring was charged with Ir(*P*<sup>*i*</sup>Pr<sub>3</sub>)<sub>2</sub>H<sub>5</sub> complex (122.0 mg, 0.24 mmol), diphenylacetonitrile (451.7 mg, 2.34 mmol) and toluene (11.8 mL). The Schlenk bomb was removed from the glovebox and the reaction mixture was heated at 80 °C. After 1 hour at 80 °C the reaction mixture was left to cool and the pressure generated in the reaction vessel (hydrogen gas) was

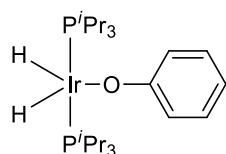
released *via* the Schlenk line (the solution turned from yellow to orange). The pressure-realising step was crucial to shift the equilibrium towards the desired product, increasing the yield. The reaction mixture was then heated again to 80 °C for a total of 3.5 hours. The reaction vessel with the orange solution was cooled down and brought back into the glovebox where the reaction mixture was concentrated under reduced pressure to give the crude product as an orange solid. The material was dissolved in toluene and recrystallised *via* addition of hexane (toluene/hexane 1:3 v/v) obtaining the complex as dark orange crystals (142.5 mg) in 67% yield.

$^1\text{H-NMR}$  (500 MHz,  $d^8\text{-THF}$ , -60 °C)  $\delta$  7.45 (m, 10H, aromatic-H), 7.25 (d,  $J = 7.9$  Hz, 4H, aromatic-H), 6.92 (t,  $J = 7.7$  Hz, 4H, aromatic-H), 6.42 (t,  $J = 7.15$  Hz, 2H, aromatic-H), 6.20 (s, 1H, CH), 2.24 (m, 6H, 6CH), 1.16 (quint,  $J = 7.0, 14.0$  Hz, 36 H, 12CH<sub>3</sub>), -21.72 (td,  $J = 8.0, 16.0$  Hz, 1H, hydride), -22.12 (td,  $J = 8.0, 16.0$  Hz, 1H, hydride).  $^{13}\text{C}\{^1\text{H}\}$  NMR (126 MHz,  $d^8\text{-THF}$ , -60 °C)  $\delta$  145.4 (N=C=C), 130.7 (CH), 129.8 (CH), 129.5 (CH), 128.8 (CH), 123.3 (CH), 117.8 (CN), 58.7 (N=C=C), 44.4 (C-P), 20.7 (CH<sub>3</sub>).  $^{31}\text{P}\{^1\text{H}\}$  NMR (202 MHz,  $d^8\text{-THF}$ , -60 °C)  $\delta$  31.9 ppm.

Elemental Analysis: calculated for (C<sub>46</sub>H<sub>65</sub>IrN<sub>2</sub>P<sub>2</sub>): C, 61.38; H, 7.28; N, 3.11; found C, 61.52; H, 7.14; N, 3.19.

MS (ES+)  $m/z$  708.3 (M-Ph<sub>2</sub>C=C=N)<sup>+</sup>.

### 3.7.9.2 Synthesis of the iridium-phenoxide intermediate 62



In a glovebox, a 10 mL Schlenk bomb equipped with magnetic stirring was charged with Ir(P<sup>*i*</sup>Pr<sub>3</sub>)<sub>2</sub>H<sub>5</sub> complex (52.5 mg, 0.1 mmol), 2-cyclohexen-1-one (188.3 mg, 2.0 mmol) and toluene (5.0 mL). The Schlenk bomb was removed from the glovebox and the reaction mixture was stirred at 25 °C for 24 hours. Over time the colour of the solution turned from pale yellow to red. The reaction mixture was then concentrated under reduced pressure yielding a sticky red solid, that was left to dry under vacuum overnight to remove all the traces of cyclohexenone. The dry complex was obtained as a deep red solid (61.6 mg) in 99% yield.

$^1\text{H NMR}$  (500 MHz, C<sub>6</sub>D<sub>6</sub>)  $\delta$  7.27-7.20 (m, 2H), 7.15 (s, 1H), 6.86 (d,  $J = 7.7$  Hz, 2H), 6.76 (t,  $J = 7.2$  Hz, 1H), 2.15 – 1.79 (m, 6H), 1.15 (dd,  $J = 7.0, 13.5$  Hz, 36H), -32.21 (t,  $J = 12.5$  Hz, 2H).  $^{31}\text{P}\{^1\text{H}\}$  NMR (202 MHz, C<sub>6</sub>D<sub>6</sub>)  $\delta$  52.47 (s).

## Crystallographic data and structure refinement for complex 62

Identification code: Complex 62

Empirical formula: C<sub>24</sub>H<sub>47</sub>IrOP<sub>2</sub>

Formula weight: 605.75 g/mol

Temperature: 99.9(5) K

Crystal system: monoclinic

Space group: P21/c

a = 8.7923(4) Å

b = 40.9817(15) Å

c = 8.5238(4) Å

α = 90 °

β = 117.264(5) °

γ = 90 °

Volume = 2730.1(2) Å<sup>3</sup>

Z = 4

μ = 10.645 mm<sup>-1</sup>

F(000) 1224

Crystal size: 0.174 × 0.102 × 0.038 mm<sup>3</sup>

Radiation CuKα (λ = 1.54184)

2θ range for data collection: 5.6270 ° to 76.3890 °

Index ranges: -10 ≤ h ≤ 10, -50 ≤ k ≤ 51, -10 ≤ l ≤ 10

Reflections collected: 29322

Data/restraints/parameters 5575/19/295

Goodness-of-fit on F<sup>2</sup>: 1.189

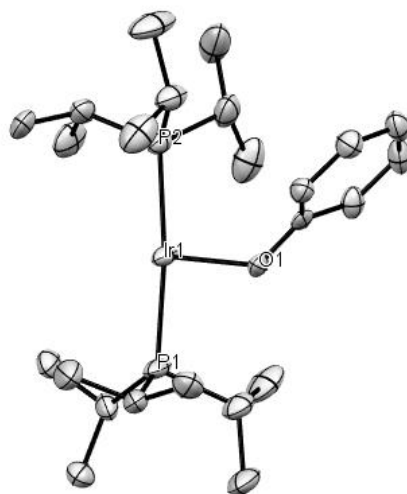
Final R indexes [I ≥ 2σ(I)] R1 = 0.0520, wR2 = 0.1104

Final R indexes [all data] R1 = 0.0540, wR2 = 0.1111

Highest diff. peak/hole :1.209/-2.319 Å

$R1 = \frac{\sum ||F_o| - |F_c||}{\sum |F_o|}$ ;  $wR2 = \frac{[\sum (w(F_o^2 - F_c^2))^2 / \sum w(F_o^2)^2]^{1/2}}{1}$

Crystal structure of complex **62** (hydrogen atoms have been omitted for clarity):



Bonds lengths:

$$\text{Ir-P2} = 2.2992(16) \text{ \AA}$$

$$\text{Ir-P1} = 2.2949(18) \text{ \AA}$$

$$\text{Ir-O} = 2.067(4) \text{ \AA}$$

$$\text{O-C1} = 1.330(8) \text{ \AA}$$

Bond and torsion angles:

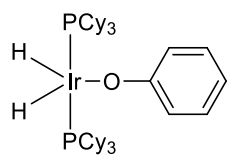
$$\text{P1-Ir-P2} = 172.86(6)^\circ$$

$$\text{O-Ir-P2} = 99.87(13)^\circ$$

$$\text{O-Ir-P1} = 87.17(13)^\circ$$

$$\text{Ir-O-C1} = 130.4(4)^\circ$$

### 3.7.9.3 Synthesis of the iridium-phenoxide complex 63 bearing tri-cyclohexylphosphines

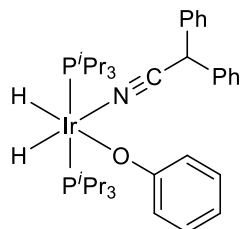


In a glovebox, a 10 mL Schlenk bomb equipped with magnetic stirring was charged with Ir(P<sup>i</sup>Pr<sub>3</sub>)<sub>2</sub>H<sub>2</sub> complex (55.3 mg, 0.07 mmol), 2-cyclohexen-1-one (140.7 mg, 1.4 mmol) and toluene (5.0 mL). The Schlenk bomb was removed from the glovebox and the reaction mixture was stirred at 25 °C for 24 hours. Over time the colour of the solution turned from pale yellow to red. The reaction mixture was then concentrated under reduced pressure yielding a sticky red solid, that was left to dry under vacuum overnight to remove all the traces of cyclohexenone. The dry complex was obtained as a deep red solid (61.9 mg) in 99% yield.

<sup>1</sup>H NMR (500 MHz, d<sup>8</sup>-toluene) δ 7.22 (t, J = 7.6 Hz, 2H), 6.78 (d, J = 7.8 Hz, 2H), 6.70 (s, 1H), 2.20-0.98 (m, 66H, 6Cy), -32.26 (t, J = 13.2 Hz, 2H). <sup>31</sup>P{<sup>1</sup>H} NMR (202 MHz, d<sup>8</sup>-toluene) δ 41.60 (s).

(Awaiting x-ray data)

### 3.7.9.4 Synthesis of the iridium-nitrile-phenoxide intermediate 65



In a glovebox, a 10 mL Schlenk bomb equipped with magnetic stirring was charged with Ir(P<sup>i</sup>Pr<sub>3</sub>)<sub>2</sub>(OPh)H<sub>2</sub> complex (36.5 mg, 0.06 mmol), diphenylacetonitrile (11.6 mg, 0.06 mmol) and toluene (3.0 mL). The Schlenk bomb was removed from the glovebox and the reaction mixture was stirred at 25 °C for 5 minutes. The reaction mixture was then concentrated under reduced pressure to obtain the complex as a dark orange solid (48.1 mg) in 99% yield.

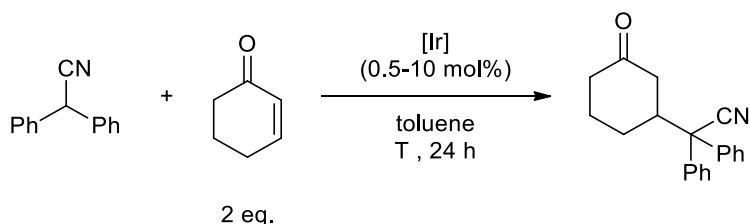
<sup>1</sup>H NMR (500 MHz, d<sup>8</sup>-toluene) δ 7.22 (bs, 6H), 7.13-6.88 (m, 8H), 6.62 (s, 1H), 4.90 (s, 1H), 2.17-1.93 (m, 6H), 1.12 (bs, 36H), -21.78 (bs, 1H), -26.41 (bs, 1H). <sup>31</sup>P{<sup>1</sup>H} NMR (202 MHz, d<sup>8</sup>-toluene) δ 35.00 (bs).

(Awaiting x-ray data)



### 3.7.10 GC time monitoring experiments

#### 3.7.10.1 General procedure for the time monitoring experiments by GC



In a glovebox, the desired iridium complex (0.01-0.2 mmol), diphenylacetonitrile (386.5 mg, 2.0 mmol) and *n*-dodecane (266.7  $\mu$ L, 200.0 mg, 1.17 mmol, GC standard) were dissolved in toluene (10 mL) in a glass 20 mL vial. Then, 2-cyclohexen-1-one (387.2  $\mu$ L, 4.0 mmol) was added and the reaction mixture was equally portioned into 10 x 4 mL glass vials equipped with a stirring bar. The vials were sealed with a Teflon lined cap. Once outside the glovebox, the reactions were heated at the required temperature (25 or 40  $^{\circ}$ C) for the required time (5, 10, 20, 40 min and 1, 2, 4, 8, 16, 24 h). Each aliquot was quenched by cooling in an ice-bath and bubbling air through the solution, and the reaction mixture was passed through a short pad of silica gel (a glass Pasteur pipette filled with 2 cm of silica gel) eluting with EtOAc (10.5 ml). The obtained solutions were analysed by GC.

#### 3.7.10.2 Catalytic hydroalkylation reaction at 40 $^{\circ}$ C with 0.5 mol% of Ir(*P*<sup>*i*</sup>Pr<sub>3</sub>)<sub>2</sub>H<sub>5</sub> (standard reaction conditions)

The general procedure from Section 3.7.10.1 was followed using Ir(*P*<sup>*i*</sup>Pr<sub>3</sub>)<sub>2</sub>H<sub>5</sub> catalyst (5.3 mg, 0.01 mmol), diphenylacetonitrile (388.5 mg, 2.0 mmol), *n*-dodecane (193.8 mg, 1.17 mmol, GC standard) and 2-cyclohexen-1-one (379.6 mg, 4.0 mmol) in toluene (10 mL) at 40  $^{\circ}$ C for a total of 24 h. At the required time point, a vial was quenched and processed according to the general procedure. The results of the time monitoring experiment are reported in Figure 3.2.

#### 3.7.10.3 Catalytic hydroalkylation reaction at 25 $^{\circ}$ C with 0.5 mol% of Ir(*P*<sup>*i*</sup>Pr<sub>3</sub>)<sub>2</sub>H<sub>5</sub> (model reaction conditions for GC studies)

The general procedure from Section 3.7.10.1 was followed using Ir(*P*<sup>*i*</sup>Pr<sub>3</sub>)<sub>2</sub>H<sub>5</sub> catalyst (5.3 mg, 0.01 mmol), diphenylacetonitrile (388.5 mg, 2.0 mmol), *n*-dodecane (193.8 mg, 1.17 mmol, GC standard) and 2-cyclohexen-1-one (379.6 mg, 4.0 mmol) in toluene (10 mL) at 25  $^{\circ}$ C for a total of 24 h. At the required time point, a vial was quenched and processed according

to the general procedure. The results of the time monitoring experiment are reported in Figure 3.3.

#### 3.7.10.4 Catalytic hydroalkylation reaction at 25 °C with 10 mol% of Ir(P<sup>i</sup>Pr<sub>3</sub>)<sub>2</sub>H<sub>5</sub> (model reaction conditions for NMR studies)

The general procedure from Section 3.7.10.1 was followed using Ir(P<sup>i</sup>Pr<sub>3</sub>)<sub>2</sub>H<sub>5</sub> catalyst (103.8 mg, 0.2 mmol), diphenylacetonitrile (386.8 mg, 2.0 mmol), *n*-dodecane (193.2 mg, 1.17 mmol, GC standard) and 2-cyclohexen-1-one (386.4 mg, 4.0 mmol) in toluene (10 mL) at 25 °C for a total of 24 h. At the required time points, a vial is quenched and processed according to the general procedure. The results of the time monitoring experiment are reported in Figure 3.4.

#### 3.7.10.5 Catalytic hydroalkylation reaction at 25 °C with 0.5 mol% of Ir(P<sup>i</sup>Pr<sub>3</sub>)<sub>2</sub>(NCCHPh<sub>2</sub>)(NCCPh<sub>2</sub>)H<sub>2</sub>

The general procedure from Section 3.7.10.1 was followed, however Ir(P<sup>i</sup>Pr<sub>3</sub>)<sub>2</sub>(NCCHPh<sub>2</sub>)(NCCPh<sub>2</sub>)H<sub>2</sub> was used as the iridium catalyst (9.1 mg, 0.01 mmol), diphenylacetonitrile (385.9 mg, 2.0 mmol), *n*-dodecane (204.5 mg, 1.17 mmol, GC standard) and 2-cyclohexen-1-one (385.1 mg, 4.0 mmol) in toluene (10 mL) at 25 °C for a total of 24 h. At the required time point, a vial was quenched and processed according to the general procedure. The results of the time monitoring experiment are reported in Figure 3.16.

#### 3.7.10.6 Catalytic hydroalkylation reaction at 25 °C with 0.5 mol% of Ir(P<sup>i</sup>Pr<sub>3</sub>)<sub>2</sub>(OPh)H<sub>2</sub>

The general procedure from Section 3.7.10.1 was followed, however Ir(P<sup>i</sup>Pr<sub>3</sub>)<sub>2</sub>(OPh)H<sub>2</sub> was used as the iridium catalyst (6.2 mg, 0.01 mmol), diphenylacetonitrile (387.0 mg, 2.0 mmol), *n*-dodecane (201.5 mg, 1.17 mmol, GC standard) and 2-cyclohexen-1-one (389.5 mg, 4.0 mmol) in toluene (10 mL) at 25 °C for a total of 24 h. At the required time point, a vial was quenched and processed according to the general procedure. The results of the time monitoring experiment are reported in Figure 3.16.

### 3.7.10.7 Catalytic hydroalkylation reaction at 25 °C with 0.5 mol% of $\text{Ir}(\text{P}^i\text{Pr}_3)_2(\text{NCCHPh}_2)(\text{NCCPh}_2)\text{H}_2$ with PhOH as an additive

#### 3.7.10.7.1 Ir/PhOH in equimolar ratio

The general procedure from Section 3.7.10.1 was followed, however  $\text{Ir}(\text{P}^i\text{Pr}_3)_2(\text{NCCHPh}_2)(\text{NCCPh}_2)\text{H}_2$  was used as the iridium catalyst (8.9 mg, 0.01 mmol) and the desired amount of PhOH was added as a stock solution (1.0 mg, 0.01 mmol). Diphenylacetonitrile (389.0 mg, 2.0 mmol), *n*-dodecane (200.3 mg, 1.17 mmol, GC standard) and 2-cyclohexen-1-one (385.6 mg, 4.0 mmol) in toluene (10 mL) at 25 °C for a total of 24 h. At the required time point, a vial was quenched and processed according to the general procedure. The results of the time monitoring experiment are reported in Figure 3.32 and also Figure 3.33.

#### 3.7.10.7.2 Ir/PhOH ratio 1:10

The general procedure from Section 3.7.10.1 was followed, however  $\text{Ir}(\text{P}^i\text{Pr}_3)_2(\text{NCCHPh}_2)(\text{NCCPh}_2)\text{H}_2$  was used as the iridium catalyst (9.3 mg, 0.01 mmol) and the desired amount of PhOH was added as a stock solution (9.7 mg, 0.10 mmol). Diphenylacetonitrile (389.0 mg, 2.0 mmol), *n*-dodecane (200.3 mg, 1.17 mmol, GC standard) and 2-cyclohexen-1-one (385.6 mg, 4.0 mmol) in toluene (10 mL) at 25 °C for a total of 24 h. At the required time point, a vial was quenched and processed according to the general procedure. The results of the time monitoring experiment are reported in Figure 3.33.

### 3.7.10.8 Catalytic hydroalkylation reaction at 25 °C with 0.5 mol% of $\text{Ir}(\text{P}^i\text{Pr}_3)_2\text{H}_5$ with PhOH as an additive

#### 3.7.10.8.1 Ir/PhOH in equimolar ratio

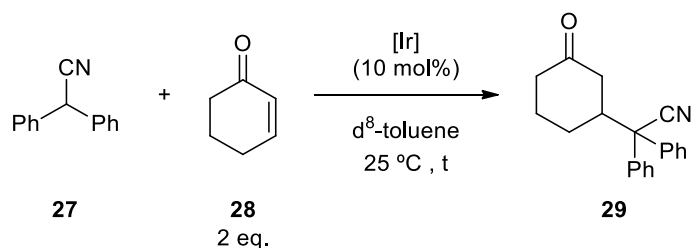
The general procedure from Section 3.7.10.1 was followed, however  $\text{Ir}(\text{P}^i\text{Pr}_3)_2\text{H}_5$  was used as the iridium catalyst (5.6 mg, 0.01 mmol) and the desired amount of PhOH was added as a stock solution (1.0 mg, 0.01 mmol). Diphenylacetonitrile (389.0 mg, 2.0 mmol), *n*-dodecane (200.3 mg, 1.17 mmol, GC standard) and 2-cyclohexen-1-one (385.6 mg, 4.0 mmol) in toluene (10 mL) at 25 °C for a total of 24 h. At the required time point, a vial was quenched and processed according to the general procedure. The results of the time monitoring experiment are reported in Figure 3.35.

### 3.7.10.8.2 Ir/PhOH ratio 1:10

The general procedure from Section 3.7.10.1 was followed, however Ir(P<sup>i</sup>Pr<sub>3</sub>)<sub>2</sub>H<sub>5</sub> was used as the iridium catalyst (5.8 mg, 0.01 mmol) and the desired amount of PhOH was added as a stock solution (9.7 mg, 0.10 mmol). Diphenylacetonitrile (389.0 mg, 2.0 mmol), *n*-dodecane (200.3 mg, 1.17 mmol, GC standard) and 2-cyclohexen-1-one (385.6 mg, 4.0 mmol) in toluene (10 mL) at 25 °C for a total of 24 h. At the required time point, a vial was quenched and processed according to the general procedure. The results of the time monitoring experiment are reported in Figure 3.35.

## 3.7.11 NMR time monitoring experiments

### 3.7.11.1 General procedure for the time monitoring experiments by NMR spectroscopy



In a glovebox, the desired iridium complex (0.012 mmol), diphenylacetonitrile (23.2 mg, 0.12 mmol), cyclohexenone (23.2 μl, 0.24 mmol) and *p*-dimethoxybenzene (3.3 mg, 0.024 mmol, NMR standard) were dissolved in d<sup>8</sup>-toluene (0.6 mL) and transferred to a J-Young NMR tube. The NMR tube was taken immediately outside the glovebox and immersed in liquid nitrogen to stop any possible reaction. Once at the instrument, all the required experiments were set up and, only after everything was ready, the NMR tube was warmed up (to avoid any condensation on the outside of the tube) and placed in the spectrometer. <sup>1</sup>H- and <sup>31</sup>P-NMR spectra were acquired at the desired time points by leaving the NMR tube inside the NMR spectrometer for the overall time of the experiment at a controlled temperature of 25 °C (298 K). The time points recorded were 5, 10, 20, 40 mins and 1, 2, 4, 8, 16, 24, (48) hours. The first time point is 5 mins instead of time zero because this is the minimum processing time required for the system (shimming and equilibration). All these NMR spectra have been acquired on a Bruker Avance III 500 MHz spectrometer.

### 3.7.11.2 Catalytic hydroalkylation reactions

#### 3.7.11.2.1 Model hydroalkylation reaction catalysed by Ir(P<sup>*i*</sup>Pr<sub>3</sub>)<sub>2</sub>H<sub>5</sub> (2)

The reaction was conducted according to the general procedure described in Section 3.7.11.1 using the Ir(P<sup>*i*</sup>Pr<sub>3</sub>)<sub>2</sub>H<sub>5</sub> catalyst (6.2 mg, 0.012 mmol), diphenylacetonitrile (23.4 mg, 0.12 mmol), 2-cyclohexenone (22.7 mg, 0.24 mmol) and p-dimethoxybenzene (3.5 mg, 0.024 mmol, NMR standard) in d<sup>8</sup>-toluene (0.6 mL) at 25 °C for 24 hours. The <sup>1</sup>H- and <sup>31</sup>P-NMR spectra are reported in Figure 3.5, Figure 3.6 and Figure 3.7.

#### 3.7.11.2.2 Hydroalkylation reaction catalysed by Ir(P<sup>*i*</sup>Pr<sub>3</sub>)<sub>2</sub>(NCCHPh<sub>2</sub>)(NCCPh<sub>2</sub>)H<sub>2</sub> (59)

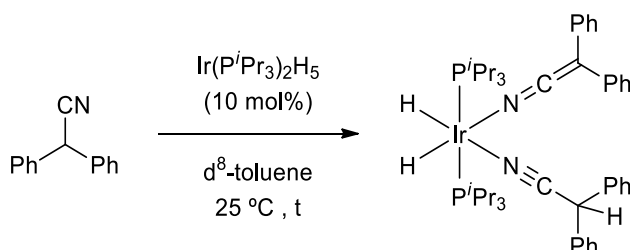
The reaction was conducted according to the general procedure described in Section 3.7.11.1 using the Ir(P<sup>*i*</sup>Pr<sub>3</sub>)<sub>2</sub>(NCCHPh<sub>2</sub>)(NCCPh<sub>2</sub>)H<sub>2</sub> intermediate as catalyst (10.6 mg, 0.012 mmol), diphenylacetonitrile (23.5 mg, 0.12 mmol), 2-cyclohexenone (23.1 mg, 0.24 mmol) and p-dimethoxybenzene (3.1 mg, 0.024 mmol, NMR standard) in d<sup>8</sup>-toluene (0.6 mL) at 25 °C for 24 hours. The <sup>1</sup>H- and <sup>31</sup>P-NMR spectra are reported in Figure 3.17 and Figure 3.18.

#### 3.7.11.2.3 Hydroalkylation reaction catalysed by Ir(P<sup>*i*</sup>Pr<sub>3</sub>)<sub>2</sub>(OPh)H<sub>2</sub> (62)

The reaction was conducted according to the general procedure described in Section 3.7.11.1 using the Ir(P<sup>*i*</sup>Pr<sub>3</sub>)<sub>2</sub>(OPh)H<sub>2</sub> intermediate as catalyst (5.4 mg, 0.012 mmol), diphenylacetonitrile (22.6 mg, 0.12 mmol) and 2-cyclohexenone (23.1 mg, 0.24 mmol) in d<sup>8</sup>-toluene (0.6 mL) at 25 °C for 24 hours. The <sup>1</sup>H- and <sup>31</sup>P-NMR spectra are reported in Figure 3.19 and Figure 3.20.

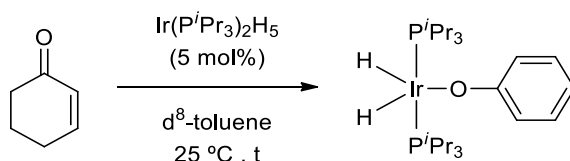
### 3.7.11.3 Reactivity investigations

#### 3.7.11.3.1 Reactivity of Ir(P<sup>*i*</sup>Pr<sub>3</sub>)<sub>2</sub>H<sub>5</sub> (2) with diphenylacetonitrile



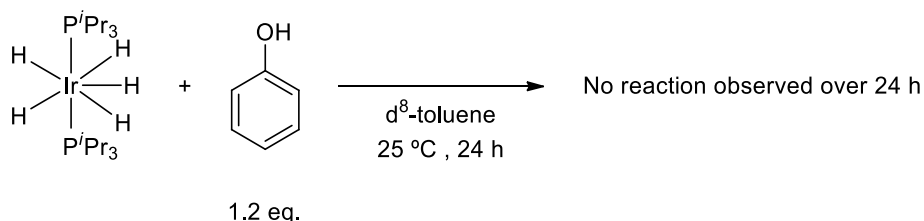
The reaction was conducted according to the general procedure described in Section 3.7.11.1 using the Ir(P<sup>*i*</sup>Pr<sub>3</sub>)<sub>2</sub>H<sub>5</sub> catalyst (6.3 mg, 0.012 mmol) and diphenylacetonitrile (24.1 mg, 0.12 mmol) in d<sup>8</sup>-toluene (0.6 mL) at 25 °C for 48 hours. The <sup>1</sup>H- and <sup>31</sup>P-NMR spectra are reported in Figure 3.8 and Figure 3.9.

### 3.7.11.3.2 Reactivity of Ir(P<sup>i</sup>Pr<sub>3</sub>)<sub>2</sub>H<sub>5</sub> (2) with cyclohexenone



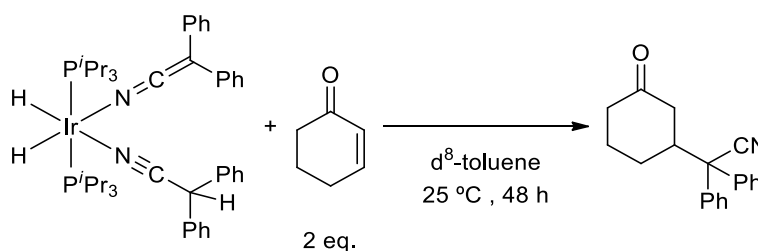
The reaction was conducted according to the general procedure described in Section 3.7.11.1 using the Ir(P<sup>i</sup>Pr<sub>3</sub>)<sub>2</sub>H<sub>5</sub> catalyst (5.7 mg, 0.012 mmol) and 2-cyclohexenone (23.5 mg, 0.24 mmol) in d<sup>8</sup>-toluene (0.6 mL) at 25 °C for 48 hours. The <sup>1</sup>H- and <sup>31</sup>P-NMR spectra are reported in Figure 3.10 and Figure 3.11.

### 3.7.11.3.3 Reactivity of Ir(P<sup>i</sup>Pr<sub>3</sub>)<sub>2</sub>H<sub>5</sub> (2) with phenol



The reaction was conducted according to the general procedure described in Section 3.7.11.1 using the Ir(P<sup>i</sup>Pr<sub>3</sub>)<sub>2</sub>H<sub>5</sub> catalyst (6.2 mg, 0.012 mmol) and phenol was added as a stock solution (1.4 mg, 0.014 mmol) in d<sup>8</sup>-toluene (0.6 mL) at 25 °C for 24 hours. The <sup>1</sup>H- and <sup>31</sup>P-NMR spectra are reported in Figure 3.36 and Figure 3.37.

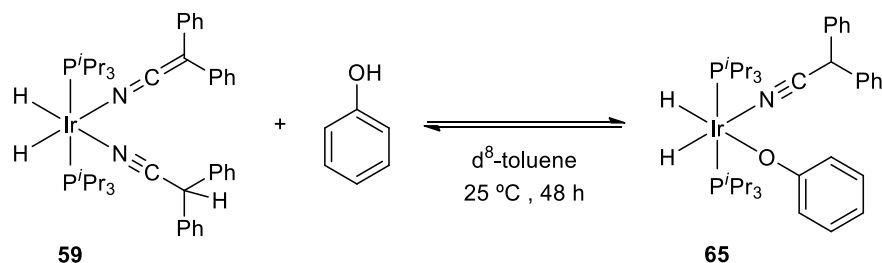
### 3.7.11.3.4 Reactivity of Ir(P<sup>i</sup>Pr<sub>3</sub>)<sub>2</sub>(NCCHPh<sub>2</sub>)(NCCPh<sub>2</sub>)H<sub>2</sub> (59) with cyclohexenone



The reaction was conducted according to the general procedure described in Section 3.7.11.1 using the Ir(P<sup>i</sup>Pr<sub>3</sub>)<sub>2</sub>(NCCHPh<sub>2</sub>)(NCCPh<sub>2</sub>)H<sub>2</sub> intermediate (5.7 mg, 0.012 mmol) and 2-cyclohexenone (23.5 mg, 0.24 mmol) in d<sup>8</sup>-toluene (0.6 mL) at 25 °C for 48 hours. The <sup>1</sup>H- and <sup>31</sup>P-NMR spectra are reported in Figure 3.21 and Figure 3.22. After the NMR experiments were completed, *n*-dodecane (11.4 mg, 10.07 mmol, GC standard) was added and the reaction mixture was passed through a short pad of silica gel (a glass Pasteur pipette filled

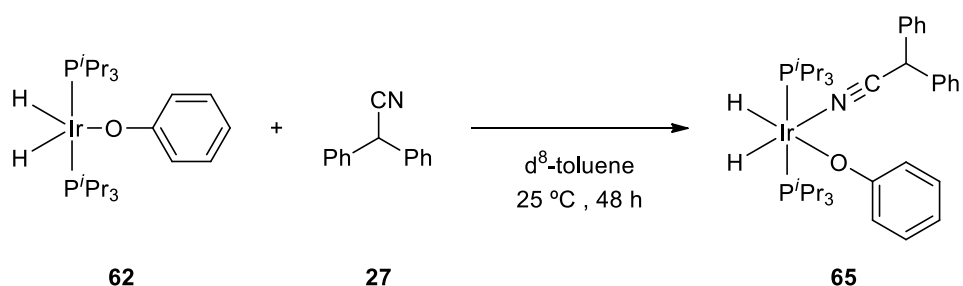
with 2 cm of silica gel) eluting with EtOAc (6.3 mL). The obtained solution was analysed by GC and results are reported in Scheme 3.29.

### 3.7.11.3.5 Reactivity of $\text{Ir}(\text{P}^i\text{Pr}_3)_2(\text{NCCHPh}_2)(\text{NCCPh}_2)\text{H}_2$ (59) with phenol



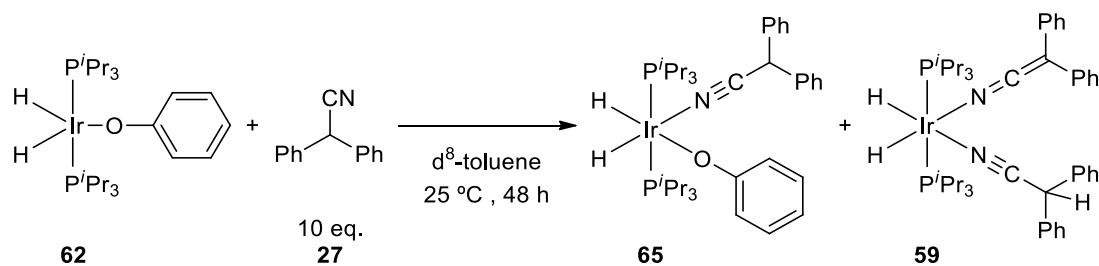
The reaction was conducted according to the general procedure described in Section 3.7.11.1 using the  $\text{Ir}(\text{P}^i\text{Pr}_3)_2(\text{NCCHPh}_2)(\text{NCCPh}_2)\text{H}_2$  (10.2 mg, 0.012 mmol) and phenol was added as a stock solution (1.1 mg, 0.012 mmol) in  $d^8$ -toluene (0.6 mL) at 25 °C for 24 hours. The  $^1\text{H}$ - and  $^{31}\text{P}$ -NMR spectra are reported in Figure 3.30 and Figure 3.31.

### 3.7.11.3.6 Reactivity of $\text{Ir}(\text{P}^i\text{Pr}_3)_2(\text{OPh})\text{H}_2$ (62) with diphenylacetonitrile in equimolar ratio



The reaction was conducted according to the general procedure described in Section 3.7.11.1 using the  $\text{Ir}(\text{P}^i\text{Pr}_3)_2(\text{OPh})\text{H}_2$  (8.1 mg, 0.012 mmol) and diphenylacetonitrile (2.3 mg, 0.012 mmol) in  $d^8$ -toluene (0.6 mL) at 25 °C for 48 hours. The  $^1\text{H}$ - and  $^{31}\text{P}$ -NMR spectra are reported in Figure 3.23 and Figure 3.24.

### 3.7.11.3.7 Reactivity of Ir(P<sup>i</sup>Pr<sub>3</sub>)<sub>2</sub>(OPh)H<sub>2</sub> (62) with diphenylacetonitrile under model reaction conditions



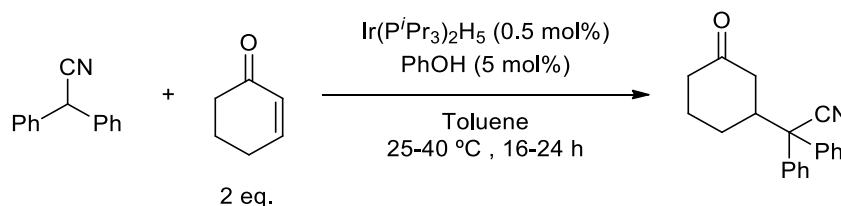
The reaction was conducted according to the general procedure described in Section 3.7.11.1 using the Ir(P<sup>i</sup>Pr<sub>3</sub>)<sub>2</sub>(OPh)H<sub>2</sub> **62** (8.8 mg, 0.012 mmol), diphenylacetonitrile (22.1 mg, 0.12 mmol) and p-dimethoxybenzene (2.7 mg, 0.024 mmol, NMR standard) in d<sup>8</sup>-toluene (0.6 mL) at 25 °C for 48 hours. The <sup>1</sup>H- and <sup>31</sup>P-NMR spectra are reported in Figure 3.28 and Figure 3.29.

### 3.7.11.4 Mixing experiment between two iridium-phenoxide complexes: Ir(P<sup>i</sup>Pr<sub>3</sub>)<sub>2</sub>(OPh)H<sub>2</sub> (62) and Ir(PCy<sub>3</sub>)<sub>2</sub>(OPh)H<sub>2</sub> (63)

In a glovebox, the desired Ir(P<sup>i</sup>Pr<sub>3</sub>)<sub>2</sub>(OPh)H<sub>2</sub> (10.2 mg, 0.016 mmol) and Ir(PCy<sub>3</sub>)<sub>2</sub>(OPh)H<sub>2</sub> (12.5 mg, 0.016 mmol) were dissolved in d<sup>8</sup>-toluene (0.6 mL) and transferred to a J-Young NMR tube. The NMR tube was taken immediately outside the glovebox and immersed in liquid nitrogen to stop any possible reaction. Once at the instrument, all the required experiments were set up and, only after everything was ready, the NMR tube was warmed up (to avoid any condensation on the outside of the tube) and placed in the spectrometer. <sup>1</sup>H- and <sup>31</sup>P-NMR spectra were acquired. The NMR tube was then maintained at 25 °C and the NMR spectra recorded again after 24 hours. The <sup>31</sup>P-NMR spectra are reported in Figure 3.15. The NMR experiments were also recorded after 3 hours at 50 °C and after 16 hours at 80 °C with no difference observed (only small new peaks formed which are likely decomposition products). All these NMR spectra have been acquired on a Bruker Avance III 500 MHz spectrometer.



### 3.7.12 Michael-type hydroalkylation catalysed by Ir(P<sup>t</sup>Pr<sub>3</sub>)<sub>2</sub>H<sub>5</sub> with phenol as an additive (10 equivalents)



#### 3.7.12.1 Control experiment without iridium at 25 °C for 24 h

In a glovebox, phenol (0.9 mg, 0.01 mmol), diphenylacetonitrile (38.8 mg, 0.20 mmol) and *n*-dodecane (26.7 μL, 19.8 mg, 0.12 mmol, GC standard) were dissolved in toluene (1 mL) in a glass 4 mL vial. Then, 2-cyclohexen-1-one (40.2 mg, 0.40 mmol) was added and the mixture was transferred to a 4 mL glass vials equipped with a stirring bar. The vial was sealed with a Teflon lined cap. Once outside the glovebox, the reaction was heated at 25 °C for 24 h. The reaction was then quenched by cooling in an ice-bath and bubbling air through the solution, and the reaction mixture was passed through a short pad of silica gel (a glass Pasteur pipette filled with 2 cm of silica gel) eluting with EtOAc (10.5 ml). The obtained solution was analysed by GC and the results are reported in Table 3.3.

#### 3.7.12.2 Tests at 25 °C, for 16 and 24 h

The tests at 25 °C, for 16 and 24 hours were the ones from the GC monitoring experiment reported in Section 3.7.10.8.2. Results are reported in Table 3.3.

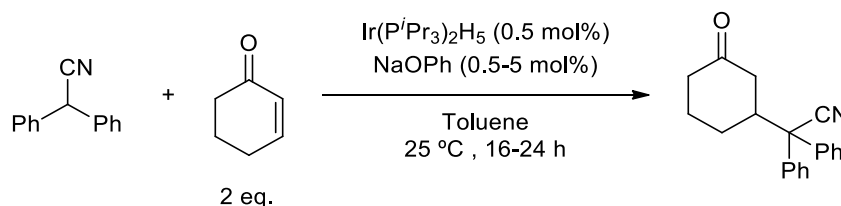
#### 3.7.12.3 Tests at 40 °C, for 16 and 24 h

In a glovebox, the Ir(P<sup>t</sup>Pr<sub>3</sub>)<sub>2</sub>H<sub>5</sub> catalyst (1.2 mg, 0.002 mmol), phenol (1.9 mg, 0.02 mmol), diphenylacetonitrile (77.5 mg, 0.40 mmol) and *n*-dodecane (53.3 μL, 39.6 mg, 0.23 mmol, GC standard) were dissolved in toluene (2 mL) in a glass 4 mL vial. Then, 2-cyclohexen-1-one (80.4 mg, 0.80 mmol) was added and the mixture was equally partitioned into 2 x 4 mL glass vials equipped with a stirring bar. The vials were sealed with a Teflon lined cap. Once outside the glovebox, the reactions were heated at 40 °C for the required time (16 or 24 h). Each aliquot was quenched by cooling in an ice-bath and bubbling air through the solution, and the reaction mixture was passed through a short pad of silica gel (a glass Pasteur pipette filled with 2 cm of silica gel) eluting with EtOAc (10.5 ml). The obtained solutions were analysed by GC and the results are reported in Table 3.3.

#### 3.7.12.4 Tests in the absence of phenol

The tests performed in the absence of phenol reported in Table 3.3 as a comparison are the results from the experiments reported in Section 3.7.10.2 and Section 3.7.10.3.

#### 3.7.13 Michael-type hydroalkylation catalysed by $\text{Ir}(\text{P}^i\text{Pr}_3)_2\text{H}_5$ with NaOPh as an additive



##### 3.7.13.1 Control experiment without iridium and 0.5 mol% of NaOPh

In a glovebox, NaOPh (0.2 mg, 0.001 mmol), diphenylacetonitrile (38.6 mg, 0.20 mmol) and *n*-dodecane (26.7  $\mu\text{L}$ , 20.0 mg, 0.12 mmol, GC standard) were dissolved in toluene (1 mL) in a glass 4 mL vial. Then, 2-cyclohexen-1-one (38.5 mg, 0.40 mmol) was added and the mixture was transferred to a 4 mL glass vial equipped with a stirring bar. The vial was sealed with a Teflon lined cap. Once outside the glovebox, the reaction was heated at 25 °C for 24 h. The reaction was then quenched by cooling it in an ice-bath and bubbling air through the solution, and the reaction mixture was passed through a short pad of silica gel (a glass Pasteur pipette filled with 2 cm of silica gel) eluting with EtOAc (10.5 mL). The obtained solution was analysed by GC and the results are reported in Table 3.4.

##### 3.7.13.2 Test with 0.5 mol% of NaOPh

In a glovebox, the  $\text{Ir}(\text{P}^i\text{Pr}_3)_2\text{H}_5$  catalyst (1.2 mg, 0.002 mmol), NaOPh (0.2 mg, 0.002 mmol), diphenylacetonitrile (77.5 mg, 0.40 mmol) and *n*-dodecane (53.3  $\mu\text{L}$ , 39.2 mg, 0.23 mmol, GC standard) were dissolved in toluene (2 mL) in a glass 4 mL vial. Then, 2-cyclohexen-1-one (80.4 mg, 0.80 mmol) was added and the mixture was equally partitioned into 2 x 4 mL glass vials equipped with a stirring bar. The vials were sealed with a Teflon lined cap. Once outside the glovebox, the reactions were heated at 25 °C for the required time (16 or 24 h). Each aliquot of the reaction was quenched by cooling in an ice-bath and bubbling air through the solution, and the reaction mixture was passed through a short pad of silica gel (a glass Pasteur pipette filled with 2 cm of silica gel) eluting with EtOAc (10.5 mL). The obtained solutions were analysed by GC and the results are reported in Table 3.4.

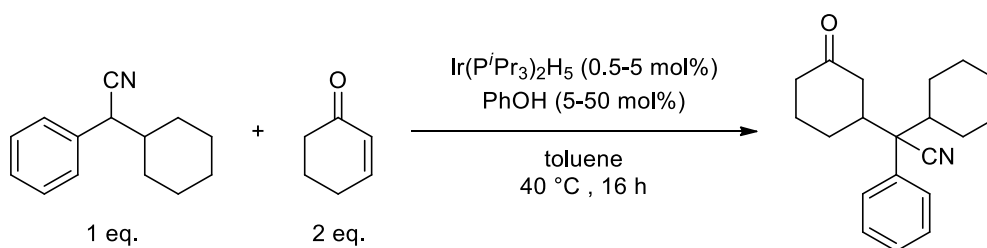
### 3.7.13.3 Test with 5 mol% of NaOPh

In a glovebox, the  $\text{Ir}(\text{P}^i\text{Pr}_3)_2\text{H}_5$  catalyst (1.2 mg, 0.002 mmol), NaOPh (2.3 mg, 0.02 mmol), diphenylacetonitrile (77.5 mg, 0.40 mmol) and *n*-dodecane (53.3  $\mu\text{L}$ , 39.2 mg, 0.23 mmol, GC standard) were dissolved in toluene (2 mL) in a glass 4 mL vial. Then, 2-cyclohexen-1-one (80.4 mg, 0.80 mmol) was added and the mixture was equally partitioned into 2 x 4 mL glass vials equipped with a stirring bar. The vials were sealed with a Teflon lined cap. Once outside the glovebox, the reactions were heated at 25 °C for the required time (16 or 24 h). Each aliquot of the reaction was quenched by cooling in an ice-bath and bubbling air through the solution, and the reaction mixture was passed through a short silica gel column (a glass Pasteur pipette filled with 2 cm of silica gel) eluting with EtOAc (10.5 mL). The obtained solutions were analysed by GC and the results are reported in Table 3.4.

### 3.7.13.4 Test in the presence of PhOH

Results reported in Table 3.4 for the yield of the same reaction performed in the presence of phenol instead that NaOH are the results of the experiments reported in Section 3.7.10.8 for 16 and 24 hours of reaction.

### 3.7.14 Michael-type hydroalkylation of 2-cyclohexen-1-one with Cy-substituted phenylacetonitrile catalysed by $\text{Ir}(\text{P}^i\text{Pr}_3)_2\text{H}_5$ with phenol as an additive



In a glovebox, cyclohexyl-phenyl- acetonitrile (123.3 mg, 0.60 mmol), *n*-dodecane (69.3 mg, 0.35 mmol, GC standard) and 2-cyclohexen-1-one (115.7 mg, 1.20 mmol) were dissolved in toluene (1.2 mL) in a glass 4 mL vial. The mixture was equally partitioned into 3 x 4 mL glass vials equipped with a stirring bar. The required amount of  $\text{Ir}(\text{P}^i\text{Pr}_3)_2\text{H}_5$  catalyst (0.001-0.1 mmol) and phenol (0.01-0.10 mmol) was added to each vial as a stock solution in toluene (0.6 mL) (see Table 3.10 below for specific amounts). The vials were sealed with a Teflon lined cap. Once outside the glovebox, the reactions were heated at 40 °C for 16 hours. Each

reaction mixture was quenched by cooling in an ice-bath and bubbling air through the solution and each one of them was passed through a short pad of silica gel (a glass Pasteur pipette filled with 2 cm of silica gel) eluting with EtOAc (10.5 ml). The obtained solutions were analysed by GC. However, instrument errors did not allow to reliably use the GC for the quantification of the reaction mixture. The products were indeed quantified after being isolated *via* flash chromatography (silica gel, eluting with 10:1, hexane/EtOAc). The amounts of isolated product are reported in Table 3.10 below.

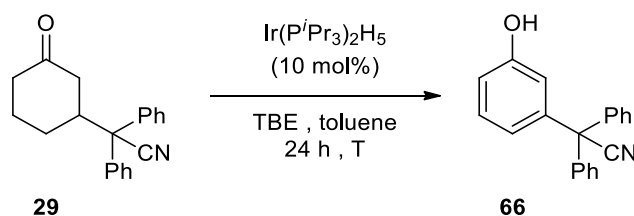
Table 3.10 Exact amounts and results for the optimisation of the Michael addition of Cy-substituted phenylacetonitriles to cyclohexenone with phenol as an additive.

| Entry | Ir (mol%) | Ir (mg) | PhOH (mg) | Product (mg) | Yield (%) |
|-------|-----------|---------|-----------|--------------|-----------|
| 1     | 0.5       | 0.5     | 0.9       | 12.9         | 21        |
| 2     | 2.5       | 2.6     | 4.7       | 26.2         | 43        |
| 3     | 5.0       | 5.2     | 9.4       | 34.7         | 57        |

### 3.7.15 Dehydrogenation of 3-substituted cyclohexanones to *meta*-substituted phenols

3.7.15.1 Attempted iridium-catalysed transfer dehydrogenation of 2-(3-oxocyclohexyl)-2,2-diphenylacetonitrile to the corresponding *meta*-substituted phenol

3.7.15.1.1 Screening of temperatures



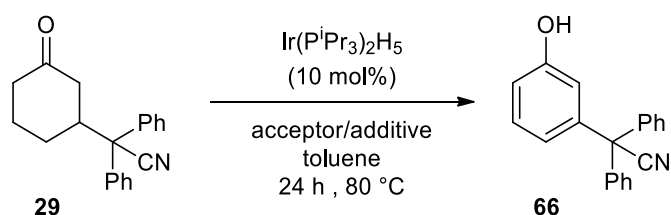
In a glovebox, the  $\text{Ir}(\text{P}^i\text{Pr}_3)_2\text{H}_5$  catalyst (10.4 mg, 0.02 mmol), 2-(3-oxocyclohexyl)-2,2-diphenylacetonitrile (57.9 mg, 0.20 mmol) and *n*-dodecane (26.7  $\mu\text{L}$ , 20.0 mg, 0.12 mmol, GC standard) were weighted in a Schlenk bomb and dissolved in toluene (1 mL). Then, TBE (258  $\mu\text{L}$ , 2.00 mmol) was added together with a stirring bar. The sealed vessel was taken outside the glovebox and heated at the required temperature for 24 hours. The reaction was then

quenched by cooling it in an ice-bath and bubbling air through the solution. The reaction mixture was passed through a short pad of silica gel (a glass Pasteur pipette filled with 2 cm of silica gel) eluting with EtOAc (10.5 ml). The obtained solution was analysed by GC and results are reported in Table 3.6. Specific amounts used for Ir(P<sup>i</sup>Pr<sub>3</sub>)<sub>2</sub>H<sub>5</sub> and 2-(3-oxocyclohexyl)-2,2-diphenylacetonitrile are reported below in Table 3.11.

Table 3.11 Exact amounts for the temperature screening for the attempted iridium-catalysed transfer dehydrogenation of 2-(3-oxocyclohexyl)-2,2-diphenylacetonitrile.

| Entry | T (°C) | Ir (mg) | 29 (mg) |
|-------|--------|---------|---------|
| 1     | 120    | 10.5    | 58.4    |
| 2     | 80     | 9.3     | 58.4    |
| 3     | 40     | 10.8    | 57.4    |

### 3.7.15.1.2 Screening of hydrogen acceptors and additives

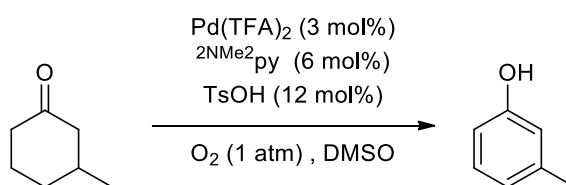


In a glovebox, the Ir(P<sup>i</sup>Pr<sub>3</sub>)<sub>2</sub>H<sub>5</sub> catalyst (10.4 mg, 0.02 mmol), 2-(3-oxocyclohexyl)-2,2-diphenylacetonitrile (57.9 mg, 0.20 mmol) and *n*-dodecane (26.7 μL, 20.0 mg, 0.12 mmol, GC standard) were weighted in a Schlenk bomb and dissolved in toluene (1 mL). Then, the additive and/or hydrogen acceptor (2.00 mmol, exact amounts are reported below in Table 3.12) were added together with a stirring bar. The sealed vessel was taken outside the glovebox and heated at 80 °C for 24 hours. The reaction was then quenched by cooling it in an ice-bath and bubbling air through the solution. The reaction mixture was passed through a short pad of silica gel (a glass Pasteur pipette filled with 2 cm of silica gel) eluting with EtOAc (10.5 ml). The obtained solution was analysed by GC and results are reported in Table 3.7.

Table 3.12 Exact amounts for the screening of acceptors and additives for the attempted iridium-catalysed transfer dehydrogenation of 2-(3-oxocyclohexyl)-2,2-diphenylacetonitrile.

| Entry | TBE (mg) | Cyclohexenone (mg) | Nitrile (mg) |
|-------|----------|--------------------|--------------|
| 1     | -        | 191.0              | -            |
| 2     | 167.1    | 191.8              | -            |
| 3     | -        | -                  | 385.9        |
| 4     | 170.3    | -                  | 386.6        |

### 3.7.15.2 Attempted ultrasound-promoted Stahl dehydrogenation



#### 3.7.15.2.1 Thermal reactions (0.36 mL)

Under air,  $\text{Pd(TFA)}_2$  (10.0 mg, 0.03 mmol), 3-methylcyclohexanone (112.2 mg, 1.00 mmol), 2-(N,N-dimethylamino)pyridine (7.3 mg, 0.06 mmol) and *p*-toluenesulfonic acid monohydrate (22.8 mg, 0.12 mmol) were charged in a 4 mL glass vial equipped with magnetic stirring and dissolved in DMSO (0.36 mL). The vial was capped (cap with septum with inlet and outlet needle) and  $\text{O}_2$  was bubbled for 10 minutes inside the reaction mixture using a balloon. The reaction mixture was heated at the required temperature (r.t. or 80 °C) for the required time (1-24 h). After cooling down the reaction mixture, *n*-dodecane (74.0  $\mu\text{L}$ , 55.5 mg, 0.33 mmol, GC standard) was added followed by EtOAc (8 mL) and a saturated solution of aqueous  $\text{NH}_4\text{Cl}$  (10 mL). The phases were separated and the aqueous phase was further re-extracted with EtOAc (3 x 8 mL). The combined organic layer was dried over  $\text{MgSO}_4$  and 1 mL was analysed by GC and GC-MS, products have been confirmed by matching with the mass spec database. Results are reported in Table 3.8

#### 3.7.15.2.2 Thermal reactions (5 mL)

Under air,  $\text{Pd(TFA)}_2$  (137.1 mg, 0.041 mmol), 3-methylcyclohexanone (1542.3 mg, 13.75 mmol), 2-(N,N-dimethylamino)pyridine (100.8 mg, 0.83 mmol) and *p*-toluenesulfonic acid monohydrate (313.9 mg, 1.65 mmol) were charged in a 20 mL glass vial equipped with

magnetic stirring and dissolved in DMSO (5.0 mL). The vial was capped (cap with septum with inlet and outlet needle) and O<sub>2</sub> was bubbled for 10 minutes inside the reaction mixture using a balloon. The reaction mixture was heated at 80 °C for the required time (1-24 h). An aliquot (0.5 mL) of the reaction mixture was taken (at the required time), diluted in EtOAc (8 mL) and *n*-dodecane (74.0 μL, 55.5 mg, 0.33 mmol, GC standard) was added followed by a saturated solution of aqueous NH<sub>4</sub>Cl (10 mL). The phases were separated and the aqueous phase was further re-extracted with EtOAc (3 x 8 mL). The combined organic layer was dried over MgSO<sub>4</sub> and 1 ml was analysed by GC and GC-MS, products have been confirmed by matching with the mass spec database. Results are reported in Table 3.8

#### 3.7.15.2.3 Reactions under ultrasound (5 mL)

Under air, Pd(TFA)<sub>2</sub> (137.1 mg, 0.041 mmol), 3-methylcyclohexanone (1542.3 mg, 13.75 mmol), 2-(*N,N*-dimethylamino)pyridine (100.8 mg, 0.83 mmol) and *p*-toluenesulfonic acid monohydrate (313.9 mg, 1.65 mmol) were charged in a 25 mL 2-neck flask and dissolved in DMSO (5.0 mL). Then, the sonochemical reactor was assembled (*see* previous chapter for the set-up, without connection to the Schlenk line). O<sub>2</sub> was bubbled for 10 minutes inside the reaction mixture using a balloon. The reactor was immersed in a water-cooling bath to maintain the solution at room temperature (25 ± 3 °C). The horn and the upper part of the reactor were cooled down from the outside by a continuous stream of compressed air. The reaction mixture was sonicated under a pulse mode (amplitude 100%). The ultrasound was applied for 10 minutes and then stopped for another 10 minutes. An aliquot (0.5 mL) of the reaction mixture was taken (at the required time), diluted in EtOAc (8 mL) and *n*-dodecane (74.0 μL, 55.5 mg, 0.33 mmol, GC standard) was added followed by a saturated solution of aqueous NH<sub>4</sub>Cl (10 mL). The phases were separated and the aqueous phase was further re-extracted with EtOAc (3 x 8 mL). The combined organic layer was dried over MgSO<sub>4</sub> and 1 ml was analysed by GC and GC-MS, products have been confirmed by matching with the mass spec database. Results are reported in Table 3.8.

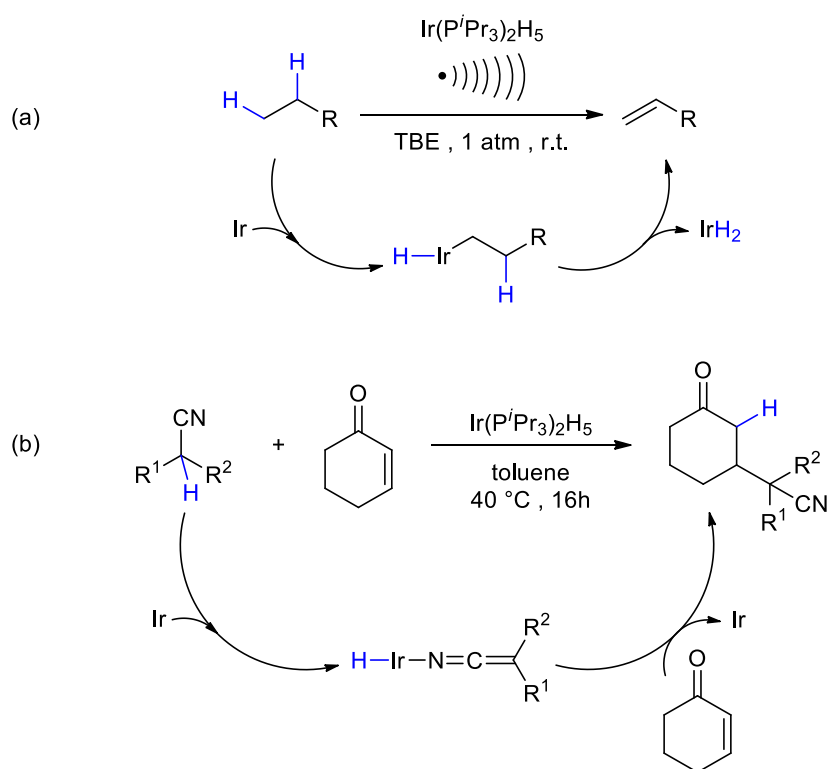
# 4

## Conclusions



## 4.1 Summary and conclusions

Activation of aliphatic C-H bonds is a fundamental challenge in organic chemistry. In this work it has been shown how this problem was tackled with two complementary approaches. First, the room-temperature sonochemical alkane dehydrogenation was described, where the alkane C-H bond is activated by an iridium complex to achieve the dehydrogenated olefin (Scheme 4.1, a). The second approach, instead, described how the C-H bond of diphenylacetone nitrile is activated by the same iridium complex to achieve the Michael addition product with cyclohexenone (Scheme 4.1, b).



Scheme 4.1 Types of iridium-mediated C-H activation reactions investigated in the present work. (a) Room-temperature sonochemical transfer alkane dehydrogenation. (b) Michael-type hydroalkylation of cyclohexenone with alkyl-aryl-nitriles.

Alkane dehydrogenation is the most economical route to convert abundant and inexpensive hydrocarbon feedstock into olefins, however relative high temperatures are still required both on industrial and lab scale for the transformation to be efficient. Aiming to tackle this issue, this work presented the development of a sonochemical approach for the alkane dehydrogenation:

- The transfer alkane dehydrogenation has been achieved at room-temperature by combining catalysis and sonochemistry.
- Ultrasound has been used as a method for chemical activation, exploiting the cavitation to provide the energy necessary to achieve the endergonic alkane dehydrogenation under extremely mild conditions, compared to what is reported for the most known homogeneous systems.
- Various literature catalysts have been tested and the iridium-pentahydride catalyst  $\text{Ir}(\text{P}^i\text{Pr}_3)_2\text{H}_5$  was found to be active under sonochemical conditions. Hence, a series of bisphosphine-iridium-pentahydride complexes bearing different trialkyl-phosphine ligands have been synthesised and tested, including two novel complexes. However, the iridium complex bearing *iso*-propyl-substituted phosphines was confirmed to be the best under the studied conditions.
- The reaction conditions have been optimised, specifically catalyst and TBE concentration, reaction time and amplitude of ultrasounds.
- A sonochemical reactor has also been developed in order to carry out these reactions under inert atmosphere.
- The alkane scope was investigated and various alkanes, both linear and cyclic from  $\text{C}_6$  to  $\text{C}_{12}$  have been tested, showing feasibility of the sonochemical approach with TONs of 1.2.
- Various experiments have been performed to gain more insights on the process. In particular, a temporal control experiment showed how the activated metal species had a short lifetime and existed only under ultrasound irradiation, which ultimately promoted the dehydrogenation.
- Catalyst deactivation has been identified as the main cause of the low activity of the system. The most common deactivation pathways, such as ligand cyclometalation and inhibition by the product, have been experimentally discarded.
- Lastly, the dct and mercury tests confirmed the homogeneous nature of the system.
- This is an important proof of concept and it also represents the first reported example of a one-step dehydrogenation of alkanes at room-temperature.

The other part of the project investigated a specific type of Michael addition. Classic Michael additions require a nucleophile bearing functional groups to effectively stabilise the charge and the use of a base, such as alkali hydroxides and alkoxides. Many transition-metal alternatives have been developed, which allowed to expand the scope of nucleophiles, however, there is only one example for the activation of a weakly acidic tertiary C-H bond. Aiming to expand this scope, an iridium-catalysed Michael-type hydroalkylation of cyclohexenone with weakly acidic nitriles has been developed in the same laboratories and operating under mild conditions. The aim of this work was to further investigate and develop this reaction:

- The weakly C-H acidic alkyl aryl nitriles scope has been successfully expanded to difficult pyridyl-substituted acetonitriles, and the corresponding hydroalkylation products have been synthesised and isolated in good to excellent yields.
- Based on the mechanistic investigations, a revised catalytic cycle has been proposed and supported with experimental data.
- The iridium-pentahydride catalyst was activated by cyclohexenone *via* a disproportionation reaction to yield the catalytically active iridium-phenoxide complex.
- The iridium-phenoxide complex has been identified as a reaction intermediate, together with two other complexes, an iridium-ylide-nitrile and an iridium-nitrile-phenoxide. The novel iridium-phenoxide and iridium-nitrile-phenoxide intermediates have also been isolated and characterised.
- The mechanistic investigations also highlighted how the iridium-phenoxide and iridium-ylide-nitrile complexes could be used as catalyst for the hydroalkylation reaction, instead of the iridium-pentahydride complex.
- It has been shown how phenol can be successfully used as an additive to improve this hydroalkylation reaction.

5

## References

1. Pérez, P. J., Alkane C-H Activation by Single-Site Metal Catalysis, *Catalysis by Metal Complexes*, Springer, New York **2012**, 38.
2. Roudesly, F.; Oble, J.; Poli, G., *Journal of Molecular Catalysis A: Chemical* **2017**, 426, 275-296.
3. Brown, W.; Foote, C.; Iverson, B.; Anslyn, E., *Organic Chemistry*. 5th ed.; Cengage Learning **2009**.
4. Cioc, R. C.; Ruijter, E.; Orru, R. V. A., *Green Chemistry* **2014**, 16 (6), 2958-2975.
5. Zhu, J. P.; Bienaymé, H., *Multicomponent Reactions*. Wiley-VCH, Weinheim **2005**.
6. Weissermel, K.; Arpe, H. J., *Industrial Organic Chemistry*. 4th ed.; Wiley-VCH, Weinheim **2003**.
7. Hofmann, A. W., *Berichte der deutschen chemischen Gesellschaft* **1883**, 16 (1), 558-560.
8. Hofmann, A. W., *Berichte der deutschen chemischen Gesellschaft* **1885**, 18 (1), 109-131.
9. Volhard, J., *Ueber Verbindungen des Thiophens, seiner Homologen und einiger Ketone mit Quecksilberchlorid*, *Justus Liebigs Ann. Chem.* **1892**, 267 (2-3), 172-185.
10. Morikawa, K.; Benedict, W. S.; Taylor, H. S., *Journal of the American Chemical Society* **1936**, 58 (8), 1445-1449.
11. Chatt, J.; Davidson, J. M., *Journal of the Chemical Society (Resumed)* **1965**, 843-855.
12. Hodges, R. J.; Garnett, J. L., *Journal of Catalysis* **1969**, 13 (1), 83-98.
13. Shilov, A. E.; Shul'pin, G. B., *Chemical Reviews* **1997**, 97 (8), 2879-2932.
14. Janowicz, A. H.; Bergman, R. G., *Journal of the American Chemical Society* **1982**, 104 (1), 352-354.
15. Hoyano, J. K.; Graham, W. A. G., *Journal of the American Chemical Society* **1982**, 104 (13), 3723-3725.
16. Jones, W. D.; Feher, F. J., *Organometallics* **1983**, 2 (4), 562-563.
17. Balcells, D.; Clot, E.; Eisenstein, O., *Chemical Reviews* **2010**, 110 (2), 749-823.
18. Gensch, T.; Hopkinson, M. N.; Glorius, F.; Wencel-Delord, J., *Chemical Society Reviews* **2016**, 45 (10), 2900-2936.
19. Frenking, G., *Theoretical Aspects of Transition Metal Catalysis*, *Topics in Organometallic Chemistry*, vol 12, Springer, Berlin **2005**, 3-3.
20. Vastine, B. A.; Hall, M. B., *Coordination Chemistry Reviews* **2009**, 253 (7), 1202-1218.
21. Collins, D. E.; Richey, F. A., *Riegel's Handbook of Industrial Chemistry*. 10th ed.; Van Nostrand Reinhold, New York **1992**.
22. Sattler, J. J. H. B.; Ruiz-Martinez, J.; Santillan-Jimenez, E.; Weckhuysen, B. M., *Chemical Reviews* **2014**, 114 (20), 10613-10653.

23. Findlater, M.; Choi, J.; Goldman, A. S.; Brookhart, M., Alkane Dehydrogenation. In *Alkane C-H Activation by Single-Site Metal Catalysis*, Springer: New York **2012**; Vol. 38, pp 113-141.
24. Choi, J.; MacArthur, A. H. R.; Brookhart, M.; Goldman, A. S., *Chemical Reviews* **2011**, *111* (3), 1761-1779.
25. Zhang, Y.; Yao, W.; Fang, H.; Hu, A.; Huang, Z., *Science Bulletin* **2015**, *60* (15), 1316.
26. Amghizar, I.; Vandewalle, L. A.; Van Geem, K. M.; Marin, G. B., *Engineering* **2017**, *3* (2), 171-178.
27. Sadrameli, S. M., *Fuel* **2015**, *140* (Supplement C), 102-115.
28. Dobereiner, G. E.; Crabtree, R. H., *Chemical Reviews* **2010**, *110* (2), 681-703.
29. Morales-Morales, D., Iridium-Mediated Alkane Dehydrogenation. In *Iridium Complexes in Organic Synthesis*, Wiley-VCH **2009**; pp 325-344.
30. Crabtree, R. H.; Mihelcic, J. M.; Quirk, J. M., *Journal of the American Chemical Society* **1979**, *101* (26), 7738-7740.
31. Crabtree, R. H.; Mellea, M. F.; Mihelcic, J. M.; Quirk, J. M., *Journal of the American Chemical Society* **1982**, *104* (1), 107-113.
32. Crabtree, R. H., *Journal of the Chemical Society, Dalton Transactions* **2001**, (17), 2437-2450.
33. Baudry, D.; Ephritikhine, M.; Felkin, H., *Journal of the Chemical Society, Chemical Communications* **1980**, (24), 1243-1244.
34. Baudry, D.; Ephritikhine, M.; Felkin, H., *Journal of the Chemical Society, Chemical Communications* **1982**, (11), 606-607.
35. Baudry, D.; Ephritikhine, M.; Felkin, H.; Holmes-Smith, R., *Journal of the Chemical Society, Chemical Communications* **1983**, (14), 788-789.
36. Burk, M. J.; Crabtree, R. H.; Parnell, C. P.; Uriarte, R. J., *Organometallics* **1984**, *3* (5), 816-817.
37. Burk, M. J.; Crabtree, R. H.; McGrath, D. V., *Journal of the Chemical Society, Chemical Communications* **1985**, (24), 1829-1830.
38. Burk, M. J.; Crabtree, R. H., *Journal of the American Chemical Society* **1987**, *109* (26), 8025-8032.
39. Felkin, H.; Fillebeen-Khan, T.; Gault, Y.; Holmes-Smith, R.; Zakrzewski, J., *Tetrahedron Letters* **1984**, *25* (12), 1279-1282.
40. Felkin, H.; Fillebeen-khan, T.; Holmes-Smith, R.; Yingrui, L., *Tetrahedron Letters* **1985**, *26* (16), 1999-2000.

41. Fujii, T.; Saito, Y., *Journal of the Chemical Society, Chemical Communications* **1990**, (10), 757-758.
42. Aoki, T.; Crabtree, R. H., *Organometallics* **1993**, 12 (2), 294-298.
43. Kumar, A.; Goldman, A. S., Recent Advances in Alkane Dehydrogenation Catalyzed by Pincer Complexes. In *The Privileged Pincer-Metal Platform: Coordination Chemistry & Applications*, van Koten, G.; Gossage, R. A., Eds. Springer International Publishing: Cham **2016**; pp 307-334.
44. Kumar, A.; Bhatti, T. M.; Goldman, A. S., *Chemical Reviews* **2017**, 117 (19), 12357-12384.
45. Moulton, C. J.; Shaw, B. L., *Journal of the Chemical Society, Dalton Transactions* **1976**, (11), 1020-1024.
46. Gupta, M.; Hagen, C.; Flesher, R. J.; Kaska, W. C.; Jensen, C. M., *Chemical Communications* **1996**, (17), 2083-2084.
47. Gupta, M.; Kaska, W.; M. Jensen, C., *Chemical Communications* **1997**, (5), 461-462.
48. Gupta, M.; Hagen, C.; Kaska, W. C.; Cramer, R. E.; Jensen, C. M., *Journal of the American Chemical Society* **1997**, 119 (4), 840-841.
49. Liu, F.; Pak, E. B.; Singh, B.; Jensen, C. M.; Goldman, A. S., *Journal of the American Chemical Society* **1999**, 121 (16), 4086-4087.
50. Jensen, C. M., *Chemical Communications* **1999**, (24), 2443-2449.
51. Xu, W.-w.; Rosini, G. P.; Krogh-Jespersen, K.; Goldman, A. S.; Gupta, M.; Jensen, C. M.; Kaska, W. C., *Chemical Communications* **1997**, (23), 2273-2274.
52. Liu, F.; Goldman, A. S., *Chemical Communications* **1999**, (7), 655-656.
53. Kanzelberger, M.; Singh, B.; Czerw, M.; Krogh-Jespersen, K.; Goldman, A. S., *Journal of the American Chemical Society* **2000**, 122 (44), 11017-11018.
54. Renkema, K. B.; Kissin, Y. V.; Goldman, A. S., *Journal of the American Chemical Society* **2003**, 125 (26), 7770-7771.
55. Niu, S.; Hall, M. B., *Journal of the American Chemical Society* **1999**, 121 (16), 3992-3999.
56. Punji, B.; Emge, T. J.; Goldman, A. S., *Organometallics* **2010**, 29 (12), 2702-2709.
57. Göttker-Schnetmann, I.; White, P.; Brookhart, M., *Journal of the American Chemical Society* **2004**, 126 (6), 1804-1811.
58. Morales-Morales, D.; Redón, R. o.; Yung, C.; Jensen, C. M., *Inorganica Chimica Acta* **2004**, 357 (10), 2953-2956.
59. Yao, W.; Zhang, Y.; Jia, X.; Huang, Z., *Angewandte Chemie International Edition* **2014**, 53 (5), 1390-1394.

60. Cavaliere, V. N.; Crestani, M. G.; Pinter, B.; Pink, M.; Chen, C.-H.; Baik, M.-H.; Mindiola, D. J., *Journal of the American Chemical Society* **2011**, *133* (28), 10700-10703.
61. Crestani, M. G.; Hickey, A. K.; Gao, X.; Pinter, B.; Cavaliere, V. N.; Ito, J.-I.; Chen, C.-H.; Mindiola, D. J., *Journal of the American Chemical Society* **2013**, *135* (39), 14754-14767.
62. Solowey, D. P.; Mane, M. V.; Kurogi, T.; Carroll, P. J.; Manor, B. C.; Baik, M.-H.; Mindiola, D. J., *Nature Chemistry* **2017**, *9* (11), 1126-1132.
63. Sakakura, T.; Abe, F.; Tanaka, M., *Chemistry Letters* **1991**, *20* (2), 297-298.
64. Sakakura, T.; Abe, F.; Tanaka, M., *Chemistry Letters* **1991**, *20* (3), 359-362.
65. Tanaka, M.; Sakakura, T., *Solar Energy Materials* **1991**, *24* (1-4), 406-412.
66. Sakakura, T.; Sodeyama, T.; Tokunaga, Y.; Tanaka, M., *Chemistry Letters* **1988**, (Vol. 17), 263 - 264.
67. Nomura, K.; Saito, Y., *Journal of the Chemical Society, Chemical Communications* **1988**, (3), 161-162.
68. Maguire, J. A.; Boese, W. T.; Goldman, A. S., *Journal of the American Chemical Society* **1989**, *111* (18), 7088-7093.
69. Maguire, J. A.; Boese, W. T.; Goldman, M. E.; Goldman, A. S., *Coordination Chemistry Reviews* **1990**, *97*, 179-192.
70. Chowdhury, A. D.; Weding, N.; Julis, J.; Franke, R.; Jackstell, R.; Beller, M., *Angewandte Chemie International Edition* **2014**, *53* (25), 6477-6481.
71. Chowdhury, A. D.; Julis, J.; Grabow, K.; Hannebauer, B.; Bentrup, U.; Adam, M.; Franke, R.; Jackstell, R.; Beller, M., *ChemSusChem* **2015**, *8* (2), 323-330.
72. Comelles, J.; Moreno-Manas, M.; Vallribera, A., Michael Additions Catalyzed by Transition Metals and Lanthanoid Species, *ChemInform* **2005**, *36* (38).
73. Takeo, S.; Yoshihiko, I.; Shimpei, T.; Hideo, K., *Bulletin of the Chemical Society of Japan* **1972**, *45* (2), 496-499.
74. Nelson, J. H.; Howells, P. N.; DeLullo, G. C.; Landen, G. L.; Henry, R. A., *The Journal of Organic Chemistry* **1980**, *45* (7), 1246-1249.
75. Christoffers, J., *European Journal of Organic Chemistry* **1998**, *1998* (7), 1259-1266.
76. Christoffers, J., *Tetrahedron Letters* **1998**, *39* (39), 7083-7084.
77. Brunner, H.; Hammer, B., *Angewandte Chemie International Edition in English* **1984**, *23* (4), 312-313.
78. Blacker, A. J.; Clarke, M. L.; Loft, M. S.; Mahon, M. F.; Williams, J. M. J., *Organometallics* **1999**, *18* (15), 2867-2873.



79. Hamashima, Y.; Hotta, D.; Sodeoka, M., *Journal of the American Chemical Society* **2002**, *124* (38), 11240-11241.
80. Watanabe, M.; Murata, K.; Ikariya, T., *Journal of the American Chemical Society* **2003**, *125* (25), 7508-7509.
81. Gómez-Bengoá, E.; Cuerva, J. M.; Mateo, C.; Echavarren, A. M., *Journal of the American Chemical Society* **1996**, *118* (36), 8553-8565.
82. Hou, Z.; Koizumi, T.-a.; Fujita, A.; Yamazaki, H.; Wakatsuki, Y., *Journal of the American Chemical Society* **2001**, *123* (24), 5812-5813.
83. Inagaki, K.; Nozaki, K.; Takaya, H., *Synlett* **1997**, *1* (01), 119-120.
84. Yao, X.; Li, C.-J., *The Journal of Organic Chemistry* **2005**, *70* (14), 5752-5755.
85. Christoffers, J.; Mann, A., *Angewandte Chemie International Edition* **2000**, *39* (15), 2752-2754.
86. Kim, Y. S.; Matsunaga, S.; Das, J.; Sekine, A.; Ohshima, T.; Shibasaki, M., *Journal of the American Chemical Society* **2000**, *122* (27), 6506-6507.
87. Bonadies, F.; Lattanzi, A.; Orelli, L. R.; Pesci, S.; Scettri, A., *Tetrahedron Letters* **1993**, *34* (47), 7649-7650.
88. Keller, E.; Feringa, B. L., *Tetrahedron Letters* **1996**, *37* (11), 1879-1882.
89. Chatani, N.; Asaumi, T.; Yorimitsu, S.; Ikeda, T.; Kakiuchi, F.; Murai, S., *Journal of the American Chemical Society* **2001**, *123* (44), 10935-10941.
90. Pan, S.; Matsuo, Y.; Endo, K.; Shibata, T., *Tetrahedron* **2012**, *68* (44), 9009-9015.
91. Lahm, G.; Opatz, T., *Organic Letters* **2014**, *16* (16), 4201-4203.
92. Mo, F.; Dong, G., *Science* **2014**, *345* (6192), 68.
93. Grützmacher, H., *Angewandte Chemie International Edition* **2008**, *47* (10), 1814-1818.
94. Lim, H. N.; Dong, G., *Angewandte Chemie International Edition* **2015**, *54* (50), 15294-15298.
95. Do, J.; Kim, S.-G., *Tetrahedron Letters* **2011**, *52* (18), 2353-2355.
96. Takaya, H.; Yoshida, K.; Isozaki, K.; Terai, H.; Murahashi, S.-I., *Angewandte Chemie International Edition* **2003**, *42* (28), 3302-3304.
97. Vogt, M.; Nerush, A.; Iron, M. A.; Leitus, G.; Diskin-Posner, Y.; Shimon, L. J. W.; Ben-David, Y.; Milstein, D., *Journal of the American Chemical Society* **2013**, *135* (45), 17004-17018.
98. Nerush, A.; Vogt, M.; Gellrich, U.; Leitus, G.; Ben-David, Y.; Milstein, D., *Journal of the American Chemical Society* **2016**, *138* (22), 6985-6997.
99. Clark, J.; Macquarrie, D., *Handbook of Green Chemistry & Technology*. Blackwell **2002**.

100. Mason, T. J., *Chemical Society Reviews* **1997**, 26 (6), 443-451.
101. Mason, T. J.; Lorimer, J. P., *Sonochemistry, theory, applications and uses of ultrasound in chemistry*, Wiley, New York **1989**.
102. Suslick, K. S., *Scientific American* **1989**, 80-86.
103. Thompson, L. H.; Doraiswamy, L. K., *Industrial & Engineering Chemistry Research* **1999**, 38 (4), 1215-1249.
104. Suslick, K. S.; Goodale, J. W.; Schubert, P. F.; Wang, H. H., *Journal of the American Chemical Society* **1983**, 105 (18), 5781-5785.
105. Kumar, R., *Journal of Organometallic Chemistry* **1977**, 136 (2), 235-239.
106. Geoffroy, G. L.; Wrighton, M. S., 2 - Metal Carbonyls. In *Organometallic Photochemistry*, Academic Press **1979**; pp 34-170.
107. Khosropour, A. R., *Ultrasonics Sonochemistry* **2008**, 15 (5), 659-664.
108. Gholap, A. R.; Venkatesan, K.; Pasricha, R.; Daniel, T.; Lahoti, R. J.; Srinivasan, K. V., *The Journal of Organic Chemistry* **2005**, 70 (12), 4869-4872.
109. Deshmukh, R. R.; Rajagopal, R.; Srinivasan, K. V., *Chemical Communications* **2001**, (17), 1544-1545.
110. Soengas, R. G.; Silva, A. M. S., *Synlett* **2012**, 23 (06), 873-876.
111. Dyker, G., *Handbook of C-H Transformations: Applications in Organic Synthesis*, Wiley **2012**.
112. Landau, S. E.; Groh, K. E.; Lough, A. J.; Morris, R. H., *Inorganic Chemistry* **2002**, 41 (11), 2995-3007.
113. Sakakura, T.; Sodeyama, T.; Sasaki, K.; Wada, K.; Tanaka, M., *Journal of the American Chemical Society* **1990**, 112 (20), 7221-7229.
114. Deeming, A. J.; Shaw, B. L., *Journal of the Chemical Society A: Inorganic, Physical, Theoretical* **1969**, (0), 597-602.
115. Cramer, R., *Inorganic Chemistry* **1962**, 1 (3), 722-723.
116. Cramer, R.; McCleverty, J. A.; Bray, J., In *Inorganic Syntheses*, John Wiley & Sons, Inc.: 1974; pp 14-18.
117. Binger, P.; Haas, J.; Glaser, G.; Goddard, R.; Krüger, C., *Chemische Berichte* **1994**, 127 (10), 1927-1929.
118. Werner, H.; Feser, R., *Zeitschrift für Naturforschung* **1980**, 35b, 689-693.
119. Suslick, K. S.; Gawienowski, J. J.; Schubert, P. F.; Wang, H. H., *The Journal of Physical Chemistry* **1983**, 87 (13), 2299-2301.

120. Mizukoshi, Y.; Nakamura, H.; Bandow, H.; Maeda, Y.; Nagata, Y., *Ultrasonics Sonochemistry* **1999**, *6* (4), 203-209.
121. Suslick, K. S.; Schubert, P. F.; Goodale, J. W., *Journal of the American Chemical Society* **1981**, *103* (24), 7342-7344.
122. Suslick, K. S., *Science* **1990**, *247* (4949), 1439-45.
123. Clerici, M. G.; Di Gioacchino, S.; Maspero, F.; Perrotti, E.; Zanobi, A., *Journal of Organometallic Chemistry* **1975**, *84* (3), 379-388.
124. Garlaschelli, L.; Khan, S. I.; Bau, R.; Longoni, G.; Koetzle, T. F., *Journal of the American Chemical Society* **1985**, *107* (24), 7212-7213.
125. Crabtree, R. H., *Chemical Reviews* **2015**, *115* (1), 127-150.
126. Garrou, P. E., *Chemical Reviews* **1985**, *85* (3), 171-185.
127. Cameron, C. J.; Felkin, H.; Fillebeen-Khan, T.; Forrow, N. J.; Guittet, E., *Journal of the Chemical Society, Chemical Communications* **1986**, (10), 801-802.
128. Ortiz, J. V.; Havlas, Z.; Hoffmann, R., *Helvetica Chimica Acta* **1984**, *67* (1), 1-17.
129. Crabtree, R. H., *The Organometallic Chemistry of the Transition Metals*. Wiley: 2009.
130. Klabunde, E. K. B. U., *Inorganic Syntheses* **1974**; Vol. XV, pp 34-38.
131. Brinkmann, S., Morris, R. H., Ramachandran, R., Park, S., Crabtree, R. H., Patel, B. P. and Pistorio, B. J., *Inorganic Syntheses* **1998**; Vol. XXXII, pp 303-308.
132. Empsall, H. D.; Hyde, E. M.; Mentzer, E.; Shaw, B. L.; Uttely, M. F., *Journal of the Chemical Society, Dalton Transactions* **1976**, (20), 2069-2074.
133. Morris, R. H., *Chemical Reviews* **2016**, *116* (15), 8588-8654.
134. Masters, C.; Shaw, B. L.; Stainbank, R. E., *Journal of the Chemical Society, Dalton Transactions* **1972**, (5), 664-667.
135. Shaw, B. L.; Stainbank, R. E., *Journal of the Chemical Society, Dalton Transactions* **1972**, (19), 2108-2112.
136. Cooper, J. W.; Roberts, B. P., *Journal of the Chemical Society, Perkin Transactions 2* **1976**, (7), 808-813.
137. Tolman, C. A., *Chemical Reviews* **1977**, *77* (3), 313-348.
138. Bilbrey, J. A.; Kazez, A. H.; Locklin, J.; Allen, W. D., *Journal of Computational Chemistry* **2013**, *34* (14), 1189-1197.
139. Desrosiers, P. J.; Cai, L.; Lin, Z.; Richards, R.; Halpern, J., *Journal of the American Chemical Society* **1991**, *113* (11), 4173-4184.
140. Janowicz, A. H.; Bergman, R. G., *Journal of the American Chemical Society* **1983**, *105* (12), 3929-3939.

141. Meima, G. R.; Menon, P. G., *Applied Catalysis A: General* **2001**, 212 (1), 239-245.
142. Widegren, J. A.; Finke, R. G., *Journal of Molecular Catalysis A: Chemical* **2003**, 198 (1), 317-341.
143. Crabtree, R. H., *Chemical Reviews* **2012**, 112 (3), 1536-1554.
144. Anton, D. R.; Crabtree, R. H., *Organometallics* **1983**, 2 (7), 855-859.
145. Campbell, K. C.; Hislop, J. S., *Journal of Catalysis* **1969**, 13 (1), 12-19.
146. Gorunova, O. N.; Novitskiy, I. M.; Grishin, Y. K.; Gloriov, I. P.; Roznyatovsky, V. A.; Khrustalev, V. N.; Kochetkov, K. A.; Dunina, V. V., *Organometallics* **2018**, 37 (17), 2842-2858.
147. Baudry, D.; Ephritikhine, M.; Felkin, H.; Zakrzewski, J., *Tetrahedron Letters* **1984**, 25 (12), 1283-1286.
148. Armarego, W. L. F.; Chai, C. L. L., *Purification of Laboratory Chemicals*. Sixth ed.; Butterworth-Heinemann, Oxford **2009**.
149. Fulmer, G. R.; Miller, A. J. M.; Sherden, N. H.; Gottlieb, H. E.; Nudelman, A.; Stoltz, B. M.; Bercaw, J. E.; Goldberg, K. I., *Organometallics* **2010**, 29 (9), 2176-2179.
150. Rybtchinski, B.; Ben-David, Y.; Milstein, D., *Organometallics* **1997**, 16 (17), 3786-3793.
151. Jia, X.; Huang, Z., *Nature Chemistry* **2016**, 8 (2), 157-161.
152. Fernández Giménez, M., *Iridium-catalysed cleavage and formation of unstrained aliphatic carbon-carbon bonds*. University of Liverpool **2017**.
153. Gu, X.; Dai, Y.; Guo, T.; Franchino, A.; Dixon, D. J.; Ye, J., *Organic Letters* **2015**, 17 (6), 1505-1508.
154. Badham, N. F.; Chen, J.-H.; Cummings, P. G.; Dell'Orco, P. C.; Diederich, A. M.; Eldridge, A. M.; Mendelson, W. L.; Mills, R. J.; Novack, V. J.; Olsen, M. A.; Rustum, A. M.; Webb, K. S.; Yang, S., *Organic Process Research & Development* **2003**, 7 (1), 101-108.
155. Di Bussolo, V.; Catelani, G.; Mastrorilli, E.; Di Bugno, C.; Giorgi, R., *Tetrahedron: Asymmetry* **1996**, 7 (12), 3585-3592.
156. Arndtsen, B. A.; Bergman, R. G., *Science* **1995**, 270 (5244), 1970.
157. Kunin, A. J.; Eisenberg, R., *Journal of the American Chemical Society* **1986**, 108 (3), 535-536.
158. Liskey, C. W.; Hartwig, J. F., *Journal of the American Chemical Society* **2013**, 135 (9), 3375-3378.
159. Simmons, E. M.; Hartwig, J. F., *Nature* **2012**, 483 (7387), 70-73.
160. Corberán, R.; Sanaú, M.; Peris, E., *Journal of the American Chemical Society* **2006**, 128 (12), 3974-3979.

161. Mas-Marzá, E.; Poyatos, M.; Sanaú, M.; Peris, E., *Inorganic Chemistry* **2004**, *43* (6), 2213-2219.
162. Linderman, R. J.; Ghannam, A.; Badejo, I., *The Journal of Organic Chemistry* **1991**, *56* (17), 5213-5216.
163. Baumann, M.; Baxendale, I. R., *Beilstein Journal of Organic Chemistry* **2013**, *9*, 2265-2319.
164. Jun, C.-H., *Chemical Communications* **1998**, (13), 1405-1406.
165. Bergman, S. D.; Storr, T. E.; Prokopcová, H.; Aelvoet, K.; Diels, G.; Meerpoel, L.; Maes, B. U. W., *Chemistry – A European Journal* **2012**, *18* (33), 10393-10398.
166. Kulago, A. A.; Van Steijvoort, B. F.; Mitchell, E. A.; Meerpoel, L.; Maes, B. U. W., *Advanced Synthesis & Catalysis* **2014**, *356* (7), 1610-1618.
167. Chen, X.; Goodhue, C. E.; Yu, J.-Q., *Journal of the American Chemical Society* **2006**, *128* (39), 12634-12635.
168. Löfberg, C.; Grigg, R.; Whittaker, M. A.; Keep, A.; Derrick, A., *The Journal of Organic Chemistry* **2006**, *71* (21), 8023-8027.
169. Bernhart, C. A.; Condamine, C.; Demarne, H.; Roncucci, R.; Gagnol, J. P.; Gautier, P. J.; Serre, M. A., *Journal of Medicinal Chemistry* **1983**, *26* (3), 451-455.
170. Klapars, A.; Waldman, J. H.; Campos, K. R.; Jensen, M. S.; McLaughlin, M.; Chung, J. Y. L.; Cvetovich, R. J.; Chen, C.-y., *The Journal of Organic Chemistry* **2005**, *70* (24), 10186-10189.
171. Newkome, G. R.; Joo, Y. J.; Evans, D. W.; Pappalardo, S.; Fronczek, F. R., *The Journal of Organic Chemistry* **1988**, *53* (4), 786-790.
172. Herold, F.; Kleps, J.; Szczęśna, B.; Anulewicz-Ostrowska, R., *Journal of Heterocyclic Chemistry* **2002**, *39* (4), 773-782.
173. Lin, Y.; Ma, D.; Lu, X., *Tetrahedron Letters* **1987**, *28* (27), 3115-3118.
174. Mestroni, G.; Zassinovich, G.; Camus, A.; Martinelli, F., *Journal of Organometallic Chemistry* **1980**, *198* (1), 87-96.
175. Alvarez, S. G.; Hasegawa, S.; Hirano, M.; Komiya, S., *Tetrahedron Letters* **1998**, *39* (29), 5209-5212.
176. Hasegawa, Y.; Gridnev, I. D.; Ikariya, T., *Bulletin of the Chemical Society of Japan* **2012**, *85* (3), 316-334.
177. Zavodnik, V. E.; Bel'skii, V. K.; Zorkii, P. M., *Journal of Structural Chemistry* **1988**, *28* (5), 793-795.
178. Ladipo, F. T.; Kooti, M.; Merola, J. S., *Inorganic Chemistry* **1993**, *32* (9), 1681-1688.

179. Choi, J.; Choliy, Y.; Zhang, X.; Emge, T. J.; Krogh-Jespersen, K.; Goldman, A. S., *Journal of the American Chemical Society* **2009**, *131* (43), 15627-15629.
180. Berry, R., *The Journal of Chemical Physics* **1960**, *32*.
181. Pannetier, G.; Fougeroux, P.; Bonnaire, R.; Platzer, N., *Journal of the Less Common Metals* **1971**, *24* (1), 83-92.
182. Fernandez, M. J.; Esteruelas, M. A.; Covarrubias, M.; Oro, L. A.; Apreda, M. C.; Foces-Foces, C.; Cano, F. H., *Organometallics* **1989**, *8* (5), 1158-1162.
183. Zhang, X.; Wang, D. Y.; Emge, T. J.; Goldman, A. S., *Inorganica Chimica Acta* **2011**, *369* (1), 253-259.
184. Hartwig, J. F., *Organotransition Metal Chemistry: From Bonding to Catalysis*. University Science Books **2010**.
185. Quin, L. D.; Verkade, J. G., *Phosphorus-31 NMR spectral properties in compound characterization and structural analysis*, Advanced Chemistry Development, University of Michigan, VCH **2004**.
186. Solymosi, K.; Latruffe, N.; Morant-Manceau, A.; Schoefs, B., *Colour Additives for Food and Beverages*, Elsevier Ltd **2015**.
187. Nirmal, N. P.; Rajput, M. S.; Prasad, R. G. S. V.; Ahmad, M., *Asian Pacific Journal of Tropical Medicine* **2015**, *8* (6), 421-430.
188. Tyman, J. H. P., *Synthetic and Natural Phenols*, Elsevier **1996**.
189. Maertens, G.; L'Homme, C.; Canesi, S., *Frontiers in Chemistry* **2015**, *2* (115).
190. Izawa, Y.; Pun, D.; Stahl, S. S., *Science* **2011**, *333* (6039), 209-213.
191. Zhang, J.; Jiang, Q.; Yang, D.; Zhao, X.; Dong, Y.; Liu, R., *Chemical Science* **2015**, *6* (8), 4674-4680.
192. Cotugno, P.; Monopoli, A.; Ciminale, F.; Milella, A.; Nacci, A., *Angewandte Chemie* **2014**, *126* (49), 13781-13785.
193. Liang, Y.-F.; Song, S.; Ai, L.; Li, X.; Jiao, N., *Green Chemistry* **2016**, *18* (24), 6462-6467.
194. Liang, Y.-F.; Li, X.; Wang, X.; Zou, M.; Tang, C.; Liang, Y.; Song, S.; Jiao, N., *Journal of the American Chemical Society* **2016**, *138* (37), 12271-12277.
195. Pun, D.; Diao, T.; Stahl, S. S., *Journal of the American Chemical Society* **2013**, *135* (22), 8213-8221.
196. Barbasiewicz, M.; Marciniak, K.; Fedoryński, M., *Tetrahedron Letters* **2006**, *47* (23), 3871-3874.